

# **Synthesis and pharmacological investigation of hybrid ligands targeting the muscarinic acetylcholine receptors**

A thesis submitted for the degree of  
Doctor of Philosophy

By

Matthew Charles Linford Wakeham

Supervisors: Prof. Peter Scammells and Dr. Ben Capuano

Monash Institute of Pharmacy and Pharmaceutical Sciences

Monash University

2019



# Table of Contents

<b>Statement of Originality</b> .....	4
<b>Abbreviations</b> .....	5
<b>Acknowledgements</b> .....	7
 <b>Chapter 1 Introduction</b> .....	9
1. G protein-coupled receptors .....	10
1.1 Classification, function and dynamics .....	10
1.2 Orthosteric ligands.....	13
1.3 Allosteric ligands .....	14
1.4 Hybrid ligands and bitopic ligands .....	16
2. Muscarinic acetylcholine receptors (mAChRs).....	19
2.1 Drugs targeting the mAChRs .....	19
2.2 Structure and activation of the mAChRs .....	22
2.3 The M <sub>1</sub> mAChR and Alzheimer's disease .....	24
2.4 The M <sub>4</sub> mAChR and schizophrenia .....	27
3. Novel design strategies to overcome issues of subtype selectivity in mAChR ligands ..	30
3.1 Allosteric agonists/ PAMs targeting the M <sub>1</sub> mAChR.....	30
3.2 Allosteric agonists/ PAMs targeting the M <sub>4</sub> mAChR .....	36
3.3 Hybrid bitopic ligands targeting the mAChRs .....	40
4. Fluorescently tagged bioactive molecules .....	47
4.1 Design of fluorescently tagged small-molecule probes .....	47
5. Summary and thesis aims.....	50
References .....	51
 <b>Chapter 2 Design, Synthesis and Evaluation of Iperoxo-BQCA Hybrid Ligands</b> .....	65
Abstract .....	67
Introduction .....	67
Results and Discussion .....	72
Conclusion .....	83
Experimental section .....	84
References .....	100

<b>Chapter 3 Structure-Activity Relationship Study of Novel M<sub>2</sub>/ M<sub>4</sub> Selective Muscarinic Acetylcholine Receptor Hybrid Ligand Partial Agonists .....</b>	<b>104</b>
Abstract .....	106
Introduction .....	107
Results and Discussion .....	114
Conclusion .....	128
Experimental section .....	130
References .....	148
 <b>Chapter 4 Investigation into the Molecular Mechanism of Efficacy and Selectivity of Iperoxo-Based Muscarinic Acetylcholine Receptor Hybrid Ligands .....</b>	 <b>152</b>
Abstract .....	154
Introduction .....	155
Results and Discussion .....	164
Conclusion .....	183
Experimental section .....	186
References .....	190
 <b>Chapter 5 Design, Synthesis and Evaluation of a Fluorophore-Tagged Muscarinic Acetylcholine Receptor Allosteric Probe .....</b>	 <b>193</b>
Abstract .....	195
Introduction .....	196
Results and Discussion .....	206
Conclusion .....	226
Experimental section .....	228
References .....	233
 <b>Chapter 6 Conclusions and Future Directions .....</b>	 <b>237</b>
 <b>Appendix .....</b>	 <b>246</b>
Supplementary Information for Chapter 2 .....	246
Supplementary Information for Chapter 3 .....	256
Supplementary Information for Chapter 4 .....	265

# **Statement of Originality**

I hereby declare that this thesis contains no material which has been accepted for the award of any other degree or diploma at any university or equivalent institution and that this thesis contains no material previously published or written by another person, except where due reference is made in the text explicitly.

Matthew Charles Linford Wakeham

## Abbreviations

ACh, acetylcholine,

AC, adenylate cyclase,

ACN, acetonitrile,

ADME, absorption, distribution,  
metabolism and excretion,

APP, amyloid precursor protein,

BBB, blood brain barrier,

BRET, bioluminescence resonance energy  
transfer,

BQCA, 1-(4-methoxybenzyl)-4-oxo-1,4-  
dihydroquinoline-3-carboxylic acid,

cAMP, cyclic adenosine monophosphate,

CHO cells, Chinese hamster ovarian cells,

CNS, central nervous system,

COSY, correlation spectroscopy,

CRC, concentration response curve,

DCM, dichloromethane,

DIPEA, diisopropylethylamine,

DMEM, Dulbecco's Modified Eagle  
Medium,

DMF, dimethylformamide,

DMSO, dimethyl sulphoxide,

EC, extracellular,

ECL, extracellular loop domain,

ESI, electrospray ionization,

FBS, foetal bovine serum,

FP, fluorescence polarisation,

FRET, Förster resonance energy transfer,

GDP, Guanosine-5'-diphosphate,

GPCR, G protein-coupled receptor,

GTP, Guanosine-5'-triphosphate,

HCTU, 2-(6-chloro-1*H*-benzotriazole-1-  
yl)-1,1,3,3-tetramethylaminium  
hexafluorophosphate,

HEPES, 2-[4-(2-hydroxyethyl)-1-  
piperazinyl]ethanesulfonic acid,

HMBC, heteronuclear multiple-bond  
correlation,

HRMS, high-resolution mass  
spectrometry,

HSQC, heteronuclear single quantum coherence,	PAM, positive allosteric modulator,
IC, intracellular,	pERK 1/2, phosphorylated ERK 1/2 protein,
IP3, inositol triphosphate,	PNS, peripheral nervous system,
IXO, iperoxo iodide,	QNB, quinuclidinyl benzilate,
KO, knockout,	RBF, round-bottomed flask,
LC-MS, liquid-chromatography mass spectrometry,	RT, room temperature,
mAChR, human muscarinic acetylcholine receptor,	SAR, structure-activity relationship,
MP, melting point,	S.E.M., standard error of the mean,
NAM, negative allosteric modulator,	TEA, triethylamine,
NMDA, <i>N</i> -methyl-D-aspartate,	TFA, trifluoroacetic acid,
NMR, nuclear magnetic resonance,	THF, tetrahydrofuran,
[ <sup>3</sup> H]NMS, tritiated <i>N</i> -methylscopolamine,	TLC, thin layer chromatography,
PBS, phosphate-buffered saline,	TM, transmembrane domain,
PLC, phospholipase C,	TOF, time of flight,
	UV, ultraviolet.

## Acknowledgments

When I began this journey I believed that I was unstoppable. Every undergraduate course that I had ever undertaken, and that I was interested in, I had easily attained a high distinction in, and for those I was less enthusiastic about, a distinction mark was nearly guaranteed. In my honours year I achieved the second highest mark in my cohort, with what I considered to be minimal exertion, and when I arrived at Monash University to undertake my PhD in medicinal chemistry, under the supervision of Professor Peter Scammells and Doctor Ben Capuano, I was sure that I would prevail similarly. I was wrong. Over the course of my PhD I have been pushed to limits that, at times, I was not sure that I could accommodate for. However, this thesis, as it is presented here, is proof that despite my own accumulated personal scepticism in my own abilities, I have indeed prevailed. I was recommended to undertake my PhD with Professor Peter Scammells by my honours supervisor, Doctor Angela Finch, whom I can honestly say was one of the best teachers I have ever had, and who is responsible for sparking my initial interest in the field of molecular pharmacology, for which I am very grateful. Initially during my PhD, at times I believed that Professor Scammells and I were practitioners of two ‘different kinds of science’ and that he, at times, did not appreciate what I believed to be my ‘creative’ approach to problem solving. However over the past years no one has done more to help me refine my ideas and develop myself as a scientist as he has, and for that I cannot possibly effectively express my true gratitude. Science is a beautiful and complicated art form, but without a robust and level-headed approach, nothing can be achieved. I am also eternally grateful to Doctor Ben Capuano, whose seemingly contradictory laid-back approach and simultaneous passion for precision and accuracy has given me much inspiration over the years, and has influenced me greatly. I would also like to thank Doctor Celine Valant and Professor Arthur Christopoulos whose guidance and support in the molecular pharmacology sections of this thesis was invaluable and without which most of

this work could not have been done. To Doctor Shane Devine and Doctor Leigh Ford I would like to express my gratitude is assisting me with the practical aspects of the chemistry sections of this thesis, and for guiding me in conducting myself safely and effectively in a chemistry laboratory. To my good friends Rosanna Wallis and Mitchell Ryan, you offered me a place to stay on many occasions when I had nowhere else to turn, without you I would have never completed this work, and I am forever in your debt. To my friends whom I met during this journey at Monash University, your tenacity, strength-of-will and light-heartedness was a constant source of emotional support, without which I could not have achieved what I have done here, and I am proud to have met each and every one of you. Finally, I would of course like to thank my family, and in particular my mother, father and brother, whom I love more than anything else in this world, and whose love, support and encouragement was at times the only thing that kept me from faulting in this endeavour. During my time at Monash I have grown, not only as a scientist, but as a person, in ways that I was not aware that I could of, and for that reason this has been the most important experience of my life.

Thank you.



# Chapter One

# Introduction

## 1. G protein-coupled receptors

### 1.1 Classification, function and dynamics

G protein-coupled receptors (GPCRs) are a class of membrane-bound receptor proteins that mediate a wide variety of physiological functions in the human body. The superfamily of human GPCRs contains over 800 members.<sup>1</sup> GPCRs are further characterised into five families based on sequence and structural similarities; rhodopsin (family A), secretin (family B), glutamate (family C), adhesion and Frizzled/Taste2, the largest of these families is the rhodopsin (family A) GPCRs which contains many important pharmaceutical targets.<sup>2-3</sup> GPCRs transmit signals across the cell membrane in response to a many varied physical stimuli including small molecules, peptides/ proteins and photons.<sup>4</sup> Signals are accepted by the extracellular region of the receptor, which induces a conformational change, and affects coupling to various intracellular signalling proteins, most notably the guanine nucleotide binding proteins (G proteins).<sup>5</sup> In the inactive state, when bound to intracellular surface of a GPCR, G proteins exist as a heterotrimeric complex of  $\alpha$ ,  $\beta$  and  $\gamma$  subunits.<sup>6</sup> Upon receptor activation the guanosine diphosphate (GDP)-bound  $\alpha$  subunit binds to a molecule of guanosine triphosphate (GTP) (displacing GDP) causing dissociation of the monomeric  $\alpha$  subunit and the dimeric  $\beta\gamma$  subunits from the receptor, which then stimulate downstream effectors.<sup>7</sup> With the assistance of GTPase, the  $\alpha$  subunit then hydrolyses GTP to GDP and reassociates with the  $\beta\gamma$  subunits and the receptor, restoring the initial state of the receptor-G protein complex and allowing for further signalling (Figure 1).<sup>8</sup>

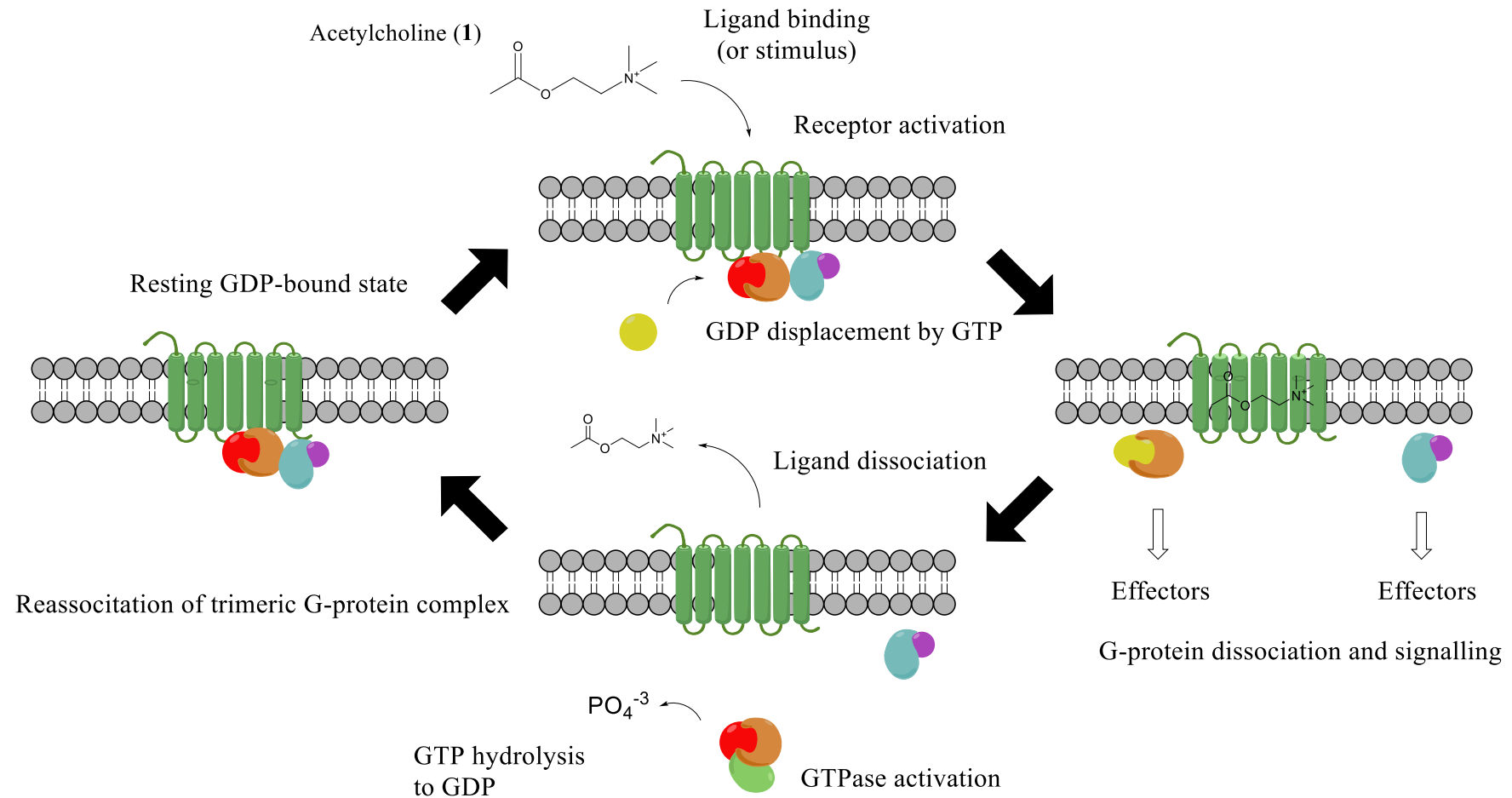


**Figure 1.** Basic mechanism of GPCR signalling via G proteins. A GPCR is shown in green, embedded in the membrane, which is shown in grey. Acetylcholine (1) is shown as a representative stimulus. GTP is depicted as yellow balls, GDP as red balls. The G protein  $\alpha$  subunit is shown in orange, the  $\beta$  subunit is shown in blue and the  $\gamma$  subunit is shown in purple. GTPase is shown in light green, associated with the G protein  $\alpha$  subunit.

GPCRs can also couple to a variety of other intracellular signalling proteins, including  $\beta$ -arrestin which is involved in regulating GPCR signalling by recruiting activated GPCRs and marking them for endocytotic internalisation via clathrin-coated vesicles.<sup>9</sup> Another important signalling pathway downstream of many GPCRs is the mitogen-activated protein kinase (MAPK) pathway, which upon activation ultimately results in phosphorylation of extracellular signal-regulated kinases (ERKs) (as well as many other signalling cascades) and which are involved in regulation of gene transcription and cell division.<sup>10</sup> The characteristic structural feature of GPCRs is their seven  $\alpha$ -helical transmembrane regions (TM1 - TM7) which are interconnected by alternating intra- and extracellular (ICL and ECL) loops.<sup>11</sup> To date, the structures of a significant number of family A GPCRs have been solved, including the rhodopsin receptor,<sup>11</sup> 1B, 2A, 2B and 2C 5-hydroxytryptamine receptors,<sup>12-15</sup>  $\beta_1$  and  $\beta_2$  adrenergic receptors,<sup>7, 16-17</sup>  $A_1$  and  $A_{2A}$  adenosine receptors,<sup>18-19</sup>  $D_2$ ,  $D_3$  and  $D_4$  dopamine receptors,<sup>20-22</sup>, CB1 and CB2 cannabinoid receptors,<sup>23-24</sup> delta-, kappa- and mu-opioid receptors<sup>25-27</sup> and the  $M_1$ - $M_4$  muscarinic acetylcholine receptors,<sup>28-31</sup> among others. As such, much is known about their physical structures, binding sites and mechanisms of receptor activation.<sup>32</sup> Comparison of x-ray crystal structures of several active and inactive-state family A GPCRs has revealed a common conformational rearrangement of the transmembrane helices (TM1-7) between upon receptor activation.<sup>33</sup> The most significant conformational change is in TM6, which undergoes rotation around its longitudinal axis, resulting in displacement of the cytoplasmic end of the helix on the order of 10 Å.<sup>33</sup> TM1, TM5 and TM7 all undergo an inward movement (towards the central binding pocket), while TM3 undergoes a slight rotation and upward movement (towards the extracellular space) (Figure 2).<sup>33</sup>

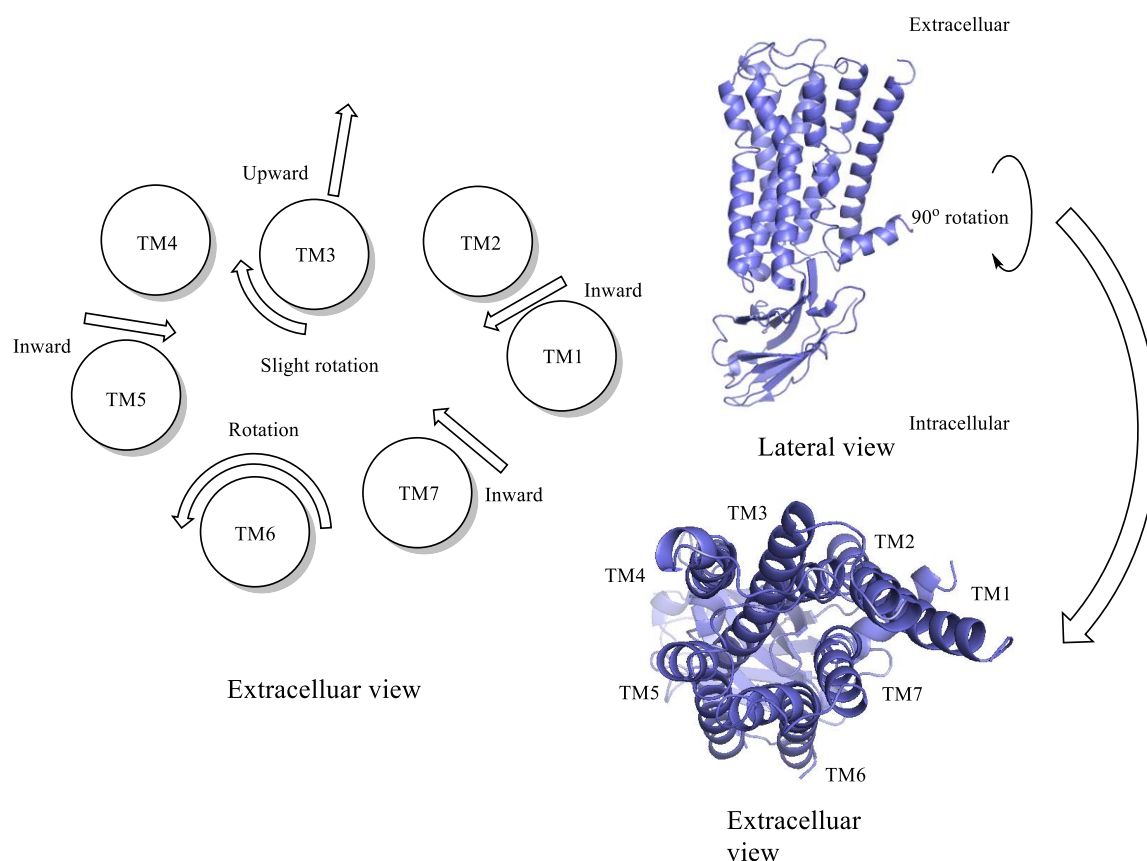


**Figure 2.** Schematic diagram showing the common conformational changes of the transmembrane helices observed between x-ray crystal structures of active and inactive-state family A GPCRs. Lateral and extracellular view of a GPCR structure shown for orientation. Graphic adapted from Tehan *et al.*<sup>33-34</sup>

## 1.2 Orthosteric ligands

In family A GPCRs the endogenous (orthosteric) binding site is typically located in the middle of the transmembrane ‘bundle’ on the extracellular face of the receptors. Ligands which bind to this site are referred to as ‘orthosteric ligands’ and depending on the degree to which they stabilise or destabilise an active receptor conformation are classified as agonists, partial agonists, antagonists or inverse agonists.<sup>35-36</sup> Agonists bind preferentially to the active state of their target receptor, antagonists bind neutrally and elicit no downstream signalling, while inverse agonists destabilise an active receptor conformation, resulting in the a reduction in intracellular signalling below that of basal levels.<sup>36</sup> The pharmacological properties of

orthosteric ligands are typically broadly quantitated by two properties, their affinity (strength of binding) and in the case of agonists and inverse agonists their efficacy (strength of signal induced by ligand binding). For agonists, partial agonists and inverse agonists of equivalent affinity the efficacy can be compared relatively from the maximum response values of each ligand in functional assays. However a more robust measure of efficacy, that is independent of ligand affinity, can be derived by fitting the data for each ligand to an operational model of agonism and constraining the affinity to a value measured in binding assays.<sup>37</sup> This method allows for a quantitative value for efficacy for each ligand that is comparable to other values, regardless of the affinities of the agonists/ partial agonists in question.

### **1.3 Allosteric ligands**

Some, and possibly all, GPCRs also contain secondary binding sites, known as ‘allosteric sites’, spatially distinct from the orthosteric site.<sup>38</sup> Ligands which bind to these sites are referred to as ‘allosteric ligands’ and can act upon their target receptor in several ways. Allosteric ligands may exert some receptor activation in their own right, referred to as allosteric agonism, or they may modulate the affinity or functional response of a co-bound orthosteric ligand, referred to as ‘allosteric modulation’ and quantitated by a term referred to as ‘cooperativity’.<sup>39</sup> Cooperativity can be positive, in which affinity and/ or efficacy of the orthosteric ligand is potentiated, neutral, in which these properties remain unchanged, or negative, in which these properties are attenuated, and allosteric ligands with these properties are referred to as positive allosteric modulators (PAMs), neutral allosteric ligands (NALs) and negative allosteric modulators (NAMs), respectively. Allosteric modulation is a probe dependent phenomenon, meaning that their activity as a PAM, NAL or NAM will depend upon the orthosteric probe with which they are co-incubated. For allosteric modulators with no intrinsic efficacy are described by a simple allosteric ternary complex model. The affinity cooperativity ( $\alpha$ ) and efficacy cooperativity ( $\beta$ ) can be estimated independently, provided that other variables (such

as allosteric ligand affinity  $K_B$ , orthosteric probe affinity,  $K_A$ ) in the model are constrained. In the cases of allosteric agonists, their intrinsic efficacy must be taken into account and their pharmacology is well described by an operational model of allosteric agonism (Figure 3).<sup>39-40</sup>

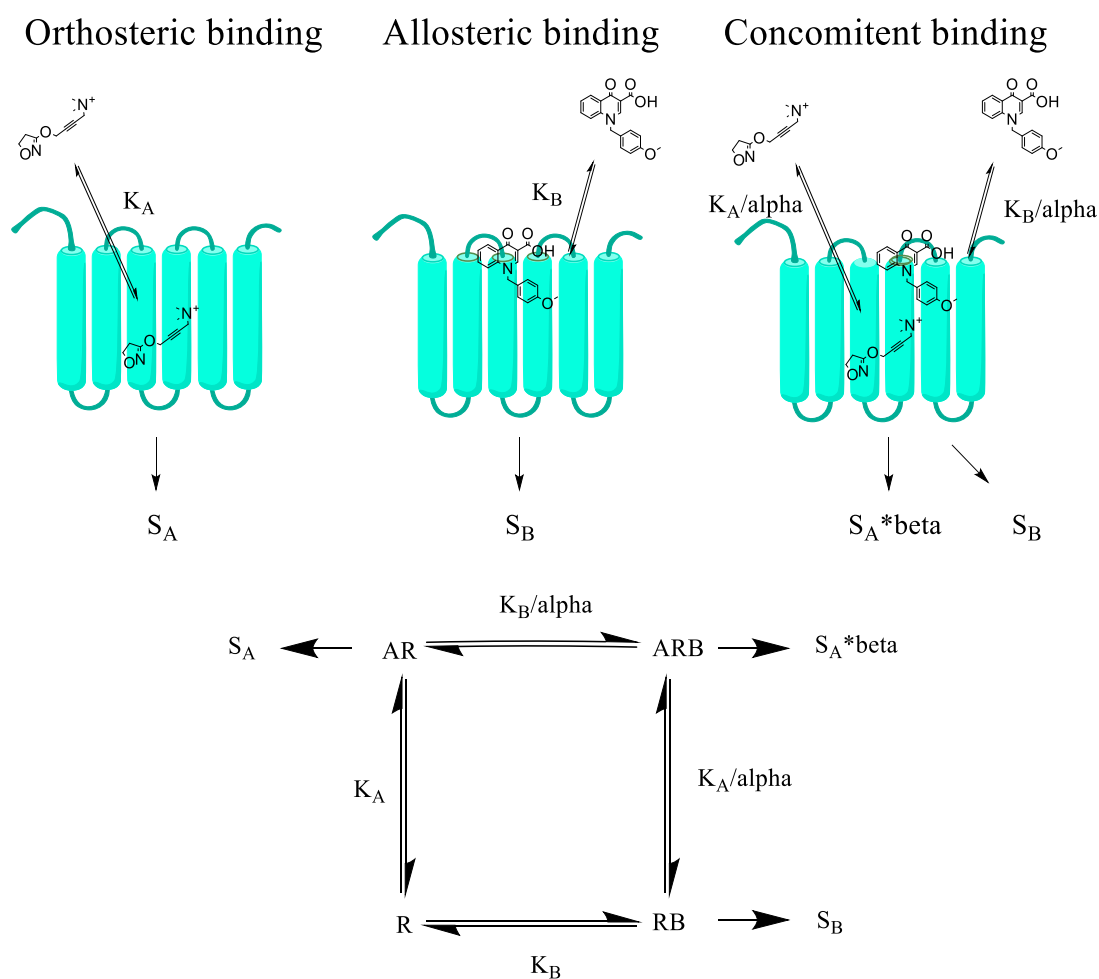


**Figure 3.** Simple operational model of allosteric agonism.  $K_A$  and  $K_B$  are the affinity constants for the orthosteric ligand and allosteric ligand binding to the orthosteric site and allosteric site, respectively.  $S_A$  and  $S_B$  represent the quantitation of some arbitrary cellular signal induced by and orthosteric ligand and allosteric ligand, respectively. ‘Alpha’ and ‘beta’ represent the cooperativity between the two ligands, ‘alpha’ refers to modulation of affinity while ‘beta’ refers to modulation of efficacy, (when both ligands are co-bound). The ligands depicted are the orthosteric agonist, iperoxo, and the allosteric potentiator, BQCA.

From a therapeutic perspective, allosteric ligands carry several potential advantages over orthosteric ligands. For purely allosteric modulators, that possess no intrinsic efficacy in their

own right (as opposed to allosteric agonists), the spatially and temporally distinct nature of their binding means that they exert no activity at their target receptor in the absence of endogenous tone. Consequently, allosteric modulators maintain normal inter-neuronal signalling ‘rhythms’ and also have an upper limit to their effect at the target receptor (i.e. a ‘ceiling’ effect), limiting the potential for overdose.<sup>38</sup> Allosteric sites are also typically less conserved than orthosteric sites and in some cases this results in differences in affinity at related receptor subtypes and hence subtype selectivity.<sup>41</sup> However selectivity in allosteric ligands can also arise from differences in cooperativity and not differences in allosteric site affinity between subtypes within subfamilies of GPCRs, inspiring the term ‘absolute subtype selectivity’; an allosteric ligand which possess neutral cooperativity at all subtypes within a subfamily of GPCRs except for one.<sup>42</sup>

#### **1.4 Hybrid ligands and bitopic ligands**

Hybrid ligands are a class of molecules that consist of two functional molecules (e.g. ligands or ‘pharmacophores’) joined by a molecular linker. There are many potential applications for the conjoining of two functional molecules. Hybrid ligands targeting two distinct (either homologous or heterologous) protein targets have been explored as synergistic/combination therapies, as well as those targeting two adjacent sites on a single protein, referred to in GPCR ligands as ‘bitopic’ (or ‘dualsteric’) ligands.<sup>43-45</sup> Bitopic ligands are based on the message-address concept in which an orthosteric ligand provides the ‘message’ (e.g. agonism and/ or affinity) and the allosteric ligand provides the ‘address’, referring to subtype selectivity.<sup>46</sup> It is important to note that not all hybrid ligands bind bitopically and not all bitopic ligands are hybrid ligands, these terms refer to the structural features of the molecule and mechanism by which it interacts with its target receptor, respectively. An example of a hybrid ligand that is both a combination therapy (i.e. targets two distinct receptors) and a bitopic ligand is THRX-198321 (**2**) (Figure 4). THRX-198321 (**2**) is a hybrid ligand which consists of a



mAChR antagonist linked to a  $\beta$ -adrenergic receptor agonist and was originally investigated as a potential treatment of COPD. Subsequently the researchers investigating THR-198321 (**2**) demonstrated the pharmacology of this ligand could not be explained by a simple orthosteric interaction, and in a detailed study demonstrated that it binds bitopically at both the M<sub>2</sub>, M<sub>3</sub> mAChRs and the  $\beta_2$ -adrenergic receptor.<sup>47-48</sup>

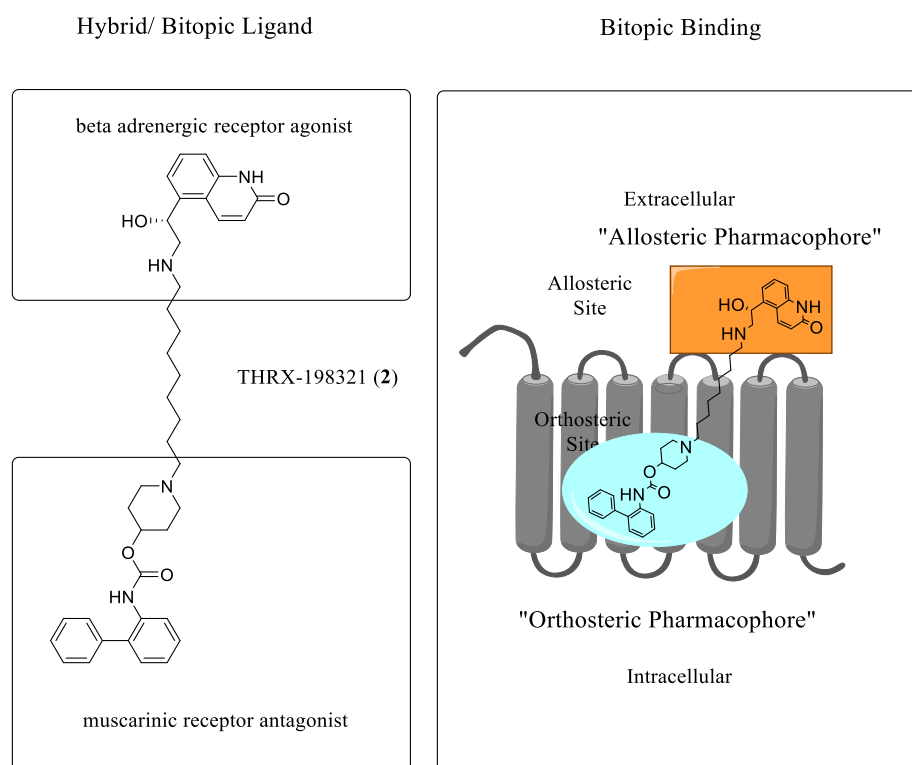


**Figure 4.** Chemical structure of combination therapy hybrid bitopic ligand, THR-198321 (**2**) and a diagram illustrating it bitopically binding to one of its target receptors, the M<sub>3</sub> mAChR.

Bitopic hybrid ligands offer a potential strategy to overcome the issues of subtype selectivity which are common among ligands targeting GPCRs. By engaging both the orthosteric and allosteric sites of a GPCR these ligands aim to exploit the lower conservation of the allosteric sites for increased subtype selectivity while maintaining high affinity and/ or efficacy that is typically associated with orthosteric ligands (Figure 4).<sup>49</sup> Bitopic binding mechanisms are highly dynamic, often consisting of multiple binding modes that can each interact or compete with one another directly at a molecular level (Figure 5).<sup>50-53</sup> As a result of

this mechanistic studies are challenging, as temporally separated allosteric or orthosteric binding events and concomitant bitopic binding may present with data from common assays that is indistinguishable.<sup>43</sup>

#### Potential Hybrid Ligand Binding Modes

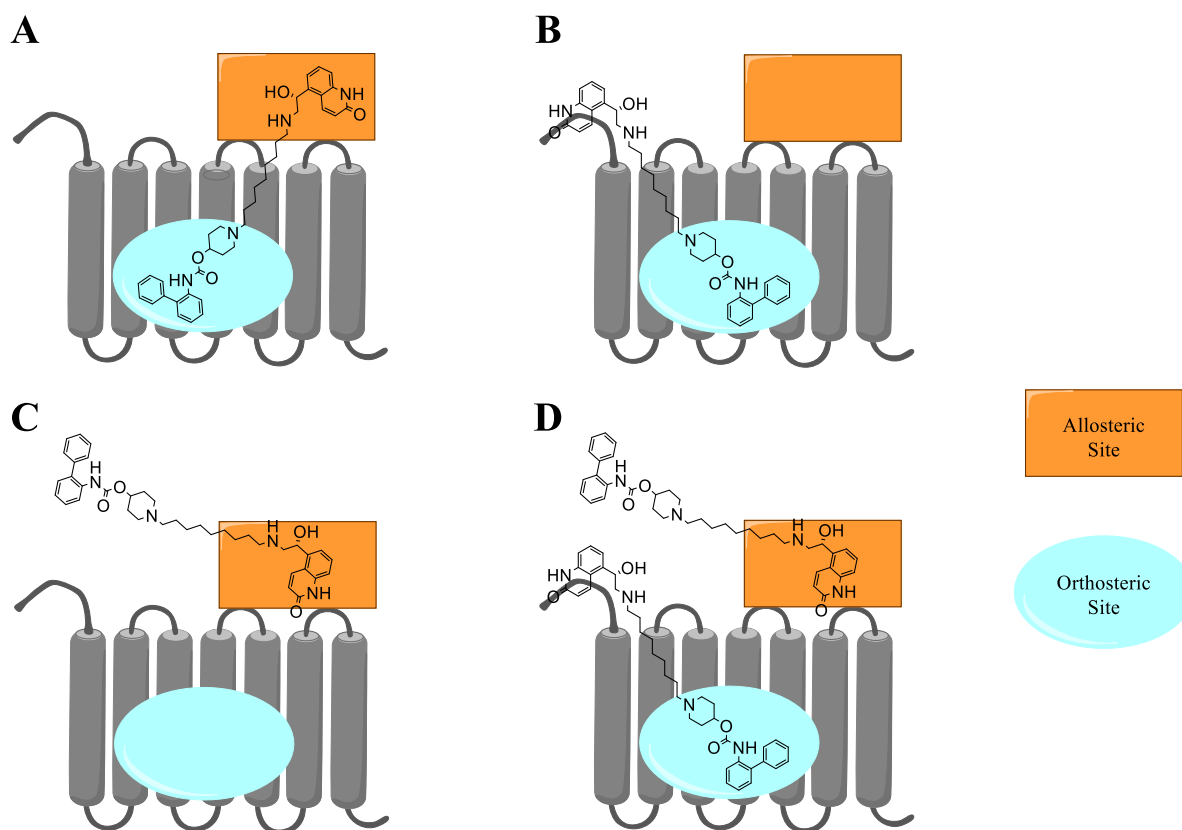


**Figure 5.** Schematic diagram of potential hybrid ligand binding modes. (A) Simultaneous bitopic binding to the allosteric and orthosteric sites. (B) Purely orthosteric binding in which the allosteric pharmacophore remains unbound to the receptor. (C) Purely allosteric binding in which the orthosteric pharmacophore remains unbound to the receptor. (D) Co-binding of two bitopic ligands, one binding purely orthosterically, the other binding purely allosterically.

Despite this, bitopic binding has been demonstrated in several designed hybrid ligands as well as discovered in examples of previously unappreciated bitopic ligands.<sup>43, 54-56</sup> In several cases the pharmacological properties (i.e. affinity, efficacy and selectivity) of the constituent monomer pharmacophores is partially preserved (or enhanced), validating hybrid bitopic ligands as potential approach to designing subtype selective agonists/ partial agonists.<sup>49, 57-58</sup>

## 2. Muscarinic acetylcholine receptors (mAChRs)

The muscarinic acetylcholine receptors (mAChRs) are a subfamily of the family A GPCRs consisting of five members, the M<sub>1</sub>-M<sub>5</sub> mAChRs, and form part of the cholinergic system in the central nervous system (CNS) and peripheral nervous system (PNS). The mAChRs are activated by the endogenous agonist acetylcholine (**1**). Studies employing mRNA hybridisation and immunocytochemical methods have revealed the relative distribution of each of the five mAChR subtypes in various human tissues.<sup>59</sup> All five subtypes are found to be expressed in the CNS, the M<sub>1</sub>, M<sub>3</sub> and M<sub>5</sub> mAChRs being expressed predominantly postsynaptically, while the M<sub>2</sub> and M<sub>4</sub> mAChRs are predominantly expressed presynaptically. The M<sub>2</sub> and M<sub>3</sub> mAChRs are also highly expressed in peripheral tissues including cardiac, smooth muscle, secretory glands and others, and off-target drug activity at these receptors is responsible for what is commonly referred to as cholinergic side effects.<sup>60</sup> The M<sub>1</sub>, M<sub>3</sub> and M<sub>5</sub> mAChRs predominantly couple intracellularly to the G<sub>q/11</sub> family of G proteins resulting activation of phospholipase C (PLC), leading to increased inositol-1,4,5-triphosphate (IP<sub>3</sub>) production, and subsequently the increased release of calcium ions (Ca<sup>2+</sup>) into the cytosol. The M<sub>2</sub> and M<sub>4</sub> mAChRs predominantly (but not exclusively<sup>61</sup>) couple to G<sub>i/o</sub> G proteins and activation of these proteins results in inhibition of adenylate cyclase (AC) which results in lower production of cyclic adenosine monophosphate (cAMP) and inhibition of voltage-gated calcium channels.<sup>59, 62</sup>

### 2.1 Drugs targeting the mAChRs

As evidenced by their broad distribution throughout the human body, the mAChRs are involved in a wide range of physiological functions, and as such have in the past and to the present been actively pursued as drug targets for the treatment of various diseases.<sup>63</sup> There are several muscarinic ligands currently used clinically including pilocarpine (**3**) and carbachol,

(4) which is used in the treatment of glaucoma, ipratropium (5), tiotropium (6) and alclidinium (7), which are used in the treatment of chronic obstructive pulmonary disease (COPD), diphenhydramine (8) and doxylamine (9), which are used as antiemetics and sleep-aids, oxybutynin (10), tolterodine (11) and solifenacin (12), which are used in the treatment of overactive bladder and urge incontinence, dicycloverine (13) and mebeverine (14), which are used in the treatment of irritable bowel syndrome, and pirenzepine (15) which has historically been used to treat peptic ulcer (Figure 6). The structural scaffold of many mAChR ligands mimics that of the endogenous agonist, ACh (1), and contain a quaternary or ionisable amine, and an ester functional group (or isostere thereof) (Figure 6).

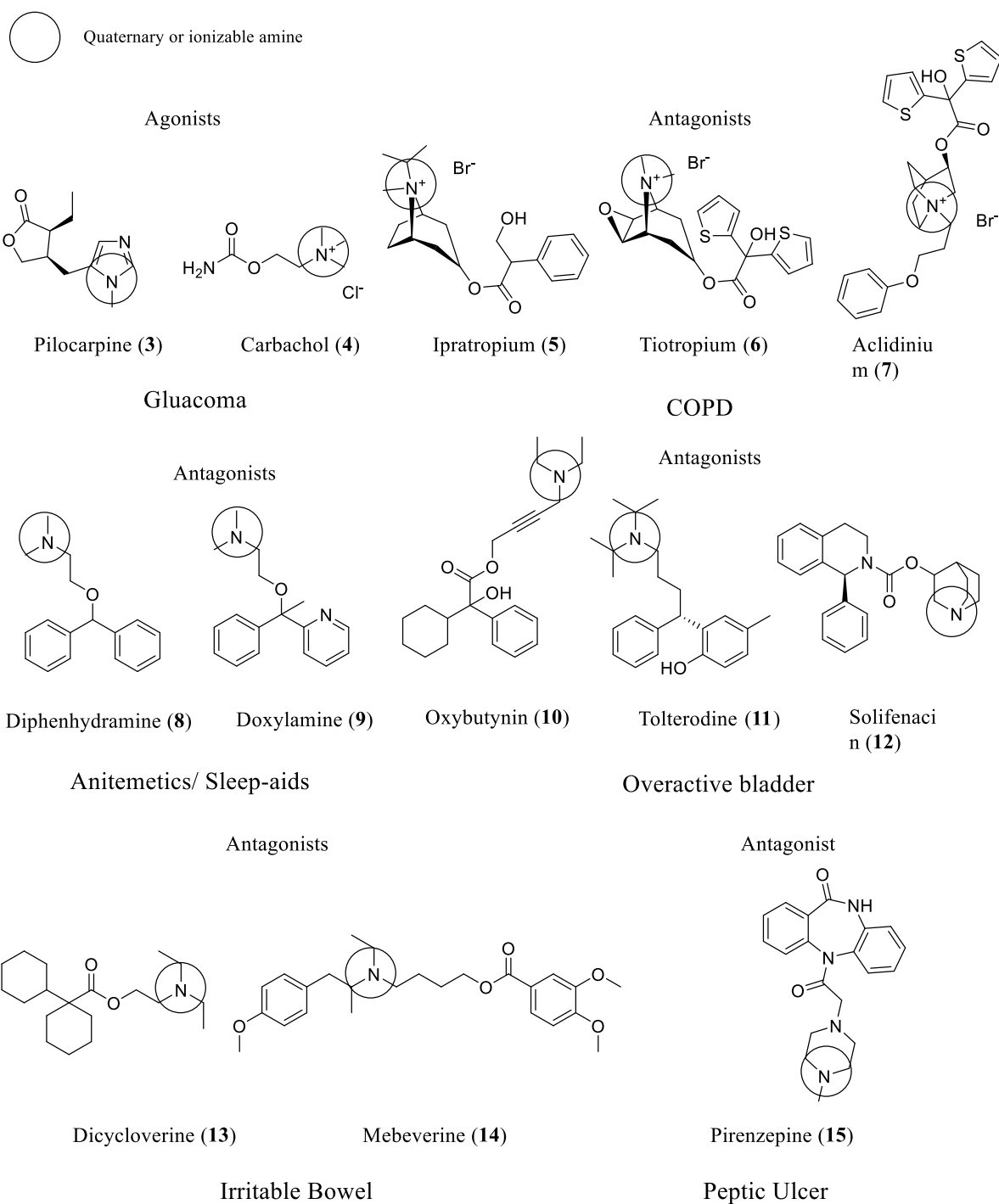


**Figure 6.** Examples of mAChR ligands with medicinal applications for a variety of conditions. Circled on each ligand is the characteristic quaternary or ionizable amine which is necessary for binding to the orthosteric site of the mAChRs.

The design of orthosteric ligands targeting the mAChRs has several common technical issues. Orthosteric mAChR ligands are typically non-selective for a single mAChR subtype, owing to the highly conserved nature of mAChR orthosteric site. Additionally a quaternary

ammonium or ionizable amine group is a necessity in mAChR orthosteric ligands. The quaternary or protonated amine group binds to a fully conserved aspartate in the orthosteric site (Asp<sup>3.32</sup>) of the mAChRs and is essential for orthosteric binding.<sup>64</sup> This means that designing ligands with suitable physiochemical properties for blood-brain barrier (BBB) penetration is a significant challenge in the design of drugs targeting the orthosteric site of mAChRs in the CNS.<sup>65</sup>

## 2.2 Structure and activation of the mAChRs

X-ray crystallographic data has revealed in molecular detail the structure, ligand binding and dynamics of the M<sub>1</sub>-M<sub>4</sub> mAChRs, by the comparison of ligand-bound active and inactive structures.<sup>28, 30-31</sup> As mentioned previously, the binding of orthosteric ligands occurs primarily to the key Asp<sup>3.32</sup> residue in the orthosteric binding pocket via a charged nitrogen ‘head’ group of the ligand (Figure 7 C). Another highly conserved residue, Asn<sup>6.52</sup> (Figure 7 C) on TM6, also makes a hydrogen bonding interaction with hydrophilic functional groups on both agonists and antagonists. The orthosteric site itself is mostly occluded in both active and inactive structures by three highly conserved tyrosines, (Tyr<sup>3.33</sup>, Tyr<sup>6.51</sup>, Tyr<sup>7.39</sup>) which form a ‘lid’ over the charged nitrogen ‘head’ group of orthosteric ligands (Figure 7 B).<sup>29</sup> The 4-hydroxyl groups of these tyrosine residues form hydrogen bonds with one-another in the active-state M<sub>2</sub> mAChR structure, and mutation of these residues to phenylalanine results in loss of agonist efficacy and coupling to intracellular signalling. Observed movement of the helices between active and inactive conformations of the M<sub>2</sub> mAChR forms part of the evidence for the model of GPCR activation discussed previously and is consistent with that model (see G protein-coupled receptors: classification, function and dynamics) (Figure 7 A).

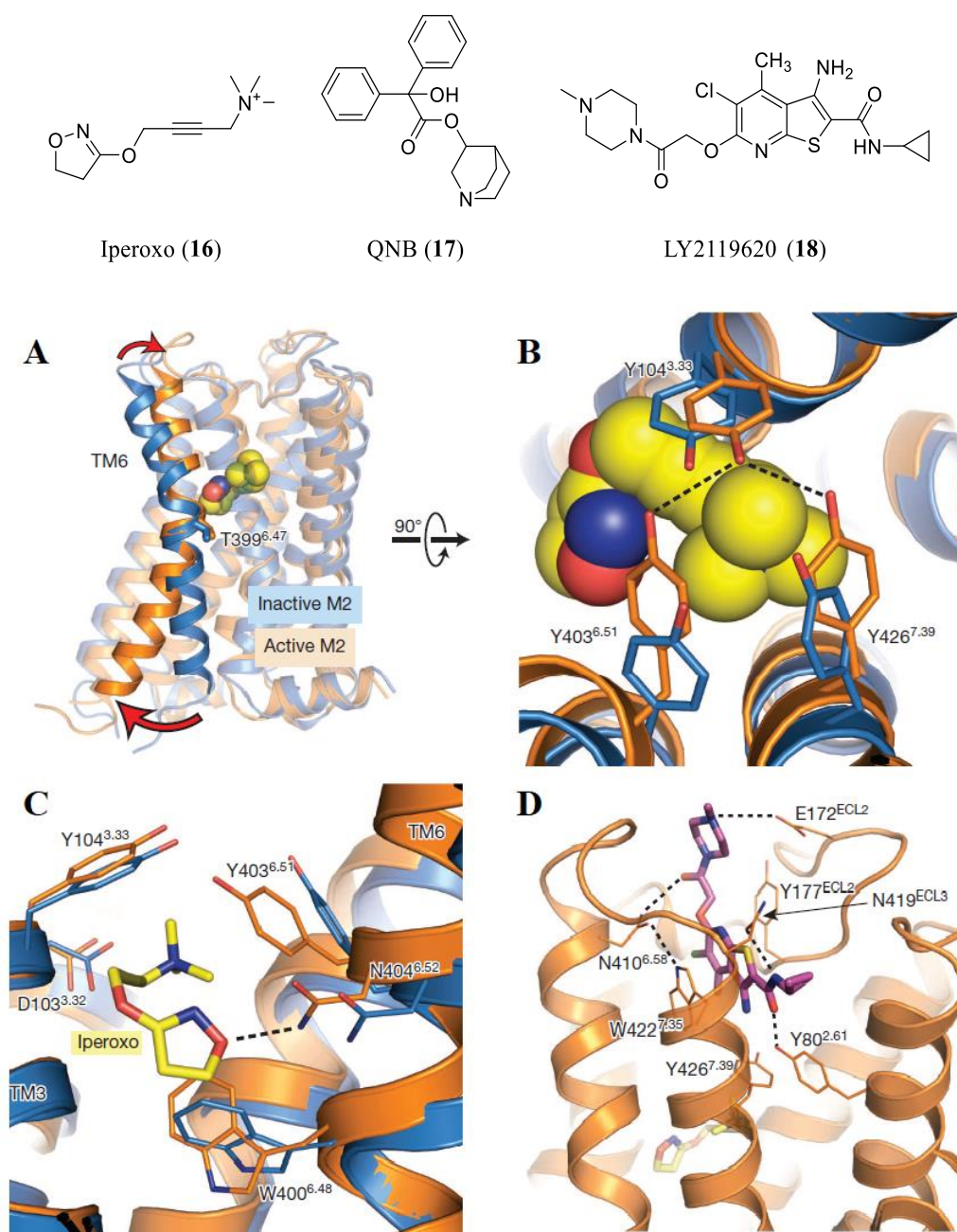


**Figure 7.** (A) Active M<sub>2</sub> mAChR (orange) bound to iperoxo (16), overlaid with the inactive 3-quinuclidinyl benzilate (QNB, 17)-bound M<sub>2</sub> mAChR crystal structure (blue) showing the location of iperoxo (16) binding and the significant displacement of TM6 upon receptor activation. (B) Closer view of the conserved tyrosine 'lid' binding to iperoxo (16). (C) View of the hydrogen bonding interaction between the dihydroisoxazole ring oxygen of iperoxo (16) and N404<sup>6.52</sup>. (D) LY2119620 (18) bound to the allosteric site of the M<sub>2</sub> mAChR. Graphic was adapted from Kruse *et al.*<sup>29</sup>

The crystal structure of the agonist, iperoxo (16), and M<sub>2</sub>/M<sub>4</sub> mAChR PAM, LY2119620 (18), co-bound to the M<sub>2</sub> mAChR provides invaluable insight into the allosteric site and

allosteric ligand binding. The ‘typical’ allosteric binding site to which LY2119620 (**18**) binds is located between ECL2 and TM6 and TM7. In the M<sub>2</sub> mAChR the key allosteric residues are Tyr177<sup>ECL2</sup> and Trp422<sup>7,35</sup> which interact directly with the aromatic core of LY2119620 (**18**). Additionally several other residues make hydrogen bonding interactions with LY2119620 (**18**) including Tyr80<sup>2,61</sup>, Asn410<sup>6,58</sup>, Asn419<sup>ECL3</sup>, or ionic interactions including Glu172<sup>ECL2</sup> (Figure 7 D).<sup>29</sup> In combination with the application of computational modelling, the x-ray data reported for the M<sub>1</sub>-M<sub>4</sub> mAChRs provides the tools necessary to derive structure-based rationalisations for complex pharmacological data and facilitates the potential for structure-based ligand design.

### 2.3 The M<sub>1</sub> mAChR and Alzheimer’s disease

Alzheimer’s disease (AD) is a neurodegenerative disease which has no definitively known cause. Symptomatically it presents with cognitive decline in memory and learning, resulting from the accumulation of  $\beta$ -amyloid plaques and neurofibrillary tangles (caused by hyperphosphorylation of tau-proteins) in the brain as the disease progresses.<sup>66-67</sup> For many decades now numerous lines of evidence have pointed towards the cholinergic hypothesis of memory dysfunction as a potential cause for cognitive decline in AD patients.<sup>68-70</sup> In post-mortem examination, AD patients have been found to have significantly reduced numbers of cholinergic neurons in the basal forebrain<sup>71</sup> as well as abnormal levels of cholinergic markers, including ACh (**1**),<sup>69</sup> its precursor choline and acetyl transferase which is essential in ACh (**1**) biosynthesis. Administration of non-selective muscarinic antagonists can exacerbate cognitive deficits in animal models<sup>72</sup> and conversely cholinergic stimulation in Alzheimer’s patients has been shown to promote cognition.<sup>68</sup>



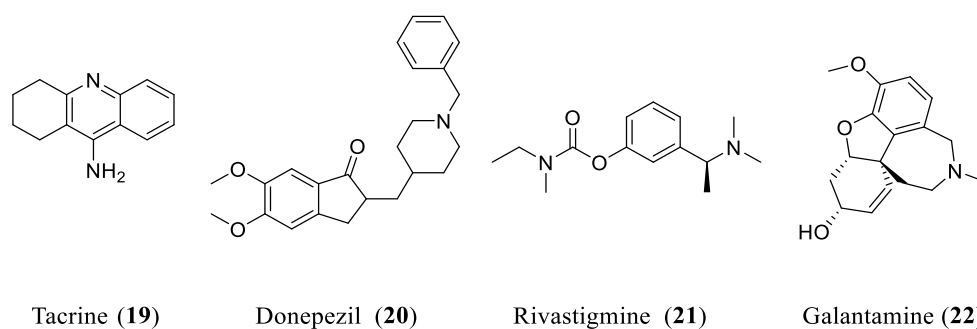


**Figure 8.** Acetylcholine esterase inhibitors, tacrine (19), donepezil (20), rivastigmine (21) and galantamine (22), which are either currently or have previously been used to treat cognitive decline in patients with Alzheimer's disease. Inhibition of acetylcholine esterase increases intra-synaptic acetylcholine, thus promoting cholinergic neurotransmission.

There are several drugs that have been or are used clinically which attempt to address this dysfunction of the cholinergic system in the CNS by inhibiting acetylcholine esterase, an enzyme responsible for ACh (1) degradation in the inter-synaptic space; tacrine, donepezil, rivastigmine and galantamine (Figure 8). However due to their non-selective mode of action, all four drugs possess significant cholinergic side effects, including gastrointestinal distress, bradycardia and hyper-salivation. Meta-analyses and randomised controlled trials measuring outcomes of patients who are prescribed acetylcholine esterase inhibitors shows only a modest benefit in slowing cognitive decline.<sup>73</sup> A more recent meta-analysis has suggested there may be no benefit for Alzheimer's patients with mild cognitive impairment or mild dementia.<sup>74</sup> One of the key 'hallmarks' of AD, the aggregation of  $\beta$ -amyloid plaques in the brain, arises due to post-translational cleavage of the precursor protein (amyloid precursor protein, APP) by a pair of secretases referred to as  $\beta$ - and  $\gamma$ - secretase. A third enzyme,  $\alpha$ -secretase, cleaves APP within the  $\beta$ -amyloid domain and thus precludes its formation (Figure 9).<sup>75</sup>

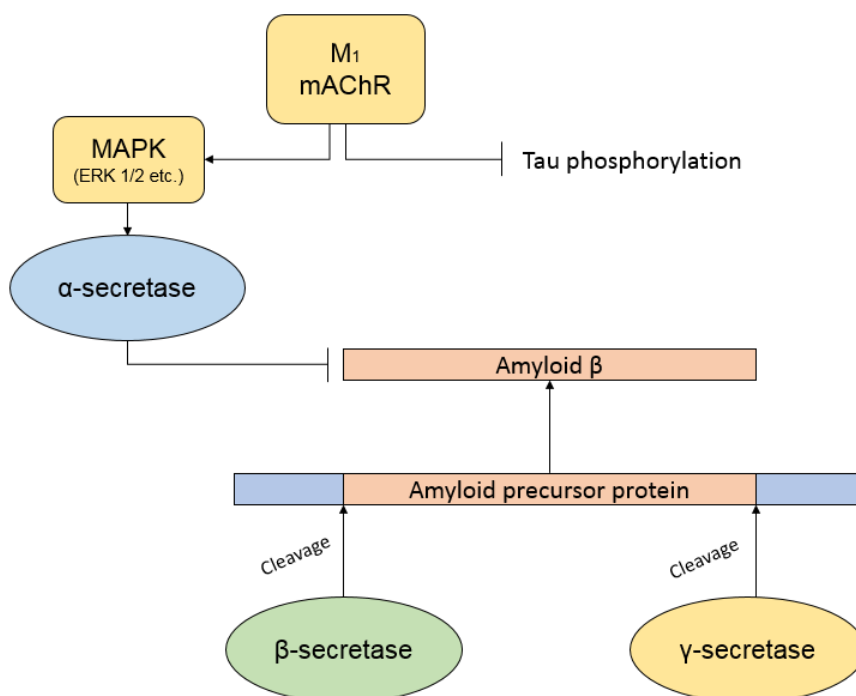


**Figure 9.** Schematic diagram showing the relationship between the M<sub>1</sub> mAChR, the  $\alpha$ -,  $\beta$ - and  $\gamma$ - secretases and their roles in processing of amyloid precursor protein to form either neurotoxic  $\beta$ -amyloid protein or benign protein products.

Activation of the M<sub>1</sub> mAChR has been found to increase levels of  $\alpha$ -secretase in the brain and ameliorate symptoms in Alzheimer's disease animal models.<sup>76</sup> Deletion of the M<sub>1</sub> mAChR has also been shown to increase amyloidogenic processes in mouse models exhibiting  $\beta$ -amyloid plaque pathology.<sup>77</sup> M<sub>1</sub> mAChR knockout mice also display increased amphetamine-induced hyperlocomotion and dopaminergic neurotransmission, suggesting the potential for the M<sub>1</sub> mAChR to treat symptoms of psychosis.<sup>78</sup>

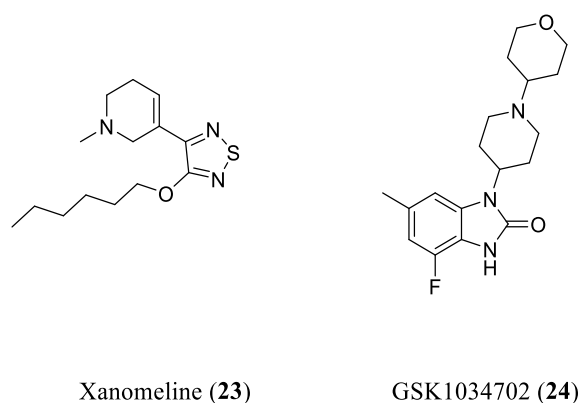


**Figure 10.** Chemical structures of  $M_1/M_4$  mAChR-preferring partial agonist, xanomeline (**23**) and  $M_1$  mAChR selective partial agonist, GSK1034702 (**24**). Both ligands have shown significant benefits to cognition in human clinical trials.

The most recent drug targeting the  $M_1$  mAChR for the treatment of cognitive dysfunction to progress to phase III clinical trials was xanomeline (**23**), a  $M_1/M_4$  mAChR preferring partial agonist (Figure 10). Xanomeline (**23**) showed significant dose-dependent reduction in hallucinations, delusions, vocal outbursts and other behavioural disturbances in Alzheimer's patients.<sup>79-80</sup> However, significant dose limiting off-target cholinergic side effects were observed (most notably gastrointestinal) which prevented the clinical advancement of xanomeline (**23**).<sup>81</sup> More recently a clinical trial of the  $M_1$  mAChR selective allosteric agonist GSK1034702 (**24**) (Figure 10) showed positive results in improving memory (specifically, immediate recall) in abstaining male smokers.<sup>82</sup> The trials of  $M_1$  mAChR targeting drugs, xanomeline (**23**) and GSK1034702 (**24**), clinically validate the  $M_1$  mAChR as a promising target for the treatment of cognitive dysfunction in Alzheimer's patients.

## 2.4 The $M_4$ mAChR and schizophrenia

Schizophrenia is a psychiatric disease that is characterised by several symptom clusters, referred to as the positive symptoms, negative symptoms, and cognitive dysfunction. Positive symptoms refers to delusions, disordered thoughts and speech, and sensory hallucinations; negative symptoms refers to deficits in emotional response including anhedonia, social

withdrawal and lack of motivation; and cognitive dysfunction in schizophrenia refers to deficits in attention, memory and learning. Schizophrenia typically presents in young adulthood however the presentation of the different symptom clusters varies significantly among patients.<sup>83</sup> The cause of schizophrenia is unknown and it has been proposed that schizophrenia arises from one or more of several genetic and/ or environmental factors, which give rise to the complex neurobiology of the disease.<sup>83-85</sup> The long-standing dopaminergic hypothesis of schizophrenia proposes that the different clusters of symptoms arise from dysfunctions in dopaminergic signalling in multiple regions of the brain, specifically positive symptoms from hyperdopaminergic activity in the mesolimbic reward pathway, and negative symptoms from hypodopaminergic activity in the medial prefrontal cortical and mesocortical pathways.<sup>86</sup> First generation antipsychotics such as chlorpromazine (a non-selective dopamine receptor antagonist) are effective for decreasing the frequency of psychotic episodes and improving positive symptoms, but showed little efficacy in treating negative symptoms or cognitive dysfunction.<sup>87</sup> Chronic usage of first generation antipsychotics is also associated with extrapyramidal side effects, limiting the long term usefulness of these drugs. Second generation antipsychotics such as clozapine, and haloperidol also possessed 5-HT<sub>2A</sub>R antagonism additionally to dopamine receptor antagonism, which resulted in reduced extrapyramidal side effects.<sup>88</sup> However these drugs also mostly fail to effectively address the negative symptoms and cognitive deficits present in schizophrenics.<sup>85</sup> More recent research has pointed towards the involvement of numerous other monoamine receptors (including, *N*-methyl-D-aspartate (NMDA) receptors, glutamate receptors and  $\gamma$ -aminobutyric acid (GABA) receptors, cannabinoid receptors, nicotinic acetylcholine receptors (nAChRs) and mAChRs) as playing integral roles in the pathogenesis and symptomology of schizophrenia.<sup>83-84, 89</sup> Designing selective agonists targeting the M<sub>4</sub> mAChR is one promising strategy that is currently being actively explored as a way of controlling dopaminergic activity as well as treating cognitive

dysfunction.<sup>90</sup> Non-selective mAChR antagonists, such as scopolamine, can induce psychosis in humans.<sup>91</sup> Conversely, mAChR stimulation has been shown to have pro-cognitive and antipsychotic properties in animal models, as well as in humans.<sup>92-93</sup> D<sub>1</sub> dopamine receptors and M<sub>4</sub> mAChRs are co-expressed in the striatum, suggesting that M<sub>4</sub> mAChR signalling could modulate dopaminergic signalling in the mesolimbic reward pathway directly.<sup>94-95</sup> In mouse models, activation M<sub>2</sub> and M<sub>4</sub> mAChRs has been shown to mediate dopaminergic and glutaminergic signalling in the nucleus accumbens (which forms part of the mesolimbic system).<sup>96</sup> Radioligand binding studies with M<sub>1</sub>/ M<sub>4</sub> mAChR selective antagonist [<sup>3</sup>H]pirenzepine on post-mortem brain samples from diagnosed schizophrenics have demonstrated reduced numbers of M<sub>1</sub> and M<sub>4</sub> mAChRs (eliminating antipsychotic usage as the cause) suggesting that mAChR signalling is impaired in these patients.<sup>97-98</sup> Numerous studies investigating administration of M<sub>4</sub> mAChR targeting agonists have demonstrated antipsychotic properties in mouse models.<sup>99-101</sup> The antipsychotic properties M<sub>1</sub>/M<sub>4</sub> selective agonist xanomeline (**23**) are abolished in M<sub>4</sub> mAChR knockout mice.<sup>102-104</sup> Additionally, M<sub>4</sub> mAChR knockout mice also display several animal model hallmarks of psychosis, including abnormal social behaviour and decreased prepulse inhibition.<sup>105</sup> The observed reduction in behavioural disturbances in clinical trials of xanomeline (**23**) in Alzheimer's patients lead to a trial being conducted evaluating its antipsychotic and pro-cognitive effects in patients with schizophrenia. The trial showed a robust dose-dependent improvement in all three symptom clusters, positive, negative and cognitive, but was again not progressed further due to intolerable gastrointestinal and other peripheral cholinergic side-effects.<sup>93</sup> Recently, Karuna Pharmaceuticals and PureTech Health have reported promising results in phase I tolerability studies for their combination therapy of xanomeline (**23**) and trospium chloride (a peripherally restricted mAChR non-selective antagonist, structure not shown), 'KarTX' (<http://karunatx.com/>). Currently Karuna Pharmaceuticals are recruiting for a phase II randomized, double-blind study

assessing the safety, tolerability, and efficacy of KarXT in hospitalized adults with diagnosed schizophrenia.<sup>106</sup> Although KarTX may circumvent the issue of mAChR subtype discrimination by blocking peripheral M<sub>2</sub> and M<sub>3</sub> mAChRs the designing of more selective ligands would eliminate the need for such combination therapies, avoiding possible side-effects of KarTX which could arise through drug-drug interactions or directly from antagonism of peripheral mAChRs.

### **3. Novel design strategies to overcome issues of subtype selectivity in mAChR ligands**

#### **3.1 Allosteric agonists/ PAMs targeting the M<sub>1</sub> mAChR**

In light of the mounting evidence for the pro-cognitive and antipsychotic action of the M<sub>1</sub> and M<sub>4</sub> mAChRs, respectively, research efforts have been directed towards the development of more selective ligands which target either or both receptors.<sup>38, 90, 107-109</sup> One approach that has been explored is that of allosteric agonist/ PAMs, which typically have greater mAChR subtype selectivity than their orthosteric agonist counterparts. The first generation allosteric agonist AC-42 was found to selectively activate the M<sub>1</sub> mAChR *in vitro* but lacked the necessary absorption, distribution, metabolism and excretion (ADME) properties for *in vivo* evaluation.<sup>110</sup>

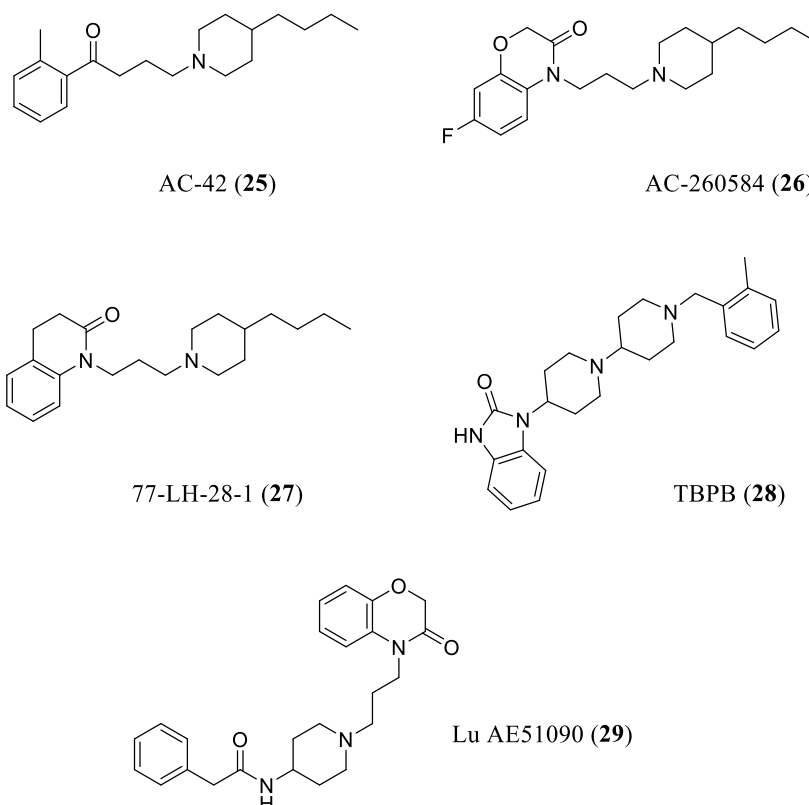


**Figure 11.** Chemical structures of early M<sub>1</sub> mAChR selective allosteric agonists, AC-42 (**25**), AC-260584 (**26**), 77-LH-28-1 (**27**), TBPB (**28**) and Lu AE51090 (**29**).

Subsequent optimisation studies lead to more metabolically stable analogues AC-260584 (**26**) and 77-LH-28-1 (**27**) which along with other early M<sub>1</sub> mAChR allosteric agonists such as TBPB (**28**) and Lu AE51090 (**29**) have all shown promising procognitive and/ or antipsychotic activity *in vivo*.<sup>111-114</sup> TBPB (**28**) has been shown to directly lower levels of  $\beta$ -amyloid production *in vitro*, further suggesting the M<sub>1</sub> mAChR as an effective target for managing the pathology of Alzheimer's disease.<sup>113</sup> BQCA (**30**) is a M<sub>1</sub> mAChR selective PAM that has generated significant interest due to its high M<sub>1</sub> mAChR subtype selectivity, high positive cooperativity with the endogenous agonist ACh (**1**) and promising results in preclinical studies.<sup>115-116</sup> Subsequent generations of analogues of BQCA (**30**) based on the quinolone scaffold (summarised in Figure 12) include compounds with improved ADME properties, and/

or compounds showing improved pharmacological results compared to BQCA (**30**) *in vitro* and in several cases in animal models.<sup>117-135</sup>

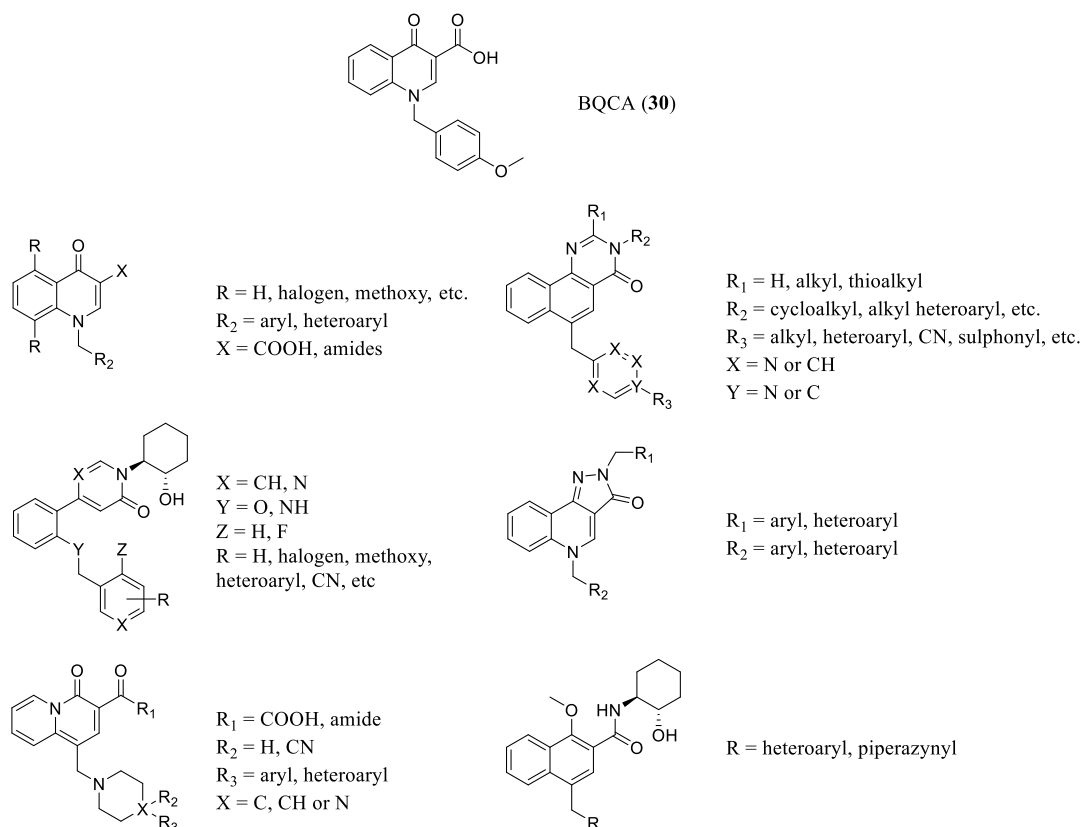


**Figure 12.** General overview of the chemical space explored surrounding the benzoquinolone scaffold of M<sub>1</sub> mAChR selective PAM, BQCA (**30**). Significant modification to the core scaffold as well as peripheral substituents has resulted in many ligands of this class which retain the property of M<sub>1</sub> mAChR selective potentiation of ACh (**1**) and/ or agonism, and which display an improved pharmacokinetic profile, and/ or improved potency, over BQCA (**30**).

HTS ‘hit’ from the NIH’s Molecular Libraries Probe Production Centers Network (MLPCN) library offered a new indole scaffold, the low potency M<sub>1</sub> mAChR selective PAM VU0108370 (**31**) (Figure 13).<sup>136</sup> Potency and selectivity were improved upon substitution of the benzylic pendant and 4,6-difluoro substitution of the indole ring, as in VU0456940 (**32**) (Figure 13).<sup>137</sup>



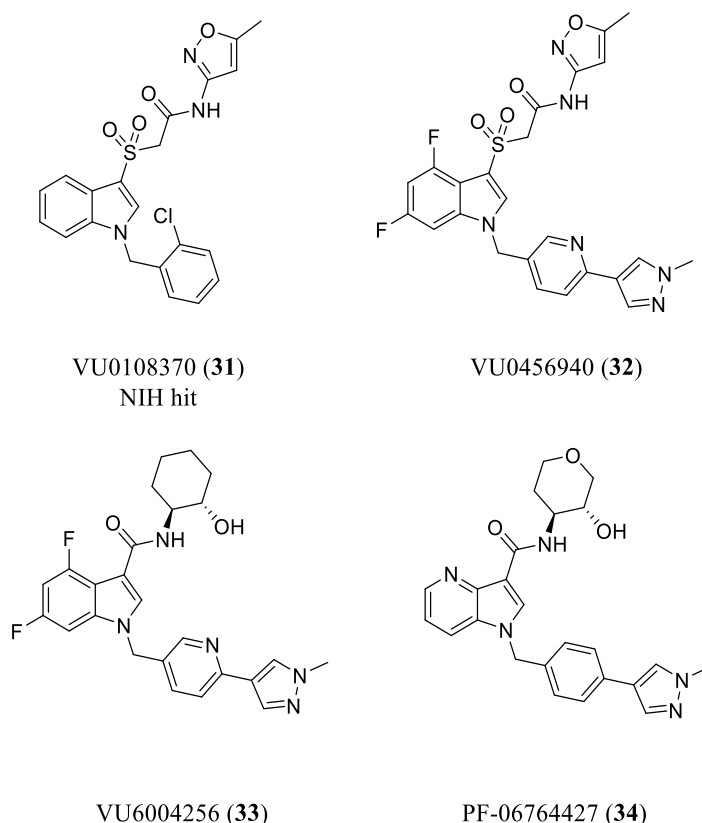


**Figure 13.** Chemical structures of indole (or azaindole)-based M<sub>1</sub> mAChR selective PAMs, based on the NIH hit, VU0108370 (**31**). Optimisation of the benzylic pendant resulted in VU0456940 (**32**). Substitution of the, indole ring and sulphonyl group with successful functional groups from previous SAR studies on the quinolone scaffold resulted in potent, selective and *in vivo* efficacious M<sub>1</sub> mAChR PAMs VU6004256 (**33**) and PF-06764427 (**34**), respectively.

Replacement of the sulphonyl group with *N*-((1*S*,2*S*)-2-hydroxycyclohexyl)amide moiety, as in VU6004256 (**33**) resulted in further improvements in potency and safety profile in mice, lacking severe adverse peripheral cholinergic side-effects.<sup>138</sup> Azaindole based analogue, PF-06764427 (**34**) displays high cooperativity and M<sub>1</sub> mAChR selectivity but lacked in its safety profile compared with VU6004256 (**33**).<sup>139</sup> The diversity of structures of subtype selective mAChR PAMs was further expanded upon by the high-throughput screening efforts at Vanderbilt Center for Neuroscience Drug Discovery, yielding compounds such as VU0119498 (**35**), VU0027414 (**36**), VU0090157 (**37**) and VU0029767 (**38**) (Figure 14). These

PAMs varied in mAChR subtype selectivity, and potentially mechanism of binding to the allosteric site.<sup>140</sup>

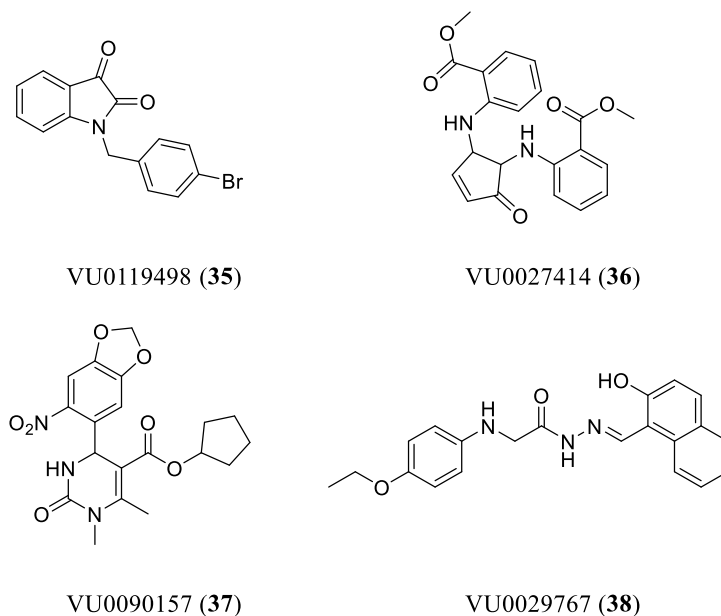


**Figure 14.** Diverse chemical structures of M<sub>1</sub> mAChR targeting 'hit' molecules discovered by the high-throughput screening efforts at Vanderbilt Center for Neuroscience Drug Discovery.

Compound VU0119498 (**35**) exhibited selectivity for the M<sub>1</sub>, M<sub>3</sub> and M<sub>5</sub> mAChRs and was further optimised to give both M<sub>1</sub> and M<sub>5</sub> mAChR selective PAMs (although only the M<sub>1</sub> mAChR selective will be discussed here), representing a third scaffold of indolone-based M<sub>1</sub> mAChR PAMs (Figure 14).<sup>141-142</sup> Similar to the indole scaffold substitution of benzylic pendant of VU0119498 (**35**) with a methyl pyrazole ring improved potency significantly, giving ML137 (**39**) and VU0448350 (**40**) (Figure 15).<sup>143</sup> Switching the indolone core to an isoindolone core, as in compounds VU0453595 (**41**) and compound **42** (Figure 15), gives a marked improvement in ADME properties, compound **42** showing good oral bioavailability in both rodent and canine animal models.<sup>138, 144-145</sup> More recently research has focused on minimising allosteric agonism in M<sub>1</sub> mAChR PAMs, which has been proposed to cause off-target peripheral mAChR activation (potentially at the M<sub>1</sub> mAChR itself), leading to cholinergic side effects.<sup>138, 145-147</sup>

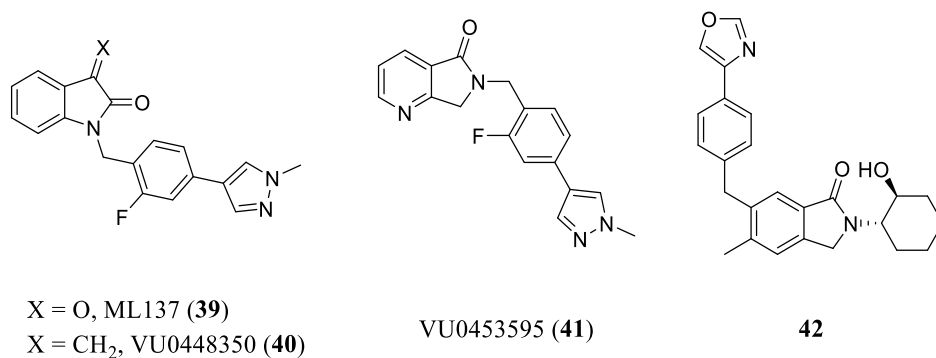


**Figure 15.** Chemical structures of indolone-based  $M_1$  mAChR selective PAMs, based on the Vanderbilt Center for Neuroscience Drug Discovery HTS hit, VU0119498 (**35**), ML137 (**39**) and VU0448350 (**40**). Isomerisation of the indolone core scaffold to isoindolone improves ADME properties in VU0453595 (**41**) and compound **42**.

From a structural perspective, it is clear that many modifications are generally advantageous to potency and/ or cooperativity across the quinolone, indoline and indolone scaffolds while maintaining similar  $M_1$  mAChR selectivity. These structural and functional similarities imply a common pharmacophore and mechanism of action for this class of  $M_1$  mAChR PAMs, which provides a basis for rational design.

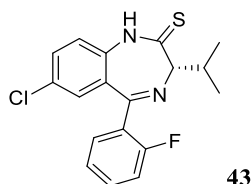


**Figure 16.** Chemical structure of  $M_1$  mAChR selective partial agonist developed by Roche, compound **43**.

Finally worthy of mention is the benzodiazepine scaffold invented at Roche, compound **43** which shows good potency in  $M_1$  mAChR expressing human cell lines (Figure 16).<sup>146</sup> However it is not clear whether this molecule fits into the same pharmacophoric or mechanistic class as the quinolone, indole and indolone-based  $M_1$  mAChR PAMs. Development of the  $M_1$  mAChR PAM scaffolds mentioned herein are currently ongoing.

### 3.2 Allosteric agonists/ PAMs targeting the M<sub>4</sub> mAChR

Preclinical studies and clinical studies pointing towards the M<sub>4</sub> mAChR as having antipsychotic properties have led to the investigation and development of M<sub>4</sub> mAChR selective ligands which are allosteric agonists and/ or PAMS. Thiochrome (**44**) was the first discovered allosteric ligand which was a M<sub>4</sub> mAChR PAM and a NAL of ACh (**1**) at the M<sub>1</sub>-M<sub>3</sub>, M<sub>5</sub> mAChR subtypes, but exhibited low affinity and poor drug-like qualities.<sup>148</sup> An important breakthrough came with the discovery of the 5-aminothieno[2,3-*c*]pyridine scaffold of M<sub>4</sub> mAChR PAM LY2033298 (**45**). LY2033298 (**45**) exhibited no allosteric agonism, instead acting as pure potentiator of ACh (**1**) at the M<sub>2</sub>/M<sub>4</sub> mAChRs.<sup>101</sup> In rodent studies, the M<sub>2</sub>/ M<sub>4</sub> mAChR selective PAM LY2033298 (**45**) was found to potentiate the antipsychotic properties of subtype non-selective mAChR agonist oxotremorine, and modulate dopamine release in the prefrontal cortex.<sup>101</sup> Structurally related analogue, LY2119620 (**46**) has similar M<sub>2</sub>/ M<sub>4</sub> mAChR selectivity and has been shown to bind to the typical allosteric site of the M<sub>2</sub> mAChR by X-ray crystallography, and to not bind to the M<sub>1</sub>, M<sub>3</sub>, M<sub>5</sub> mAChR subtypes by Schober *et al.* employing a radiolabelled derivative,<sup>29, 149</sup> as opposed to thiochrome (**45**) which gains selectivity via differences in cooperativity at the M<sub>1</sub>-M<sub>5</sub> mAChR subtypes.<sup>148</sup>

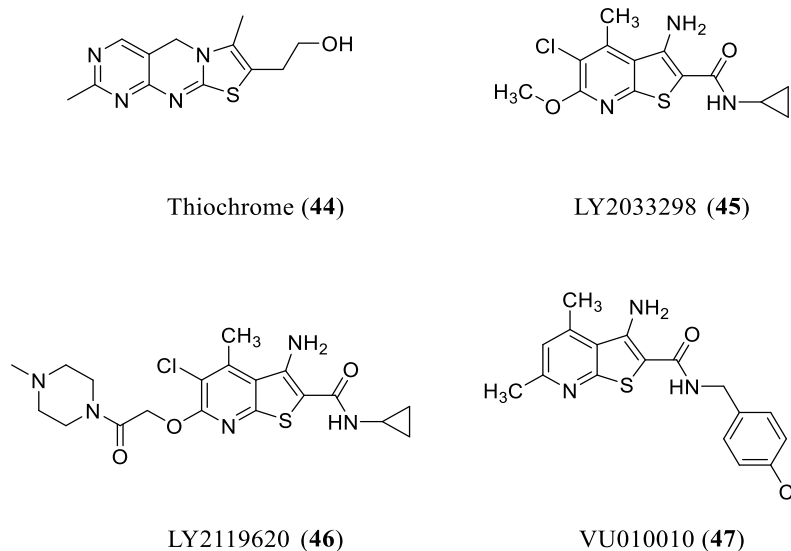


**Figure 17.** Chemical structures of early M<sub>4</sub> mAChR PAMs; thiochrome (**44**), LY2033298 (**45**), LY2119620 (**46**) and VU010010 (**47**).

Subsequent optimisation of the of LY2033298 (**45**), substituting the pyridine ring and amide group lead to VU010010 (**47**), which showed high potency and good cooperativity with ACh (**1**) in cells expressing rat M<sub>4</sub> mAChRs.<sup>99</sup> VU010010 (**47**) was found to increase carbachol (**4**) induced depression of transmission at excitatory (but not inhibitory) synapses in the hippocampus in *ex vivo* studies, suggesting the importance of the M<sub>4</sub> mAChR in memory and learning.<sup>99</sup> However when administered alone, VU010010 (**47**) lacked *in vivo* activity, likely due to its poor pharmacokinetic profile. Many amide substituted derivatives of VU010010 (**47**) have been reported including VU0152099 (**48**) and VU0152100 (ML108) (**49**), which maintain potency and which show improved CNS penetration in rats.<sup>150</sup> However, poor metabolic stability due to hydroxylation of the 6-methyl group of the pyridine ring limited VU0152099 (**48**) and VU0152100 (ML108) (**49**) from being pursued further. Replacement of the labile 6-methyl with ethers, and subsequent SAR studies, resulted in ML173 (**50**), which showed greatly improved microsomal stability.<sup>151</sup> However ML173 (**50**) also displayed 25-fold preference for the human over the rat M<sub>4</sub> mAChR, an issue which arises due to the lack of evolutionary pressure to conserve the allosteric sites of GPCRs.

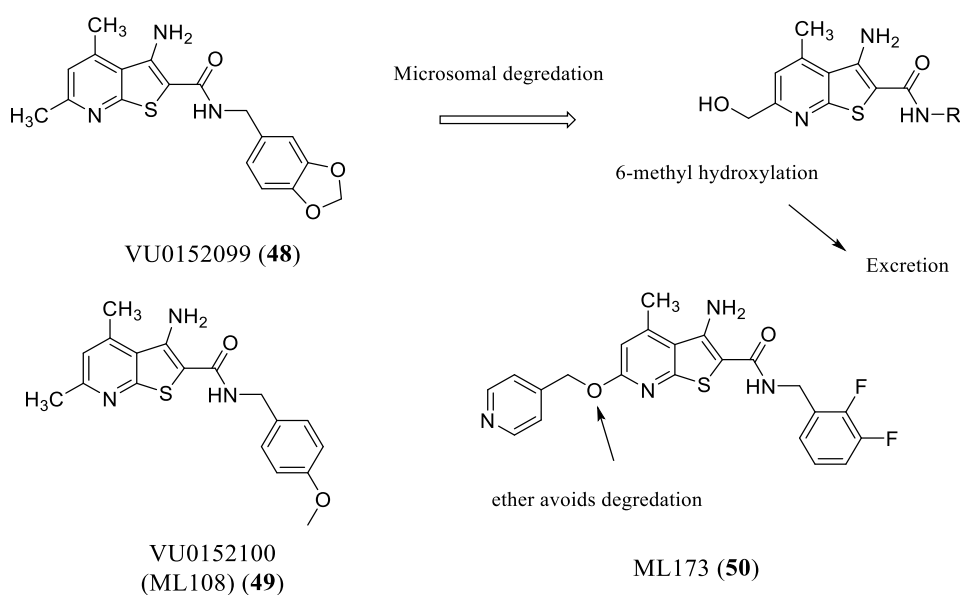


**Figure 18.** Chemical structures of M<sub>4</sub> mAChR selective PAMs VU0152099 (**48**) and VU0152100 (**49**) which are degraded *in vivo* by 6-methyl hydroxylation, and ML173 (**50**) which overcomes this issue by employing a substituted ether at the 6- position.

This species bias presents a significant challenge for optimisation because it somewhat invalidates preclinical rodent study data, making it very difficult to evaluate candidate molecules for safety and efficacy *in vivo*. Subsequent generations of M<sub>4</sub> mAChR PAMs, expanded further on the 5-aminothieno[2,3-*c*]pyridine scaffold and focused on the two main issues, the species bias between rat and human M<sub>4</sub> mAChRs and the ADME profile of the compounds, emphasising CNS penetration and metabolic stability. Two new scaffolds have since been emerged, including a benzothiazole-based ligand, ML293 (**51**), from Vanderbilt Center for Neuroscience Drug and the discovery and the 5-amino-thieno[2,3-*c*]pyridazine-based ligand from Wood *et al.* (**52**) (Figure 19).<sup>152-153</sup>

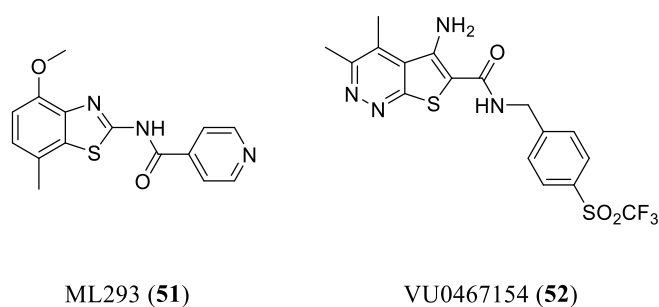


**Figure 19.** Two novel scaffolds of M<sub>4</sub> mAChR selective PAMs, ML293 (**51**) and VU0467154 (**52**), both of which demonstrate an improved pharmacokinetic profiles over previous scaffolds.

The benzothiazole-based ligand, ML293 (**51**) has a low micromolar potency however shows good CNS penetration in rats when orally administered, making it an interesting potential candidate for further optimisation.<sup>152</sup> The pyridazine-based ligand described by Wood *et al.*, VU0467154 (**52**), also displayed favourable pharmacokinetic properties but lacked in potency at the human M<sub>4</sub> mAChR (although has applications as a tool in rat models).<sup>153-154</sup>

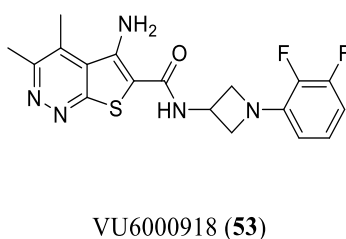


**Figure 20.** Chemical structure of VU6000918 (**53**) which showed demonstrated promising efficacy in preclinical rat models of psychosis.

More recently SAR surrounding azetidine-derived amides of these pyridazine ligands has culminated in the discovery of VU6000918 (**53**), which achieves high potency, good pharmacokinetic properties and has demonstrated a 74% reduction in amphetamine induced hyperlocomotion in rats with 3 mg/ kg.<sup>155</sup> As with the M<sub>1</sub> mAChR PAMs mentioned previously, the development of these M<sub>4</sub> mAChR PAMs is currently ongoing.

### 3.3 Hybrid and bitopic ligands targeting the mAChRs

One potentially interesting observation is that there are numerous structurally and functionally diverse examples of subtype selective mAChR ligands which display evidence for a bitopic binding mechanism.<sup>43-45</sup> The previously mentioned M<sub>1</sub> mAChR selective agonist AC-42 (**54**) (Figure 21) shows evidence in binding and functional assays that is inconsistent with either a purely allosteric or purely orthosteric binding mode.<sup>56</sup> The M<sub>1</sub> mAChR affinity and functional response of AC-42 (**54**) are rightward shifted by orthosteric antagonist atropine, indicative of a competitive interaction. However AC-42 (**54**) also slows [<sup>3</sup>H]*N*-methylscopolamine ([<sup>3</sup>H]NMS) dissociation in non-equilibrium kinetic binding experiments suggestive of an allosteric interaction. Confounding the issue, mutational studies point to the extracellular region between TM1 and TM3 as the binding site of AC-42 (**54**) and orthosteric mutations, Y381A and W101A, which significantly reduce the affinity of orthosteric agonists ACh (**1**) and pilocarpine (**3**), actually increase the affinity of AC-42 (**54**).

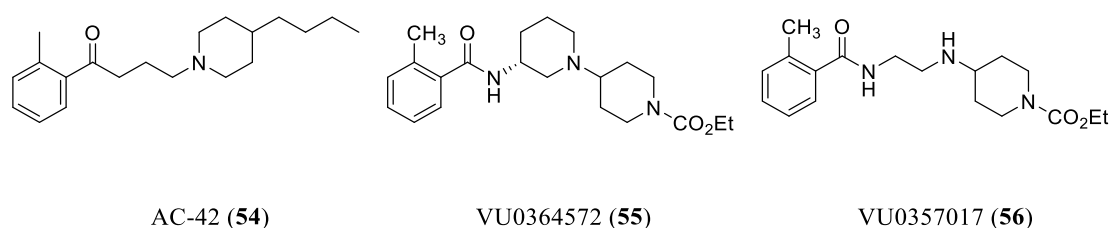


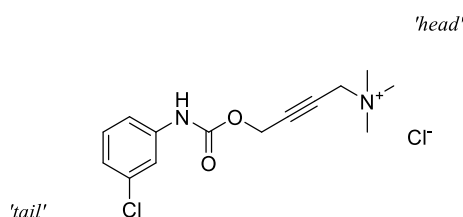
**Figure 21.** Chemical structures of M<sub>1</sub> mAChR selective bitopic agonists; AC-42 (**54**), VU0364572 (**55**) and VU0357017 (**56**).

Structurally related ligands 77-LH-28-1 (**27**), TBPB (**28**), Lu AE51090 (**29**), VU0364572 (**55**) and VU0357017 (**56**) all display similar M<sub>1</sub> mAChR selective partial agonism and have also all shown evidence for both orthosteric and allosteric binding, implying a general bitopic binding mechanism for this class of M<sub>1</sub> mAChR selective partial agonists.<sup>54, 112, 114, 156-158</sup> The (formally assumed orthosteric) M<sub>1</sub>/M<sub>4</sub> mAChR-preferring agonist McN-A-343 (**57**) was



shown to interact via a bitopic binding mechanism at the M<sub>2</sub> mAChR by Valant *et al.* in 2008.<sup>51</sup>

The group showed the quaternary ammonium orthosteric ‘head’ group activates the receptor while the allosteric ‘tail’ region of McN-A-343 (**57**) interacts with the allosteric site and exerts negative cooperativity with the head group.



McN-A-343 (**57**)

**Figure 22.** Chemical structure of M<sub>1</sub>/M<sub>4</sub> mAChR preferring partial agonist, McN-A-343 (**57**).

Upon mutation of one core allosteric epitope at the M<sub>2</sub> mAChR (Y177A<sup>ECL2</sup>) the allosteric tail of McN-A-343 (**57**) was no longer able to exert negative cooperativity with the head group, and hence the potency of the parent compound increased. Potentially, bitopic binding has also been seen in the subtype selective mAChR antagonist, ADFX-384 (**58**), which belongs to a set of structurally related antagonists (compounds **59-62**, Figure 23) which possess M<sub>1</sub>/M<sub>4</sub> mAChR or M<sub>2</sub>/M<sub>4</sub> mAChR subtype selectivity.<sup>159</sup>

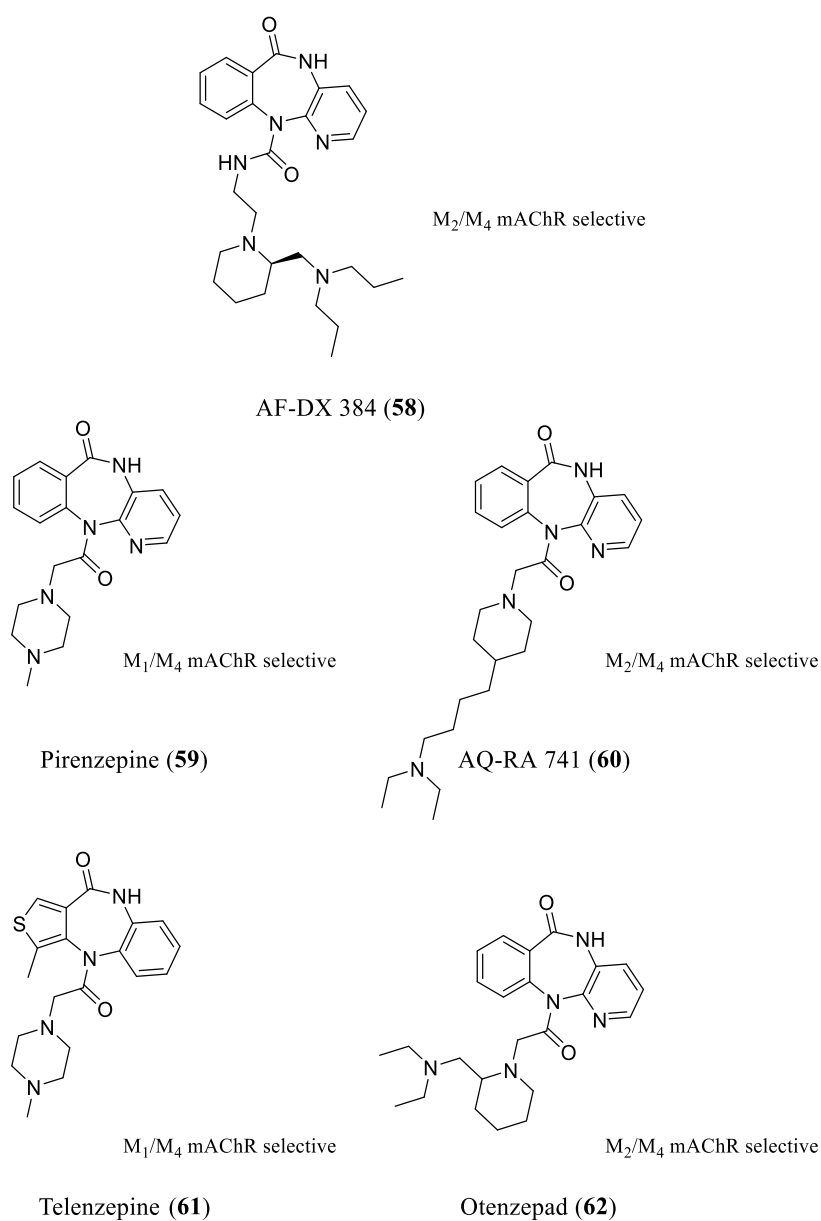


**Figure 23.** Chemical structure of the potentially bitopic mAChR selective antagonist AF-DX 384 (**58**), and structurally related selective mAChR antagonists, pirenzepine (**59**), AQ-RA 741 (**60**), telenzepine (**61**) and otenzepad (**62**).

There are several examples of serendipitously discovered mAChR bitopic ligands including *N*-desmethylozapine (**63**), Pirenzepine-(15)-BODIPY (**64**), THRX-160209 (**65**) and THRX-198321 (**66**), which with the exception of *N*-desmethylozapine (**63**) are antagonists (Figure 24).<sup>47-48, 160-161</sup>

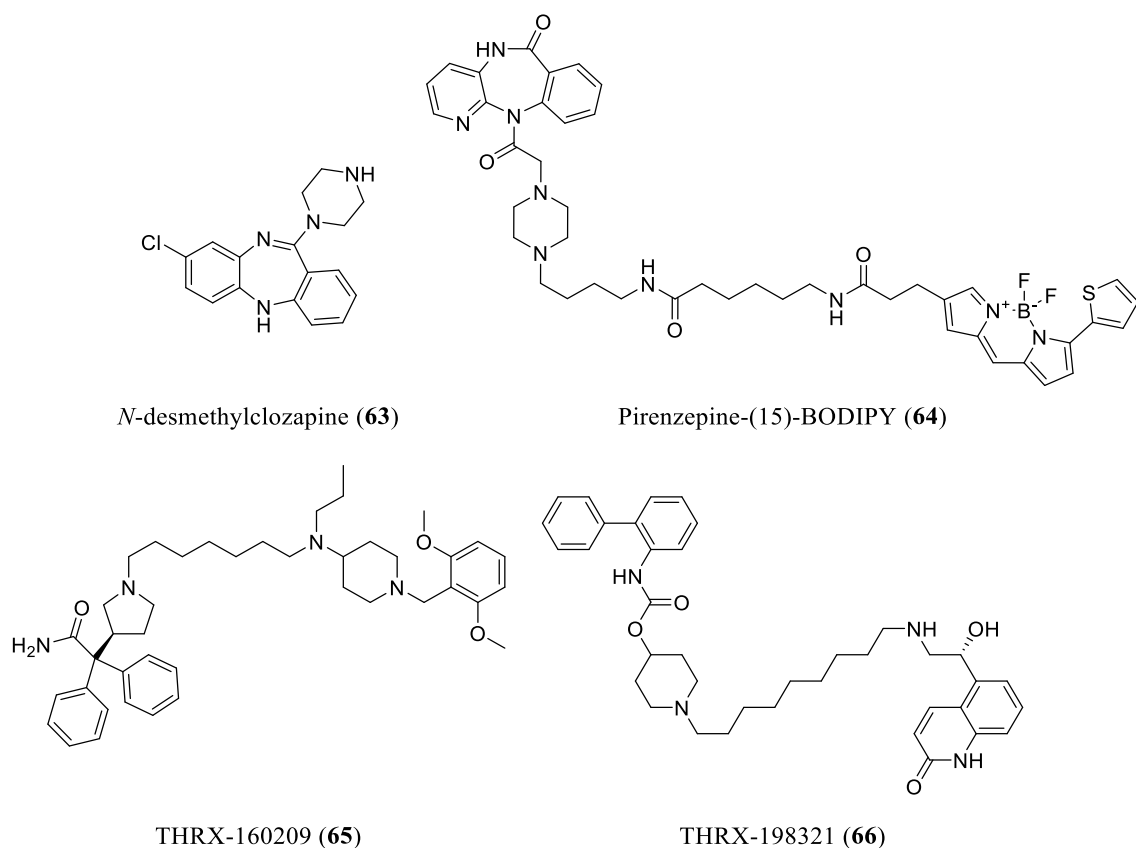


**Figure 24.** Chemical structures of serendipitously discovered mACHR bitopic ligands; *N*-desmethylozapine (**63**), pirenzepine-(15)-BODIPY (**64**), THRX-160209 (**65**) and THRX-198321 (**66**).

The apparent frequency with which bitopic ligands have been incidentally discovered tends to suggest the ubiquity of the phenomena, which implies that there may be many examples of currently unrealised bitopic ligands. The evidence presented for a bitopic mechanism for *N*-desmethylozapine (**63**), pirenzepine-(15)-BODIPY (**64**), THRX-160209 (**65**) and THRX-198321 (**66**) is briefly outlined below in Table 1.

---

**Table 1.** Bitopic ligands targeting mAChRs and evidence for their bitopic mechanism

Ligand	Target receptor	Evidence for bitopic interaction
<i>N</i> -desmethylozapine ( <b>63</b> )	M <sub>1</sub> mAChR	<ul style="list-style-type: none"><li>- Competes with both allosteric and orthosteric ligands</li><li>- Sensitive to allosteric and orthosteric mutations</li></ul>
Pirenzepine-(15)-BODIPY ( <b>64</b> )	M <sub>1</sub> mAChR	<ul style="list-style-type: none"><li>- Competes with orthosteric ligands</li><li>- Insensitive to allosteric modulation at specific linker lengths</li><li>- Sensitive to allosteric and orthosteric mutations</li><li>- Docking consistent with bitopic binding mode</li></ul>
THR-160209 ( <b>65</b> )	M <sub>2</sub> mAChR	<ul style="list-style-type: none"><li>- Affinity greater than constituent monomers</li><li>- M<sub>2</sub> mAChR selectivity</li><li>- [<sup>3</sup>H]THR-160209 displaced by orthosteric and allosteric ligands</li></ul>
THR-198321 ( <b>66</b> )	M <sub>2</sub> mAChR/ $\beta_2$ AR	<ul style="list-style-type: none"><li>- Affinity greater than monomers</li><li>- Competes with orthosteric ligands</li><li>- Changes dissociation of orthosteric radioligands (implies allosteric interaction)</li></ul>

---

Several designed examples of mAChR bitopic partial agonists have also been reported including iper-6-phth (**67a**), iper-6-naph (**67b**), isox-6-phth (**68a**) and isox-6-naph (**68b**), which consist of a potent agonist (iperoxo or isoxazole) and the M<sub>2</sub> mAChR selective NAM, W84 (**71**), or derivatives thereof (Figure 25). These hybrid ligands acquire selectivity for the M<sub>2</sub> mAChR by a mechanism of interacting orthosteric and allosteric ligand binding ensembles, which determine the efficacy of each ligand differentially at each of the M<sub>1</sub>-M<sub>5</sub> mAChR subtypes.<sup>49-50</sup>

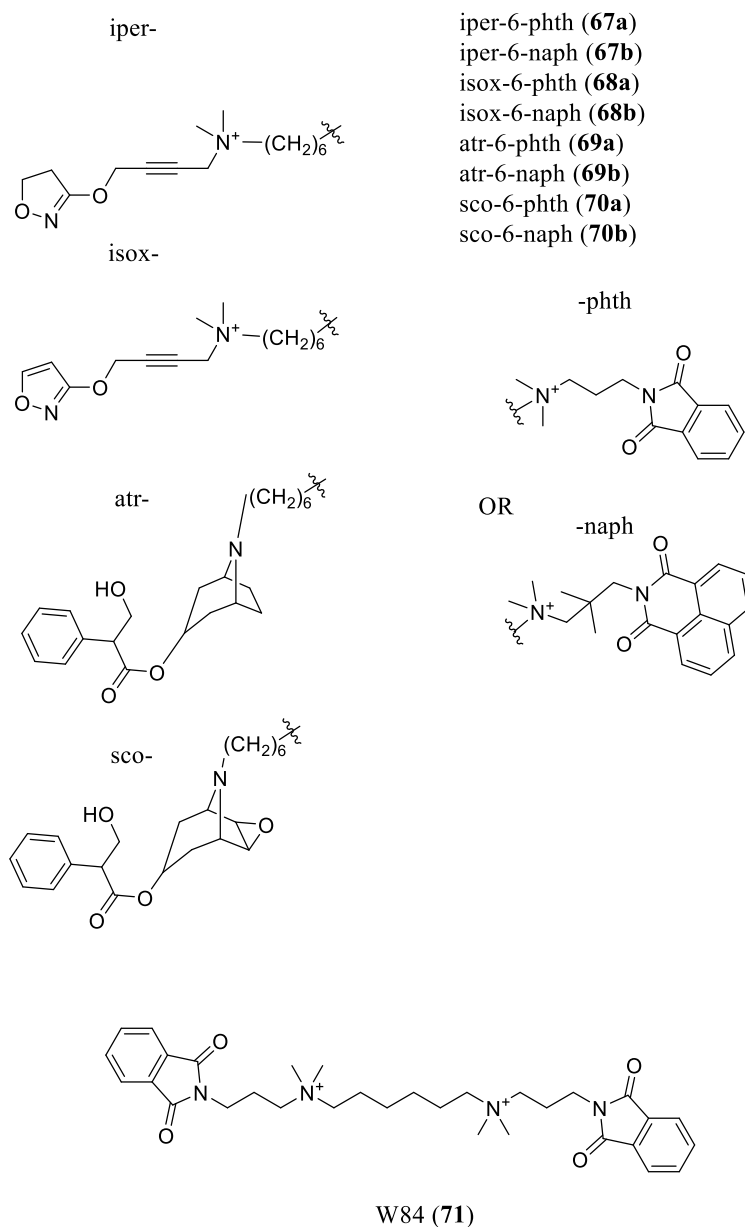
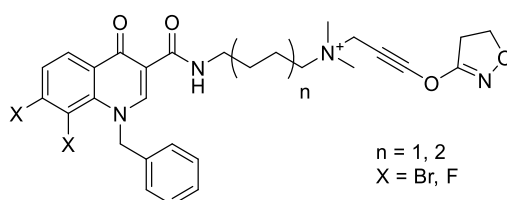


**Figure 25.** Generalised chemical structure of designed mAChR bitopic ligands consisting of agonists (iperoxo, iper-, isoxazole, isox-), antagonists (atropine, atr-, scopolamine, sco-), and the NAM, W84 (**71**) (-phth, **a**) or a naphthyl derivative (-naph, **b**).

Similarly, hybrid antagonists atr-6-phth (**69a**), atr-6-naph (**69b**), sco-6-phth (**70a**), sco-6-naph (**70b**), consisting of orthosteric antagonists atropine or scopolamine and allosteric derivatives of W84, and also display some moderate preference for the M<sub>2</sub> mAChR at the level of affinity.<sup>162</sup> Several hybrid bitopic ligands consisting of a derivative of the M<sub>1</sub> mAChR

selective agonist/ PAM BQCA and iperoxo have been reported, and exhibit linker length dependent partial agonism at the M<sub>1</sub> mAChR.<sup>163-164</sup>



BQCA-iperoxo

**Figure 26.** Generalised chemical structure of BQCA-iperoxo hybrid ligands.

However, these BQCA-iperoxo hybrids (Figure 26) have not been assessed for selectivity over the remaining M<sub>2</sub>-M<sub>5</sub> mAChR subtypes. Interestingly, some low-efficacy derivatives of BQCA-iperoxo have also been shown to be protean agonists, which induce agonism in inactive receptors and inverse agonism in active receptors.<sup>165</sup> Modifying the linker length of BQCA-iperoxo type ligands can be employed to rationally design these protean agonists.<sup>166</sup> A key feature that is common to many examples of hybrid ligands (designed and discovered) is subtype selectivity. The mechanisms of bitopic binding appear to be intrinsically linked to mechanisms of mAChR ligand selectivity. From this, it seems likely that the understanding of the molecular dynamics of bitopic ligands will reveal much about mechanisms of subtype selectivity for mAChRs, and potentially family A GPCRs generally. However, only further investigation will tell whether mAChR hybrid bitopic ligands will be able to overcome the significant challenges associated with the development of selective agonists for the mAChRs in the CNS. Regardless, these molecules are useful probes whose investigation will likely yield valuable insight into the molecular mechanisms by which mAChR ligands, both orthosteric and allosteric, gain subtype selectivity.

## 4. Fluorescently tagged bioactive molecules

Fluorescently tagging bioactive molecules has a huge number of potential applications in the biological sciences for understanding the localisation and molecular scale interactions of proteins and small-molecules. Generally, the fluorescent tagging of bioactive molecules is achieved by genetic manipulation of a protein of interest to form a fluorescent chimeric protein, or by chemical modification of a small-molecule ligand such that it fluoresces.<sup>167</sup> Two important applications in pharmaceutical science are the visualisation of fluorescent proteins to monitor localisation (for example GPCR internalisation and trafficking), and the use of fluorescently tagged ligands for the measurement of the binding kinetics or affinity of an unlabelled test ligand.<sup>168</sup> The latter being a versatile and safer alternative the use radiolabelled ligands, which are commonly used for the determination of the kinetic and binding properties of unlabelled test ligands, or of the radioligand itself. Techniques which employ several fluorescently tagged bioactive molecules, such as fluorescence resonant energy transfer (FRET) and bioluminescence resonance energy transfer (BRET) are particularly powerful, allowing for the simultaneous determination, in real-time, of protein localisation and trafficking within the cell as well as molecular scale protein-protein or protein-ligand interactions, when coupled with an appropriate visualisation technique (such as confocal microscopy).<sup>169</sup>

### 4.1 Design of fluorescently tagged small-molecule probes

Small molecule fluorescent probes typically consist of a ligand, covalently joined to a fluorophore by a molecule linker.<sup>170</sup> Examples exist where the fluorophore has been incorporated directly into the pharmacophore of a single ligand (such as the CB<sub>2</sub> cannabinoid receptor probe described by Petrov *et al.*),<sup>171</sup> however such a design strategy requires that the receptor binding pocket be somewhat flexible, and tolerate the incorporation of the fluorophore into the ligand scaffold, to avoid significant affinity losses.<sup>171</sup> For hybrid fluorescent ligands

conjoined by a linker there are several important considerations in designing a suitable probe, such as linker length, attachment point (to both the fluorophore and ligand), and the physiochemical properties (importantly lipophilicity) of the resultant probe.<sup>172</sup> Generally, there will be an optimal linker length, at which affinity of the probe is highest. However, the relationship between linker length and probe affinity is not necessarily a simple one, such as the  $\beta_2$  adrenoreceptor targeting probes reported by Martikkala *et al.*, for which both short and long linker length probes could displace orthosteric ligand propranolol, but the intermediate linker length probe could not.<sup>173</sup> Attachment of the linker to the ligand needs to be done at a point where the ligand scaffold is suitably structurally flexible to the additional steric bulk of the linker and fluorophore.<sup>168</sup> This decision needs to be informed by SAR information of the ligand as well as preferably some structural knowledge about the bound ligand-receptor complex to predict a suitable attachment point which will not interfere with the binding of the probe.<sup>174</sup> Attachment point of the linker to the fluorophore tag is less critical but also an important consideration as some chemical modifications may interfere with the fluorescent properties of the fluorophore.<sup>175</sup> However many commercially available fluorophores come with a reactive functional group installed for convenient synthetic attachment to a target bioactive molecule. Upon synthesis, the pharmacology of small-molecule fluorescent probes must be rigorously validated to ensure that, following addition of the fluorophore/ linker, they retain the desired binding and functional properties for the intended application.<sup>168</sup> Hybrid ligands such as fluorescently tagged GPCR ligands are typically large molecules, and as such consideration of their lipophilicity must be taken into account when designing them. When designing a probe, attempts should be made such that its lipophilicity does not exceed that of (for example) the Lipinski rules,<sup>176</sup> such that the probe retains reasonable water solubility for an aqueous assay environment and to limit non-specific uptake of the probe into cellular membranes which could interfere with the accuracy, precision and/ or resolution of



measurements made using the probe.<sup>172</sup> Due to the highly lipophilic nature of the commonly used polymethylene-based linkers, some researchers have employed polyethyleneglycol-like or polypeptide-based linkers to limit lipophilicity of in their probe designs.<sup>177-178</sup> Several fluorescent probes targeting the mAChRs have been reported including probes based on orthosteric antagonist, tolterodine (**72**), the M<sub>1</sub>/ M<sub>4</sub> mAChR selective orthosteric antagonist, telenzepine (**73**), and the M<sub>1</sub> mAChR selective bitopic/ allosteric agonist, AC-42 (**74**).<sup>179-181</sup>

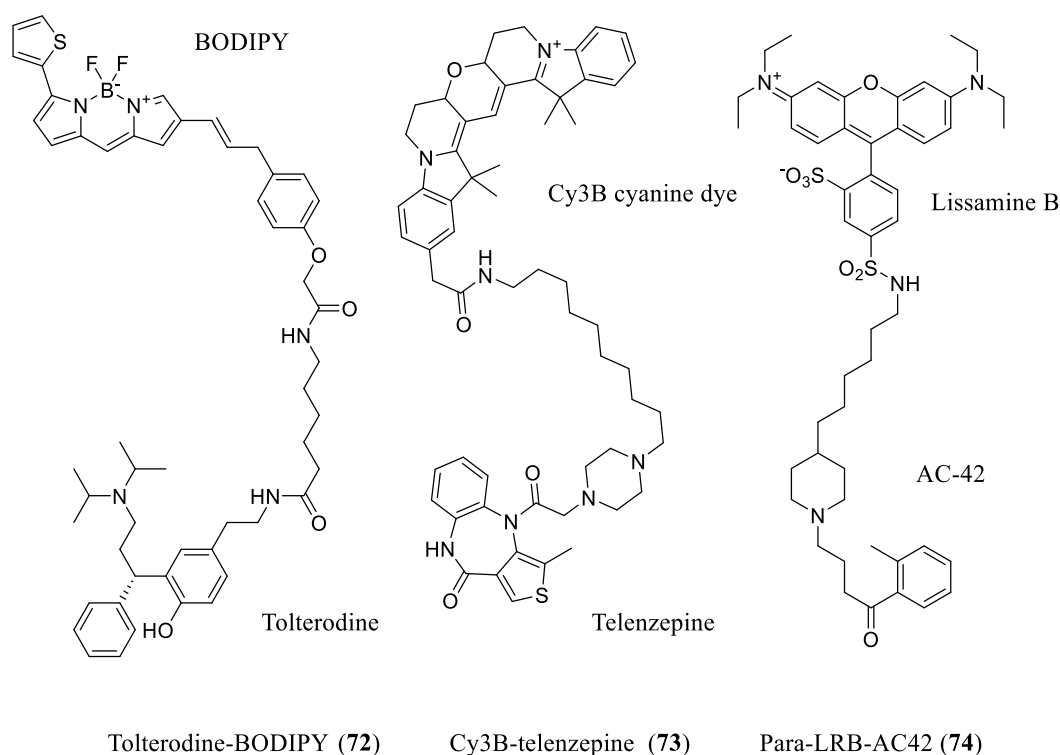


**Figure 27.** Chemical structures of fluorescent tracer ligands targeting the mAChRs; tolterodine-BODIPY (**72**), Cy3B-telenzepine (**73**) and para-LRB-AC42 (**74**).

At this current time, as mAChR allosteric site targeting fluorescent tracer has not been reported. Application of such a probe would yield invaluable information regarding the structure, function and dynamics of allosteric ligand binding to the mAChRs, and additionally would have applications in screening for of allosteric ligands, which will likely ultimately lead to the development of more potent and selective drugs targeting these receptors.

## 5. Summary and thesis aims

The mAChRs have in the past and up to the present been actively pursued in both academia and industry as therapeutic targets for a range of diseases. Most recently, the M<sub>1</sub> and M<sub>4</sub> mAChRs have become of targets interest for the treatment of cognitive disorders, such as Alzheimer's disease and schizophrenia. Due to the high degree of homology between the M<sub>1</sub>-M<sub>5</sub> mAChR subtypes the development of single subtype selective ligands has proven to be a significant challenge. In this introduction we have highlighted several contemporary approaches to overcoming this issue of selectivity in mAChR ligand design, including the development of allosteric ligands and the lesser explored concept of bitopic hybrid ligands. The focus of chapters 2 and 3 of this thesis was to develop an M<sub>1</sub> or M<sub>4</sub> mAChR selective hybrid agonist. However, development of these hybrid agonists was found to be limited due to an apparent inverse correlation between their selectivity and efficacy. As such, in chapter 4 our aim was to uncover the molecular mechanism that determined this apparent inverse correlation, such as to explore the mechanism by which these ligands gain selectivity, and to determine the viability of designing a high efficacy/ high selectivity mAChR hybrid agonist. In chapter 5 our aim was to develop a fluorescently tagged probe molecule, which could be used as a tool for determining allosteric site affinity of ligands at the mAChRs, and which would be appropriate for adapting to a HTS method. Overall, this work aims to increase our understanding of mAChR hybrid ligand agonist selectivity, and to aid in the future development of selective mAChR drugs, for the treatment of cognitive disorders.

## ■ REFERENCES

- (1) Lander, E. S.; Linton, L. M.; Birren, B.; Nusbaum, C.; Zody, M. C.; Baldwin, J.; Devon, K.; Dewar, K.; Doyle, M.; FitzHugh, W.; Funke, R.; Gage, D.; Harris, K.; Heaford, A.; Howland, J.; Kann, L.; Lehoczky, J.; LeVine, R.; McEwan, P.; McKernan, K.; Meldrim, J.; Mesirov, J. P.; Miranda, C.; Morris, W.; Naylor, J.; Raymond, C.; Rosetti, M.; Santos, R.; Sheridan, A.; Sougnez, C.; Stange-Thomann, N.; Stojanovic, N.; Subramanian, A.; Wyman, D.; Rogers, J.; Sulston, J.; Ainscough, R.; Beck, S.; Bentley, D.; Burton, J.; Clee, C.; Carter, N.; Coulson, A.; Deadman, R.; Deloukas, P.; Dunham, A.; Dunham, I.; Durbin, R.; French, L.; Grafham, D.; Gregory, S.; Hubbard, T.; Humphray, S.; Hunt, A.; Jones, M.; Lloyd, C.; McMurray, A.; Matthews, L.; Mercer, S.; Milne, S.; Mullikin, J. C.; Mungall, A.; Plumb, R.; Ross, M.; Shownkeen, R.; Sims, S.; Waterston, R. H.; Wilson, R. K.; Hillier, L. W.; McPherson, J. D.; Marra, M. A.; Mardis, E. R.; Fulton, L. A.; Chinwalla, A. T.; Pepin, K. H.; Gish, W. R.; Chissole, S. L.; Wendl, M. C.; Delehaunty, K. D.; Miner, T. L.; Delehaunty, A.; Kramer, J. B.; Cook, L. L.; Fulton, R. S.; Johnson, D. L.; Minx, P. J.; Clifton, S. W.; Hawkins, T.; Branscomb, E.; Predki, P.; Richardson, P.; Wenning, S.; Slezak, T.; Doggett, N.; Cheng, J.-F.; Olsen, A.; Lucas, S.; Elkin, C.; Uberbacher, E.; Frazier, M.; Gibbs, R. A.; Muzny, D. M.; Scherer, S. E.; Bouck, J. B.; Sodergren, E. J.; Worley, K. C.; Rives, C. M.; Gorrell, J. H.; Metzker, M. L.; Naylor, S. L.; Kucherlapati, R. S.; Nelson, D. L.; Weinstock, G. M.; Sakaki, Y.; Fujiyama, A.; Hattori, M.; Yada, T.; Toyoda, A.; Itoh, T.; Kawagoe, C.; Watanabe, H.; Totoki, Y.; Taylor, T.; Weissbach, J.; Heilig, R.; Saurin, W.; Artiguenave, F.; Brottier, P.; Bruls, T.; Pelletier, E.; Robert, C.; Wincker, P.; Rosenthal, A.; Platzer, M.; Nyakatura, G.; Taudien, S.; Rump, A.; Smith, D. R.; Doucette-Stamm, L.; Rubenfield, M.; Weinstock, K.; Lee, H. M.; Dubois, J.; Yang, H.; Yu, J.; Wang, J.; Huang, G.; Gu, J.; Hood, L.; Rowen, L.; Madan, A.; Qin, S.; Davis, R. W.; Federspiel, N. A.; Abola, A. P.; Proctor, M. J.; Roe, B. A.; Chen, F.; Pan, H.; Ramser, J.; Lehrach, H.; Reinhardt, R.; McCombie, W. R.; de la Bastide, M.; Dedhia, N.; Blöcker, H.; Hornischer, K.; Nordsiek, G.; Agarwala, R.; Aravind, L.; Bailey, J. A.; Bateman, A.; Batzoglu, S.; Birney, E.; Bork, P.; Brown, D. G.; Burge, C. B.; Cerutti, L.; Chen, H.-C.; Church, D.; Clamp, M.; Copley, R. R.; Doerks, T.; Eddy, S. R.; Eichler, E. E.; Furey, T. S.; Galagan, J.; Gilbert, J. G. R.; Harmon, C.; Hayashizaki, Y.; Haussler, D.; Hermjakob, H.; Hokamp, K.; Jang, W.; Johnson, L. S.; Jones, T. A.; Kasif, S.; Kasprzyk, A.; Kennedy, S.; Kent, W. J.; Kitts, P.; Koonin, E. V.; Korf, I.; Kulp, D.; Lancet, D.; Lowe, T. M.; McLysaght, A.; Mikkelsen, T.; Moran, J. V.; Mulder, N.; Pollara, V. J.; Ponting, C. P.; Schuler, G.; Schultz, J.; Slater, G.; Smit, A. F. A.; Stupka, E.; Szustakowki, J.; Thierry-Mieg, D.; Thierry-Mieg, J.; Wagner, L.; Wallis, J.; Wheeler, R.; Williams, A.; Wolf, Y. I.; Wolfe, K. H.; Yang, S.-P.; Yeh, R.-F.; Collins, F.; Guyer, M. S.; Peterson, J.; Felsenfeld, A.; Wetterstrand, K. A.; Myers, R. M.; Schmutz, J.; Dickson, M.; Grimwood, J.; Cox, D. R.; Olson, M. V.; Kaul, R.; Raymond, C.; Shimizu, N.; Kawasaki, K.; Minoshima, S.; Evans, G. A.; Athanasiou, M.; Schultz, R.; Patrinos, A.; Morgan, M. J. Initial sequencing and analysis of the human genome. *Nature* **2001**, *409*, 860.
- (2) Fredriksson, R.; Lagerström, M. C.; Lundin, L.-G.; Schiöth, H. B. The G-Protein-Coupled Receptors in the Human Genome Form Five Main Families. Phylogenetic Analysis, Paralogon Groups, and Fingerprints. *Mol. Pharmacol.* **2003**, *63*, 1256.
- (3) Sriram, K.; Insel, P. A. GPCRs as targets for approved drugs: How many targets and how many drugs? *Mol. Pharmacol.* **2018**, *96*, 251-58.
- (4) Lagerstrom, M. C.; Schioth, H. B. Structural diversity of G protein-coupled receptors and significance for drug discovery. *Nat. Rev. Drug Discov.*, **2008**, *7*, 339-57.
- (5) Rosenbaum, D. M.; Rasmussen, S. G. F.; Kobilka, B. K. The structure and function of G-protein-coupled receptors. *Nature* **2009**, *459*, 356-63.

- (6) Wess, J. Molecular basis of muscarinic receptor function. *Trends Pharmacol. Sci.* **1993**, *14*, 308-313.
- (7) Rasmussen, S. G. F.; DeVree, B. T.; Zou, Y.; Kruse, A. C.; Chung, K. Y.; Kobilka, T. S.; Thian, F. S.; Chae, P. S.; Pardon, E.; Calinski, D.; Mathiesen, J. M.; Shah, S. T. A.; Lyons, J. A.; Caffrey, M.; Gellman, S. H.; Steyaert, J.; Skiniotis, G.; Weis, W. I.; Sunahara, R. K.; Kobilka, B. K. Crystal structure of the  $\beta$ 2 adrenergic receptor–Gs protein complex. *Nature* **2011**, *477*, 549.
- (8) Milligan, G.; Kostenis, E. Heterotrimeric G-proteins: a short history. *Br. J. Pharmacol.* **2006**, *147 Suppl 1*, S46-55.
- (9) Smith, J. S.; Rajagopal, S. The  $\beta$ -arrestins: Multifunctional regulators of G protein-coupled receptors. *J. Biol. Chem.* **2016**, *291*, 8969-77.
- (10) Goldsmith, Z. G.; Dhanasekaran, D. N. G protein regulation of MAPK networks. *Oncogene* **2007**, *26*, 3122-42.
- (11) Zhou, X. E.; Melcher, K.; Xu, H. E. Structure and activation of rhodopsin. *Acta Pharmacol. Sin.* **2012**, *33*, 291-9.
- (12) A common antagonistic mechanism for class A GPCRs revealed by the structure of the human 5-HT<sub>1B</sub> serotonin receptor bound to an antagonist. <http://www.rcsb.org/structure/5V54>.
- (13) Structures of the 5-HT<sub>2A</sub> receptor in complex with the antipsychotics risperidone and zotepin. <http://www.rcsb.org/structure/6A94>.
- (14) McCorvy, J. D.; Wacker, D.; Wang, S.; Agegnehu, B.; Liu, J.; Lansu, K.; Tribo, A. R.; Olsen, R. H. J.; Che, T.; Jin, J.; Roth, B. L. Structural determinants of 5-HT<sub>2B</sub> receptor activation and biased agonism. *Nat. struct. mol. biol.* **2018**, *25*, 787-796.
- (15) Peng, Y.; McCorvy, J. D.; Harpsøe, K.; Lansu, K.; Yuan, S.; Popov, P.; Qu, L.; Pu, M.; Che, T.; Nikolajsen, L. F.; Huang, X. P.; Wu, Y.; Shen, L.; Bjorn-Yoshimoto, W. E.; Ding, K.; Wacker, D.; Han, G. W.; Cheng, J.; Katritch, V.; Jensen, A. A.; Hanson, M. A.; Zhao, S.; Gloriam, D. E.; Roth, B. L.; Stevens, R. C.; Liu, Z. J. 5-HT<sub>2C</sub> Receptor Structures Reveal the Structural Basis of GPCR Polypharmacology. *Cell* **2018**, *172*, 719-730.
- (16) Warne, T.; Serrano-Vega, M. J.; Baker, J. G.; Moukhametzianov, R.; Edwards, P. C.; Henderson, R.; Leslie, A. G.; Tate, C. G.; Schertler, G. F. Structure of a beta<sub>1</sub>-adrenergic G-protein-coupled receptor. *Nature* **2008**, *454*, 486-91.
- (17) Cherezov, V.; Rosenbaum, D. M.; Hanson, M. A.; Rasmussen, S. G.; Thian, F. S.; Kobilka, T. S.; Choi, H. J.; Kuhn, P.; Weis, W. I.; Kobilka, B. K.; Stevens, R. C. High-resolution crystal structure of an engineered human beta<sub>2</sub>-adrenergic G protein-coupled receptor. *Science (New York, N.Y.)* **2007**, *318*, 1258-65.
- (18) Jaakola, V. P.; Griffith, M. T.; Hanson, M. A.; Cherezov, V.; Chien, E. Y.; Lane, J. R.; Ijzerman, A. P.; Stevens, R. C. The 2.6 angstrom crystal structure of a human A<sub>2A</sub> adenosine receptor bound to an antagonist. *Science (New York, N.Y.)* **2008**, *322*, 1211-7.
- (19) Draper-Joyce, C. J.; Khoshouei, M.; Thal, D. M.; Liang, Y. L.; Nguyen, A. T. N.; Furness, S. G. B.; Venugopal, H.; Baltos, J. A.; Plitzko, J. M.; Danev, R.; Baumeister, W.; May, L. T.; Wootten, D.; Sexton, P. M.; Glukhova, A.; Christopoulos, A. Structure of the adenosine-bound human adenosine A<sub>1</sub> receptor-Gi complex. *Nature* **2018**, *558*, 559-563.
- (20) Chien, E. Y.; Liu, W.; Zhao, Q.; Katritch, V.; Han, G. W.; Hanson, M. A.; Shi, L.; Newman, A. H.; Javitch, J. A.; Cherezov, V.; Stevens, R. C. Structure of the human dopamine D<sub>3</sub> receptor in complex with a D<sub>2</sub>/D<sub>3</sub> selective antagonist. *Science (New York, N.Y.)* **2010**, *330*, 1091-5.
- (21) Wang, S.; Che, T.; Levit, A.; Shoichet, B. K.; Wacker, D.; Roth, B. L. Structure of the D<sub>2</sub> dopamine receptor bound to the atypical antipsychotic drug risperidone. *Nature* **2018**, *555*, 269-273.

- (22) Wang, S.; Wacker, D.; Levit, A.; Che, T.; Betz, R. M.; McCorvy, J. D.; Venkatakrishnan, A. J.; Huang, X. P.; Dror, R. O.; Shoichet, B. K.; Roth, B. L. D4 dopamine receptor high-resolution structures enable the discovery of selective agonists. *Science (New York, N.Y.)* **2017**, *358*, 381-386.
- (23) Krishna Kumar, K.; Shalev-Benami, M.; Robertson, M. J.; Hu, H.; Banister, S. D.; Hollingsworth, S. A.; Latorraca, N. R.; Kato, H. E.; Hilger, D.; Maeda, S.; Weis, W. I.; Farrens, D. L.; Dror, R. O.; Malhotra, S. V.; Kobilka, B. K.; Skiniotis, G. Structure of a Signaling Cannabinoid Receptor 1-G Protein Complex. *Cell* **2019**, *176*, 448-458.e12.
- (24) Li, X.; Hua, T.; Vemuri, K.; Ho, J. H.; Wu, Y.; Wu, L.; Popov, P.; Benchama, O.; Zvonok, N.; Locke, K.; Qu, L.; Han, G. W.; Iyer, M. R.; Cinar, R.; Coffey, N. J.; Wang, J.; Wu, M.; Katritch, V.; Zhao, S.; Kunos, G.; Bohn, L. M.; Makriyannis, A.; Stevens, R. C.; Liu, Z. J. Crystal Structure of the Human Cannabinoid Receptor CB2. *Cell* **2019**, *176*, 459-467.e13.
- (25) Che, T.; Majumdar, S.; Zaidi, S. A.; Ondachi, P.; McCorvy, J. D.; Wang, S.; Mosier, P. D.; Uprety, R.; Vardy, E.; Krumm, B. E.; Han, G. W.; Lee, M. Y.; Pardon, E.; Steyaert, J.; Huang, X. P.; Strachan, R. T.; Tribo, A. R.; Pasternak, G. W.; Carroll, F. I.; Stevens, R. C.; Cherezov, V.; Katritch, V.; Wacker, D.; Roth, B. L. Structure of the Nanobody-Stabilized Active State of the Kappa Opioid Receptor. *Cell* **2018**, *172*, 55-67.e15.
- (26) Fenalti, G.; Zatsepin, N. A.; Betti, C.; Giguere, P.; Han, G. W.; Ishchenko, A.; Liu, W.; Guillemyn, K.; Zhang, H.; James, D.; Wang, D.; Weierstall, U.; Spence, J. C.; Boutet, S.; Messerschmidt, M.; Williams, G. J.; Gati, C.; Yefanov, O. M.; White, T. A.; Oberthuer, D.; Metz, M.; Yoon, C. H.; Barty, A.; Chapman, H. N.; Basu, S.; Coe, J.; Conrad, C. E.; Fromme, R.; Fromme, P.; Tourwe, D.; Schiller, P. W.; Roth, B. L.; Ballet, S.; Katritch, V.; Stevens, R. C.; Cherezov, V. Structural basis for bifunctional peptide recognition at human delta-opioid receptor. *Nat. struct. mol. biol.* **2015**, *22*, 265-8.
- (27) Koehl, A.; Hu, H.; Maeda, S.; Zhang, Y.; Qu, Q.; Paggi, J. M.; Latorraca, N. R.; Hilger, D.; Dawson, R.; Matile, H.; Schertler, G. F. X.; Granier, S.; Weis, W. I.; Dror, R. O.; Manglik, A.; Skiniotis, G.; Kobilka, B. K. Structure of the micro-opioid receptor-Gi protein complex. *Nature* **2018**, *558*, 547-52.
- (28) Thal, D. M.; Sun, B.; Feng, D.; Nawaratne, V.; Leach, K.; Felder, C. C.; Bures, M. G.; Evans, D. A.; Weis, W. I.; Bachhawat, P.; Kobilka, T. S.; Sexton, P. M.; Kobilka, B. K.; Christopoulos, A. Crystal structures of the M1 and M4 muscarinic acetylcholine receptors. *Nature* **2016**, *531*, 335-40.
- (29) Kruse, A. C.; Ring, A. M.; Manglik, A.; Hu, J.; Hu, K.; Eitel, K.; Hubner, H.; Pardon, E.; Valant, C.; Sexton, P. M.; Christopoulos, A.; Felder, C. C.; Gmeiner, P.; Steyaert, J.; Weis, W. I.; Garcia, K. C.; Wess, J.; Kobilka, B. K. Activation and allosteric modulation of a muscarinic acetylcholine receptor. *Nature* **2013**, *504*, 101-6.
- (30) Kruse, A. C.; Hu, J.; Pan, A. C.; Arlow, D. H.; Rosenbaum, D. M.; Rosemond, E.; Green, H. F.; Liu, T.; Chae, P. S.; Dror, R. O.; Shaw, D. E.; Weis, W. I.; Wess, J.; Kobilka, B. K. Structure and dynamics of the M3 muscarinic acetylcholine receptor. *Nature* **2012**, *482*, 552-6.
- (31) Haga, K.; Kruse, A. C.; Asada, H.; Yurugi-Kobayashi, T.; Shiroishi, M.; Zhang, C.; Weis, W. I.; Okada, T.; Kobilka, B. K.; Haga, T.; Kobayashi, T. Structure of the human M2 muscarinic acetylcholine receptor bound to an antagonist. *Nature* **2012**, *482*, 547-51.
- (32) Kobilka, B. K. G protein coupled receptor structure and activation. *Biochim. biophys. acta.* **2007**, *1768*, 794-807.
- (33) Tehan, B. G.; Bortolato, A.; Blaney, F. E.; Weir, M. P.; Mason, J. S. Unifying Family A GPCR Theories of Activation. *Pharmacol. Ther.* **2014**, *143*, 51-60.
- (34) Manglik, A.; Kim, T. H.; Masureel, M.; Altenbach, C.; Yang, Z.; Hilger, D.; Lerch, M. T.; Kobilka, T. S.; Thian, F. S.; Hubbell, W. L.; Prosser, R. S.; Kobilka, B. K. Structural

Insights into the Dynamic Process of beta2-Adrenergic Receptor Signaling. *Cell* **2015**, *161*, 1101-1111.

(35) Lebon, G.; Warne, T.; Tate, C. G. Agonist-bound structures of G protein-coupled receptors. *Curr. Opin. Struct. Biol.* **2012**, *22*, 482-90.

(36) Kenakin, T. Agonists, partial agonists, antagonists, inverse agonists and agonist/antagonists? *Trends Pharmacol. Sci.* **1987**, *8*, 423-426.

(37) Black J. W.; Leff, P. Operational models of pharmacological agonism. *Proc. R. Soc. Lond. [Biol]* **1983**, *220*, 141-162.

(38) Conn, P. J.; Christopoulos, A.; Lindsley, C. W. Allosteric modulators of GPCRs: a novel approach for the treatment of CNS disorders. *Nat. Rev. Drug Discov.* **2009**, *8*, 41-54.

(39) Christopoulos, A.; Kenakin, T. G Protein-Coupled Receptor Allosterism and Complexing. *Pharmacol. Rev.* **2002**, *54*, 323-74.

(40) Kenakin, T. Allosteric Agonist Modulators. *J. Recept. Signal Transduct.* **2007**, *27*, 247-259.

(41) Wenthur, C. J.; Gentry, P. R.; Mathews, T. P.; Lindsley, C. W. Drugs for Allosteric Sites on Receptors. *Annu. Rev. Pharmacol. Toxicol.* **2014**, *54*, 165-184.

(42) Lazareno, S.; Gharagozloo, P.; Kuonen, D.; Popham, A.; Birdsall, N. J. M. Subtype-Selective Positive Cooperative Interactions between Brucine Analogues and Acetylcholine at Muscarinic Receptors: Radioligand Binding Studies. *Mol. Pharmacol.* **1998**, *53*, 573-89.

(43) Valant, C.; Robert Lane, J.; Sexton, P. M.; Christopoulos, A. The best of both worlds? Bitopic orthosteric/allosteric ligands of G protein-coupled receptors. *Annu. Rev. Pharmacol. Toxicol.* **2012**, *52*, 153-78.

(44) Lane, R. J.; Sexton, P. M.; Christopoulos, A. Bridging the gap: bitopic ligands of G-protein-coupled receptors. *Trends Pharmacol. Sci.* **2013**, *34*, 59-66.

(45) Kamal, M.; Jockers, R. Bitopic ligands: all-in-one orthosteric and allosteric. *FI000 Biol. Rep.* **2009**, *1*, 77.

(46) Portoghese, P. S. Bivalent ligands and the message-address concept in the design of selective opioid receptor antagonists. *Trends Pharmacol. Sci.* **1989**, *10*, 230-5.

(47) Steinfeld, T.; Hughes, A. D.; Klein, U.; Smith, J. A.; Mammen, M. THRX-198321 Is a Bifunctional Muscarinic Receptor Antagonist and beta-2-Adrenoceptor Agonist (MABA) That Binds in a Bimodal and Multivalent Manner *Mol. Pharmacol.* **2010**, *79*, 389-99.

(48) Steinfeld, T.; Mammen, M.; Smith, J. A.; Wilson, R. D.; Jasper, J. R. A Novel Multivalent Ligand That Bridges the Allosteric and Orthosteric Binding Sites of the M2 Muscarinic Receptor. *Mol. Pharmacol.* **2007**, *72*, 291-302.

(49) Disingrini, T.; Muth, M.; Dallanoce, C.; Barocelli, E.; Bertoni, S.; Kellershohn, K.; Mohr, K.; De Amici, M.; Holzgrabe, U. Design, Synthesis, and Action of Oxotremorine-Related Hybrid-Type Allosteric Modulators of Muscarinic Acetylcholine Receptors. *J. Med. Chem.* **2006**, *49*, 366-372.

(50) Bock, A.; Bermudez, M.; Krebs, F.; Matera, C.; Chirinda, B.; Sydow, D.; Dallanoce, C.; Holzgrabe, U.; De Amici, M.; Lohse, M. J.; Wolber, G.; Mohr, K. Ligand Binding Ensembles Determine Graded Agonist Efficacies at a G Protein-coupled Receptor. *J. Biol. Chem.* **2016**, *291*, 16375-89.

(51) Valant, C.; Gregory, K. J.; Hall, N. E.; Scammells, P. J.; Lew, M. J.; Sexton, P. M.; Christopoulos, A. A Novel Mechanism of G Protein-coupled Receptor Functional Selectivity: Muscarinic partial agonist McN-A-343 as a bitopic orthosteric/allosteric ligand. *J. Biol. Chem.* **2008**, *283*, 29312-21.

(52) Bock, A.; Chirinda, B.; Krebs, F.; Messerer, R.; Bätz, J.; Muth, M.; Dallanoce, C.; Klighenthal, D.; Tränkle, C.; Hoffmann, C.; De Amici, M.; Holzgrabe, U.; Kostenis, E.; Mohr, K. Dynamic ligand binding dictates partial agonism at a g protein-coupled receptor. *Nat. Chem. Biol.* **2014**, *10*, 18-20.

- (53) Bermudez, M.; Bock, A.; Krebs, F.; Holzgrabe, U.; Mohr, K.; Lohse, M. J.; Wolber, G. Ligand-Specific Restriction of Extracellular Conformational Dynamics Constrains Signaling of the M2 Muscarinic Receptor. *ACS Chem. Biol.* **2017**, *12*, 1743-48.
- (54) Keov, P.; Valant, C.; Devine, S. M.; Lane, J. R.; Scammells, P. J.; Sexton, P. M.; Christopoulos, A.. Reverse Engineering of the Selective Agonist TBPB Unveils Both Orthosteric and Allosteric Modes of Action at the M1 Muscarinic Acetylcholine Receptor. *Mol. Pharmacol.* **2013**, *84*, 425-37.
- (55) Keov, P.; López, L.; Devine, S. M.; Valant, C.; Lane, J. R.; Scammells, P. J.; Christopoulos, A.; Sexton, P. M.; A. Molecular mechanisms of bitopic ligand engagement with the M1 muscarinic acetylcholine receptor. *J. Biol. Chem.* **2014**, *289*, 23817-37.
- (56) Avlani, V. A.; Langmead, C. J.; Guida, E.; Wood, M. D.; Tehan, B. G.; Herdon, H. J.; Watson, J. M.; Sexton, P. M.; Christopoulos, A. Orthosteric and allosteric modes of interaction of novel selective agonists of the M1 muscarinic acetylcholine receptor. *Mol. Pharmacol.* **2010**, *78*, 94-104.
- (57) Narlawar, R.; Lane, J. R.; Doddareddy, M.; Lin, J.; Brussee, J.; Ijzerman, A. P. Hybrid ortho/allosteric ligands for the adenosine A(1) receptor. *J. Med. Chem.* **2010**, *53*, 3028-37.
- (58) Shonberg, J.; Draper-Joyce, C.; Mistry, S. N.; Christopoulos, A.; Scammells, P. J.; Lane, J. R.; Capuano, B. Structure–Activity Study of N-((trans)-4-(2-(7-Cyano-3,4-dihydroisoquinolin-2(1H)-yl)ethyl)cyclohexyl)-1H-indole-2-carboxamide (SB269652), a Bitopic Ligand That Acts as a Negative Allosteric Modulator of the Dopamine D2 Receptor. *J. Med. Chem.* **2015**, *58*, 5287-307.
- (59) Caulfield, M. P. Muscarinic receptors--characterization, coupling and function. *Pharmacol. Ther.* **1993**, *58*, 319-79.
- (60) Nathanson, N. M. Synthesis, trafficking, and localization of muscarinic acetylcholine receptors. *Pharmacol. Ther.* **2008**, *119*, 33-43.
- (61) Ashkenazi, A.; Winslow, J. W.; Peralta, E. G.; Peterson, G. L.; Schimerlik, M. I.; Capon, D. J.; Ramachandran, J. An M2 muscarinic receptor subtype coupled to both adenylyl cyclase and phosphoinositide turnover. *Science (New York, N.Y.)* **1987**, *238*, 672-5.
- (62) van Koppen, C. J.; Kaiser, B. Regulation of muscarinic acetylcholine receptor signaling. *Pharmacol. Ther.* **2003**, *98*, 197-220.
- (63) Matera, C.; Tata, A. M. Pharmacological approaches to targeting muscarinic acetylcholine receptors. *Recent Pat. CNS Drug Discov.* **2014**, *9*, 85-100.
- (64) Suga, H.; Sawyer, G.; Ehlert, F. Mutagenesis of Nucleophilic Residues near the Orthosteric Binding Pocket of M-1 and M-2 Muscarinic receptors: Effect on the Binding of Nitrogen Mustard Analogs of Acetylcholine and McN-A-343. **2010**, *78*, 745-55.
- (65) Davie, B. J.; Christopoulos, A.; Scammells, P. J. Development of M1 mAChR allosteric and bitopic ligands: prospective therapeutics for the treatment of cognitive deficits. *ACS Chem. Neurosci.* **2013**, *4*, 1026-48.
- (66) Fisher, A. M1 muscarinic agonists target major hallmarks of Alzheimer's disease--the pivotal role of brain M1 receptors. *Neurodegener. Dis.* **2008**, *5*, 237-40.
- (67) Fisher, A.; Pittel, Z.; Haring, R.; Bar-Ner, N.; Kliger-Spatz, M.; Natan, N.; Egozi, I.; Sonogo, H.; Marcovitch, I.; Brandeis, R. M1 muscarinic agonists can modulate some of the hallmarks in Alzheimer's disease. *J. Mol. Neurosci.* **2003**, *20*, 349-356.
- (68) Bartus, R. T.; Dean, R. L., 3rd; Beer, B.; Lippa, A. S. The cholinergic hypothesis of geriatric memory dysfunction. *Science (New York, N.Y.)* **1982**, *217*, 408-14.
- (69) Francis, P. T.; Palmer, A. M.; Snape, M.; Wilcock, G. K. The cholinergic hypothesis of Alzheimer's disease: a review of progress. *J. Neurol. Neurosurg. Psychiatry* **1999**, *66*, 137-47.
- (70) Contestabile, A. The history of the cholinergic hypothesis. *Behav. Brain Res.* **2011**, *221*, 334-40.

- (71) Whitehouse, P. J.; Price, D. L.; Struble, R. G.; Clark, A. W.; Coyle, J. T.; Delon, M. R. Alzheimer's disease and senile dementia: loss of neurons in the basal forebrain. *Science (New York, N.Y.)* **1982**, *215*, 1237-9.
- (72) Young, J. W.; Powell, S. B.; Geyer, M. A. Mouse pharmacological models of cognitive disruption relevant to schizophrenia. *Neuropharmacol.* **2012**, *62*, 1381-90.
- (73) Deardorff, W. J.; Feen, E.; Grossberg, G. T. The Use of Cholinesterase Inhibitors Across All Stages of Alzheimer's Disease. *Drugs Aging* **2015**, *32*, 537-47.
- (74) Han, J.-Y.; Besser, L. M.; Xiong, C.; Kukull, W. A.; Morris, J. C. Cholinesterase Inhibitors May Not Benefit Mild Cognitive Impairment and Mild Alzheimer Disease Dementia. *Alzheimer Dis. Assoc. Disord.* **2019**, *33*, 87-94.
- (75) Irvine, G. B.; El-Agnaf, O. M.; Shankar, G. M.; Walsh, D. M. Protein Aggregation in the Brain: The Molecular Basis for Alzheimer's and Parkinson's Diseases. *Mol. Med.* **2008**, *14*, 451-64.
- (76) Thathiah, A.; De Strooper, B. The role of G protein-coupled receptors in the pathology of Alzheimer's disease. *Nat. Rev. Neurosci.* **2011**, *12*, 73-87.
- (77) Davis, A. A.; Fritz, J. J.; Wess, J.; Lah, J. J.; Levey, A. I. Deletion of the M1 Muscarinic Acetylcholine Receptors Increases Amyloid Pathology In Vitro and In Vivo. *J. Neurosci.* **2010**, *30*, 4190-6.
- (78) Gerber, D. J.; Sotnikova, T. D.; Gainetdinov, R. R.; Huang, S. Y.; Caron, M. G.; Tonegawa, S. Hyperactivity, elevated dopaminergic transmission, and response to amphetamine in M1 muscarinic acetylcholine receptor-deficient mice. *Proc. Natl. Acad. Sci. U. S. A.* **2001**, *98*, 15312-7.
- (79) Bodick, N. C.; Offen, W. W.; Levey, A. I.; Cutler, N. R.; Gauthier, S. C.; Satlin, A.; Shannon, H. E.; Tollefson, G. D.; Rasmussen, K.; Bymaster, F. P.; Hurley, D. J.; Potter, W. Z.; Paul, S. M.; Effects of xanomeline, a selective muscarinic receptor agonist, on cognitive function and behavioral symptoms in Alzheimer's disease. *Arch. Neurol.* **1997**, *54*, 465-73.
- (80) Bodick, N. C.; Offen, W. W.; Shannon, H. E.; Satterwhite, J.; Lucas, R.; van Lier, R.; Paul, S. M. The selective muscarinic agonist xanomeline improves both the cognitive deficits and behavioral symptoms of Alzheimer disease. *Alzheimer Dis. Assoc. Disord.* **1997**, *11 Suppl 4*, S16-22.
- (81) Bender, A. M.; Jones, C. K.; Lindsley, C. W. Classics in Chemical Neuroscience: Xanomeline. *ACS Chem. Neurosci.* **2017**, *8*, 435-43.
- (82) Nathan, P. J.; Watson, J.; Lund, J.; Davies, C. H.; Peters, G.; Dodds, C. M.; Swirski, B.; Lawrence, P.; Bentley, G. D.; O'Neill, B. V.; Robertson, J.; Watson, S.; Jones, G. A.; Maruff, P.; Croft, R. J.; Laruelle, M.; Bullmore, E. T. The potent M1 receptor allosteric agonist GSK1034702 improves episodic memory in humans in the nicotine abstinence model of cognitive dysfunction. *Int. J. Neuropsychopharmacol.* **2013**, *16*, 721-31.
- (83) Haller, C. S.; Padmanabhan, J. L.; Lizano, P.; Torous, J.; Keshavan, M. Recent advances in understanding schizophrenia. *F1000Prime Rep.* **2014**, *6*, 57.
- (84) Insel, T. R. Rethinking schizophrenia. *Nature* **2010**, *468*, 187-93.
- (85) Thaker, G. K.; Carpenter Jr, W. T. Advances in schizophrenia. *Nat. Med.* **2001**, *7*, 667-71.
- (86) Carlsson, A. The current status of the dopamine hypothesis of schizophrenia. *Neuropsychopharmacology* **1988**, *1*, 179-86.
- (87) Kane, J.; Honigfeld, G.; Singer, J.; Meltzer, H. Clozapine for the treatment-resistant schizophrenic. A double-blind comparison with chlorpromazine. *Arch. Gen. Psychiatry* **1988**, *45*, 789-96.
- (88) Rummel-Kluge, C.; Komossa, K.; Schwarz, S.; Hunger, H.; Schmid, F.; Kissling, W.; Davis, J. M.; Leucht, S. Second-generation antipsychotic drugs and extrapyramidal side effects: a systematic review and meta-analysis of head-to-head comparisons. *Schizophr. Bull.* **2012**, *38*, 167-177.



- (89) Ishiguro, H.; Horiuchi, Y.; Ishikawa, M.; Koga, M.; Imai, K.; Suzuki, Y.; Morikawa, M.; Inada, T.; Watanabe, Y.; Takahashi, M.; Someya, T.; Ujike, H.; Iwata, N.; Ozaki, N.; Onaivi, E. S.; Kunugi, H.; Sasaki, T.; Itokawa, M.; Arai, M.; Niizato, K.; Iritani, S.; Naka, I.; Ohashi, J.; Kakita, A.; Takahashi, H.; Nawa, H.; Arinami, T. Brain cannabinoid CB2 receptor in schizophrenia. *Biol. Psychiatry* **2010**, *67*, 974-82.
- (90) Yohn, S. E.; Conn, P. J. Positive allosteric modulation of M1 and M4 muscarinic receptors as potential therapeutic treatments for schizophrenia. *Neuropharmacology* **2018**, *136*, 438-48.
- (91) Yeomans, J. S. Role of Tegmental Cholinergic Neurons in Dopaminergic Activation, Antimuscarinic Psychosis and Schizophrenia. *Neuropsychopharmacology* **2003**, *12*, 3-16.
- (92) Andersen, M. B.; Croy, C. H.; Dencker, D.; Werge, T.; Bymaster, F. P.; Felder, C. C.; Fink-Jensen, A. Antipsychotic-like effect of the muscarinic acetylcholine receptor agonist BuTAC in non-human primates. *PloS One* **2015**, *10*, e0122722.
- (93) Shekhar, A.; Potter, W.; Lienemann, J.; Sundblad, K.; Lightfoot, J.; Herrera, J.; Unverzagt, F.; Bymaster, F.; Felder, C. Efficacy of xanomeline, a selective muscarinic agonist, in treating schizophrenia: a double-blind, placebo controlled study, *ACNP 40th Annual Meeting*, **2001**; 9-13.
- (94) Ince, E.; Ciliax, B. J.; Levey, A. I. Differential expression of D1 and D2 dopamine and m4 muscarinic acetylcholine receptor proteins in identified striatonigral neurons. *Synapse (New York, N.Y.)* **1997**, *27*, 357-66.
- (95) Santiago, M. P.; Potter, L. T. Biotinylated m4-toxin demonstrates more M4 muscarinic receptor protein on direct than indirect striatal projection neurons. *Brain Res* **2001**, *894*, 12-20.
- (96) Shin, J. H.; Adrover, M. F.; Wess, J.; Alvarez, V. A. Muscarinic regulation of dopamine and glutamate transmission in the nucleus accumbens. *Proc. Natl. Acad. Sci. U. S. A.* **2015**, *112*, 8124-9.
- (97) Crook, J. M.; Tomaskovic-Crook, E.; Copolov, D. L.; Dean, B. Low Muscarinic Receptor Binding in Prefrontal Cortex From Subjects With Schizophrenia: A Study of Brodmann's Areas 8, 9, 10, and 46 and the Effects of Neuroleptic Drug Treatment. *Am. J. Psychiatry* **2001**, *158*, 918-25.
- (98) Zavitsanou, K.; Katsifis, A.; Mattner, F.; Huang, X. F. Investigation of M1/M4 Muscarinic Receptors in the Anterior Cingulate Cortex in Schizophrenia, Bipolar Disorder, and Major Depression Disorder. *Neuropsychopharmacology* **2004**, *29*, 619-25.
- (99) Shirey, J. K.; Xiang, Z.; Orton, D.; Brady, A. E.; Johnson, K. A.; Williams, R.; Ayala, J. E.; Rodriguez, A. L.; Wess, J.; Weaver, D.; Niswender, C. M.; Conn, P. J. An allosteric potentiator of M4 mAChR modulates hippocampal synaptic transmission. *Nat. Chem. Biol.* **2008**, *4*, 42-50.
- (100) Brady, A. E.; Jones, C. K.; Bridges, T. M.; Kennedy, J. P.; Thompson, A. D.; Heiman, J. U.; Breining, M. L.; Gentry, P. R.; Yin, H.; Jadhav, S. B.; Shirey, J. K.; Conn, P. J.; Lindsley, C. W. Centrally Active Allosteric Potentiators of the M4 Muscarinic Acetylcholine Receptor Reverse Amphetamine-Induced Hyperlocomotor Activity in Rats. *J. Pharmacol. Exp. Ther.* **2008**, *327*, 941-53.
- (101) Leach, K.; Loiacono, R. E.; Felder, C. C.; McKinzie, D. L.; Mogg, A.; Shaw, D. B.; Sexton, P. M.; Christopoulos, A. Molecular mechanisms of action and in vivo validation of an M4 muscarinic acetylcholine receptor allosteric modulator with potential antipsychotic properties. *Neuropsychopharmacology* **2010**, *35*, 855-69.
- (102) Thomsen, M.; Wess, J.; Fulton, B. S.; Fink-Jensen, A.; Caine, S. B. Modulation of prepulse inhibition through both M1 and M4 muscarinic receptors in mice. *Psychopharmacology* **2010**, *208*, 401-16.
- (103) Dencker, D.; Wörtwein, G.; Weikop, P.; Jeon, J.; Thomsen, M.; Sager, T. N.; Mørk, A.; Woldbye, D. P. D.; Wess, J.; Fink-Jensen, A. Involvement of a Subpopulation of Neuronal M4

Muscarinic Acetylcholine Receptors in the Antipsychotic-like Effects of the M1/ M4 Preferring Muscarinic Receptor Agonist Xanomeline. *J. Neurosci.* **2011**, *31*, 5905-8.

(104) Woolley, M. L.; Carter, H. J.; Gartlon, J. E.; Watson, J. M.; Dawson, L. A. Attenuation of amphetamine-induced activity by the non-selective muscarinic receptor agonist, xanomeline, is absent in muscarinic M4 receptor knockout mice and attenuated in muscarinic M1 receptor knockout mice. *Eur. J. Pharmacol.* **2009**, *603*, 147-9.

(105) Koshimizu, H.; Leiter, L. M.; Miyakawa, T. M4 muscarinic receptor knockout mice display abnormal social behavior and decreased prepulse inhibition. *Mol. Brain* **2012**, *5*, 10.

(106) KarTX clinical trial. <https://clinicaltrials.gov/ct2/show/study/NCT03697252>

(107) Bymaster, F. P.; Felder, C.; Ahmed, S.; McKinzie, D. Muscarinic Receptors as a Target for Drugs Treating Schizophrenia. *Curr. Drug Targets CNS Neurol. Disord.* **2002**, *1*, 163-81.

(108) Foster, D. J.; Choi, D. L.; Conn, P. J.; Rook, J. M. Activation of M1 and M4 muscarinic receptors as potential treatments for Alzheimer's disease and schizophrenia. *Neuropsychiatr. Dis. Treat.* **2014**, *10*, 183-91.

(109) Langmead, C. J.; Watson, J.; Reavill, C. Muscarinic acetylcholine receptors as CNS drug targets. *Pharmacol. Ther.* **2008**, *117*, 232-43.

(110) Spalding, T. A.; Trotter, C.; Skjaerbaek, N.; Messier, T. L.; Currier, E. A.; Burstein, E. S.; Li, D.; Hacksell, U.; R Brann, M. R. Discovery of an ectopic activation site on the M(1) muscarinic receptor. *Mol. Pharmacol.* **2002**, *61*, 1297-302.

(111) Bradley, S. R.; Lamah, J.; Ohrmund, L.; Son, T.; Bajpai, A.; Nguyen, D.; Friberg, M.; Burstein, E. S.; Spalding, T. A.; Ott, T. R.; Schiffer, H. H.; Tabatabaei, A.; McFarland, K.; Davis, R. E.; Bonhaus, D. W. AC-260584, an orally bioavailable M(1) muscarinic receptor allosteric agonist, improves cognitive performance in an animal model. *Neuropharmacology* **2010**, *58*, 365-73.

(112) Langmead, C. J.; Austin, N. E.; Branch, C. L.; Brown, J. T.; Buchanan, K. A.; Davies, C. H.; Forbes, I. T.; Fry, V. A.; Hagan, J. J.; Herdon, H. J.; Jones, G. A.; Jeggo, R.; Kew, J. N.; Mazzali, A.; Melarange, R.; Patel, N.; Pardoe, J.; Randall, A. D.; Roberts, C.; Roopun, A.; Starr, K. R.; Teriakidis, A.; Wood, M. D.; Whittington, M.; Wu, Z.; Watson, J. Characterization of a CNS penetrant, selective M1 muscarinic receptor agonist, 77-LH-28-1. *Br. J. Pharmacol.* **2008**, *154*, 1104-15.

(113) Jones, C. K.; Brady, A. E.; Davis, A. A.; Xiang, Z.; Bubser, M.; Tantawy, M. N.; Kane, A. S.; Bridges, T. M.; Kennedy, J. P.; Bradley, S. R.; Peterson, T. E.; Ansari, M. S.; Baldwin, R. M.; Kessler, R. M.; Deutch, A. Y.; Lah, J. J.; Levey, A. I.; Lindsley, C. W.; Conn, P. J. Novel selective allosteric activator of the M1 muscarinic acetylcholine receptor regulates amyloid processing and produces antipsychotic-like activity in rats. *J. Neurosci.* **2008**, *28*, 10422-33.

(114) Sams, A. G.; Hentzer, M.; Mikkelsen, G. K.; Larsen, K.; Bundgaard, C.; Plath, N.; Christoffersen, C. T.; Bang-Andersen, B. Discovery of N-{1-[3-(3-oxo-2,3-dihydrobenzo[1,4]oxazin-4-yl)propyl]piperidin-4-yl}-2-phenylac etamide (Lu AE51090): an allosteric muscarinic M1 receptor agonist with unprecedented selectivity and procognitive potential. *J. Med. Chem.* **2010**, *53*, 6386-97.

(115) Ma, L.; Seager, M. A.; Wittmann, M.; Jacobson, M.; Bickel, D.; Burno, M.; Jones, K.; Graufelds, V. K.; Xu, G.; Pearson, M.; McCampbell, A.; Gaspar, R.; Shughrue, P.; Danziger, A.; Regan, C.; Flick, R.; Pascarella, D.; Garson, S.; Doran, S.; Kreatsoulas, C.; Veng, L.; Lindsley, C. W.; Shipe, W.; Kuduk, S.; Sur, C.; Kinney, G.; Seabrook, G. R.; Ray, W. J. Selective activation of the M1 muscarinic acetylcholine receptor achieved by allosteric potentiation. *Proc. Natl. Acad. Sci. U. S. A.* **2009**, *106*, 15950-5.

(116) Shirey, J. K.; Brady, A. E.; Jones, P. J.; Davis, A. A.; Bridges, T. M.; Kennedy, J. P.; Jadhav, S. B.; Menon, U. N.; Xiang, Z.; Watson, M. L.; Christian, E. P.; Doherty, J. J.; Quirk, M. C.; Snyder, D. H.; Lah, J. J.; Levey, A. I.; Nicolle, M. M.; Lindsley, C. W.; Conn, P. J. A

selective allosteric potentiator of the M1 muscarinic acetylcholine receptor increases activity of medial prefrontal cortical neurons and restores impairments in reversal learning. *J. Neurosci.* **2009**, *29*, 14271-86.

(117) Uslaner, J. M.; Eddins, D.; Puri, V.; Cannon, C. E.; Sutcliffe, J.; Chew, C. S.; Pearson, M.; Vivian, J. A.; Chang, R. K.; Ray, W. J.; Kuduk, S. D.; Wittmann, M. The muscarinic M1 receptor positive allosteric modulator PQCA improves cognitive measures in rat, cynomolgus macaque, and rhesus macaque. *Psychopharmacology* **2013**, *225*, 21-30.

(118) Mistry, S. N.; Valant, C.; Sexton, P. M.; Capuano, B.; Christopoulos, A.; Scammells, P. J. Synthesis and Pharmacological Profiling of Analogues of Benzyl Quinolone Carboxylic Acid (BQCA) as Allosteric Modulators of the M1 Muscarinic Receptor. *J. Med. Chem.* **2013**, *56*, 5151-72.

(119) Kuduk, S. D.; Beshore, D. C. SAR studies on carboxylic acid series M(1) selective positive allosteric modulators (PAMs). *Curr. Top. Med. Chem.* **2014**, *14*, 1738-54.

(120) Kuduk, S. D.; Di Marco, C. N.; Chang, R. K.; Ray, W. J.; Ma, L.; Wittmann, M.; Seager, M. A.; Koeplinger, K. A.; Thompson, C. D.; Hartman, G. D.; Bilodeau, M. T. Heterocyclic fused pyridone carboxylic acid M(1) positive allosteric modulators. *Bioorg. Med. Chem. Lett.* **2010**, *20*, 2533-7.

(121) Kuduk, S. D.; Di Marco, C. N.; Cofre, V.; Ray, W. J.; Ma, L.; Wittmann, M.; Seager, M. A.; Koeplinger, K. A.; Thompson, C. D.; Hartman, G. D.; Bilodeau, M. T. Fused heterocyclic M1 positive allosteric modulators. *Bioorg. Med. Chem. Lett.* **2011**, *21*, 2769-72.

(122) Mistry, S. N.; Jörg, M.; Lim, H.; Vinh, N. B.; Sexton, P. M.; Capuano, B.; Christopoulos, A.; Lane, J. R.; Scammells, P. J. 4-Phenylpyridin-2-one Derivatives: A Novel Class of Positive Allosteric Modulator of the M1 Muscarinic Acetylcholine Receptor. *J. Med. Chem.* **2016**, *59*, 388-409.

(123) Mistry, S. N.; Lim, H.; Jörg, M.; Capuano, B.; Christopoulos, A.; Lane, J. R.; Scammells, P. J. Novel Fused Arylpyrimidinone Based Allosteric Modulators of the M1 Muscarinic Acetylcholine Receptor. *ACS Chem. Neurosci.* **2016**, *7*, 647-61.

(124) Davoren, J. E.; Lee, C.-W.; Garnsey, M.; Brodney, M. A.; Cordes, J.; Dlugolenski, K.; Edgerton, J. R.; Harris, A. R.; Helal, C. J.; Jenkinson, S.; Kauffman, G. W.; Kenakin, T. P.; Lazzaro, J. T.; Lotarski, S. M.; Mao, Y.; Nason, D. M.; Northcott, C.; Nottebaum, L.; O'Neil, S. V.; Pettersen, B.; Popiolek, M.; Reinhart, V.; Salomon-Ferrer, R.; Steyn, S. J.; Webb, D.; Zhang, L.; Grimwood, S. Discovery of the Potent and Selective M1 PAM-Agonist N-[(3R,4S)-3-Hydroxytetrahydro-2H-pyran-4-yl]-5-methyl-4-[4-(1,3-thiazol-4-yl)benzyl]pyridine-2-carboxamide (PF-06767832): Evaluation of Efficacy and Cholinergic Side Effects. *J. Med. Chem.* **2016**, *59*, 6313-28.

(125) Dallagnol, J. C. C.; Khajehali, E.; van der Westhuizen, E. T.; Jörg, M.; Valant, C.; Gonçalves, A. G.; Capuano, B.; Christopoulos, A.; Scammells, P. J.; Synthesis and Pharmacological Evaluation of Heterocyclic Carboxamides: Positive Allosteric Modulators of the M1 Muscarinic Acetylcholine Receptor with Weak Agonist Activity and Diverse Modulatory Profiles. *J. Med. Chem.* **2018**, *61*, 2875-94.

(126) Davoren, J. E.; Lee, C. W.; Garnsey, M.; Brodney, M. A.; Cordes, J.; Dlugolenski, K.; Edgerton, J. R.; Harris, A. R.; Helal, C. J.; Jenkinson, S.; Kauffman, G. W.; Kenakin, T. P.; Lazzaro, J. T.; Lotarski, S. M.; Mao, Y.; Nason, D. M.; Northcott, C.; Nottebaum, L.; O'Neil, S. V.; Pettersen, B.; Popiolek, M.; Reinhart, V.; Salomon-Ferrer, R.; Steyn, S. J.; Webb, D.; Zhang, L.; Grimwood, S. Discovery of the Potent and Selective M1 PAM-Agonist N-[(3R,4S)-3-Hydroxytetrahydro-2H-pyran-4-yl]-5-methyl-4-[4-(1,3-thiazol-4-yl)benzyl]pyridine-2-carboxamide (PF-06767832): Evaluation of Efficacy and Cholinergic Side Effects. *J. Med. Chem.* **2016**, *59*, 6313-28.

- (127) Davoren, J. E.; O'Neil, S. V.; Anderson, D. P.; Brodney, M. A.; Chenard, L.; Dlugolenski, K.; Edgerton, J. R.; Green, M.; Garnsey, M.; Grimwood, S.; Harris, A. R.; Kauffman, G. W.; LaChapelle, E.; Lazzaro, J. T.; Lee, C. W.; Lotarski, S. M.; Nason, D. M.; Obach, R. S.; Reinhart, V.; Salomon-Ferrer, R.; Steyn, S. J.; Webb, D.; Yan, J.; Zhang, L. Design and optimization of selective azaindole amide M1 positive allosteric modulators. *Bioorg. Med. Chem. Lett.* **2016**, *26*, 650-5.
- (128) Yang, F. V.; Shipe, W. D.; Bunda, J. L.; Nolt, M. B.; Wisnoski, D. D.; Zhao, Z.; Barrow, J. C.; Ray, W. J.; Ma, L.; Wittmann, M.; Seager, M. A.; Koeplinger, K. A.; Hartman, G. D.; Lindsley, C. W. Parallel synthesis of N-biaryl quinolone carboxylic acids as selective M1 positive allosteric modulators. *Bioorg. Med. Chem. Lett.* **2010**, *20*, 531-6.
- (129) Kuduk, S. D.; Beshore, D. C.; Dimarco, C. N.; Greshock, T. J.; Aryl methyl benzoquinazolinone M1 receptor positive allosteric modulators. *U. S. patent US20160229813A1* **2017**.
- (130) Mistry, S. N.; Lim, H.; Jorg, M.; Capuano, B.; Christopoulos, A.; Lane, J. R.; Scammells, P. J. Novel Fused Arylpyrimidinone Based Allosteric Modulators of the M1 Muscarinic Acetylcholine Receptor. *ACS Chem. Neurosci.* **2016**, *7*, 647-61.
- (131) Han, C.; Chatterjee, A.; Noetzel, M. J.; Panarese, J. D.; Smith, E.; Chase, P.; Hodder, P.; Niswender, C.; Conn, P. J.; Lindsley, C. W.; Stauffer, S. R. Discovery and SAR of muscarinic receptor subtype 1 (M1) allosteric activators from a molecular libraries high throughput screen. Part 1: 2,5-dibenzyl-2H-pyrazolo[4,3-c]quinolin-3(5H)-ones as positive allosteric modulators. *Bioorg. Med. Chem. Lett.* **2015**, *25*, 384-8.
- (132) Kuduk, S. D.; Chang, R. K.; Di Marco, C. N.; Ray, W. J.; Ma, L.; Wittmann, M.; Seager, M. A.; Koeplinger, K. A.; Thompson, C. D.; Hartman, G. D.; Bilodeau, M. T. Quinolizidinone carboxylic acids as CNS penetrant, selective m1 allosteric muscarinic receptor modulators. *ACS Med. Chem. Lett.* **2010**, *1*, 263-7.
- (133) Kuduk, S. D.; Chang, R. K.; Di Marco, C. N.; Pitts, D. R.; Greshock, T. J.; Ma, L.; Wittmann, M.; Seager, M. A.; Koeplinger, K. A.; Thompson, C. D.; Hartman, G. D.; Bilodeau, M. T.; Ray, W. J. Discovery of a selective allosteric M1 receptor modulator with suitable development properties based on a quinolizidinone carboxylic acid scaffold. *J. Med. Chem.* **2011**, *54*, 4773-80.
- (134) Kuduk, S. D.; Chang, R. K.; Greshock, T. J.; Ray, W. J.; Ma, L.; Wittmann, M.; Seager, M. A.; Koeplinger, K. A.; Thompson, C. D.; Hartman, G. D.; Bilodeau, M. T. Identification of amides as carboxylic Acid surrogates for quinolizidinone-based m1 positive allosteric modulators. *ACS Med. Chem. Lett.* **2012**, *3*, 1070-4.
- (135) Kuduk, S. D.; Di Marco, C. N.; Saffold, J. R.; Ray, W. J.; Ma, L.; Wittmann, M.; Koeplinger, K. A.; Thompson, C. D.; Hartman, G. D.; Bilodeau, M. T.; Beshore, D. C. Identification of a methoxynaphthalene scaffold as a core replacement in quinolizidinone amide M1 positive allosteric modulators. *Bioorg. Med. Chem. Lett.* **2014**, *24*, 1417-20.136.
- (136) Reid, P. R.; Bridges, T. M.; Sheffler, D. J.; Cho, H. P.; Lewis, L. M.; Days, E.; Daniels, J. S.; Jones, C. K.; Niswender, C. M.; Weaver, C. D.; Conn, P. J.; Lindsley, C. W.; Wood, M. R. Discovery and optimization of a novel, selective and brain penetrant M1 positive allosteric modulator (PAM): the development of ML169, an MLPCN probe. *Bioorg. Med. Chem. Lett.* **2011**, *21*, 2697-701.
- (137) Tarr, J. C.; Turlington, M. L.; Reid, P. R.; Utley, T. J.; Sheffler, D. J.; Cho, H. P.; Klar, R.; Pancani, T.; Klein, M. T.; Bridges, T. M.; Morrison, R. D.; Blobaum, A. L.; Xiang, Z.; Daniels, J. S.; Niswender, C. M.; Conn, P. J.; Wood, M. R.; Lindsley, C. W. Targeting selective activation of M(1) for the treatment of Alzheimer's disease: further chemical optimization and pharmacological characterization of the M(1) positive allosteric modulator ML169. *ACS Chem. Neurosci.* **2012**, *3*, 884-95.

- (138) Rook, J. M.; Abe, M.; Cho, H. P.; Nance, K. D.; Luscombe, V. B.; Adams, J. J.; Dickerson, J. W.; Remke, D. H.; Garcia-Barrantes, P. M.; Engers, D. W.; Engers, J. L.; Chang, S.; Foster, J. J.; Blobaum, A. L.; Niswender, C. M.; Jones, C. K.; Conn, P. J.; Lindsley, C. W. Diverse Effects on M1 Signaling and Adverse Effect Liability within a Series of M1 Ago-PAMs. *ACS Chem. Neurosci.* **2017**, *8*, 866-83.
- (139) Davoren, J. E.; O'Neil, S. V.; Anderson, D. P.; Brodney, M. A.; Chenard, L.; Dlugolenski, K.; Edgerton, J. R.; Green, M.; Garnsey, M.; Grimwood, S.; Harris, A. R.; Kauffman, G. W.; LaChapelle, E.; Lazzaro, J. T.; Lee, C.-W.; Lotarski, S. M.; Nason, D. M.; Obach, R. S.; Reinhart, V.; Salomon-Ferrer, R.; Steyn, S. J.; Webb, D.; Yan, J.; Zhang, L. Design and optimization of selective azaindole amide M1 positive allosteric modulators. *Bioorg. Med. Chem. Lett.* **2016**, *26*, 650-5.
- (140) Marlo, J. E.; Niswender, C. M.; Days, E. L.; Bridges, T. M.; Xiang, Y.; Rodriguez, A. L.; Shirey, J. K.; Brady, A. E.; Nalywajko, T.; Luo, Q.; Austin, C. A.; Williams, M. B.; Kim, K.; Williams, R.; Orton, D.; Brown, H. A.; Lindsley, C. W.; Weaver, C. D.; Conn, P. J. Discovery and characterization of novel allosteric potentiators of M1 muscarinic receptors reveals multiple modes of activity. *Mol. Pharmacol.* **2009**, *75*, 577-88.
- (141) Wold, E. A.; Chen, J.; Cunningham, K. A.; Zhou, J. Allosteric Modulation of Class A GPCRs: Targets, Agents, and Emerging Concepts. *J. Med. Chem.* **2018**, *62*, 88-127.
- (142) Bridges, T. M.; Kennedy, J. P.; Cho, H. P.; Breininger, M. L.; Gentry, P. R.; Hopkins, C. R.; Conn, P. J.; Lindsley, C. W. Chemical lead optimization of a pan G(q) mAChR M(1), M(3), M(5) positive allosteric modulator (PAM) lead. Part I: Development of the first highly selective M(5) PAM. *Bioorg. Med. Chem. Lett.* **2010**, *20*, 558-62.
- (143) Melancon, B. J.; Poslusney, M. S.; Gentry, P. R.; Tarr, J. C.; Sheffler, D. J.; Mattmann, M. E.; Bridges, T. M.; Utley, T. J.; Daniels, J. S.; Niswender, C. M.; Conn, P. J.; Lindsley, C. W.; Wood, M. R. Isatin replacements applied to the highly selective, muscarinic M1 PAM ML137: continued optimization of an MLPCN probe molecule. *Bioorg. Med. Chem. Lett.* **2013**, *23*, 412-6.
- (144) Ghoshal, A.; Rook, J. M.; Dickerson, J. W.; Roop, G. N.; Morrison, R. D.; Jalan-Sakrikar, N.; Lamsal, A.; Noetzel, M. J.; Poslusney, M. S.; Wood, M. R.; Melancon, B. J.; Stauffer, S. R.; Xiang, Z.; Daniels, J. S.; Niswender, C. M.; Jones, C. K.; Lindsley, C. W.; Conn, P. J. Potentiation of M1 Muscarinic Receptor Reverses Plasticity Deficits and Negative and Cognitive Symptoms in a Schizophrenia Mouse Model. *Neuropsychopharmacology* **2016**, *41*, 598-610.
- (145) Davoren, J. E.; Garnsey, M.; Pettersen, B.; Brodney, M. A.; Edgerton, J. R.; Fortin, J.-P.; Grimwood, S.; Harris, A. R.; Jenkinson, S.; Kenakin, T.; Lazzaro, J. T.; Lee, C.-W.; Lotarski, S. M.; Nottebaum, L.; O'Neil, S. V.; Popiolek, M.; Ramsey, S.; Steyn, S. J.; Thorn, C. A.; Zhang, L.; Webb, D. Design and Synthesis of  $\gamma$ - and  $\delta$ -Lactam M1 Positive Allosteric Modulators (PAMs): Convulsion and Cholinergic Toxicity of an M1-Selective PAM with Weak Agonist Activity. *J. Med. Chem.* **2017**, *60*, 6649-63.
- (146) Flohr, A.; Hutter, R.; Mueller, B.; Bohnert, C.; Pellisson, M.; Schaffhauser, H. Discovery of the first low-shift positive allosteric modulators for the muscarinic M1 receptor. *Bioorg. Med. Chem. Lett.* **2017**, *27*, 5415-9.
- (147) Alt, A.; Pendri, A.; Bertekap, R. L., Jr.; Li, G.; Benitex, Y.; Nophsker, M.; Rockwell, K. L.; Burford, N. T.; Sum, C. S.; Chen, J.; Herbst, J. J.; Ferrante, M.; Hendricson, A.; Cvijic, M. E.; Westphal, R. S.; O'Connell, J.; Banks, M.; Zhang, L.; Gentles, R. G.; Jenkins, S.; Loy, J.; Macor, J. E. Evidence for Classical Cholinergic Toxicity Associated with Selective Activation of M1 Muscarinic Receptors. *J. Pharmacol. Exp. Ther.* **2016**, *356*, 293-304.
- (148) Lazareno, S.; Dolezal, V.; Popham, A.; Birdsall, N. J. Thiochrome enhances acetylcholine affinity at muscarinic M4 receptors: receptor subtype selectivity via cooperativity rather than affinity. *Mol. Pharmacol.* **2004**, *65*, 257-66.

- (149) Schober, D. A.; Croy, C. H.; Xiao, H.; Christopoulos, A.; Felder, C. C. Development of a Radioligand, [3H]-LY2119620, to Probe the Human M2 and M4 Muscarinic Receptor Allosteric Binding Sites. *Mol. Pharmacol.* **2014**, *86*, 116-23.
- (150) Brady, A. E.; Jones, C. K.; Bridges, T. M.; Kennedy, J. P.; Thompson, A. D.; Heiman, J. U.; Breininger, M. L.; Gentry, P. R.; Yin, H.; Jadhav, S. B.; Shirey, J. K.; Conn, P. J.; Lindsley, C. W. Centrally active allosteric potentiators of the M4 muscarinic acetylcholine receptor reverse amphetamine-induced hyperlocomotor activity in rats. *J. Pharmacol. Exp. Ther.* **2008**, *327*, 941-53.
- (151) Kennedy, J. P.; Bridges, T. M.; Gentry, P. R.; Brogan, J. T.; Kane, A. S.; Jones, C. K.; Brady, A. E.; Shirey, J. K.; Conn, P. J.; Lindsley, C. W. Synthesis and structure-activity relationships of allosteric potentiators of the m(4) muscarinic acetylcholine receptor. *ChemMedChem.* **2009**, *4*, 1600-7.
- (152) Salovich, J. M.; Vinson, P. N.; Sheffler, D. J.; Lamsal, A.; Utley, T. J.; Blobaum, A. L.; Bridges, T. M.; Le, U.; Jones, C. K.; Wood, M. R.; Daniels, J. S.; Conn, P. J.; Niswender, C. M.; Lindsley, C. W.; Hopkins, C. R. Discovery of N-(4-methoxy-7-methylbenzo[d]thiazol-2-yl)isonicotinamide, ML293, as a novel, selective and brain penetrant positive allosteric modulator of the muscarinic 4 (M4) receptor. *Bioorg. Med. Chem. Lett.* **2012**, *22*, 5084-8.
- (153) Wood, M. R.; Noetzel, M. J.; Poslusney, M. S.; Melancon, B. J.; Tarr, J. C.; Lamsal, A.; Chang, S.; Luscombe, V. B.; Weiner, R. L.; Cho, H. P.; Bubser, M.; Jones, C. K.; Niswender, C. M.; Wood, M. W.; Engers, D. W.; Brandon, N. J.; Duggan, M. E.; Conn, P. J.; Bridges, T. M.; Lindsley, C. W. Challenges in the development of an M4 PAM in vivo tool compound: The discovery of VU0467154 and unexpected DMPK profiles of close analogs. *Bioorg. Med. Chem. Lett.* **2017**, *27*, 171-5.
- (154) Bubser, M.; Bridges, T. M.; Dencker, D.; Gould, R. W.; Grannan, M.; Noetzel, M. J.; Lamsal, A.; Niswender, C. M.; Daniels, J. S.; Poslusney, M. S.; Melancon, B. J.; Tarr, J. C.; Byers, F. W.; Wess, J.; Duggan, M. E.; Dunlop, J.; Wood, M. W.; Brandon, N. J.; Wood, M. R.; Lindsley, C. W.; Conn, P. J.; Jones, C. K. Selective activation of M4 muscarinic acetylcholine receptors reverses MK-801-induced behavioral impairments and enhances associative learning in rodents. *ACS Chem. Neurosci.* **2014**, *5*, 920-42.
- (155) Tarr, J. C.; Wood, M. R.; Noetzel, M. J.; Bertron, J. L.; Weiner, R. L.; Rodriguez, A. L.; Lamsal, A.; Byers, F. W.; Chang, S.; Cho, H. P.; Jones, C. K.; Niswender, C. M.; Wood, M. W.; Brandon, N. J.; Duggan, M. E.; Conn, P. J.; Bridges, T. M.; Lindsley, C. W. Challenges in the development of an M4 PAM preclinical candidate: The discovery, SAR, and in vivo characterization of a series of 3-aminoazetidine-derived amides. *Bioorg. Med. Chem. Lett.* **2017**, *27*, 2990-5.
- (156) Lebois, E. P.; Digby, G. J.; Sheffler, D. J.; Melancon, B. J.; Tarr, J. C.; Cho, H. P.; Miller, N. R.; Morrison, R.; Bridges, T. M.; Xiang, Z.; Daniels, J. S.; Wood, M. R.; Conn, P. J.; Lindsley, C. W. Development of a highly selective, orally bioavailable and CNS penetrant M1 agonist derived from the MLPCN probe ML071. *Bioorg. Med. Chem. Lett.* **2011**, *21*, 6451-5.
- (157) Melancon, B. J.; Gogliotti, R. D.; Tarr, J. C.; Saleh, S. A.; Chauder, B. A.; Lebois, E. P.; Cho, H. P.; Utley, T. J.; Sheffler, D. J.; Bridges, T. M.; Morrison, R. D.; Daniels, J. S.; Niswender, C. M.; Conn, P. J.; Lindsley, C. W.; Wood, M. R. Continued optimization of the MLPCN probe ML071 into highly potent agonists of the hM1 muscarinic acetylcholine receptor. *Bioorg. Med. Chem. Lett.* **2012**, *22*, 3467-72.
- (158) Digby, G. J.; Utley, T. J.; Lamsal, A.; Sevel, C.; Sheffler, D. J.; Lebois, E. P.; Bridges, T. M.; Wood, M. R.; Niswender, C. M.; Lindsley, C. W.; Conn, P. J. Chemical modification of the M(1) agonist VU0364572 reveals molecular switches in pharmacology and a bitopic binding mode. *ACS Chem. Neurosci.* **2012**, *3*, 1025-36.

- (159) Trankle, C.; Andresen, I.; Lambrecht, G.; Mohr, K. M2 receptor binding of the selective antagonist AF-DX 384: possible involvement of the common allosteric site. *Mol. Pharmacol.* **1998**, *53*, 304-12.
- (160) Sur, C.; Mallorga, P. J.; Wittmann, M.; Jacobson, M. A.; Pascarella, D.; Williams, J. B.; Brandish, P. E.; Pettibone, D. J.; Scolnick, E. M.; Conn, P. J. N-desmethylozapine, an allosteric agonist at muscarinic 1 receptor, potentiates N-methyl-D-aspartate receptor activity. *Proc. Natl Acad. Sci. U. S. A.* **2003**, *100*, 13674-9.
- (161) Daval, S. B.; Kellenberger, E.; Bonnet, D.; Utard, V.; Galzi, J. L.; Ilien, B. Exploration of the orthosteric/allosteric interface in human M1 muscarinic receptors by bitopic fluorescent ligands. *Mol. Pharmacol.* **2013**, *84*, 71-85.
- (162) Schmitz, J.; van der May, D.; Bermudez, M.; Klöckner, J.; Schrage, R.; Kostenis, E.; Tränkle, C.; Wolber, G.; Mohr, K.; Holzgrabe, U. Dualsteric Muscarinic Antagonists—Orthosteric Binding Pose Controls Allosteric Subtype Selectivity. *J. Med. Chem.* **2014**, *57*, 6739–50.
- (163) Messerer, R.; Kauk, M.; Volpato, D.; Alonso Canizal, M. C.; Klockner, J.; Zabel, U.; Nuber, S.; Hoffmann, C. FRET Studies of Quinolone-Based Bitopic Ligands and Their Structural Analogues at the Muscarinic M1 Receptor. *ACS Chem. Biol.* **2017**, *12*, 833-43.
- (164) Chen, X.; Klöckner, J.; Holze, J.; Zimmermann, C.; Seemann, W. K.; Schrage, R.; Bock, A.; Mohr, K.; Tränkle, C.; Holzgrabe, U.; Decker, M. Rational Design of Partial Agonists for the Muscarinic M1 Acetylcholine Receptor. *J. Med. Chem.* **2015**, *58*, 560-76.
- (165) Kenakin, T. Functional Selectivity through Protean and Biased Agonism: Who Steers the Ship? *Mol. Pharmacol.* **2007**, *72*, 1393-401.
- (166) De Min, A.; Matera, C.; Bock, A.; Holze, J.; Kloeckner, J.; Muth, M.; Traenkle, C.; De Amici, M.; Kenakin, T.; Holzgrabe, U.; Dallanocce, C.; Kostenis, E.; Mohr, K.; Schrage, R. A New Molecular Mechanism To Engineer Protean Agonism at a G Protein–Coupled Receptor. *Mol. Pharmacol.* **2017**, *91*, 348-56.
- (167) Middleton, R. J.; Kellam, B. Fluorophore-tagged GPCR ligands. *Curr. Opin. Chem. Biol.* **2005**, *9*, 517-25.
- (168) Vernall, A. J.; Hill, S. J.; Kellam, B. The evolving small-molecule fluorescent-conjugate toolbox for Class A GPCRs. *Br. J. Pharmacol.* **2014**, *171*, 1073-84.
- (169) Stoddart, L. A.; White, C. W.; Nguyen, K.; Hill, S. J.; Pflieger, K. D., Fluorescence- and bioluminescence-based approaches to study GPCR ligand binding. *Br J Pharmacol* **2016**, *173* (20), 3028-37.
- (170) Jacobson, K. A., Functionalized Congener Approach to the Design of Ligands for G Protein-Coupled Receptors (GPCRs). *Bioconjugate Chem* **2009**, *20* (10), 1816-1835.
- (171) Petrov, R. R.; Ferrini, M. E.; Jaffar, Z.; Thompson, C. M.; Roberts, K.; Diaz, P., Design and evaluation of a novel fluorescent CB2 ligand as probe for receptor visualization in immune cells. *Bioorg. Med. Chem. Lett.* **2011**, *21* (19), 5859-62.
- (172) Leopoldo, M.; Lacivita, E.; Berardi, F.; Perrone, R., Developments in fluorescent probes for receptor research. *Drug Discov. Today* **2009**, *14* (13), 706-712.
- (173) Martikkala, E.; Lehmusto, M.; Lilja, M.; Rozwandowicz-Jansen, A.; Lunden, J.; Tomohiro, T.; Hanninen, P.; Petaja-Repo, U.; Harma, H., Cell-based beta2-adrenergic receptor-ligand binding assay using synthesized europium-labeled ligands and time-resolved fluorescence. *Anal. Biochem* **2009**, *392* (2), 103-9.
- (174) Ma, Z.; Du, L.; Li, M., Toward Fluorescent Probes for G-Protein-Coupled Receptors (GPCRs). *J. Med. Chem.* **2014**, *57* (20), 8187-8203.
- (175) Beijia, M.; Afonso, C. A. M.; Martinho, J. M. G. Synthesis and applications of Rhodamine derivatives as fluorescent probes. *Chem. Soc. Rev.* **2009**, *38*, 2410-33.

- (176) Lipinski, C. A.; Lombardo, F.; Dominy, B. W.; Feeney, P. J. Experimental and computational approaches to estimate solubility and permeability in drug discovery and development settings. *Adv. Drug Deliv. Rev.* **2001**, *46*, 3-26.
- (177) Stoddart, L. A.; Vernall, A. J.; Denman, J. L.; Briddon, S. J.; Kellam, B.; Hill, S. J. Fragment Screening at Adenosine-A3 Receptors in Living Cells Using a Fluorescence-Based Binding Assay. *Chem. Biol.* **2012**, *19*, 1105-15.
- (178) Baker, J. G.; Adams, L. A.; Salchow, K.; Mistry, S. N.; Middleton, R. J.; Hill, S. J.; Kellam, B. Synthesis and characterization of high-affinity 4,4-difluoro-4-bora-3a,4a-diaza-s-indacene-labeled fluorescent ligands for human beta-adrenoceptors. *J. Med. Chem.* **2011**, *54*, 6874-87.
- (179) Jones, L. H.; Randall, A.; Napier, C.; Trevethick, M.; Sreckovic, S.; Watson, J. Design and synthesis of a fluorescent muscarinic antagonist. *Bioorg. Med. Chem. Lett.* **2008**, *18*, 825-7.
- (180) Hern, J. A.; Baig, A. H.; Mashanov, G. I.; Birdsall, B.; Corrie, J. E.; Lazareno, S.; Molloy, J. E.; Birdsall, N. J. Formation and dissociation of M1 muscarinic receptor dimers seen by total internal reflection fluorescence imaging of single molecules. *Proc. Natl. Acad. Sci. U. S. A.* **2010**, *107*, 2693-8.
- (181) Daval, S. B.; Valant, C.; Bonnet, D.; Kellenberger, E.; Hibert, M.; Galzi, J.-L.; Ilien, B. Fluorescent Derivatives of AC-42 To Probe Bitopic Orthosteric/Allosteric Binding Mechanisms on Muscarinic M1 Receptors. *J. Med. Chem.* **2012**, *55*, 2125-43.



# Chapter Two

## **Declaration of Contributions for Chapter Two**

In this chapter the initial concept design for the hybrid ligands and some preliminary synthesis of these compounds is attributed to Dr. Briana J. Davie. The synthesis of all of the ligands presented in this chapter was performed by myself. The pharmacological assaying/evaluation of the aforementioned ligands was also performed by myself, including all analysis. The cloned hM<sub>1</sub>-M<sub>5</sub> muscarinic acetylcholine cell lines used in this work were provided by the laboratory of Dr. Arthur Christopoulos. General guidance in the pharmacological analysis was also provided by Dr. Arthur Christopoulos and Dr. Celine Valant.

# Subtype Selectivity and Efficacy of Iperoxo-BQCA Muscarinic Acetylcholine Receptor Hybrid Ligands

**ABSTRACT:** Agonists for the human M<sub>1</sub> and M<sub>4</sub> muscarinic acetylcholine receptors (mAChRs) are attractive compounds for the treatment of cognitive disorders, such as Alzheimer's disease and schizophrenia. However past efforts to optimise a ligand for selective agonism at any one of the M<sub>1</sub>-M<sub>5</sub> mAChR subtypes has proven to be a significant challenge. Recently, research efforts have demonstrated that hybrid ligands may offer a potential solution to the issue of subtype selectivity. In an attempt to design an M<sub>1</sub> mAChR selective partial agonist by hybridizing an M<sub>1</sub> mAChR selective positive allosteric modulator (BQCA) and a potent agonist (iperoxo), we unexpectedly found that these ligands possessed moderate M<sub>2</sub>/M<sub>4</sub> mAChR selectivity, and that the M<sub>4</sub> mAChR selectivity could be augmented by truncation or removal of the allosteric pharmacophore. Evaluation of truncated derivatives of the hybrid ligands at the M<sub>1</sub>-M<sub>5</sub> mAChR subtypes suggests that the allosteric pharmacophore of iperoxo-based mAChR hybrid ligands plays a negative role in their M<sub>2</sub>/M<sub>4</sub> mAChR selectivity, which arises from addition of the linear *N*-alkyl linker alone, provided the *N*-alkyl chain length is sufficient.

## ■ INTRODUCTION

The human M<sub>1</sub> and M<sub>4</sub> muscarinic acetylcholine receptors (mAChRs) have previously been established as promising targets for the treatment of Alzheimer's disease and schizophrenia.<sup>1-10</sup> Clinical data for the M<sub>1</sub>/M<sub>4</sub> mAChR preferring partial agonist, xanomeline, showed a significant reduction in cognitive impairment in patients with Alzheimer's disease<sup>2-3</sup> and schizophrenia.<sup>4</sup> However, patient dropout rates from the clinical trials to date have been high, due to intolerable gastrointestinal and other cholinergic side-effects.<sup>3</sup> The observed side-

effects have been largely attributed to off-target activity at the related M<sub>2</sub> and M<sub>3</sub> mAChR subtypes.<sup>10-11</sup> The issue of low subtype selectivity is common to most orthosteric mAChR ligands (for example the potent agonist, 4-[(4,5-dihydro-3-isoxazolyl)oxy]-*N,N,N*-trimethyl-2-butyln-1-aminium iodide (iperoxo) (**1**)) and putatively arises due to the high degree of conservation of the orthosteric site of the mAChRs.<sup>12</sup> However the mAChRs possess as many as two spatially distinct ‘allosteric’ sites that are less conserved and thus offer more opportunities for attaining greater receptor subtype selectivity.<sup>13</sup> Allosteric modulators targeting these sites are of particular interest in the treatment of CNS disorders,<sup>14</sup> as they can modulate signaling dependent on the presence of endogenous ligand and thus maintain the normal inter-neuronal signaling patterns.<sup>15</sup> 1-(4-Methoxybenzyl)-4-oxo-1,4-dihydro-3-quinolinecarboxylic acid (BQCA) (**2**) is a first generation M<sub>1</sub> mAChR selective positive allosteric modulator (PAM).<sup>16</sup> Despite the successive improvements in the generations of compounds based on **2**, even in structurally diverse M<sub>1</sub> mAChR PAMs, the affinities of these compounds have remained in the low micromolar range,<sup>17-19</sup> suggesting that mAChR allosteric sites may be intrinsically weakly interacting binding sites. However, in the past decade several groups have reported hybrid ligands for the mAChRs that consist of two ligands (or more generally ‘pharmacophores’) that are joined by a molecular linker.<sup>20-21</sup> Many of these hybrid ligands are reported to engage the mAChRs both allosteric and orthosterically, concurrently or concomitantly, referred to as ‘bitopic’ or ‘dualsteric’ receptor binding.<sup>22-29</sup> Bitopic hybrid ligands offer an attractive solution to the issues of low potency, affinity and/or selectivity of either allosteric or orthosteric ligands as they engage both allosteric and orthosteric sites and so can, in principal, possess some of the favourable traits of both types of ligands (i.e. selectivity and potency).<sup>20-21</sup> This carries the caveat that bitopic hybrid ligands lose the temporally and spatially distinct binding that characterises allosteric ligands, and with it the favourable properties it may offer in the treatment of CNS disorders with regard to maintaining

normal inter-neuronal signaling patterns.<sup>20-21</sup> However, the partial clinical success of xanomeline clearly demonstrates that, provided selectivity can be maintained, an orthosteric binding mechanism does not exclude the potential for clinical viability.<sup>2-3</sup> Additionally hybrid ligands are typically larger molecules which may limit their blood-brain barrier (BBB) penetration, however this is not a significant consideration for this proof-of-concept study.

The molecular mechanisms of receptor-ligand binding that have been proposed to explain the observed pharmacology of these hybrid ligands are complex, in some cases comprising of multiple distinctive allosteric and orthosteric binding modes that can each interact with one another.<sup>20, 23, 27, 29-33</sup> To date, rational hybrid ligand design strategies have focused on the conjoining of known allosteric and orthosteric pharmacophores with an appropriate length molecular linker.<sup>21-22, 24, 29, 34</sup> This approach has been used to show that conjoining of the M<sub>2</sub> mAChR selective negative allosteric modulator (NAM) ‘W-84’ and an orthosteric agonist oxotremorine, predictably produces partial agonist hybrids, with selective an apparent preference for M<sub>2</sub> mAChR similar to the parent allosteric ligand.<sup>22</sup> Similarly, several studies have shown that the pharmacology of mAChR hybrid ligands can be reconstituted by the coincubation of its monomeric units.<sup>23, 25, 34</sup> This has prompted the suggestion that it may be possible to rationally design selective hybrid ligand full agonists for the mAChRs, by combining a selective PAM and a highly efficacious agonist. For example, compound **1**, a highly efficacious mAChR agonist,<sup>35</sup> that is selectively potentiated by the PAM, **2** at the M<sub>1</sub> mAChR (Figure 1).<sup>16</sup>

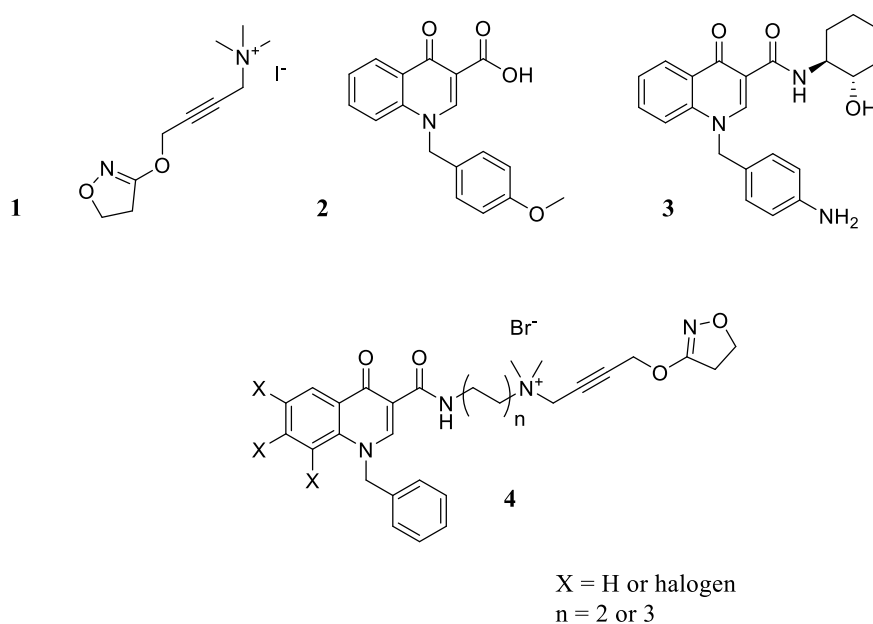


**Figure 1.** Chemical structures of iperexo (4-[(4,5-dihydro-3-isoxazolyl)oxy]-*N,N,N*-trimethyl-2-butyne-1-aminium iodide) (**1**), a subtype non-selective mAChR agonist, BQCA (1-(4-methoxybenzyl)-4-oxo-1,4-dihydro-3-quinolinecarboxylic acid) (**2**), an M<sub>1</sub> mAChR selective allosteric modulator, BQCA-derivative (1-(4-aminobenzyl)-*N*-((1*S*,2*S*)-2-hydroxycyclohexyl)-4-oxo-1,4-dihydroquinoline-3-carboxamide) (**3**), presumably an M<sub>1</sub> mAChR selective allosteric modulator, and a general structure of the series of M<sub>2</sub>/M<sub>4</sub> mAChR selective BQCA-iperexo hybrid ligands previously reported (**4**).<sup>24, 34</sup>

Recently, several hybrid ligands derived from **1** and **2** have been reported (e.g. compound **4**, Figure 1).<sup>24, 34</sup> In these studies, compound **4** and analogs behaved as partial agonists, contradictory to what might be expected, given the potent functional response observed with the incubation of the constituent monomers.<sup>24, 34</sup> However, the partial agonism of **4** and its derivatives is consistent with a steric clash between the linker and several conserved tyrosine residues (Y<sup>3.34</sup>, Y<sup>6.51</sup> and Y<sup>7.39</sup>) that occlude the mAChR orthosteric site and are important for receptor activation,<sup>36</sup> and so is likely an unavoidable consequence of the introduction of the linker. Compound **4** and its derivatives have not been evaluated for their mAChR subtype selectivity, and so a comparison to the selectivity of the constituent allosteric monomer cannot be made.<sup>24, 34</sup> However, discrepancies between the optimised structures of **4** compared with

monomer **2** tend to suggest that the allosteric pharmacophore of **4** is unable to bind homologously to its constituent allosteric monomer, **2**, or act cooperatively with the orthosteric pharmacophore, iperoxo.<sup>24, 34, 37</sup> A possible explanation for this is that the linker attachment point of **4** restricts the conformation of the allosteric pharmacophore, prohibiting it from engaging the allosteric site homologously to its constituent allosteric monomer. A previous SAR study has shown that substitution of the 3-carboxylic acid is generally detrimental to the activity of **2**.<sup>37</sup> This result suggests that attachment of the linker to the benzylic ‘pendant’ moiety of **2** (Figure 1) may be a more advantageous compared to the 3-carboxylic acid attachment point, that has been previously explored.<sup>24, 34</sup> Reported here is a series of hybrid ligands consisting of **1** and a closely related analogue of BQCA, **3**, attached by an amide linker at the unexplored 4-position of the benzylic ‘pendant’.

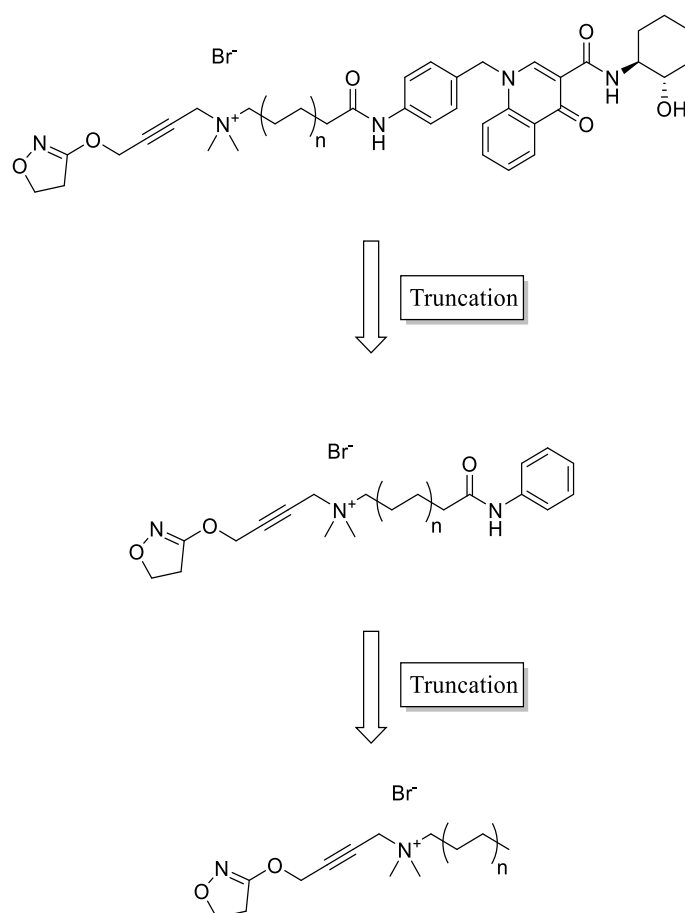


**Figure 2.** Proposed molecular truncations to the hybrid ligands for comparative structure-function analysis at the  $\text{M}_1$ - $\text{M}_5$  mAChRs.

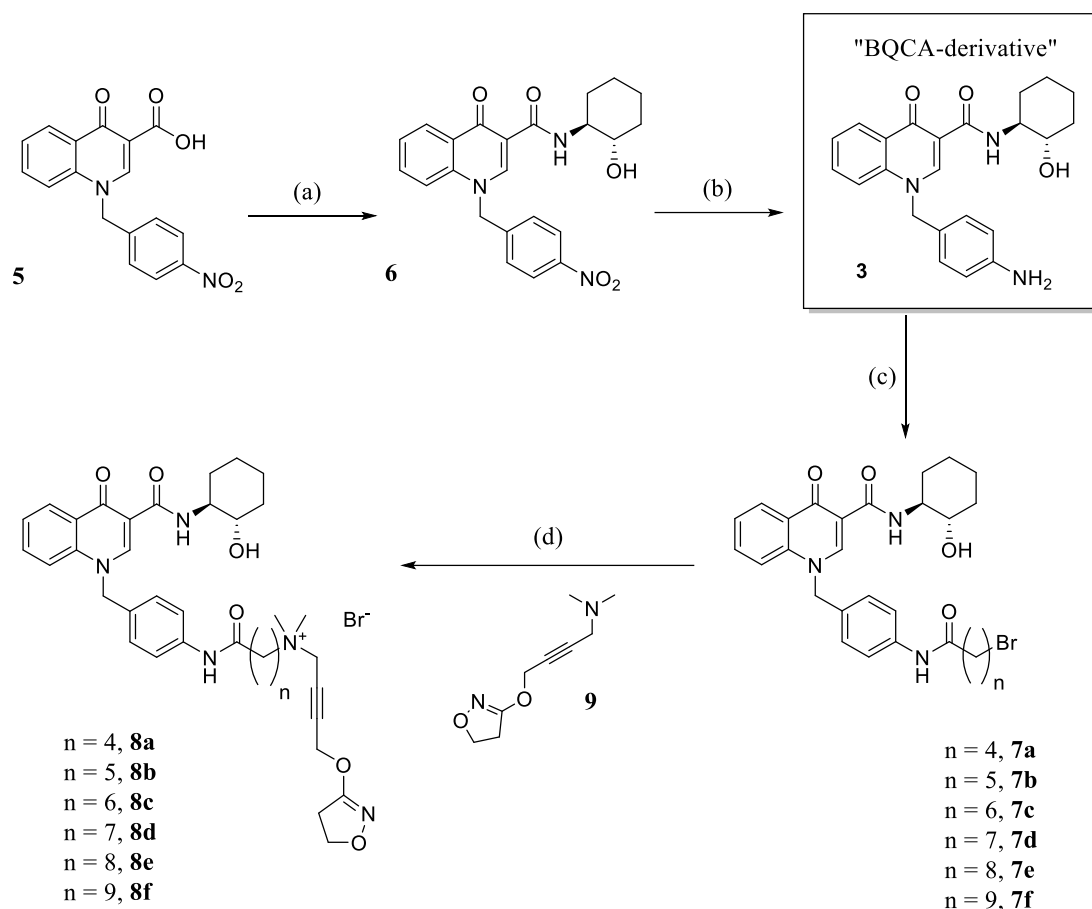
Examination of the pharmacology of our hybrid ligands showed that they possess moderate M<sub>2</sub>/M<sub>4</sub> mAChR selectivity at linker lengths with non-optimal potency and maximum response. To determine the structural features of hybrid ligands based on **1** that affect mAChR subtype selectivity we synthesised a series of truncated hybrid ligands (Figure 2), and evaluated them at the M<sub>1</sub>-M<sub>5</sub> mAChRs by pERK 1/2 and radioligand binding assays.

## ■ RESULTS AND DISCUSSION

**Chemistry.** We initially planned to use BQCA (**2**) as the allosteric pharmacophore for the hybrid ligands. The synthetic route retained an ethyl ester as a protecting group throughout the synthesis, prior to being hydrolysed in the final step. However, the target hybrid ligands were unstable under the hydrolytic conditions necessary to de-protect the ester. Accordingly, it was decided that the 3-carboxylic acid of **2** would be functionalised to the corresponding (1*S*,2*S*)-2-hydroxycyclohexyl amide derivative **3**. The 3-carboxylic acid of **2** has been shown to be non-essential for its PAM / agonist activity and the (1*S*,2*S*)-2-hydroxycyclohexyl amide moiety has previously been shown to be beneficial for both efficacy and functional cooperativity with acetylcholine, in related analogues.<sup>17-19, 37</sup> The incorporation of the 2-hydroxycyclohexyl amide moiety into our design (in place of a carboxylic acid) obviated the associated problems with the protection and deprotection steps. This minor adjustment allows amide coupling reagents to be used to attach the linker to **3**, without the need to deprotect the ester. This approach was found to be applicable to all linker lengths synthesised.



**Scheme 1. Synthesis of hybrid ligands consisting of iperoxo and a derivative of BQCA connected by a polymethylene amide linker<sup>a</sup>**

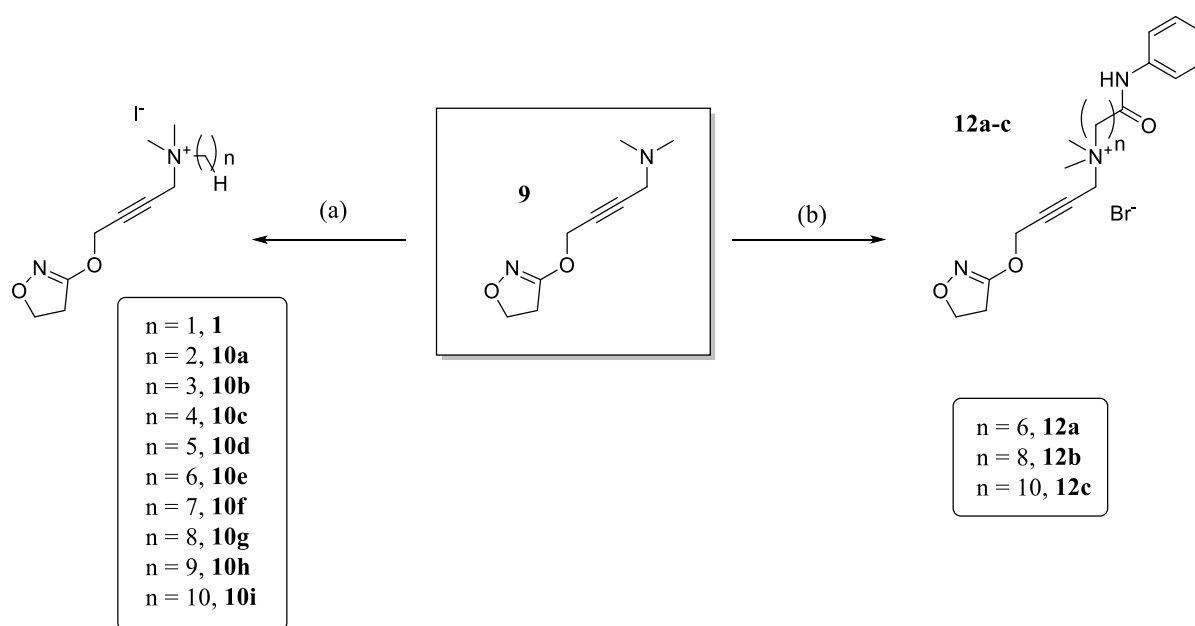


<sup>a</sup>Reagents and conditions: (a) (1*S*,2*S*)-2-aminocyclohexan-1-ol HCl, HCTU, DIPEA, 1:1 DMF:DCM, rt, 75%; (b) Pd/C, H<sub>2</sub> (1 atm), DMF, rt, 67%; (c) bromoalkanoic acid, HCTU, DIPEA, 1:1 DMF:DCM, rt, 58–95%; (d) **9**, DIPEA, ACN, reflux, 9–40%.

The synthesis of **5** was performed according the general methods previously described for the synthesis of related analogues of **2**.<sup>37–38</sup> Compound **5** was then amide coupled to (1*S*,2*S*)-2-aminocyclohexan-1-ol using HCTU coupling reagent in DCM:DMF (1:1), with DIPEA as the base to form compound **6**. Coupling of the terminal-bromoalkanoic acids to the aromatic amine of **3** was achieved again using HCTU. The synthesis of **9** was carried out according to a previously reported method.<sup>39</sup> Synthesis of products **8a–f** was achieved by refluxing the bromoalkanamide intermediates **7a–f** with **9** in ACN and DIPEA as the base. The yields for

compounds **8a-f** were lower than expected due to competing elimination and hydrolysis reactions of the bromoalkanamides. Hydrolysis of the bromoalkanamides could be limited by the use of dry solvents however the elimination side reaction was more difficult to avoid because of the higher temperatures required to promote quaternisation of iperoxo-base, **9**. Ultimately the yields were deemed acceptable for producing sufficient quantities of these compounds for initial proof-of-concept pharmacological evaluation.

**Scheme 2. Synthesis of truncated hybrid ligands and substituted analogs<sup>a</sup>**



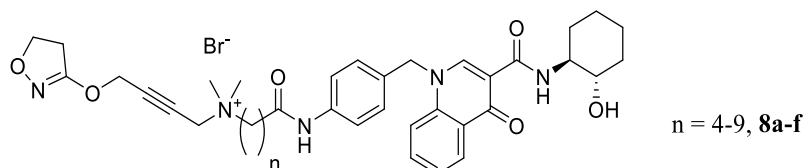
<sup>a</sup>Reagents and conditions: (a) *N*-alkyl iodide, KI:K<sub>2</sub>CO<sub>3</sub> (1:1) cat., ACN, reflux, 31–75%; (b) bromoalkanamide (**11a-c** Supplementary Information), ACN, DIPEA, reflux, 32–64%.

*N*-Alkylation of **9** to form products **1** and **10a-i** was carried out according the method described by Messerer *et al.*<sup>34</sup> Compounds **11a-c** were prepared employing HCTU coupling reagent (Supplementary Information). Synthesis of products **12a-c** was achieved as for **8a-f**, by refluxing **11a-c** with **9** and DIPEA in ACN. Starting material and other minor-byproducts were separable from the product by flash column chromatography (FCC), using a small mass to product ratio of silica, or by preparative HPLC.

**Evaluation of the hybrid ligands at the M<sub>1</sub>-M<sub>5</sub> mAChRs.** Hybrid ligands **8a-f** were first evaluated at the M<sub>1</sub> mAChR by ERK1/2 peak phosphorylation assay in Flp-In-CHO cells over expressing the M<sub>1</sub> mAChR, to determine the optimal linker length for the hybrids in terms of potency and maximum response. The ERK1/2 assay was chosen because ERK phosphorylation is a downstream effector of many pathways coupled to the mAChRs, including both G<sub>i</sub> and G<sub>s</sub> G protein activation. Thus, the pERK1/2 assay allows both G<sub>i</sub> and G<sub>s</sub> coupled mAChR subtypes to be evaluated and compared using a single assay type. Consistent with previously reported mAChR hybrid ligands (e.g. compound **4**) we found the hybrid ligands to behave as partial agonists, with the C6-C8 polymethylene linkers, **8c-e**, to be optimal, in the sense that they possessed higher maximum response and potency values than shorter or longer linker lengths evaluated at the M<sub>1</sub> mAChR.<sup>22, 24, 26, 28-29, 34</sup> Accordingly, compounds **8c-e** were then evaluated at the remaining M<sub>2</sub>-M<sub>5</sub> mAChRs in Flp-In-CHO cells (M<sub>2</sub>, M<sub>4</sub>-M<sub>5</sub> mAChRs) or CHO-K1 (M<sub>3</sub> mAChR) by the same pERK 1/2 concentration-response assay. The binding affinities of **8c-e**, at the M<sub>1</sub>-M<sub>5</sub> mAChRs were also measured in the same cell lines by competition radioligand binding assay with [<sup>3</sup>H]NMS. From these measurements of pERK 1/2 response and affinity we were also able to determine the efficacy of **8c-e** at the M<sub>1</sub>-M<sub>5</sub> mAChRs.

Compounds **8c-e** displayed no improvement in selectivity towards the M<sub>1</sub> mAChR over **1**, contradictorily showing a significant decrease in efficacy at the M<sub>1</sub> versus M<sub>2</sub> or M<sub>4</sub> mAChRs. Surprisingly the non-optimal linker hybrid, **8e**, displayed significant differences in efficacy between the M<sub>2</sub> or M<sub>4</sub> versus the M<sub>1</sub>/M<sub>3</sub>/M<sub>5</sub> mAChRs (Table 1). These observations were consistent with those of related mAChR hybrid ligands that also have shown preferential attenuation of efficacy at the G<sub>as</sub> coupled M<sub>1</sub>/M<sub>3</sub>/M<sub>5</sub> mAChRs versus the G<sub>ai</sub> coupled M<sub>2</sub>/M<sub>4</sub> mAChRs at non-optimal linker lengths.<sup>33</sup>

**Evaluation of the truncated hybrid ligands at the M<sub>1</sub>-M<sub>5</sub> mAChRs.** To examine the roles of the structural features of the **8c-e** in mAChR subtype selectivity a series of truncated hybrid ligands, **10a-i** and **12a-c** (Scheme 2), was designed and synthesised to identify regions of the ligand important for selectivity and potency. We first wished to ascertain that **3** maintained functional cooperativity with **1**, comparable to related analogues in the literature. Interaction assays of the allosteric monomer **3** and orthosteric monomer **1** were performed (Supplementary Information) and the cooperativity of **3** with **1** was found to be comparable to related analogues in the literature ( $\log \alpha = 2.20 \pm 0.30$  and  $\log \alpha\beta = 1.30 \pm 0.20$ ).<sup>37</sup> Our hybrid ligands, **8a-f**, were first examined by pERK 1/2 assay at the M<sub>1</sub> mAChR to evaluate which linker lengths gave the optimal potency and maximum response. The most potent hybrid ligands with the highest maximum response, **8c-e**, were then examined at the M<sub>1</sub>-M<sub>5</sub> mAChRs by pERK 1/2 and competitive radioligand binding assay. From the pERK 1/2 and radioligand binding data we then calculated the efficacy of **8c-e**.

**Table 1.** Functional and binding data for hybrid ligands (**8a-f**) at the M<sub>1</sub>–M<sub>5</sub> mAChRs

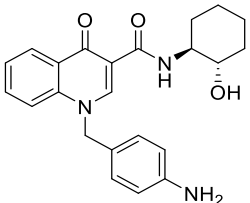
Cpd	n	mAChR	pEC <sub>50</sub> <sup>a</sup>	E <sub>max</sub> <sup>b</sup>	pK <sub>i</sub> <sup>c</sup>	log τ <sub>c</sub> <sup>d</sup>
<b>1</b> (IXO)	n/a	M <sub>1</sub>	9.46 ± 0.35	100 ± 2	7.62 ± 0.13	1.89 ± 0.10
	n/a	M <sub>2</sub>	10.23 ± 0.19	100 ± 4	8.70 ± 0.02	2.02 ± 0.15
	n/a	M <sub>3</sub>	9.42 ± 0.31	100 ± 2	6.84 ± 0.14	1.84 ± 0.13
	n/a	M <sub>4</sub>	10.43 ± 0.17	100 ± 2	8.18 ± 0.07	2.04 ± 0.12
	n/a	M <sub>5</sub>	9.52 ± 0.16	100 ± 4	7.83 ± 0.23	1.67 ± 0.11
<b>8a</b>	4	M <sub>1</sub>	7.09 ± 0.07	77 ± 3	-	-
<b>8b</b>	5	M <sub>1</sub>	7.13 ± 0.07	88 ± 3	-	-
<b>8c</b>	6	M <sub>1</sub>	7.85 ± 0.07	98 ± 3	7.32 ± 0.22	0.66 ± 0.11 <sup>*†e</sup>
	6	M <sub>2</sub>	9.04 ± 0.06	103 ± 2	7.49 ± 0.12	1.65 ± 0.05
	6	M <sub>3</sub>	8.68 ± 0.08	89 ± 2	6.29 ± 0.14	1.00 ± 0.02
	6	M <sub>4</sub>	9.27 ± 0.08	96 ± 3	7.30 ± 0.18	1.92 ± 0.12
	6	M <sub>5</sub>	8.10 ± 0.20	86 ± 6	6.95 ± 0.07	0.63 ± 0.09 <sup>†e</sup>
<b>8d</b>	7	M <sub>1</sub>	7.72 ± 0.06	100 ± 2	6.84 ± 0.13	1.02 ± 0.14 <sup>*†e</sup>
	7	M <sub>2</sub>	8.93 ± 0.07	107 ± 2	6.86 ± 0.18	2.29 ± 0.13
	7	M <sub>3</sub>	8.11 ± 0.09	93 ± 3	5.64 ± 0.14	1.04 ± 0.02
	7	M <sub>4</sub>	8.95 ± 0.09	94 ± 3	6.63 ± 0.14	2.07 ± 0.12
	7	M <sub>5</sub>	7.96 ± 0.16	71 ± 4	6.33 ± 0.12	0.81 ± 0.08
<b>8e</b>	8	M <sub>1</sub>	7.56 ± 0.08	97 ± 4	6.75 ± 0.19	0.76 ± 0.13 <sup>*†e</sup>
	8	M <sub>2</sub>	8.48 ± 0.05	107 ± 2	6.81 ± 0.14	1.81 ± 0.12
	8	M <sub>3</sub>	7.55 ± 0.11	66 ± 4	5.82 ± 0.20	0.66 ± 0.04 <sup>†e</sup>
	8	M <sub>4</sub>	8.67 ± 0.07	88 ± 2	6.46 ± 0.22	1.73 ± 0.12
	8	M <sub>5</sub>	7.77 ± 0.20	58 ± 5	6.33 ± 0.15	0.21 ± 0.07 <sup>†e</sup>
<b>8f</b>	9	M <sub>1</sub>	7.03 ± 0.14	74 ± 3	-	-

<sup>a</sup>pEC<sub>50</sub> values are the negative logarithm of the concentration of a ligand that was able to elicit 50 % the maximum achievable response by that ligand as determined by fitting a 3-parameter concentration-response curve to the data. <sup>b</sup>E<sub>max</sub> values are the maximum response measured by a ligand, as a percentage of the maximum response achievable by the full agonist, iperxo (IXO, **1**). <sup>c</sup>pK<sub>i</sub> values are the negative logarithm of the inhibition constant for each ligand, as determined by competition radioligand binding assays with [<sup>3</sup>H]NMS and fitting the data to a one-site inhibition binding model. <sup>d</sup>Log τ<sub>c</sub> is the ligand efficacy, corrected for receptor expression, as determined by fitting the functional ERK 1/2 phosphorylation concentration-response data for each ligand to an operational model of agonism and constraining the model by the measured values of affinity for each ligand at each of the respective mAChR subtype. <sup>e</sup>\* and <sup>†</sup> denote a statistically significant difference in efficacy versus the M<sub>2</sub> or M<sub>4</sub> mAChRs, respectively. Data was statistically analysed using Bonferroni's multiple comparison test, 2-way ANOVA. Values not measured are denoted '-'. Data represent the mean ± S.E. of 3 independent experiments performed in duplicate.

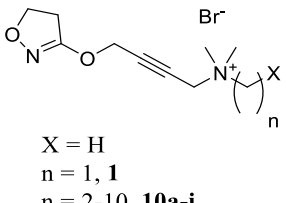
The hybrid ligands, **8a-f**, displayed the highest potency and maximum response at the M<sub>1</sub> mAChR at linker lengths of C6-C8 carbons, **8c-e**. The hybrid ligands were generally

partial agonists with potencies ranging from approximately 100 nM to 10 nM, at the M<sub>1</sub> mAChR. When compounds **8c-e** were evaluated at the remaining M<sub>2</sub>-M<sub>5</sub> mAChR subtypes they displayed a wider range on potencies from approximately 100 nM to 1 nM, and a range of affinities from approximately 3 μM to 30 nM. The hybrid ligand with the highest potency was **8c** which had a pEC<sub>50</sub> of 9.27 ± 0.08 at the M<sub>4</sub> mAChR. Unfortunately none of the hybrid ligands evaluated at the M<sub>1</sub>-M<sub>5</sub> mAChRs possessed any selectivity for the M<sub>1</sub> mAChR, instead in fact displaying generally lower efficacy at the M<sub>1</sub>/M<sub>3</sub>/M<sub>5</sub> mAChRs versus the M<sub>2</sub>/M<sub>4</sub> mAChRs, relative to iperoxo, **1**. This reduction in efficacy at the M<sub>1</sub>/M<sub>3</sub>/M<sub>5</sub> mAChRs interestingly results in some slight selectivity for the M<sub>2</sub>/M<sub>4</sub>, and this is most pronounced in the least potent and least efficacious hybrid ligand, **8e**. To examine the structural features responsible for this preference for the M<sub>2</sub>/M<sub>4</sub> mAChRs over the M<sub>1</sub>/M<sub>3</sub>/M<sub>5</sub> mAChRs at the level of efficacy, we then examined the truncated hybrid ligands, **10a-i** and **12a-c** by pERK 1/2 concentration-response functional assay at the M<sub>1</sub> mAChR. Representative compounds bearing C6, C8 and C10 linker lengths, were then examined at the M<sub>2</sub> – M<sub>5</sub> mAChRs by functional and radioligand binding assay to evaluate their selectivity.

**Table 2.** Functional and binding data for the truncated hybrid ligands **3**, **10a-i**, **12a-c** at the M<sub>1</sub>-M<sub>5</sub> mAChRs

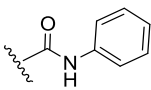


**3**



X = H  
n = 1, **1**  
n = 2-10, **10a-i**

X = N-phenylamide =



n = 6, 8 or 10, **12a-c**

Cpd	n	X	mAChR	pEC <sub>50</sub> <sup>a</sup>	E <sub>max</sub> <sup>b</sup>	pK <sub>i</sub> <sup>c</sup>	Log τ <sub>c</sub>
<b>3</b>	n/a	n/a	M <sub>1</sub>	6.19 ± 0.12	72 ± 4	5.64 ± 0.38	0.57 ± 0.11
<b>10a</b>	2	H	M <sub>1</sub>	7.80 ± 0.05	68 ± 2	-	-
<b>10b</b>	3	H	M <sub>1</sub>	7.35 ± 0.05	70 ± 2	-	-
<b>10c</b>	4	H	M <sub>1</sub>	7.32 ± 0.11	67 ± 5	-	-
<b>10d</b>	5	H	M <sub>1</sub>	6.58 ± 0.11	79 ± 5	-	-

<b>10e</b>	6	H	M <sub>1</sub>	7.78 ± 0.17	58 ± 6	5.63 ± 0.14	1.92 ± 0.26
			M <sub>2</sub>	8.01 ± 0.21	85 ± 6	6.51 ± 0.23	1.51 ± 0.22
			M <sub>3</sub>	7.52 ± 0.18	89 ± 6	5.60 ± 0.23	1.25 ± 0.25
			M <sub>4</sub>	8.32 ± 0.14	83 ± 3	6.19 ± 0.04	2.12 ± 0.13
			M <sub>5</sub>	7.67 ± 0.22	71 ± 6	6.14 ± 0.04	1.48 ± 0.23
<b>10f</b>	7	H	M <sub>1</sub>	7.13 ± 0.18	56 ± 4	-	-
<b>10g</b>	8	H	M <sub>1</sub>	7.72 ± 0.38	28 ± 2	5.70 ± 0.14	1.73 ± 0.20 <sup>†e</sup>
			M <sub>2</sub>	7.23 ± 0.28	62 ± 6	5.93 ± 0.22	1.30 ± 0.30
			M <sub>3</sub>	7.71 ± 0.47	31 ± 6	5.44 ± 0.23	1.43 ± 0.34 <sup>*†e</sup>
			M <sub>4</sub>	7.95 ± 0.22	61 ± 4	5.70 ± 0.26	2.22 ± 0.25
			M <sub>5</sub>	7.08 ± 0.23	55 ± 5	5.49 ± 0.17	1.53 ± 0.24
<b>10h</b>	9	H	M <sub>1</sub>	5.83 ± 0.45	8 ± 3	-	-
<b>10i</b>	10	H	M <sub>1</sub>	nd	nd	5.83 ± 0.17	-3
			M <sub>2</sub>	6.36 ± 0.22	38 ± 7	6.33 ± 0.38	0.09 ± 0.52 <sup>†e</sup>
			M <sub>3</sub>	nd	nd	6.03 ± 0.38	-3
			M <sub>4</sub>	7.05 ± 0.12	37 ± 6	5.61 ± 0.28	1.60 ± 0.22 <sup>*e</sup>
			M <sub>5</sub>	nd	nd	5.09 ± 0.12	-3
<b>12a</b>	6	<i>N</i> -phenylamide	M <sub>1</sub>	6.49 ± 0.18	19 ± 2	4.82 ± 0.06	1.43 ± 0.18 <sup>*†e</sup>
			M <sub>2</sub>	6.75 ± 0.24	58 ± 6	5.33 ± 0.06	1.55 ± 0.31
			M <sub>3</sub>	6.43 ± 0.23	29 ± 4	4.38 ± 0.10	1.49 ± 0.23 <sup>†e</sup>
			M <sub>4</sub>	6.65 ± 0.14	50 ± 4	4.69 ± 0.09	1.95 ± 0.14
			M <sub>5</sub>	5.89 ± 0.08	62 ± 3	4.77 ± 0.11	1.05 ± 0.08
<b>12b</b>	8	<i>N</i> -phenylamide	M <sub>1</sub>	7.11 ± 0.09	64 ± 3	5.87 ± 0.08	0.99 ± 0.09 <sup>†e</sup>
			M <sub>2</sub>	7.70 ± 0.12	92 ± 4	6.50 ± 0.07	1.27 ± 0.17
			M <sub>3</sub>	7.23 ± 0.08	75 ± 3	5.40 ± 0.11	1.27 ± 0.08
			M <sub>4</sub>	7.74 ± 0.09	88 ± 3	5.93 ± 0.06	1.80 ± 0.09
			M <sub>5</sub>	7.29 ± 0.15	72 ± 4	5.31 ± 0.10	1.93 ± 0.15
<b>12c</b>	10	<i>N</i> -phenylamide	M <sub>1</sub>	6.95 ± 0.42	7 ± 2	5.92 ± 0.08	-0.79 ± 0.11 <sup>*†e</sup>
			M <sub>2</sub>	7.72 ± 0.17	73 ± 5	5.97 ± 0.13	1.09 ± 0.13
			M <sub>3</sub>	7.72 ± 0.42	18 ± 3	5.29 ± 0.11	-0.58 ± 0.23 <sup>*†e</sup>
			M <sub>4</sub>	7.66 ± 0.08	74 ± 2	5.62 ± 0.09	1.58 ± 0.09
			M <sub>5</sub>	6.29 ± 0.25	18 ± 2	5.56 ± 0.10	-0.51 ± 0.06 <sup>*†e</sup>

<sup>a</sup>pEC<sub>50</sub> values are the negative logarithm of the concentration of a ligand that was able to elicit 50% the maximum achievable response by that ligand as determined by fitting a 3-parameter concentration-response curve to the data. <sup>b</sup>E<sub>max</sub> values are the maximum response measured by a ligand, as a percentage of the maximum response achievable by the full agonist, iperoxo (IXO, **1**). <sup>c</sup>pK<sub>i</sub> values are the negative logarithm of the inhibition constant for each ligand, as determined by competition radioligand binding assays with [<sup>3</sup>H]NMS and fitting the data to a one-site inhibition binding model. <sup>d</sup>Log τ<sub>c</sub> is the ligand efficacy (corrected for receptor expression) as determined by fitting the functional ERK 1/2 phosphorylation concentration-response data for each ligand to an operational model of agonism and constraining the model by the measured values of affinity for each ligand at each of the respective mAChR subtype. Instances where no ligand efficacy was observed Log τ<sub>c</sub> was fixed to -3. <sup>e</sup>\* and <sup>†</sup> denote a statistically significant difference in efficacy versus the M<sub>2</sub> or M<sub>4</sub> mAChRs, respectively. Data was statistically analysed using Bonferroni's multiple comparison test, 2-way ANOVA. Values not measured are denoted '-'. Compounds which gave no determinable response in the specified assay are denoted 'nd'. Data represent the mean ± S.E. of 3 independent experiments performed in duplicate.

Generally, the truncated hybrid ligands, **10a-i** and **12a-c**, possessed a consistent affinity of 1-10  $\mu$ M across the M<sub>1</sub>-M<sub>5</sub> mAChR subtypes while the potency and maximum response values varied more prominently between ligands and mAChR subtypes (Figure 4, Table 2). The maximum response of **10a-i** was dependent only on the linker length of the ligand, with the response decreasing as linker length increased (Table 2). The longest linker derivative, **10i**, gave a response so low at the M<sub>1</sub>/M<sub>3</sub>/M<sub>5</sub> mAChR that a reliable measurement could not be distinguished from baseline (Table 2). Interestingly, the efficacy of **10i** (IXO-C10), was also found to be significantly higher at the M<sub>4</sub> mAChR compared to the M<sub>2</sub> mAChR, while approximately maintaining efficacy with **1** at the M<sub>4</sub> mAChR (Table 1). In contrast, the *N*-phenyl amide bearing truncated hybrids, **12a-c**, displayed an optimal linker length, similar to the hybrid ligands, **8a-f**. The optimal linker length was found to be the C8 derivative, **12b**, that gave the greatest potency and maximum response of this subset of compounds, **12a-c**, at the M<sub>1</sub>-M<sub>5</sub> mAChRs (Table 2). The C10 linker length truncated hybrid ligands, **10i** (IXO-C10) and **12c** (IXO-C10-phen), both displayed comparably greater selectivity for the M<sub>2</sub>/M<sub>4</sub> > M<sub>1</sub>/M<sub>3</sub>/M<sub>5</sub> mAChRs than the C6 or C8 ligands, **8c,e** (hybrid-C6, hybrid-C8), **10e,g** (IXO-C6, IXO-C8), and **12a,b** (IXO-C6-phen, IXO-C8-phen).



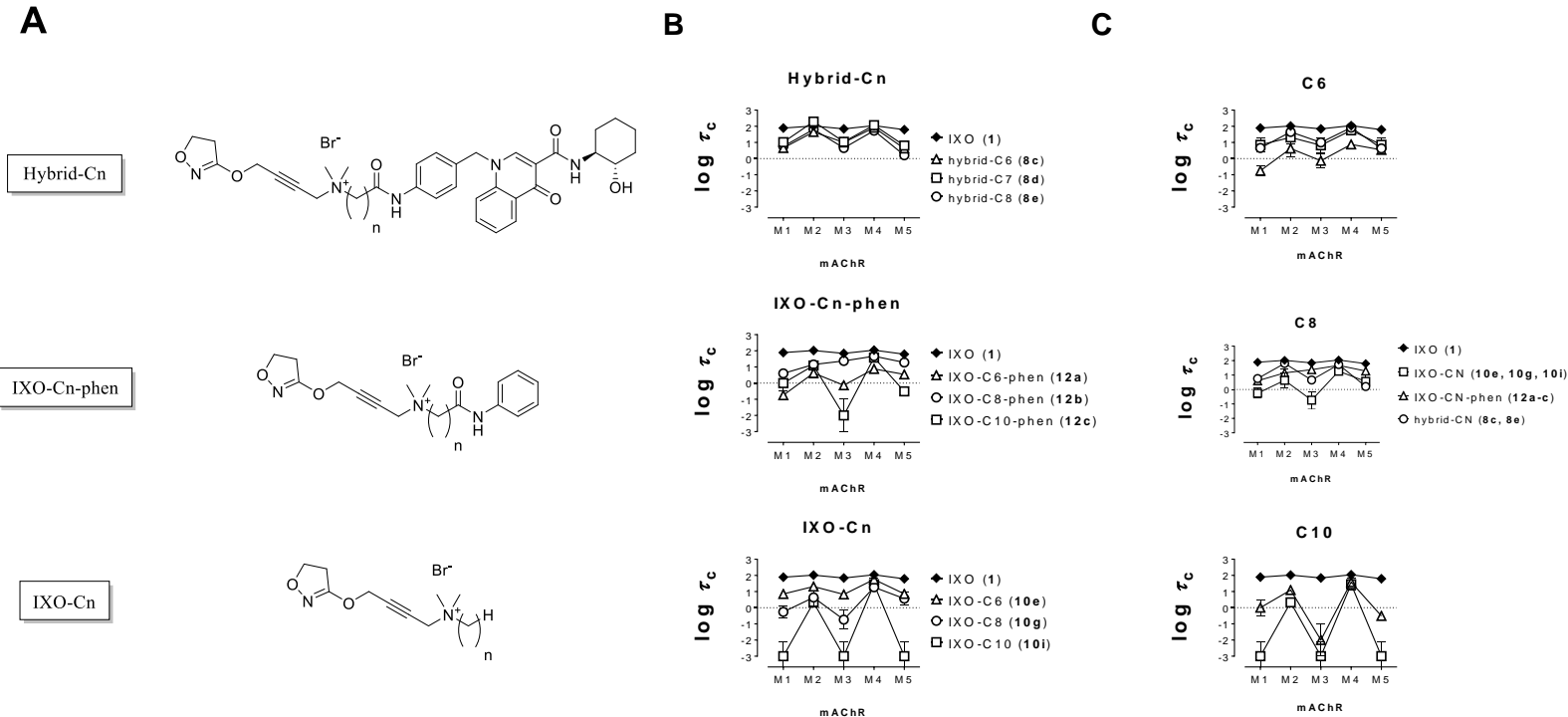


**Figure 4. Effect of terminal substituent and linker length on ligand efficacy of hybrid and truncated hybrid ligands at the M<sub>1</sub>-M<sub>5</sub> mAChR subtypes.** (A) Generalised structures of hybrid ligands ('hybrid-Cn'), and the truncated hybrid ligands ('IXO-Cn-phen' and 'IXO-Cn'). The graphs show (B, top) compounds with **3** as the terminal substituent (hybrid-Cn), (B, middle) truncated compounds with and *N*-phenyl amide as the terminal substituent (IXO-Cn-phen), (B, bottom) truncated compounds with no terminal substituent (IXO-Cn). (C, top) shows the compounds bearing six (C6) linear polymethylene units in their linker (**8c**, **10e**, **12a**), (C, middle) eight (C8) units (**8e**, **10g**, **12b**) and (C, bottom) ten (C10) units (**10i**, **12c**). Log  $\tau_c$  is the ligand efficacy, corrected for receptor expression, as determined by fitting the functional ERK 1/2 phosphorylation concentration-response data for each ligand to an operational model of agonism and constraining the model by the measured values of affinity (Table 1, Table 2) for each ligand at each of the M<sub>1</sub>-M<sub>5</sub> mAChR subtypes. Each data point represents the mean  $\pm$  S. E. of 3 independent experiments, performed in duplicate.

The M<sub>1</sub>-M<sub>5</sub> mAChR efficacy data for the hybrid ligands, **8c,e**, and truncated hybrid ligands **10d,g,i** and **12a-c** were analysed by stratifying the compounds by their linker length (C6, C8 or C10) and terminal ‘allosteric’ substituent (i.e. ‘hybrid-Cn’, ‘IXO-Cn-phen’ or ‘IXO-Cn’) (Figure 4 A). Comparison of the efficacy of the ligands by terminal substituent reveals that truncation of the allosteric pharmacophore to the IXO-Cn-phen derivatives, **12a-c**, increases the M<sub>2</sub>/M<sub>4</sub> mAChR selectivity. Except at the optimal linker length, **12b** (IXO-C8-phen), at which efficacy was highest and M<sub>2</sub>/M<sub>4</sub> mAChR subtype selectivity was lowest (Figure 4 B). The IXO-Cn ligands, **10a-i**, showed a simple linker length dependent decrease in efficacy at the M<sub>1</sub>/M<sub>3</sub>/M<sub>5</sub> > M<sub>2</sub>/M<sub>4</sub> mAChRs, compared with **1** (Figure 4 B). Comparison of the efficacy of the ligands, stratified by their linker length (C6, C8 or C10), at the M<sub>1</sub>-M<sub>5</sub> mAChR subtypes, reveals that functionalisation of the ‘allosteric’ pharmacophore of the hybrid ligand structure at shorter linker lengths (C6 and C8) is less important to the efficacy of the ligands, than at longer linker lengths (C10) (Figure 4 C). The presence of similar M<sub>2</sub>/M<sub>4</sub> > M<sub>1</sub>/M<sub>3</sub>/M<sub>5</sub> mAChR selectivity in the truncated hybrids ligands, **10a-i** and **12a-c**, and the hybrid ligands, **8a-f**, suggests that this selectivity does not result from a receptor-ligand interaction with the allosteric pharmacophore, but rather more likely with the linker. However, the fact the both the hybrid ligands, **8a-f**, and compounds **12a-c** exhibit an optimal linker (in terms of potency and maximum response) at a linker length of approximately C8 polymethylene units, tends to suggest that the allosteric pharmacophore (or *N*-phenyl amide in **12a-c**) has some positive effect on agonism at this linker length. It seems likely that one or more of the common structural features between the allosteric pharmacophore of the hybrid ligands **8a-f** and the *N*-phenyl amide of compounds **12a-c** makes an allosteric interaction with the mAChRs which positively affects the potency and maximum response of the ligands. However, it seems that, counter intuitively, this proposed additional allosteric interaction with the mAChRs, while it increases the potency and maximum response of the compounds, seemingly simultaneously

reduces the M<sub>2</sub>/M<sub>4</sub> mAChR selectivity which is observed in the longer or shorter linker length ligands, **8a-b,f** and **12a,c**, or in the longer linker-only ligand, **10i**.

## ■ CONCLUSIONS

Herein is presented a series of hybrid ligands consisting of a potent orthosteric ligand, iperoxo, **1**, and a functionally equivalent derivative of BQCA, **3**, and the analysis of their mAChR subtype selectivity at the level of efficacy. It was found that the hybrid ligands possessed little selectivity at optimal linker lengths, however at non-optimal linker lengths some apparent preference for the M<sub>2</sub>/M<sub>4</sub> mAChRs was observed. To understand the structural basis of these observations we synthesized a series of truncated hybrid ligands, and similarly assayed them across the M<sub>1</sub>-M<sub>5</sub> mAChRs. The truncated hybrid ligands were found to possess similar pharmacological properties to the hybrid ligands in terms of M<sub>2</sub>/M<sub>4</sub> mAChR selectivity. The pharmacology of the M<sub>2</sub>/M<sub>4</sub> mAChR selective truncated hybrid ligands was well described by the mechanism of conformational restriction of the extracellular domain proposed by Bermudez *et al.*,<sup>33</sup> and this mechanism in turn explains why no allosteric pharmacophore is necessary to achieve the desirable M<sub>2</sub>/M<sub>4</sub> mAChR selectivity. However as of yet we have no clear explanation as to why the hybrid ligands (hybrid-C6, **8c**, hybrid-C7, **8d**, and hybrid-C8, **8e**) and some of the truncated hybrid ligands (IXO-C6, **10e**, IXO-C8, **10g**, and IXO-C8-phen, **12b**) show little or no selectivity for the M<sub>2</sub>/M<sub>4</sub> mAChRs. It is plausible that these ligands may bind differentially to the allosteric vestibule of the mAChRs in their dominant binding pose, in such a conformation that they do not obstruct the allosteric site and hence have lower or abolished selectivity. Furthermore it is interesting to note that the selectivity of other mAChR hybrid ligands, which have been proposed to bind bitopically (such as those described by Disingri *et al.*<sup>22</sup>), closely resembles the selectivity observed (i.e. preference for the M<sub>2</sub>/M<sub>4</sub> mAChRs) in our truncated hybrid ligands (e.g. IXO-C10, **10i**), which bare no allosteric

pharmacophore and hence cannot bind bitopically. This may suggest that some mAChR hybrid ligands have been misclassified as bitopic, when in fact they gain selectivity by the mechanism of conformational restriction of the allosteric vestibule proposed by Bermudez *et al.*,<sup>33</sup> and that this may be the most common mechanism by which mAChR hybrid ligand agonists gain selectivity. In our experiments, IXO-C10, **10i**, showed significantly higher efficacy at the M<sub>4</sub> versus M<sub>2</sub> mAChRs, possibly suggesting that conformational restriction of the extracellular domain may affect the M<sub>2</sub> and M<sub>4</sub> mAChR efficacy differentially in some cases, either due to subtle structural differences in the M<sub>2</sub> and M<sub>4</sub> mAChR subtypes, differential coupling to intracellular G proteins or due to differences in ligand binding conformations between these subtypes. We suggest that the addition of an *N*-alkyl linker to more selective orthosteric pharmacophores may yield ligands with improved selectivity for the M<sub>2</sub> or M<sub>4</sub> mAChRs. Additionally, we have found that the truncated hybrid ligand IXO-C10-phen, **12c**, retains good efficacy at the M<sub>2</sub> and M<sub>4</sub> mAChRs (M<sub>2</sub> mAChR:  $\log \tau_c = 1.09 \pm 0.13$ , M<sub>4</sub> mAChR:  $\log \tau_c = 1.58 \pm 0.09$ ) as well as approximately 10-fold selectivity over the remaining M<sub>1</sub>/M<sub>3</sub>/M<sub>5</sub> mAChR subtypes (M<sub>1</sub> mAChR:  $\log \tau_c = -0.79 \pm 0.11$ , M<sub>3</sub> mAChR:  $\log \tau_c = -0.58 \pm 0.23$ , M<sub>5</sub> mAChR:  $\log \tau_c = -0.51 \pm 0.06$ ). This structure contains several regions (allosteric pharmacophore, orthosteric pharmacophore and linker) which could potentially be further expanded upon via a SAR study to optimise its efficacy and selectivity and may serve as a suitable lead compound for the development of a purely M<sub>2</sub> or M<sub>4</sub> mAChR selective hybrid ligand.

## ■ EXPERIMENTAL SECTION

**Chemistry.** All materials were reagent grade and purchased commercially from Sigma-Aldrich or Matrix Scientific. Anhydrous solvents were obtained from a MBraun MB SPS-800

Solvent Purification System. Analytical thin layer chromatography (TLC) was performed on Silica Gel 60 F254 pre-coated plates (0.25 mm, Merck ART 5554) and visualised using ultraviolet light, iodine, potassium permanganate or ninhydrin as necessary. Silica gel 40–63 micron (Davisil) was used for silica gel flash chromatography.  $^1\text{H}$  NMR spectra were recorded on a Bruker Avance 400 MHz Ultrashield Plus spectrometer at 400.13 MHz. Chemical shifts ( $\delta_{\text{H}}$ ) for all  $^1\text{H}$  NMR spectra are reported in parts per million (ppm) using the central peak of the deuterated solvent chemical shift as the reference:  $\text{CDCl}_3$  (7.26) and  $d_6$ -DMSO (2.50).<sup>40</sup> Each resonance was assigned according to the following convention: chemical shift ( $\delta$ ) (multiplicity, coupling constant(s) in Hz, number of protons). Coupling constants ( $J$ ) are reported to the nearest 0.1 Hz. In reporting the spectral data, the following abbreviations have been used: s, singlet; d, doublet; t, triplet; q, quartet; p, pentet; m, multiplet; br, broad; app, apparent; as well as combinations of these where appropriate.  $^{13}\text{C}$  NMR spectra were recorded at 100.62 MHz using a Bruker Avance 400 MHz Ultrashield Plus spectrometer. Chemical shifts ( $\delta$ ) for all  $^{13}\text{C}$  NMR spectra are reported in parts per million (ppm), using the center peak of the deuterated solvent chemical shift as the reference:  $\text{CDCl}_3$  (77.16) and  $d_6$ -DMSO (39.52).<sup>40</sup> HSQC, HMBC and COSY spectra were obtained using the standard Bruker pulse sequence to assist with structural assignment of the compounds. LC-MS was performed on an Agilent 1200 Series coupled to the 6120 quadrupole mass spectrometer. Elution was also monitored at 254 nm. HRMS analyses were recorded in the specified ion mode using an Agilent 6224 TOF LC-MS coupled to an Agilent 1290 Infinity (Agilent, Palo Alto, CA). Analytical reverse-phase HPLC was performed on a Waters HPLC system using a Phenomenex® Luna C8 (2) 100Å column (150 × 4.6 mm, 5  $\mu\text{m}$ ) and a binary solvent system; solvent A: 0.1% TFA/ $\text{H}_2\text{O}$ ; solvent B: 0.1% TFA/ACN. Isocratic elution was carried out using the following protocol (time, % solvent A, % solvent B): 0 min, 100, 0; 10 min, 20, 80; 11 min, 20, 80; 12 min, 100, 0; 20 min, 100, 0; at a flow rate of 1.0 mL/min monitored at 214 and/ or 254 nm

using a Waters 996 Photodiode Array detector. Characterisation requirements for final compounds were set as:  $^1\text{H}$  NMR,  $^{13}\text{C}$  NMR, LC-MS, HPLC (254 nm and 214 nm) purity >95%.

Synthesis of 1-(4-nitrobenzyl)-4-oxo-1,4-dihydroquinoline-3-carboxylic acid **5**,<sup>38</sup> Iperoxo-base **9** and subsequently iperoxo **1**<sup>39</sup> was carried out according to literature procedures (Supplementary Information).

***N*-((1*S*,2*S*)-2-Hydroxycyclohexyl)-1-(4-nitrobenzyl)-4-oxo-1,4-dihydroquinoline-3-carboxamide (**6**).** 1-(4-Nitrobenzyl)-4-oxo-1,4-dihydroquinoline-3-carboxylic acid (**5**) (2.19 g, 6.74 mmol), HCTU (3.23 g, 8.03 mmol) and (1*S*,2*S*)-2-aminocyclohexan-1-ol•HCl (1.04 g, 6.88 mmol) were dissolved in DMF (20 mL) and stirred at rt under  $\text{N}_2$ . *N,N*-Diisopropylethylamine (4.0 mL, 3.0 g, 23 mmol) in DCM (20 mL) was added dropwise over 45 min. Stirring, under  $\text{N}_2$  was continued overnight (17 h). The DCM was removed under vacuum and the solution was diluted with aqueous HCl (20 mL, 2 M) and extracted with ethyl acetate (3 × 30 mL). The organics were washed with saturated  $\text{NaHCO}_3$  (aq) (30 mL), distilled water (30 mL) and brine (30 mL), dried over anhydrous  $\text{MgSO}_4$  and the solvent removed under vacuum. The crude product was purified by FCC, with silica as the stationary phase and DCM–DCM/methanol (19:1) as the gradient mobile phase. The product was a orange solid; 2.28 g, 75%.  $^1\text{H}$  NMR ( $d_6$ -DMSO)  $\delta$  10.07 (d,  $J$  = 7.6 Hz, 1H), 9.12 (s, 1H), 8.36 (dd,  $J$  = 8.1, 1.4 Hz, 1H), 8.20 (d,  $J$  = 6.6 Hz, 2H), 7.73 (ddd,  $J$  = 8.6, 7.0, 1.6 Hz, 1H), 7.63 (d,  $J$  = 8.5 Hz, 1H), 7.51 (ddd,  $J$  = 7.9, 7.1, 0.7 Hz, 1H, H6), 7.46 (d,  $J$  = 8.8 Hz, 2H), 5.97 (s, 2H), 4.82 (d,  $J$  = 5.0 Hz, 1H), 3.82–3.60 (m, 1H), 3.48–3.36 (m, 1H), 2.08–1.97 (m, 1H), 1.92–1.80 (m, 1H), 1.71–1.52 (m, 2H), 1.40–1.16 (m, 4H).  $^{13}\text{C}$  NMR ( $d_6$ -DMSO)  $\delta$  176.3, 164.2, 149.5, 147.5, 144.4, 139.4, 133.6, 128.1, 127.9, 126.8, 125.7, 124.5, 118.2, 112.2, 71.7, 55.6, 54.1, 34.2,

31.1, 24.2, 23.7.  $m/z$  MS (TOF ES<sup>+</sup>) C<sub>23</sub>H<sub>23</sub>N<sub>3</sub>O<sub>5</sub> [M+H]<sup>+</sup> calcd, 422.2; found, 422.2. LC-MS:  $t_R$  = 5.91 min.

**1-(4-Aminobenzyl)-*N*-((1*S*,2*S*)-2-hydroxycyclohexyl)-4-oxo-1,4-dihydroquinoline-3-carboxamide (3).** *N*-((1*S*,2*S*)-2-Hydroxycyclohexyl)-1-(4-nitrobenzyl)-4-oxo-1,4-dihydroquinoline-3-carboxamide (**6**) (1.60 g, 3.80 mmol) was dissolved in DMF (24 mL). Pd/C (10% w/w, 160 mg) was added and the solution was stirred under hydrogen gas for 3 h. Once the starting material was no longer detectable by LC-MS the solution was filtered and washed through Celite<sup>TM</sup> with methanol (30 mL). The methanol was removed from the collected organics, slowly under vacuum, at which point a white precipitate formed which was filtered and washed with cold H<sub>2</sub>O, giving the product as a fine white solid; 1.00 g, 67%. <sup>1</sup>H NMR (*d*<sub>6</sub>-DMSO)  $\delta$  10.09 (d,  $J$  = 7.6 Hz, 1H), 8.96 (s, 1H), 8.33 (dd,  $J$  = 8.1, 1.5 Hz, 1H), 7.86 (d,  $J$  = 8.6 Hz, 1H), 7.76 (ddd,  $J$  = 8.6, 5.7, 1.6 Hz, 1H), 7.50 (ddd,  $J$  = 7.9, 7.1, 0.8 Hz, 1H), 6.96 (d,  $J$  = 8.4 Hz, 2H), 6.51 (d,  $J$  = 8.5 Hz, 2H), 5.52 (s, 2H), 5.14 (s, 2H), 4.81 (d,  $J$  = 5.0 Hz, 1H), 3.76–3.56 (m, 1H), 3.44–3.35 (m, 1H), 2.05–1.95 (m, 1H), 1.93–1.79 (m, 1H), 1.71–1.53 (m, 2H), 1.38–1.08 (m, 4H); <sup>13</sup>C NMR (*d*<sub>6</sub>-DMSO)  $\delta$  175.6, 164.0, 148.6, 148.1, 139.2, 132.7, 128.1, 127.4, 126.1, 125.0, 122.0, 118.0, 114.0, 111.1, 71.3, 55.9, 53.7, 33.8, 30.7, 23.8, 23.3.  $m/z$  MS (TOF ES<sup>+</sup>) C<sub>23</sub>H<sub>25</sub>N<sub>3</sub>O<sub>3</sub> [M+H]<sup>+</sup> calcd, 392.2; found, 392.2. LC-MS:  $t_R$  = 4.98 min.

**General procedure for the synthesis of terminal-bromoalkanamide BQCA derivatives.** 1-(4-Aminobenzyl)-*N*-((1*S*,2*S*)-2-hydroxycyclohexyl)-4-oxo-1,4-dihydroquinoline-3-carboxamide (**3**) (256  $\mu$ mol, 1 eq.), HCTU (307  $\mu$ mol, 1.2 eq.) and the appropriate terminal-bromoalkanoic acid (307  $\mu$ mol, 1.2 eq.) were dissolved in DMF (2 mL) and stirred under N<sub>2</sub> at room temperature. *N,N*-Diisopropylethylamine (DIPEA) (59 mg, 0.46 mmol, 1.8 eq.) in DCM (2 mL) was added dropwise over 30 min, and stirring continued for 6 h. The DCM was removed under vacuum and the reaction mixture was then diluted with

distilled water (10 mL). The precipitate which formed was filtered and washed with a small volume of cold ethyl acetate, then suspended in a 1:1 solution of saturated NaHCO<sub>3</sub> (aq) and distilled water and stirred vigorously for 30 min, before being vacuum filtered again. The resulting solid was then re-dissolved in DCM (10 mL) and washed with sat. NaHCO<sub>3</sub> solution (5 mL), dH<sub>2</sub>O (5 mL) and brine (5 mL) before being dried over anhydrous MgSO<sub>4</sub> and the solvent removed *in vacuo* to afford the target compound.

**1-(4-(5-Bromopentanamido)benzyl)-N-((1S,2S)-2-hydroxycyclohexyl)-4-oxo-1,4-dihydroquinoline-3-carboxamide (7a).** Off-white solid; 82.4 mg, 58%. <sup>1</sup>H NMR (*d*<sub>6</sub>-DMSO) δ 10.09 (d, *J* = 7.3 Hz, 1H), 9.94 (s, 1H), 9.04 (s, 1H), 8.34 (d, *J* = 7.8 Hz, 1H), 7.79–7.68 (m, 2H), 7.55 (d, *J* = 8.0 Hz, 2H), 7.52–7.46 (m, 1H, H<sub>6</sub>), 7.18 (d, *J* = 8.6 Hz, 2H), 5.71 (s, 2H), 4.83 (s, 1H, OH), 3.74–3.64 (m, 1H), 3.51 (t, *J* = 6.5 Hz, 2H), 3.44–3.36 (m, 1H) 2.30 (t, *J* = 7.3 Hz, 2H), 2.07–1.97 (m, 1H), 1.91–1.73 (m, 3H), 1.69–1.52 (m, 4H), 1.45–1.15 (m, 4H); <sup>13</sup>C NMR (*d*<sub>6</sub>-DMSO) δ 176.1, 171.4, 164.4, 149.1, 139.6, 139.4, 133.3, 130.7, 127.9, 127.6, 126.6, 125.5, 119.9, 118.4, 111.8, 71.7, 56.0, 54.1, 36.1, 35.2, 34.2, 32.2, 31.1, 27.5, 24.2, 24.1. *m/z* MS (TOF ES<sup>+</sup>) C<sub>28</sub>H<sub>32</sub>BrN<sub>3</sub>O<sub>4</sub> [M+H]<sup>+</sup> calcd, 554.2; found, 554.1. LC-MS: *t*<sub>R</sub> = 6.02 min.

**1-(4-(6-Bromohexanamido)benzyl)-N-((1S,2S)-2-hydroxycyclohexyl)-4-oxo-1,4-dihydroquinoline-3-carboxamide (7b).** Off-white solid; 99.7 mg, 86%. <sup>1</sup>H NMR (*d*<sub>6</sub>-DMSO) δ 10.09 (d, *J* = 7.3 Hz, 1H), 9.93 (s, 1H), 9.04 (s, 1H), 8.34 (d, *J* = 7.8 Hz, 1H), 7.79–7.69 (m, 2H), 7.55 (d, *J* = 8.0 Hz, 2H), 7.52–7.46 (m, 1H, H<sub>6</sub>), 7.18 (d, *J* = 8.1 Hz, 2H), 5.70 (s, 2H), 4.83 (s, 1H), 3.75–3.64 (m, 1H), 3.51 (t, *J* = 6.5 Hz, 2H), 3.44–3.36 (m, 1H) 2.27 (t, *J* = 8.1 Hz, 2H), 2.07–1.97 (m, 1H), 1.92–1.73 (m, 3H), 1.69–1.52 (m, 4H), 1.45–1.15 (m, 6H). <sup>13</sup>C NMR (*d*<sub>6</sub>-DMSO) δ 176.1, 171.6, 164.4, 149.1, 139.6, 139.4, 133.3, 130.6, 127.9, 127.6, 126.6, 125.5, 119.9, 118.4, 111.8, 71.7, 56.1, 54.1, 36.6, 35.5, 34.2, 32.5, 31.1, 27.7, 24.7, 24.2, 23.7. *m/z* MS (TOF ES<sup>+</sup>) C<sub>29</sub>H<sub>34</sub>BrN<sub>3</sub>O<sub>4</sub> [M+H]<sup>+</sup> calcd, 568.2; found, 568.2. LC-MS: *t*<sub>R</sub> = 6.14 min.



**1-(4-(7-Bromoheptanamido)benzyl)-N-((1S,2S)-2-hydroxycyclohexyl)-4-oxo-1,4-dihydroquinoline-3-carboxamide (7c).** Off-white solid; 140.1 mg, 93%. <sup>1</sup>H NMR (*d*<sub>6</sub>-DMSO)  $\delta$  10.09 (d, *J* = 7.6 Hz, 1H), 9.91 (s, 1H), 9.04 (s, 1H), 8.34 (d, *J* = 7.7 Hz, 1H), 7.78–7.70 (m, 2H), 7.55 (d, *J* = 8.6 Hz, 2H), 7.49 (ddd, *J* = 8.0, 6.2, 1.8 Hz, 1H, H<sub>6</sub>), 7.17 (d, *J* = 8.6 Hz, 2H), 5.70 (s, 2H), 4.83 (s, 1H), 3.74–3.64 (m, 1H), 3.50 (t, *J* = 6.7 Hz, 2H), 3.43–3.36 (m, 1H), 2.26 (t, *J* = 7.4 Hz, 2H), 2.07–1.97 (m, 1H), 1.91–1.82 (m, 1H), 1.81–1.72 (m, 2H), 1.69–1.44 (m, 4H), 1.44–1.15 (m, 8H). <sup>13</sup>C NMR (*d*<sub>6</sub>-DMSO)  $\delta$  175.7, 171.3, 163.9, 148.6, 139.1, 139.0, 132.9, 130.2, 127.4, 127.1, 126.1, 125.1, 119.4, 118.0, 111.4, 71.2, 55.6, 53.7, 36.2, 35.2, 33.7, 32.1, 30.7, 27.7, 27.3, 24.9, 23.8, 23.3. *m/z* MS (TOF ES<sup>+</sup>) C<sub>30</sub>H<sub>36</sub>BrN<sub>3</sub>O<sub>4</sub> [M+H]<sup>+</sup> calcd, 582.2; found, 582.4. LC-MS: *t*<sub>R</sub> = 6.31 min.

**1-(4-(8-Bromooctanamido)benzyl)-N-((1S,2S)-2-hydroxycyclohexyl)-4-oxo-1,4-dihydroquinoline-3-carboxamide (7d).** Off-white solid; 150.1 mg, 95%. <sup>1</sup>H NMR (*d*<sub>6</sub>-DMSO)  $\delta$  10.09 (d, *J* = 7.6 Hz, 1H), 9.90 (s, 1H), 9.04 (s, 1H), 8.34 (d, *J* = 7.7 Hz, 1H), 7.79–7.70 (m, 2H), 7.55 (d, *J* = 8.5 Hz, 2H), 7.52–7.46 (m, 1H), 7.17 (d, *J* = 8.6 Hz, 2H), 5.70 (s, 2H), 4.82 (d, *J* = 5.0 Hz, 1H), 3.74–3.63 (m, 1H), 3.51 (t, *J* = 6.7 Hz, 2H), 3.44–3.36 (m, 1H), 2.25 (t, *J* = 7.4 Hz, 2H), 2.07–1.97 (m, 1H), 1.92–1.72 (m, 3H), 1.69–1.48 (m, 4H), 1.41–1.15 (m, 10H). <sup>13</sup>C NMR (*d*<sub>6</sub>-DMSO)  $\delta$  176.1, 171.8, 164.3, 149.1, 139.6, 139.5, 133.3, 130.6, 127.9, 127.6, 126.6, 125.5, 119.9, 118.4, 111.8, 71.7, 56.0, 54.1, 36.7, 35.7, 34.2, 32.5, 31.1, 28.9, 28.3, 27.9, 25.4, 24.2, 23.7. *m/z* MS (TOF ES<sup>+</sup>) C<sub>31</sub>H<sub>38</sub>BrN<sub>3</sub>O<sub>4</sub> [M+H]<sup>+</sup> calcd, 596.2; found, 596.2. LC-MS: *t*<sub>R</sub> = 6.45 min.

**1-(4-(9-Bromononanamido)benzyl)-N-((1S,2S)-2-hydroxycyclohexyl)-4-oxo-1,4-dihydroquinoline-3-carboxamide (7e).** Off-white solid; 100.9 mg, 65%. <sup>1</sup>H NMR (*d*<sub>6</sub>-DMSO)  $\delta$  10.09 (d, *J* = 7.5 Hz, 1H), 9.90 (s, 1H), 9.04 (s, 1H), 8.34 (d, *J* = 8.4 Hz), 7.78–7.69 (m, 2H), 7.55 (d, *J* = 8.5 Hz, 2H), 7.52–7.46 (m, 1H), 7.17 (d, *J* = 8.5 Hz, 2H), 5.70 (s, 2H), 4.82 (d, *J* = 4.6 Hz, 1H), 3.75–3.62 (m, 2H), 3.49 (t, *J* = 6.7 Hz, 2H), 3.43–3.36 (m, 1H), 2.25

(t,  $J = 7.3$  Hz, 3H), 2.07–1.98 (m, 1H), 1.90–1.71 (m, 3H), 1.69–1.42 (m, 4H), 1.39–1.15 (m, 12H).  $^{13}\text{C}$  NMR ( $d_6$ -DMSO)  $\delta$  176.1, 171.8, 164.4, 149.1, 139.6, 139.5, 133.3, 130.6, 127.9, 127.6, 126.6, 125.5, 119.9, 118.4, 111.8, 71.7, 56.0, 54.1, 36.8, 35.7, 34.2, 32.7, 31.1, 29.1, 29.0, 28.4, 28.0, 25.5, 24.2, 23.7.  $m/z$  MS (TOF ES<sup>+</sup>)  $\text{C}_{32}\text{H}_{40}\text{BrN}_3\text{O}_4$   $[\text{M}+\text{H}]^+$  calcd, 610.2; found, 610.2. LC-MS:  $t_R = 6.64$  min.

**1-(4-(10-Bromodecanamido)benzyl)-*N*-((1*S*,2*S*)-2-hydroxycyclohexyl)-4-oxo-1,4-dihydroquinoline-3-carboxamide (7f).** Off-white solid; 120.6 mg, 76%.  $^1\text{H}$  NMR ( $d_6$ -DMSO)  $\delta$  10.09 (d,  $J = 7.5$  Hz, 1H), 9.90 (s, 1H), 9.04 (s, 1H), 8.34 (d,  $J = 8.4$  Hz, 1H), 7.78–7.69 (m, 2H), 7.55 (d,  $J = 8.5$  Hz, 2H), 7.52–7.46 (m, 1H), 7.17 (d,  $J = 8.5$  Hz, 2H), 5.70 (s, 2H), 4.82 (d,  $J = 4.6$  Hz, 1H), 3.75–3.62 (m, 2H), 3.49 (t,  $J = 6.7$  Hz, 2H), 3.43–3.36 (m, 1H), 2.25 (t,  $J = 7.3$  Hz, 3H), 2.07–1.98 (m, 1H), 1.90–1.71 (m, 3H), 1.69–1.42 (m, 4H), 1.39–1.15 (m, 14H).  $^{13}\text{C}$  NMR ( $d_6$ -DMSO)  $\delta$  176.1, 171.8, 164.4, 149.0, 139.6, 139.5, 133.3, 130.6, 127.9, 127.6, 126.6, 125.5, 119.8, 118.4, 111.8, 71.7, 56.1, 54.1, 36.8, 35.7, 34.1, 32.7, 31.1, 29.2, 29.1, 29.0, 28.5, 27.9, 25.5, 24.2, 23.7.  $m/z$  MS (TOF ES<sup>+</sup>)  $\text{C}_{33}\text{H}_{42}\text{BrN}_3\text{O}_4$   $[\text{M}+\text{H}]^+$  calcd, 624.2; found, 623.8. LC-MS:  $t_R = 6.85$  min.

**General procedure for the synthesis of ligands 8a-f and 12a-c.** The appropriate terminal-bromoalkanamide BQCA derivative (**7a–f**) (250  $\mu\text{mol}$ , 1.0 eq.) or terminal-bromoalkanamide (**11a–c**) (250  $\mu\text{mol}$ , 1.0 eq.) and 4-((4,5-dihydroisoxazol-3-yl)oxy)-*N,N*-dimethylbut-2-yn-1-amine (iperoxo-base **9**) (375  $\mu\text{mol}$ , 1.5 eq.) were dissolved in chloroform (1 mL) and heated to reflux for 48 h. The solvent was then removed *in vacuo* and the resulting residue chromatographed on 15 mass equivalents of silica (gradient mobile phase: 100% DCM - 90% DCM/ 10% methanol), the appropriate fractions combined and the solvent removed *in vacuo* to yield the target molecule.

***N*-(4-((4,5-Dihydroisoxazol-3-yl)oxy)but-2-yn-1-yl)-5-((4-((3-(((1*S*,2*S*)-2-hydroxycyclohexyl)carbamoyl)-4-oxoquinolin-1(4*H*)-yl)methyl)phenyl)amino)-*N,N*-**

**dimethyl-5-oxopentan-1-aminium bromide (8a).** Light orange solid; 43.2 mg, 32%.  $^1\text{H}$  NMR ( $\text{CDCl}_3$ )  $\delta$  10.25 (app s, 1H), 9.93 (s, 1H), 8.86 (s, 1H), 8.38 (d,  $J = 7.4$  Hz, 1H), 7.73 (d,  $J = 7.8$  Hz, 2H), 7.56 (t,  $J = 7.20$  Hz, 1H), 7.43 (d,  $J = 8.4$  Hz, 1H), 7.37 (t,  $J = 7.3$  Hz, 1H), 7.01 (d,  $J = 7.8$  Hz, 2H), 5.38 (s, 2H), 4.74 (s, 2H), 4.62 (s, 2H), 4.37 (t,  $J = 9.6$  Hz, 2H), 3.78 (br s, 2H), 3.53–3.41 (br m, 1H), 3.24 (s, 6H), 2.94 (t,  $J = 9.6$  Hz, 2H), 2.61–2.22 (br m, 2H), 2.09–1.93 (br m, 2H), 1.82–1.58 (br m, 7H), 1.46–1.12 (br m, 5H).  $^{13}\text{C}$  NMR ( $\text{CDCl}_3$ )  $\delta$  176.7, 171.5, 166.8, 166.5, 148.4, 139.2, 139.1, 133.1, 129.2, 127.7, 127.1, 126.9, 125.4, 120.5, 117.1, 111.2, 86.8, 75.6, 75.4, 70.1, 63.6, 57.3, 57.1, 55.4, 54.9, 50.3, 35.4, 34.3, 32.9, 31.4, 24.6, 24.0, 22.0, 21.5.  $m/z$  MS (TOF ES+)  $\text{C}_{37}\text{H}_{46}\text{N}_5\text{O}_6$   $[\text{M}]^+$  calcd, 656.3; found 656.3. LC-MS:  $t_R = 3.10$  min.

***N*-(4-((4,5-Dihydroisoxazol-3-yl)oxy)but-2-yn-1-yl)-6-((4-((3-(((1*S*,2*S*)-2-hydroxycyclohexyl)carbamoyl)-4-oxoquinolin-1(4*H*)-yl)methyl)phenyl)amino)-*N,N*-dimethyl-6-oxohexan-1-aminium bromide (8b).** Light orange solid; 22.0 mg, 17%.  $^1\text{H}$  NMR ( $\text{CDCl}_3$ )  $\delta$  10.26 (app s, 1H), 9.94 (s, 1H), 8.86 (s, 1H), 8.38 (d,  $J = 7.5$  Hz, 1H), 7.75 (d,  $J = 7.6$  Hz, 2H), 7.57 (t,  $J = 7.2$  Hz, 1H), 7.43 (d,  $J = 8.4$  Hz, 1H), 7.38 (t,  $J = 7.4$  Hz, 1H), 7.00 (d,  $J = 7.7$  Hz, 2H), 5.39 (s, 2H), 4.74 (s, 2H), 4.62 (s, 2H), 4.37 (t,  $J = 9.6$  Hz, 2H), 3.78 (br s, 2H), 3.52–3.42 (br m, 1H), 3.23 (s, 6H), 2.94 (t,  $J = 9.6$  Hz, 2H), 2.60–2.23 (br m, 2H), 2.10–1.93 (br m, 2H), 1.83–1.58 (br m, 7H), 1.46–1.12 (br m, 7H).  $^{13}\text{C}$  NMR ( $\text{CDCl}_3$ )  $\delta$  176.7, 172.3, 166.8, 166.6, 148.3, 139.4, 139.3, 133.1, 128.8, 127.8, 127.1, 125.4, 125.0, 120.5, 117.1, 111.2, 86.7, 75.7, 75.6, 70.1, 64.2, 57.2, 57.1, 55.5, 54.8, 50.7, 34.3, 32.9, 31.9, 31.4, 25.0, 24.7, 24.5, 22.7, 21.9.  $m/z$  MS (TOF ES+)  $\text{C}_{38}\text{H}_{48}\text{N}_5\text{O}_6$   $[\text{M}]^+$  calcd, 670.4; found, 670.4. LC-MS:  $t_R = 3.12$  min.

***N*-(4-((4,5-Dihydroisoxazol-3-yl)oxy)but-2-yn-1-yl)-7-((4-((3-(((1*S*,2*S*)-2-hydroxycyclohexyl)carbamoyl)-4-oxoquinolin-1(4*H*)-yl)methyl)phenyl)amino)-*N,N*-dimethyl-7-oxoheptan-1-aminium bromide (8c).** Light orange solid; 19.7 mg, 15%.  $^1\text{H}$

NMR (CDCl<sub>3</sub>)  $\delta$  10.25 (app s, 1H), 9.93 (s, 1H), 8.86 (s, 1H), 8.38 (d,  $J$  = 7.4 Hz, 1H), 7.73 (d,  $J$  = 7.8 Hz, 2H), 7.56 (t,  $J$  = 7.2 Hz, 1H), 7.43 (d,  $J$  = 8.4 Hz, 1H), 7.37 (t,  $J$  = 7.3 Hz, 1H), 7.01 (d,  $J$  = 7.8 Hz, 2H), 5.38 (s, 2H), 4.74 (s, 2H), 4.62 (s, 2H), 4.37 (t,  $J$  = 9.6 Hz, 2H), 3.78 (br m, 2H), 3.53 – 3.41 (br m, 1H), 3.24 (s, 6H), 2.94 (t,  $J$  = 9.6 Hz, 2H), 2.61 – 2.22 (br m, 2H), 2.09 – 1.93 (br m, 2H), 1.82–1.58 (br m, 7H), 1.46–1.12 (br m, 9H). <sup>13</sup>C NMR (CDCl<sub>3</sub>)  $\delta$  176.7, 172.7, 166.8, 166.6, 148.3, 139.5, 139.3, 133.1, 128.7, 127.8, 127.1, 127.0, 125.4, 120.5, 117.1, 111.2, 86.7, 75.7, 75.6, 70.1, 64.3, 57.3, 57.1, 55.6, 54.8, 50.5, 36.9, 34.4, 31.4, 29.7, 27.6, 25.0, 24.8, 24.7, 24.0, 22.0.  $m/z$  MS (TOF ES<sup>+</sup>) C<sub>39</sub>H<sub>50</sub>N<sub>5</sub>O<sub>6</sub> [M]<sup>+</sup> calcd, 684.4; found, 684.4; LC-MS:  $t_R$  = 3.21 min.

***N*-(4-((4,5-Dihydroisoxazol-3-yl)oxy)but-2-yn-1-yl)-8-((4-((3-(((1*S*,2*S*)-2-hydroxycyclohexyl)carbamoyl)-4-oxoquinolin-1(4*H*)-yl)methyl)phenyl)amino)-*N,N*-dimethyl-8-oxooctan-1-aminium bromide (8d).** Light orange solid; 12.1 mg, 9%. <sup>1</sup>H NMR (CDCl<sub>3</sub>)  $\delta$  10.25 (app s, 1H), 9.93 (s, 1H), 8.86 (s, 1H), 8.38 (d,  $J$  = 7.4 Hz, 1H), 7.73 (d,  $J$  = 7.8 Hz, 2H), 7.56 (t,  $J$  = 7.2 Hz, 1H), 7.43 (d,  $J$  = 8.4 Hz, 1H), 7.37 (t,  $J$  = 7.3 Hz, 1H), 7.01 (d,  $J$  = 7.8 Hz, 2H), 5.38 (s, 2H), 4.74 (s, 2H), 4.62 (s, 2H), 4.37 (t,  $J$  = 9.6 Hz, 2H), 3.78 (br m, 2H), 3.53–3.41 (br m, 1H), 3.24 (s, 6H), 2.94 (t,  $J$  = 9.6 Hz, 2H), 2.61–2.22 (br m, 2H), 2.09–1.93 (br m, 2H), 1.82–1.58 (br m, 7H), 1.46–1.12 (br m, 11H). <sup>13</sup>C NMR (CDCl<sub>3</sub>)  $\delta$  176.7, 172.9, 166.8, 166.6, 148.1, 139.6, 139.3, 133.2, 128.6, 127.8, 127.3, 127.0, 125.4, 120.5, 117.0, 111.2, 86.6, 75.7, 75.5, 70.1, 64.2, 57.3, 57.1, 55.6, 54.8, 50.4, 36.6, 34.3, 32.9, 31.4, 27.8, 27.5, 25.3, 25.0, 24.7, 24.0, 22.1;  $m/z$  MS (TOF ES<sup>+</sup>) C<sub>40</sub>H<sub>52</sub>N<sub>5</sub>O<sub>6</sub> [M]<sup>+</sup> calcd, 698.4, found 698.4. LC-MS:  $t_R$  = 3.22 min.

***N*-(4-((4,5-Dihydroisoxazol-3-yl)oxy)but-2-yn-1-yl)-9-((4-((3-(((1*S*,2*S*)-2-hydroxycyclohexyl)carbamoyl)-4-oxoquinolin-1(4*H*)-yl)methyl)phenyl)amino)-*N,N*-dimethyl-9-oxononan-1-aminium bromide (8e).** Light orange solid; 18.9 mg, 17%. <sup>1</sup>H NMR (CDCl<sub>3</sub>)  $\delta$  10.25 (app s, 1H), 9.93 (s, 1H), 8.86 (s, 1H), 8.38 (d,  $J$  = 7.4 Hz, 1H), 7.73 (d,  $J$  =

7.8 Hz, 2H), 7.56 (t,  $J = 7.2$  Hz, 1H), 7.43 (d,  $J = 8.4$  Hz, 1H), 7.37 (t,  $J = 7.3$  Hz, 1H), 7.01 (d,  $J = 7.8$  Hz, 2H), 5.38 (s, 2H), 4.74 (s, 2H), 4.62 (s, 2H), 4.37 (t,  $J = 9.6$  Hz, 2H), 3.78 (br m, 2H), 3.53–3.41 (br m, 1H), 3.24 (s, 6H), 2.94 (t,  $J = 9.6$  Hz, 2H), 2.61–2.22 (br m, 2H), 2.09–1.93 (br m, 2H), 1.82–1.58 (br m, 7H), 1.46–1.12 (br m, 13H).  $^{13}\text{C}$  NMR ( $\text{CDCl}_3$ )  $\delta$  176.7, 172.9, 166.8, 166.7, 148.2, 139.6, 139.3, 133.1, 128.6, 127.9, 127.2, 127.0, 125.4, 120.6, 117.1, 111.2, 86.6, 75.7, 75.6, 70.1, 64.4, 57.3, 57.1, 55.6, 54.7, 50.7, 35.9, 34.3, 33.9, 33.1, 28.1, 26.0, 25.9, 25.6, 25.1, 24.7, 23.9, 22.4.  $m/z$  MS (TOF ES+)  $\text{C}_{41}\text{H}_{54}\text{N}_5\text{O}_6$   $[\text{M}]^+$  calcd, 712.4, found 712.4. LC-MS:  $t_R = 3.35$  min.

***N*-(4-((4,5-Dihydroisoxazol-3-yl)oxy)but-2-yn-1-yl)-10-((4-((3-(((1*S*,2*S*)-2-hydroxycyclohexyl)carbamoyl)-4-oxoquinolin-1(4*H*)-yl)methyl)phenyl)amino)-*N,N*-dimethyl-10-oxodecan-1-aminium bromide (8f).** Light orange solid; 51.4 mg, 40%.  $^1\text{H}$  NMR ( $\text{CDCl}_3$ )  $\delta$  10.25 (app s, 1H), 9.93 (s, 1H), 8.86 (s, 1H), 8.38 (d,  $J = 7.4$  Hz, 1H), 7.73 (d,  $J = 7.8$  Hz, 2H), 7.56 (t,  $J = 7.2$  Hz, 1H), 7.43 (d,  $J = 8.4$  Hz, 1H), 7.37 (t,  $J = 7.3$  Hz, 1H), 7.01 (d,  $J = 7.8$  Hz, 2H), 5.38 (s, 2H), 4.74 (s, 2H), 4.62 (s, 2H), 4.37 (t,  $J = 9.6$  Hz, 2H), 3.78 (br m, 2H), 3.53–3.41 (br m, 1H), 3.24 (s, 6H), 2.94 (t,  $J = 9.6$  Hz, 2H), 2.61–2.22 (br m, 2H), 2.09–1.93 (br m, 2H), 1.82–1.58 (br m, 7H), 1.46–1.12 (br m, 15H).  $^{13}\text{C}$  NMR ( $\text{CDCl}_3$ )  $\delta$  176.8, 172.9, 166.7, 166.6, 148.2, 139.5, 139.3, 133.1, 128.6, 127.8, 127.2, 127.0, 125.4, 120.6, 117.1, 111.2, 86.6, 75.7, 75.6, 70.1, 64.3, 57.2, 57.1, 55.7, 54.8, 50.4, 37.1, 34.3, 32.9, 32.2, 31.4, 29.6, 28.4, 26.4, 25.5, 25.3, 24.7, 23.9, 22.4.  $m/z$  MS (TOF ES+)  $\text{C}_{42}\text{H}_{56}\text{N}_5\text{O}_6$   $[\text{M}]^+$  calcd, 726.4; found, 726.4. LC-MS:  $t_R = 3.55$  min.

**General procedure for the synthesis of compounds 1 and 10a-i.** 4-((4,5-Dihydroisoxazol-3-yl)oxy)-*N,N*-dimethylbut-2-yn-1-amine (**9**) (160  $\mu\text{mol}$ , 1.0 eq.) was dissolved in an excess of alkyl iodide (5–20 eq.). The solution was stirred at rt for 24–48 h. If iperoxo-base **9** was found to be present at this point by LC-MS the reaction was sealed and

heated gently to 60 °C on a water bath until starting material was no longer detectable. Solvent was removed in vacuum and the product washed with ethyl acetate: petroleum ether (1:1).

**4-((4,5-Dihydroisoxazol-3-yl)oxy)-*N*-ethyl-*N*,*N*-dimethylbut-2-yn-1-aminium iodide (10a).** White solid; 39.4 mg, 70%. <sup>1</sup>H NMR (*d*<sub>6</sub>-DMSO)  $\delta$  4.93 (t, *J* = 1.7, 2H), 4.43 (t, *J* = 1.7, 2H), 4.32 (t, *J* = 9.6 Hz, 2H), 3.42 (q, *J* = 7.3 Hz, 2H), 3.05 (s, 6H), 3.02 (t, *J* = 9.6 Hz, 2H), 1.26 (t, *J* = 7.3 Hz, 3H). <sup>13</sup>C NMR (*d*<sub>6</sub>-DMSO)  $\delta$  166.7, 85.9, 76.1, 69.6, 58.9, 57.2, 52.9, 49.2, 32.2, 7.9. *m/z* MS (TOF ES+) C<sub>11</sub>H<sub>19</sub>N<sub>2</sub>O<sub>2</sub>+ [M]<sup>+</sup> calcd, 211.1; found, 211.1. LC-MS: *t*<sub>R</sub> = 1.04 min.

**4-((4,5-Dihydroisoxazol-3-yl)oxy)-*N*,*N*-dimethyl-*N*-propylbut-2-yn-1-aminium iodide (10b).** White solid; 18.1 mg, 31%. <sup>1</sup>H NMR (CDCl<sub>3</sub>)  $\delta$  4.92 (t, *J* = 1.5 Hz, 2H), 4.82 (t, *J* = 1.5 Hz, 2H), 4.44 (t, *J* = 9.6 Hz, 2H), 3.65–3.55 (m, 2H), 3.45 (s, 6H), 3.03 (t, *J* = 9.6 Hz, 2H), 1.91–1.75 (m, 2H), 1.07 (t, *J* = 7.3 Hz, 3H). <sup>13</sup>C NMR (*d*<sub>6</sub>-DMSO)  $\delta$  166.7, 86.0, 76.2, 69.6, 64.6, 57.2, 53.4, 49.8, 32.2, 15.5, 10.4. *m/z* MS (TOF ES+) C<sub>12</sub>H<sub>21</sub>N<sub>2</sub>O<sub>2</sub>+ [M]<sup>+</sup> calcd, 225.2; found, 225.2. LC-MS: *t*<sub>R</sub> = 1.80 min.

***N*-Butyl-4-((4,5-dihydroisoxazol-3-yl)oxy)-*N*,*N*-dimethylbut-2-yn-1-aminium iodide (10c).** White solid; 26.5 mg, 44%. <sup>1</sup>H NMR (CDCl<sub>3</sub>)  $\delta$  4.86 (t, *J* = 1.5 Hz, 2H), 4.83 (t, *J* = 1.5 Hz, 2H), 4.43 (t, *J* = 9.6 Hz, 2H), 3.73–3.58 (m, 2H), 3.45 (s, 6H), 3.02 (t, *J* = 9.6 Hz, 2H), 1.81–1.66 (m, 2H), 1.52–1.40 (m, 2H), 1.01 (t, *J* = 7.3 Hz, 2H). <sup>13</sup>C NMR (CDCl<sub>3</sub>)  $\delta$  166.9, 87.1, 75.7, 70.2, 64.5, 57.4, 55.3, 51.0, 33.1, 24.9, 19.6, 13.8. *m/z* MS (TOF ES+) C<sub>13</sub>H<sub>23</sub>N<sub>2</sub>O<sub>2</sub>+ [M]<sup>+</sup> calcd, 239.2; found, 239.2. LC-MS: *t*<sub>R</sub> = 1.79 min.

***N*-(4-((4,5-Dihydroisoxazol-3-yl)oxy)but-2-yn-1-yl)-*N*,*N*-dimethylpentan-1-aminium iodide (10d).** White solid; 40.0 mg, 64%. <sup>1</sup>H NMR (CDCl<sub>3</sub>)  $\delta$  4.85 (t, *J* = 1.5 Hz, 2H), 4.83 (t, *J* = 1.5 Hz, 2H), 4.44 (t, *J* = 9.6 Hz, 2H), 3.69–3.58 (m, 2H), 3.44 (s, 6H), 3.03 (t, *J* = 9.7 Hz, 2H), 1.84–1.68 (m, 2H), 1.44–1.35 (m, 4H), 0.94 (t, *J* = 6.9 Hz, 3H). <sup>13</sup>C NMR (CDCl<sub>3</sub>)  $\delta$

166.9, 87.2, 75.6, 70.2, 64.8, 57.3, 55.3, 51.0, 33.1, 28.2, 22.7, 22.4, 14.0. *m/z* MS (TOF ES+)  $C_{14}H_{25}N_2O_2 + [M]^+$  calcd, 253.2; found, 253.2. LC-MS:  $t_R = 1.80$  min.

***N*-(4-((4,5-Dihydroisoxazol-3-yl)oxy)but-2-yn-1-yl)-*N,N*-dimethylhexan-1-aminium iodide (10e).** White solid; 43.2 mg, 66%.  $^1H$  NMR ( $CDCl_3$ )  $\delta$  4.87 (t,  $J = 1.5$  Hz, 2H), 4.83 (t,  $J = 1.5$  Hz, 2H), 4.44 (t,  $J = 9.6$  Hz, 2H), 3.68–3.57 (m, 2H), 3.45 (s, 6H), 3.03 (t,  $J = 9.6$  Hz, 2H), 1.82–1.68 (m, 2H), 1.49–1.21 (m, 6H), 0.90 (t,  $J = 7.1$  Hz, 3H).  $^{13}C$  NMR ( $d_6$ -DMSO)  $\delta$  166.7, 86.0, 76.1, 69.6, 63.2, 57.2, 53.2, 49.8, 32.3, 30.6, 25.3, 21.8, 21.7, 13.8. *m/z* MS (TOF ES+)  $C_{15}H_{27}N_2O_2 + [M]^+$  calcd, 267.2; found, 267.2. LC-MS:  $t_R = 1.79$  min.

***N*-(4-((4,5-Dihydroisoxazol-3-yl)oxy)but-2-yn-1-yl)-*N,N*-dimethylheptan-1-aminium iodide (10f).** White solid; 48.0 mg, 71%.  $^1H$  NMR ( $CDCl_3$ )  $\delta$  4.87 (t,  $J = 1.5$  Hz, 2H), 4.83 (t,  $J = 1.5$  Hz, 2H), 4.44 (t,  $J = 9.6$  Hz, 2H), 3.69 – 3.55 (m, 2H), 3.45 (s, 6H), 3.03 (t,  $J = 9.6$  Hz, 2H), 1.82–1.67 (m, 2H), 1.47–1.15 (m, 8H), 0.88 (t,  $J = 6.9$  Hz, 3H).  $^{13}C$  NMR ( $CDCl_3$ )  $\delta$  166.9, 87.2, 75.8, 70.3, 64.8, 57.5, 55.4, 51.1, 33.2, 31.0, 29.0, 26.2, 23.1, 22.7, 14.2. *m/z* MS (TOF ES+)  $C_{16}H_{29}N_2O_2 + [M]^+$  calcd, 281.2; found, 281.2. LC-MS:  $t_R = 1.80$  min.

***N*-(4-((4,5-Dihydroisoxazol-3-yl)oxy)but-2-yn-1-yl)-*N,N*-dimethyloctan-1-aminium iodide (10g).** White solid; 113.1 mg, 75 %.  $^1H$  NMR ( $CDCl_3$ )  $\delta$  4.88 (t,  $J = 1.5$  Hz, 2H), 4.83 (t,  $J = 1.5$  Hz, 2H), 4.43 (t,  $J = 9.6$  Hz, 2H), 3.70–3.57 (m, 2H), 3.45 (s, 6H), 3.02 (t,  $J = 9.6$  Hz, 2H), 1.82–1.70 (m, 2H), 1.45–1.15 (m, 12H), 0.86 (t,  $J = 6.8$  Hz, 2H).  $^{13}C$  NMR ( $CDCl_3$ )  $\delta$  166.9, 87.0, 75.8, 70.2, 64.7, 57.5, 55.3, 51.0, 33.1, 31.8, 29.3, 29.2, 26.3, 23.1, 22.8, 14.2. *m/z* MS (TOF ES+)  $C_{17}H_{31}N_2O_2 + [M]^+$  calcd, 295.2; found, 295.2. LC-MS:  $t_R = 1.81$  min.

***N*-(4-((4,5-Dihydroisoxazol-3-yl)oxy)but-2-yn-1-yl)-*N,N*-dimethylnonan-1-aminium iodide (10h).** White solid; 132.8 mg, 68 %.  $^1H$  NMR ( $CDCl_3$ )  $\delta$  4.88 (t,  $J = 1.5$  Hz, 2H), 4.83 (t,  $J = 1.5$  Hz, 2H), 4.42 (t,  $J = 9.6$  Hz, 2H), 3.71–3.56 (m, 2H), 3.45 (s, 6H), 3.02 (t,  $J = 9.6$  Hz, 2H), 1.83–1.69 (m, 2H), 1.46–1.16 (m, 14H), 0.86 (t,  $J = 6.8$  Hz, 3H);  $^{13}C$  NMR ( $CDCl_3$ )

$\delta$  166.9, 87.0, 75.8, 70.2, 64.7, 57.5, 55.3, 51.0, 33.1, 31.9, 29.5, 29.3, 29.1, 26.3, 23.1, 22.8, 14.3;  $m/z$  MS (TOF ES+)  $C_{18}H_{33}N_2O_2$   $[M]^+$  calcd, 309.3; found, 309.3. LC-MS:  $t_R$  = 1.82 min.

***N*-(4-((4,5-Dihydroisoxazol-3-yl)oxy)but-2-yn-1-yl)-*N,N*-dimethyldecan-1-aminium iodide (10i).** White solid; 20.1 mg, 66 %.  $^1H$  NMR ( $CDCl_3$ )  $\delta$  4.88 (t,  $J$  = 1.5 Hz, 2H), 4.83 (t,  $J$  = 1.5 Hz, 2H), 4.42 (t,  $J$  = 9.6 Hz, 2H), 3.71–3.56 (m, 2H), 3.45 (s, 6H), 3.02 (t,  $J$  = 9.6 Hz, 2H), 1.83–1.69 (m, 2H), 1.47–1.15 (m, 16H), 0.86 (t,  $J$  = 6.8 Hz, 3H).  $^{13}C$  NMR ( $CDCl_3$ )  $\delta$  166.7, 86.9, 75.8, 70.2, 64.7, 57.5, 55.3, 51.0, 33.1, 31.9, 29.5, 29.3, 29.1, 28.9, 26.3, 23.1, 22.8, 14.3;  $m/z$  MS (TOF ES+)  $C_{19}H_{35}N_2O_2$   $[M]^+$  calcd, 323.3; found, 323.3. LC-MS:  $t_R$  = 1.82 min.

***N*-(4-((4,5-Dihydroisoxazol-3-yl)oxy)but-2-yn-1-yl)-*N,N*-dimethyl-7-oxo-7-(phenylamino)heptan-1-aminium bromide (12a)** Light yellow oil; 29.3 mg, 69 %.  $^1H$  NMR ( $CDCl_3$ )  $\delta$  9.17 (s, 1H), 7.80–7.74 (m, 2H), 7.29–7.22 (m, 2H), 7.03 (tt,  $J$  = 7.6/ 1.1 Hz, 1H), 4.82–4.79 (m, 2H), 4.71–4.68 (m, 2H), 4.41 (t,  $J$  = 9.6 Hz, 2H), 3.72–3.63 (m, 2H), 3.31 (s, 6H), 2.99 (t,  $J$  = 9.6 Hz, 2H), 2.49 (t,  $J$  = 7.6 Hz, 2H), 1.83–1.67 (m, 4H), 1.53–1.36 (m, 4H).  $^{13}C$  NMR ( $CDCl_3$ )  $\delta$  172.5, 166.9, 139.1, 128.8, 123.7, 120.0, 86.9, 75.7, 70.2, 64.5, 57.3, 55.1, 47.7, 37.2, 33.0, 27.8, 25.2, 25.0, 22.17.  $m/z$  MS (TOF ES+)  $C_{22}H_{32}N_3O_3$   $[M]^+$  calcd, 386.2; found, 386.2. LC-MS:  $t_R$  = 4.725 min.

***N*-(4-((4,5-Dihydroisoxazol-3-yl)oxy)but-2-yn-1-yl)-*N,N*-dimethyl-9-oxo-9-(phenylamino)nonan-1-aminium bromide (12b)** Light yellow oil; 34.1 mg, 78 %.  $^1H$  NMR ( $CDCl_3$ )  $\delta$  9.04 (s, 1H), 7.72 (d,  $J$  = 8.0 Hz, 2H), 7.29–7.21 (m, 2H), 7.02 (t,  $J$  = 7.2 Hz, 1H), 4.83–4.72 (m, 4H), 4.39 (t,  $J$  = 9.6 Hz, 2H), 3.64–3.51 (m, 2H), 3.32 (s, 6H), 2.98 (t,  $J$  = 9.6 Hz, 2H), 2.48 (t,  $J$  = 7.2 Hz, 2H), 1.79–1.63 (m, 4H), 1.43–1.27 (m, 8H).  $^{13}C$  NMR ( $CDCl_3$ )  $\delta$  172.7, 166.9, 139.1, 128.9, 123.8, 120.2, 86.7, 75.9, 70.2, 64.6, 57.4, 54.9, 47.7, 37.3, 33.1, 28.7, 28.5, 28.4, 25.9, 25.4, 22.2.  $m/z$  MS (TOF ES+)  $C_{24}H_{36}N_3O_3$   $[M]^+$  calcd, 414.3; found, 414.3. LC-MS:  $t_R$  = 5.25 min.



***N*-(4-((4,5-Dihydroisoxazol-3-yl)oxy)but-2-yn-1-yl)-*N,N*-dimethyl-11-oxo-11-(phenylamino)undecan-1-aminium bromide (12c)** Light yellow oil; 22.7 mg, 70 %. <sup>1</sup>H NMR (CDCl<sub>3</sub>) δ 8.70 (s, 1H), 7.66 (d, *J* = 8.0 Hz, 2H), 7.25 (t, *J* = 8.0 Hz, 2H), 7.02 (t, *J* = 7.2 Hz, 1H), 4.82-4.72 (m, 4H), 4.40 (t, *J* = 9.6 Hz, 2H), 3.64-3.53 (m, 2H), 3.33 (s, 6H) 2.98 (t, *J* = 9.6 Hz, 2H), 2.44 (t, *J* = 7.2 Hz, 2H), 1.78-1.62 (m, 4H), 1.41-1.23 (m, 12H). <sup>13</sup>C NMR (CDCl<sub>3</sub>) δ 172.5, 166.9, 138.9, 128.9, 123.8, 120.2, 86.7, 75.9, 70.2, 64.5, 58.5, 57.4, 54.9, 50.6, 37.5, 33.0, 29.0, 28.9, 28.8, 28.7, 26.0, 25.6, 22.8. *m/z* MS (TOF ES+) C<sub>26</sub>H<sub>40</sub>N<sub>3</sub>O<sub>3</sub><sup>+</sup> [M]<sup>+</sup> calcd, 442.30; found, 442.3. LC-MS: *t<sub>R</sub>* = 5.81 min.

**Pharmacology.** *Cell culture.* Flp-In-CHO cells stably expressing human muscarinic M<sub>1</sub>, M<sub>2</sub>, M<sub>4</sub>, M<sub>5</sub>, or CHO-K<sub>1</sub> expressing the M<sub>3</sub> receptors were cultured at 37 °C in 5% CO<sub>2</sub> in F-12 (Ham) (M<sub>1</sub>) or Dulbecco's modified Eagle media (M<sub>2</sub> – M<sub>5</sub>) supplemented with 10% (M<sub>1</sub>) or 5% (M<sub>2</sub> – M<sub>5</sub>) (v/v) FBS.

*ERK 1/2 phosphorylation assay plate preparation.* Cells were seeded into transparent 96-well plates at 25 × 10<sup>3</sup> cells per well and grown for 6 - 8 h. Cells were then washed once with phosphate-buffered saline (PBS) and incubated in serum-free media (180 or 160 μL per well, depending on the intended assay) at 37 °C) for at least 8 h, to allow phosphorylated ERK1/2 levels to subside.

*Concentration-response curves (CRCs).* Cells were plated in 180 μL media per well. A stock solution of acetylcholine (10<sup>-2</sup> M) was made up in cold PBS. Stock solutions of the test ligands (10<sup>-2</sup> M) were made up in warm DMSO. Dilutions of all ligands were made up in FBS-free media at ten times (10×) the required concentration and added to stock plates. Cells were incubated at 37 °C with 20 μL of ligand solution at the appropriate concentration per well until peak phosphorylation occurred at which point the assay was terminated.

*Allosteric-orthosteric ligand interaction assays.* As for CRCs, except that cells were plated in 160  $\mu\text{L}$  media per well. 20  $\mu\text{L}$  of both allosteric ligand and orthosteric ligands were added immediately in succession.

*Assay termination and data collection.* Agonist-stimulated ERK1/2 phosphorylation was terminated by the removal of drugs and the addition of 100  $\mu\text{L}$  p/well of *SureFire*<sup>TM</sup> lysis buffer. The cell lysates were agitated for 5-10 min. Following agitation, 10  $\mu\text{L}$  of cell lysates were transferred into a 384-well white opaque Optiplat<sup>TM</sup>, followed by addition of 8.3  $\mu\text{L}$  of a solution of reaction buffer / activation buffer / acceptor beads / donor beads in a ratio of 60/10/0.3/0.3 (v/ v/ v/ v) under green light conditions. The plates were then incubated at 37 °C in the dark for 1 h and fluorescence was measured on a Envision<sup>TM</sup> plate reader (PerkinElmer) using standard settings.

*Radioligand equilibrium whole cell binding assay plate preparation.* Cells were seeded into white opaque Isoplates<sup>TM</sup> at  $10 \times 10^3$  cells per well and then grown at 37 °C for 20-24 h. Cells were then washed twice with 50  $\mu\text{L}$  of cold HEPES-buffered saline, then 140 or 160  $\mu\text{L}$  of cold HEPES-buffered saline was added per well.

*Orthosteric competition binding assay protocol.* Stock solutions of each ligand ( $10^{-2}$  M) were made up in cold HEPES-buffered saline. Dilutions of all ligands were made up in cold HEPES-buffered saline at ten times ( $10\times$ ) the required concentration and added to stock plates on ice. Cells were equilibrated at 25 °C for 4 h with 20  $\mu\text{L}$  of test ligand solution and 20  $\mu\text{L}$  of 1 nM [<sup>3</sup>H]NMS (total volume 200  $\mu\text{L}$  per well).

*Allosteric interaction assay protocol.* Stock solutions of each orthosteric ligand ( $10^{-2}$  M) were made up in cold HEPES-buffered saline. Stock solutions of the interacting allosteric ligands of choice ( $10^{-2}$  M) were made up in warm DMSO. Dilutions of all ligands were made up in cold HEPES-buffered saline at ten times ( $10\times$ ) the required concentration and added to

stock plates. Cells were equilibrated at 4 °C for 4 h with 20 µL of ACh, 20 µL of allosteric ligand solution and 20 µL of 1 nM [<sup>3</sup>H]NMS (total volume 200 µL per well).

*Assay termination and data collection.* Assays were terminated by media removal of the assay buffer and by washing twice with 50 µL 0.9% NaCl solution. Microscint-20 scintillation liquid (100 µL per well) was then added to each well and the plates covered. The levels of remaining bound radioligand, were measured in counts per minute (cpm) on the Microbeta2TM LumiJET 2460 microplate counter (PerkinElmer).

*Data analysis.* All data analysis was managed using Prism 6 software (GraphPad Software, San Diego, CA).

Whole cell equilibrium competition radioligand binding experiments were fitted to a one-site competition binding equation (1) to estimate the p*K<sub>i</sub>* for each ligand. The equation assumes that there is only one-site the ligands bind to and that the binding is reversible and at equilibrium:

$$Y = bottom + \frac{top - bottom}{1 + 10^{[I] - \log(10^{K_i(1 + \frac{[A]}{K_A})})}} \quad (1)$$

where Y is the percentage (vehicle control) binding, top and bottom are the total and non-specific binding, respectively. [A] and [I] are the concentrations of [<sup>3</sup>H]NMS, and competing “cold” ligand respectively, *K<sub>A</sub>* and *K<sub>i</sub>* are the equilibrium dissociation constants of [<sup>3</sup>H]NMS and the “cold” ligand, respectively. The efficacy (*τ*) of several ligands was determined by fitting the functional data to an operational model of agonism (2):

$$Y = \frac{E_{max} - Basal}{1 + (\frac{10^{\log K_A + 10[L]}}{10^{\log \tau + [L]}})^n} \quad (2)$$

where Y is the measured response, *E<sub>max</sub>* and basal are the top and bottom asymptotes of the curve, respectively, *K<sub>A</sub>* equilibrium dissociation constant for the ligand being tested, [L] is the concentration of ligand in solution, *τ* is the efficacy of the ligand being tested and n is the transducer slope. The efficacy values were then normalised to the M<sub>4</sub> mAChR values, to give

the ‘corrected efficacy’ ( $\tau_c$ ), to account for the varying receptor expression in each cell line used by the following equation:

$$\log \tau_c = \log \tau - \log\left(\frac{B_{max_{Mx}}}{B_{max_{M4}}}\right) \quad (3)$$

where  $\tau_c$  is the corrected efficacy,  $\tau$  is the measured efficacy (as determined by equation 2),  $B_{max}$  is the maximum counts recorded when the mAChR in question is incubated with a saturating concentration of [ $^3$ H]NMS, at mAChR M<sub>x</sub>, where x gives the subtype in question, compared to the M<sub>4</sub> mAChR.

## ■ REFERENCES

- (1) Fisher, A.; Pittel, Z.; Haring, R.; Bar-Ner, N.; Kliger-Spatz, M.; Natan, N.; Egozi, I.; Sonogo, H.; Marcovitch, I.; Brandeis, R. M1 muscarinic agonists can modulate some of the hallmarks in Alzheimer’s disease. *J. Mol. Neurosci.* **2003**, *20*, 349-56.
- (2) Bodick, N. C.; Offen, W. W.; Levey, A. I.; Cutler, N. R.; Gauthier, S. C.; Satlin, A.; Shannon, H. E.; Tollefson, G. D.; Rasmussen, K.; Bymaster, F. P.; Hurley, D. J.; Potter, W. Z.; Paul, S. M.; Effects of xanomeline, a selective muscarinic receptor agonist, on cognitive function and behavioral symptoms in Alzheimer's disease. *Arch. Neurol.* **1997**, *54*, 465-73.
- (3) Bodick, N. C.; Offen, W. W.; Shannon, H. E.; Satterwhite, J.; Lucas, R.; van Lier, R.; Paul, S. M. The selective muscarinic agonist xanomeline improves both the cognitive deficits and behavioral symptoms of Alzheimer disease. *Alzheimer Dis. Assoc. Disord.* **1997**, *11 Suppl 4*, S16-22.
- (4) Shekhar, A.; Potter, W.; Lienemann, J.; Sundblad, K.; Lightfoot, J.; Herrera, J.; Unverzagt, F.; Bymaster, F.; Felder, C. Efficacy of xanomeline, a selective muscarinic agonist, in treating schizophrenia: a double-blind, placebo controlled study, *ACNP 40th Annual Meeting*, **2001**; 9-13.
- (5) Shekhar, A.; Potter, W. Z.; Lightfoot, J.; Lienemann, J.; Dubé, S.; Mallinckrodt, C.; Bymaster, F. P.; McKinzie, D. L.; Felder, C. C. Selective Muscarinic Receptor Agonist Xanomeline as a Novel Treatment Approach for Schizophrenia. *Am. J. Psychiatry* **2008**, *165*, 1033–9.
- (6) Davis, A. A.; Fritz, J. J.; Wess, J.; Lah, J. J.; Levey, A. I. Deletion of the M1 Muscarinic Acetylcholine Receptors Increases Amyloid Pathology In Vitro and In Vivo. *J. Neurosci.* **2010**, *30*, 4190-6.
- (7) Zavitsanou, K.; Katsifis, A.; Mattner, F.; Xu-Feng, H. Investigation of M1/M4 muscarinic receptors in the anterior cingulate cortex in schizophrenia, bipolar disorder, and major depression disorder. *Neuropsychopharmacology* **2004**, *29*, 619-25.
- (8) Medeiros, R.; Kitazawa, M.; Caccamo, A.; Baglietto-Vargas, D.; Estrada-Hernandez, T.; Cribbs, D. H.; Fisher, A.; LaFerla, F. M. Loss of Muscarinic M(1) Receptor Exacerbates Alzheimer's Disease–Like Pathology and Cognitive Decline. *Am. J. Pathol.* **2011**, *179*, 980-91.
- (9) Shannon, H. E.; Rasmussen, K.; Bymaster, F. P.; Hart, J. C.; Peters, S. C.; Swedberg, M. D. B.; Jeppesen, L.; Sheardown, M. J.; Sauerberg, P.; Fink-Jensen, A. Xanomeline, an M1/M4

preferring muscarinic cholinergic receptor agonist, produces antipsychotic-like activity in rats and mice. *Schizophr. Res.* **2000**, *42*, 249-59.

(10) Andersen, M. B.; Fink.-Jensen, A.; Peacock, L.; Gerlach, J.; Bymaster, F.; Lundbæk, J. A.; Werge, T. The Muscarinic M1/M4 Receptor Agonist Xanomeline Exhibits Antipsychotic-Like Activity in *Cebus apella* Monkeys. *Neuropsychopharmacology* **2003**, *28*, 1168-75.

(11) Mirza, N. R.; Peters, D.; Sparks, R. G. Xanomeline and the Antipsychotic Potential of Muscarinic Receptor Subtype Selective Agonists. *CNS Drug Rev.* **2003**, *9*, 159-86.

(12) Gregory, K. J.; Sexton, P. M.; Christopoulos, A. Allosteric Modulation of Muscarinic Acetylcholine Receptors. *Curr. Neuropharmacol.* **2007**, *5*, 157-67.

(13) Wootten, D.; Christopoulos, A.; Sexton, P. M. Emerging paradigms in GPCR allostery: implications for drug discovery. *Nat. Rev. Drug Discov.* **2013**, *12*, 630-44.

(14) Conn, P. J.; Christopoulos, A.; Lindsley, C. W. Allosteric modulators of GPCRs: a novel approach for the treatment of CNS disorders. *Nat. Rev. Drug Discov.* **2009**, *8*, 41-54.

(15) Kruse, A. C.; Kobilka, B. K.; Gautam, D.; Sexton, P. M.; Christopoulos, A.; Wess, J. Muscarinic acetylcholine receptors: novel opportunities for drug development. *Nat. Rev. Drug Discov.* **2014**, *13*, 549-60.

(16) Ma, L.; Seager, M. A.; Wittmann, M.; Jacobson, M.; Bickel, D.; Burno, M.; Jones, K.; Graufelds, V. K.; Xu, G.; Pearson, M.; McCampbell, A.; Gaspar, R.; Shughrue, P.; Danziger, A.; Regan, C.; Flick, R.; Pascarella, D.; Garson, S.; Doran, S.; Kreatsoulas, C.; Veng, L.; Lindsley, C. W.; Shipe, W.; Kuduk, S.; Sur, C.; Kinney, G.; Seabrook, G. R.; Ray, W. J. Selective activation of the M1 muscarinic acetylcholine receptor achieved by allosteric potentiation. *Proc. Natl. Acad. Sci.* **2009**, *106*, 15950-5.

(17) Mistry, S. N.; Jorg, M.; Lim, H.; Vinh, N. B.; Sexton, P. M.; Capuano, B.; Christopoulos, A.; Lane, J. R.; Scammells, P. J. 4-Phenylpyridin-2-one Derivatives: A Novel Class of Positive Allosteric Modulator of the M1 Muscarinic Acetylcholine Receptor. *J. Med. Chem.* **2016**, *59*, 388-409.

(18) Dallagnol, J. C. C.; Khajehali, E.; van der Westhuizen, E. T.; Jörg, M.; Valant, C.; Gonçalves, A. G.; Capuano, B.; Christopoulos, A.; Scammells, P. J.; Synthesis and Pharmacological Evaluation of Heterocyclic Carboxamides: Positive Allosteric Modulators of the M1 Muscarinic Acetylcholine Receptor with Weak Agonist Activity and Diverse Modulatory Profiles. *J. Med. Chem.* **2018**, *61*, 2875-94.

(19) Khajehali, E.; Valant, C.; Jörg, M.; Tobin, A. B.; Conn, P. J.; Lindsley, C. W.; Sexton, P. M.; Scammells, P. J.; Christopoulos, A. Probing the binding site of novel selective positive allosteric modulators at the M1 muscarinic acetylcholine receptor. *Biochem. Pharmacol.* **2018**, *154*, 243-54.

(20) Lane, R. J.; Sexton, P. M.; Christopoulos, A. Bridging the gap: bitopic ligands of G-protein-coupled receptors. *Trends Pharmacol. Sci.* **2013**, *34*, 59-66.

(21) Valant, C.; Robert Lane, J.; Sexton, P. M.; Christopoulos, A. The best of both worlds? Bitopic orthosteric/allosteric ligands of G protein-coupled receptors. *Annu. Rev. Pharmacol. Toxicol.* **2012**, *52*, 153-78.

(22) Disingrini, T.; Muth, M.; Dallanoce, C.; Barocelli, E.; Bertoni, S.; Kellershohn, K.; Mohr, K.; De Amici, M.; Holzgrabe, U. Design, Synthesis, and Action of Oxotremorine-Related Hybrid-Type Allosteric Modulators of Muscarinic Acetylcholine Receptors. *J. Med. Chem.* **2006**, *49*, 366-72.

(23) Valant, C.; Gregory, K. J.; Hall, N. E.; Scammells, P. J.; Lew, M. J.; Sexton, P. M.; Christopoulos, A. A Novel Mechanism of G Protein-coupled Receptor Functional Selectivity: Muscarinic partial agonist McN-A-343 as a bitopic orthosteric/allosteric ligand. *J. Biol. Chem.* **2008**, *283*, 29312-21.

- (24) Chen, X.; Klöckner, J.; Holze, J.; Zimmermann, C.; Seemann, W. K.; Schrage, R.; Bock, A.; Mohr, K.; Tränkle, C.; Holzgrabe, U.; Decker, M. Rational Design of Partial Agonists for the Muscarinic M1 Acetylcholine Receptor. *J. Med. Chem.* **2015**, *58*, 560-76.
- (25) Keov, P.; Valant, C.; Devine, S. M.; Lane, J. R.; Scammells, P. J.; Sexton, P. M.; Christopoulos, A.. Reverse Engineering of the Selective Agonist TBPB Unveils Both Orthosteric and Allosteric Modes of Action at the M1 Muscarinic Acetylcholine Receptor. *Mol. Pharmacol.* **2013**, *84*, 425-37.
- (26) Steinfeld, T.; Hughes, A. D.; Klein, U.; Smith, J. A.; Mammen, M. THRX-198321 Is a Bifunctional Muscarinic Receptor Antagonist and beta-2-Adrenoceptor Agonist (MABA) That Binds in a Bimodal and Multivalent Manner *Mol. Pharmacol.* **2010**, *79*, 389–99.
- (27) Keov, P.; López, L.; Devine, S. M.; Valant, C.; Lane, J. R.; Scammells, P. J.; Christopoulos, A.; Sexton, P. M.; A. Molecular mechanisms of bitopic ligand engagement with the M1 muscarinic acetylcholine receptor. *J. Biol. Chem.* **2014**, *289*, 23817-37.
- (28) Steinfeld, T.; Mammen, M.; Smith, J. A.; Wilson, R. D.; Jasper, J. R. A Novel Multivalent Ligand That Bridges the Allosteric and Orthosteric Binding Sites of the M2 Muscarinic Receptor. *Mol. Pharmacol.* **2007**, *72*, 291-302.
- (29) Schmitz, J.; van der May, D.; Bermudez, M.; Klöckner, J.; Schrage, R.; Kostenis, E.; Tränkle, C.; Wolber, G.; Mohr, K.; Holzgrabe, U. Dualsteric Muscarinic Antagonists—Orthosteric Binding Pose Controls Allosteric Subtype Selectivity. *J. Med. Chem.* **2014**, *57*, 6739–50.
- (30) Bock, A.; Chirinda, B.; Krebs, F.; Messerer, R.; Bätz, J.; Muth, M.; Dallanoce, C.; Kligenthal, D.; Tränkle, C.; Hoffmann, C.; De Amici, M.; Holzgrabe, U.; Kostenis, E.; Mohr, K. Dynamic ligand binding dictates partial agonism at a g protein–coupled receptor. *Nat. Chem. Biol.* **2014**, *10*, 18-20.
- (31) Mohr, K.; Tränkle, C.; Kostenis, E.; Barocelli, E.; De Amici, M.; Holzgrabe, U., Rational design of dualsteric GPCR ligands: quests and promise. *Br J Pharmacol.* **2010**, *159* (5), 997-1008..
- (32) Bock, A.; Bermudez, M.; Krebs, F.; Matera, C.; Chirinda, B.; Sydow, D.; Dallanoce, C.; Holzgrabe, U.; De Amici, M.; Lohse, M. J.; Wolber, G.; Mohr, K. Ligand Binding Ensembles Determine Graded Agonist Efficacies at a G Protein-coupled Receptor. *J. Biol. Chem.* **2016**, *291*, 16375-89.
- (33) Bermudez, M.; Bock, A.; Krebs, F.; Holzgrabe, U.; Mohr, K.; Lohse, M. J.; Wolber, G. Ligand-Specific Restriction of Extracellular Conformational Dynamics Constrains Signaling of the M2 Muscarinic Receptor. *ACS Chem. Biol.* **2017**, *12*, 1743-48.
- (34) Messerer, R.; Kauk, M.; Volpato, D.; Alonso Canizal, M. C.; Klockner, J.; Zabel, U.; Nuber, S.; Hoffmann, C. FRET Studies of Quinolone-Based Bitopic Ligands and Their Structural Analogues at the Muscarinic M1 Receptor. *ACS Chem. Biol.* **2017**, *12*, 833-43.
- (35) Schrage, R.; Seemann, W. K.; Klöckner, J.; Dallanoce, C.; Racké, K.; Kostenis, E.; De Amici, M.; Holzgrabe, U.; Mohr, K. Agonists with supraphysiological efficacy at the muscarinic M2 ACh receptor. *Br. J. Pharmacol.* **2013**, *169*, 357-70.
- (36) Kruse, A. C.; Ring, A. M.; Manglik, A.; Hu, J.; Hu, K.; Eitel, K.; Hubner, H.; Pardon, E.; Valant, C.; Sexton, P. M.; Christopoulos, A.; Felder, C. C.; Gmeiner, P.; Steyaert, J.; Weis, W. I.; Garcia, K. C.; Wess, J.; Kobilka, B. K. Activation and allosteric modulation of a muscarinic acetylcholine receptor. *Nature* **2013**, *504*, 101-6.
- (37) Mistry, S. N.; Valant, C.; Sexton, P. M.; Capuano, B.; Christopoulos, A.; Scammells, P. J. Synthesis and Pharmacological Profiling of Analogues of Benzyl Quinolone Carboxylic Acid (BQCA) as Allosteric Modulators of the M1 Muscarinic Receptor. *J. Med. Chem.* **2013**, *56*, 5151-72.
- (38) Davie, B. J.; Valant, C.; White, J. M.; Sexton, P. M.; Capuano, B.; Christopoulos, A.; Scammells, P. J. Synthesis and Pharmacological Evaluation of Analogues of Benzyl Quinolone

Carboxylic Acid (BQCA) Designed to Bind Irreversibly to an Allosteric Site of the M1 Muscarinic Acetylcholine Receptor. *J. Med. Chem.* **2014**, *57*, 5405-18.

(39) Kloeckner, J.; Schmitz, J.; Holzgrabe, U. Convergent, short synthesis of the muscarinic superagonist iperovo. *Tetrahedron Lett.* **2010**, *51*, 3470-2.

(40) Gottlieb, H. E.; Kotlyar, V.; Nudelman, A. NMR Chemical Shifts of Common Laboratory Solvents as Trace Impurities. *J. Org. Chem.* **1997**, *62*, 7512-5.

# Chapter Three



## **Declaration of Contributions for Chapter Three**

The design and synthesis of all of the ligands presented in this chapter was performed by myself. The pharmacological assaying/ evaluation of the aforementioned ligands was also performed by myself, including all analysis. The cloned hM<sub>1</sub>-M<sub>5</sub> muscarinic acetylcholine cell lines used in this work were provided by the laboratory of Dr. Arthur Christopoulos. General guidance in the pharmacological analysis was also provided by Dr. Arthur Christopoulos and Dr. Celine Valant.

# Structure-Activity Relationship Study of Novel M<sub>2</sub>/ M<sub>4</sub> Selective Muscarinic Acetylcholine Receptor Hybrid Ligand Partial Agonists

**ABSTRACT:** In chapter 2 we identified several iperoxo-based truncated hybrid ligands which possessed good potency and selectivity for the M<sub>2</sub>/M<sub>4</sub> mAChRs. Noting the potential therapeutic relevance of an M<sub>4</sub> mAChR selective agonist we have explored these structures here in this chapter in an attempt to optimise their potency and M<sub>4</sub> mAChR selectivity. We have explored substitutions to all regions of the molecule including the orthosteric pharmacophore, linker and terminal allosteric substituent. Our results show that substitution of the orthosteric pharmacophore for a more M<sub>1</sub>/M<sub>4</sub> mAChR selective, but lower efficacy, ligand (McN-A-343) results in a loss of activity, demonstrating the necessity of a high efficacy agonist as the orthosteric pharmacophore when designing mAChR hybrid-ligand agonists. Substitution of the linker with heteroatoms or a heteroaliphatic ring gave ligands which displayed lower potency and selectivity than their alkyl linker counterparts, suggesting that this region of the molecule is intolerant of both polar and sterically bulky substitution. Modification of the terminal allosteric phenyl group of our lead compound yielded several interesting compounds which display varied efficacy values and selectivity, including two low efficacy ligands with good selectivity for the M<sub>2</sub> and M<sub>4</sub> mAChRs, respectively. However, an apparent interdependence of efficacy and selectivity was observed for all of the compounds evaluated which limited further optimization towards a highly efficacious M<sub>4</sub> mAChR selective agonist. We propose that there may be a molecular mechanistic explanation for this apparent interdependence of selectivity and efficacy which may limit further optimisation.

## ■ INTRODUCTION

Family A (rhodopsin-like) G protein-coupled receptors (GPCRs) are a class of membrane bound receptor proteins that contains many important pharmaceutical targets, constituting approximately one quarter of currently approved drugs.<sup>1-3</sup> Structurally, GPCRs consist of seven alpha-helices that traverse the cell membrane and are connected by extracellular and intracellular ‘loops’.<sup>4</sup> GPCRs bind to an endogenous ligand at their so called ‘orthosteric’ site, which in the family A GPCRs is located in the middle of the helix ‘bundle’, approximately half-way across the cell membrane.<sup>5</sup> Many, and potentially all, GPCRs also possess secondary binding sites referred to as ‘allosteric’ binding sites which are typically less conserved and thus offer more opportunities for selectivity.<sup>6</sup> Ligands which engage both the allosteric and orthosteric sites simultaneously are referred to as ‘bitopic’ (or ‘dualsteric’) ligands, and usually consist of two ligands (or ‘pharmacophores’) connected by a molecular linker (Figure 1).<sup>7-9</sup>

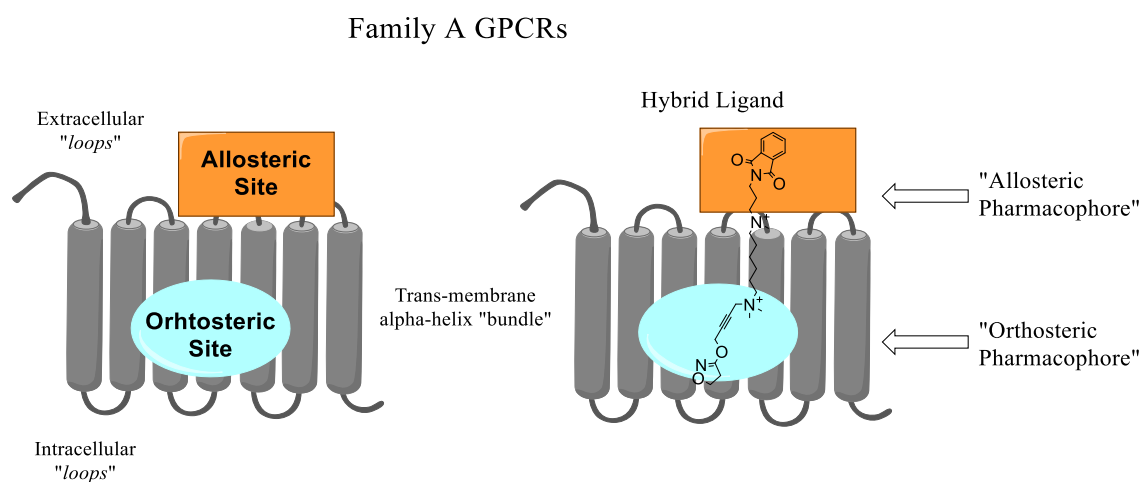


**Figure 1.** Schematic diagram of a family A GPCR and a hybrid ligand bound to a family A GPCR in a ‘bitopic’ or ‘dualsteric’ binding mode.

The muscarinic acetylcholine receptors are a sub-family of the family A GPCRs that contains five members, the M<sub>1</sub>-M<sub>5</sub> mAChRs. Each of the M<sub>1</sub>-M<sub>5</sub> mAChR subtypes are involved in pharmaceutically relevant biological processes and both antagonist and agonist drugs

targeting the mAChRs are used clinically.<sup>10-11</sup> Activation of the M<sub>1</sub> and M<sub>4</sub> mAChRs has previously been established as a promising pharmaceutical target for the treatment of Alzheimer's disease and schizophrenia, respectively.<sup>12-19</sup> However, designing subtype selective mAChR agonists has proven a significant challenge,<sup>13-14</sup> presumably due to the homologous structure of the orthosteric site across the M<sub>1</sub>-M<sub>5</sub> mAChR subtypes,<sup>20-23</sup> to which most mAChR agonists typically exclusively bind. As a result, mAChR agonism is usually accompanied by off-target side effects at the related mAChR subtypes. Hybrid ligands offer an attractive solution to the issue of subtype selectivity as they have the potential to interact with the mAChRs outside the orthosteric site to less conserved, allosteric regions of the receptor, which can potentially engender the hybrid ligands with subtype selectivity.<sup>24-27</sup>

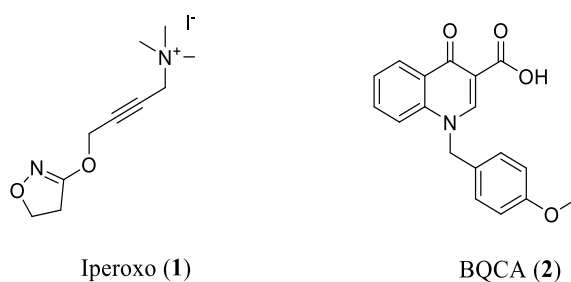


**Figure 2.** Chemical structures of full-agonist, iperoxo (4-[(4,5-dihydro-3-isoxazolyl)oxy]-N,N,N-trimethyl-2-butyne-1-aminium iodide) (1) and M<sub>1</sub> mAChR selective PAM, BQCA (1-(4-methoxybenzyl)-4-oxo-1,4-dihydro-3-quinolinecarboxylic acid) (2).

In chapter 2, we explored the conjoining of a potent agonist, iperoxo (1), and a positive allosteric modulator (PAM)/ agonist, BQCA (2), in an attempt to design an M<sub>1</sub> mAChR selective partial agonist (Figure 2). We found the selectivity of the resultant hybrid ligands to be, unexpectedly, partially selective towards the M<sub>2</sub>/ M<sub>4</sub> mAChR instead of the M<sub>1</sub> mAChR. Noting the potential clinical significance of an M<sub>4</sub> mAChR selective agonist, we then attempted

to elucidate the mechanism of this selectivity as well as to improve the M<sub>4</sub> mAChR selectivity and potency of these ligands.

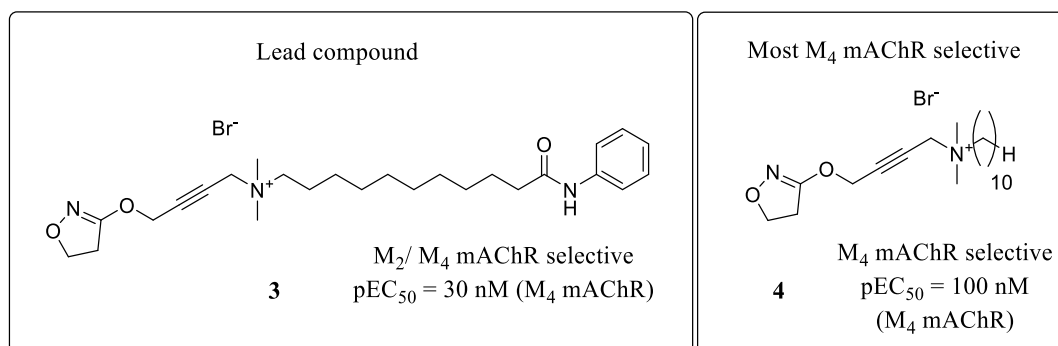


**Figure 3.** Structures of the more potent lead compound (*N*-(4-((4,5-dihydroisoxazol-3-yl)oxy)but-2-yn-1-yl)-*N,N*-dimethyl-11-oxo-11-(phenylamino)undecan-1-aminium bromide) (**3**) and the most M<sub>4</sub> mAChR selective ligand (*N*-(4-((4,5-dihydroisoxazol-3-yl)oxy)but-2-yn-1-yl)-*N,N*-dimethyldecan-1-aminium iodide) (**4**), identified in a previous study (Chapter 2).

We identified *N*-(4-((4,5-dihydroisoxazol-3-yl)oxy)but-2-yn-1-yl)-*N,N*-dimethyl-11-oxo-11-(phenylamino)undecan-1-aminium bromide (**3**) as a potent agonist with significant M<sub>2</sub>/M<sub>4</sub> mAChR selectivity and *N*-(4-((4,5-dihydroisoxazol-3-yl)oxy)but-2-yn-1-yl)-*N,N*-dimethyldecan-1-aminium bromide (**4**) as having significant selectivity for the M<sub>4</sub>>M<sub>2</sub>>>M<sub>1</sub>/M<sub>3</sub>/M<sub>5</sub> mAChRs at the level of efficacy, albeit with relatively lower potency compared with compound **3** (Figure 3). This study demonstrated the previously unacknowledged importance of the *N*-linker for selectivity of iperoxo-based mAChR hybrid ligands and that non-ligand ‘allosteric’ pharmacophores can be employed to achieve high potency and selective agonists, such as compound **3**. In our initial hybrid ligand structure-activity relationship (SAR) study, M<sub>2</sub>/M<sub>4</sub> mAChR selectivity and efficacy of these ligands appeared to be inversely related. That is, only either selectivity or high potency could be attained in a single ligand, but not both properties. Given the noteworthy improvement in

selectivity observed in the (subtype non-selective) mAChR agonist, iperoxo, upon hybridization we also speculated that this effect may be more pronounced upon the hybridization of a more selective orthosteric agonist. In this study, we wanted to look at several aspects of the mAChR hybrid ligand structure eluded as potentially interesting by our previous study in chapter 2. These included substituting the orthosteric pharmacophore for a more selective one, substituting the *N*-linker of the hybrid ligands and expanding on the SAR study surrounding substitution of the phenyl ring of compound **3**.

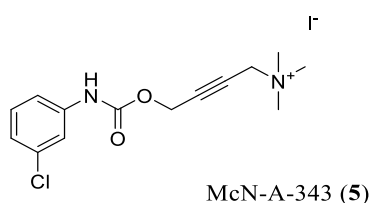


**Figure 4.** Chemical structure of the M<sub>1</sub>/M<sub>4</sub> mAChR preferring partial agonist, McN-A-343 (4-(((3-chlorophenyl)carbamoyl)oxy)-*N,N,N*-trimethylbut-2-yn-1-aminium iodide) (**5**).

McN-A-343 (**5**) is an M<sub>1</sub>/ M<sub>4</sub> mAChR preferring partial agonist which has shown evidence for acting at the mAChRs by a bitopic mechanism (Figure 4).<sup>28</sup> McN-A-343 **5** also, unlike iperoxo (**1**), distinguishes between the M<sub>2</sub> and M<sub>4</sub> mAChRs.<sup>29</sup> For these reasons we looked at swapping the subtype non-selective agonist (orthosteric pharmacophore), iperoxo (**1**), for McN-A-343 (**5**) as the orthosteric pharmacophore of our hybrid ligands.<sup>30</sup> We also looked at substituting the *N*-linker of our hybrid ligands with structural motifs from a class of diaryldiazepinone based selective mAChR antagonists, which includes telenzepine (**6**), pirenzepine (**7**), AF-DX 384 (**8**), otenzepad (**9**), AQ-RA 741 (**10**), among others (Figure 5).

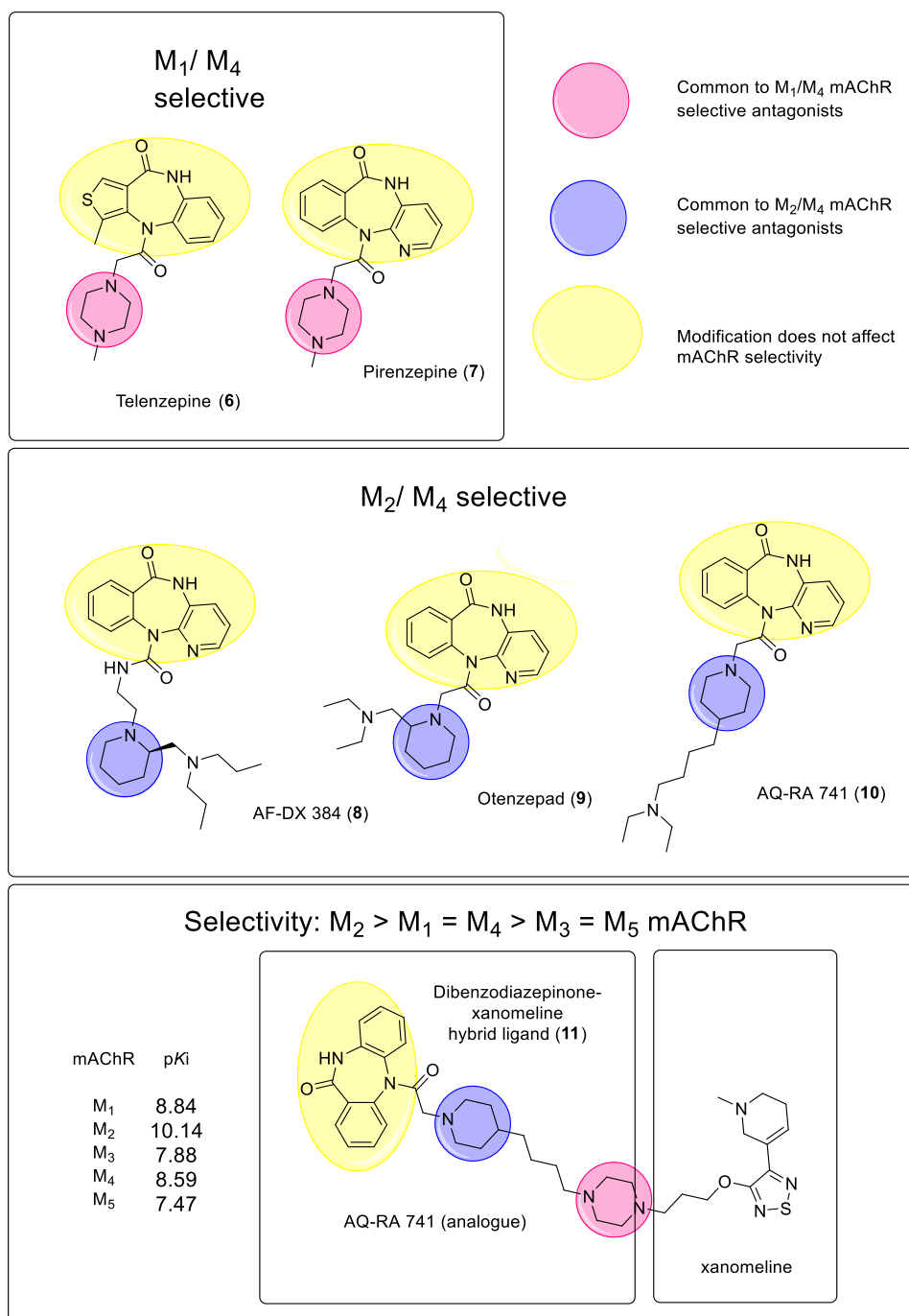


**Figure 5.** Chemical structures of mAChR subtype-selective antagonists; telenzepine (6), pirenzepine (7), AF-DX 384 (8), otenzepad (9), AQ-RA 741 (10) and a dibenzodiazepinone-xanomeline hybrid ligand (11), previously described by She *et al.*<sup>31</sup>

Based on comparison of the structures of the M<sub>1</sub>/ M<sub>4</sub> mAChR selective antagonists, telenzepine (**6**) and pirenzepine (**7**), and the M<sub>2</sub>/ M<sub>4</sub> mAChR selective antagonists, AF-DX 384 (**8**), otenzepad (**9**) and AQ-RA 741 (**10**), we hypothesized that the heteroaliphatic rings (piperazine in M<sub>1</sub>/ M<sub>4</sub> mAChR selective ligands and piperidine in the M<sub>2</sub>/M<sub>4</sub> mAChR selective ligands) may play a role in the selectivity of these ligands (Figure 5). Furthermore AF-DX 384 has shown evidence of interacting with the mAChRs allosterically,<sup>32</sup> which in turn suggests that the structurally related diaryldiazepinone ligands (Figure 5) may also act by a more complex mechanism than previously thought. From these two points, we speculated that incorporation of these heteroaliphatic rings into our hybrid ligands may augment their selectivity at the level of affinity in favour of either the M<sub>1</sub>/ M<sub>4</sub> mAChR (if a piperazine were installed) or M<sub>2</sub>/ M<sub>4</sub> mAChR (if a piperidine were installed). She *et al.* recently demonstrated that the M<sub>2</sub> mAChR affinity selectivity could be augmented by hybridising the orthosteric partial agonist xanomeline and a dibenzodiazepinone-type derivative of AQ-RA 741 (Figure 5). Intriguingly this ligand contains both the piperazinyl and piperidinyl motifs and as expected as consequence of our hypothesis, has greatest affinity at the M<sub>2</sub>>M<sub>1</sub>=M<sub>4</sub> mAChRs, similar to the diaryldiazepinone ligands from which it is derived. However when the full diaryldiazepinone pharmacophore (Figure 5) is incorporated into a hybrid ligand with the partial agonist xanomeline mAChR agonism is lost.<sup>31</sup> We suspected that the loss of efficacy of this ligand results from conformational restriction of the active state of the allosteric site<sup>33</sup> by the dibenzodiazepinone antagonist core. In our ligand design, we hoped to maintain ligand efficacy and so removed much of the diaryldiazepinone core, leaving only a phenyl ring, such that the resultant hybrids structurally resembled our lead mAChR hybrid ligand, **1**, for the sake of comparison (Figure 6).



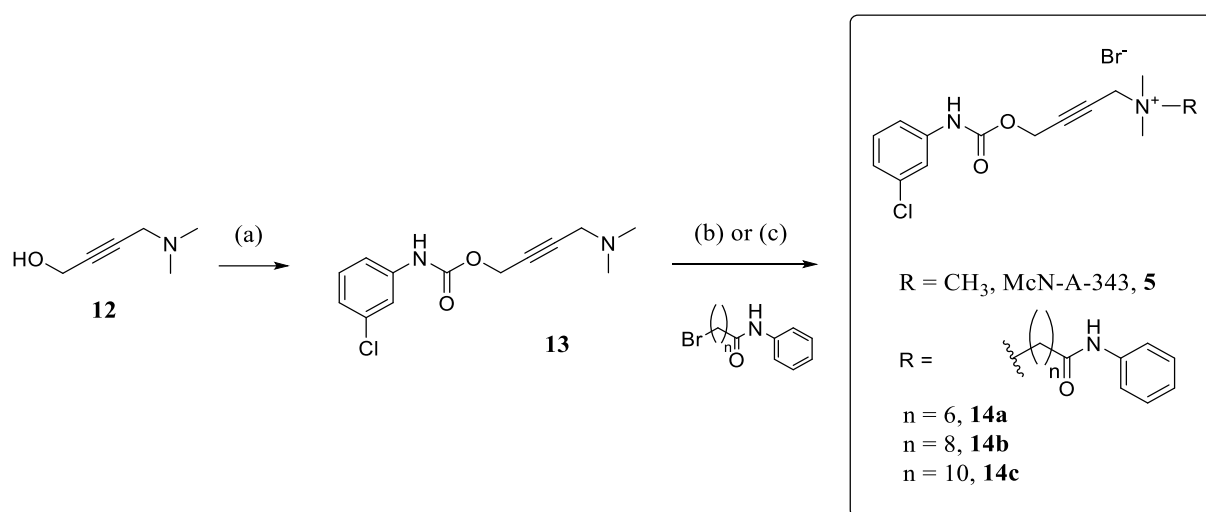


bulk, hydrogen bonding and electron donating properties, and the trifluoromethyl was chosen because of its hydrogen bonding and electron withdrawing properties.

## ■ RESULTS AND DISCUSSION

**Chemistry.** The synthesis of McN-A-343-base **13** was carried out by combining the synthesis of 4-(*N,N*-dimethylamino)but-2-yn-1-ol (**12**) reported by Klockner *et al.*<sup>34</sup> and then forming the carbamide with 3-chlorophenylisocyanate and base, similar to previously reported methods (Scheme 1).<sup>28, 35-36</sup> Overall the yields are comparable to previously reported methods.<sup>35</sup>

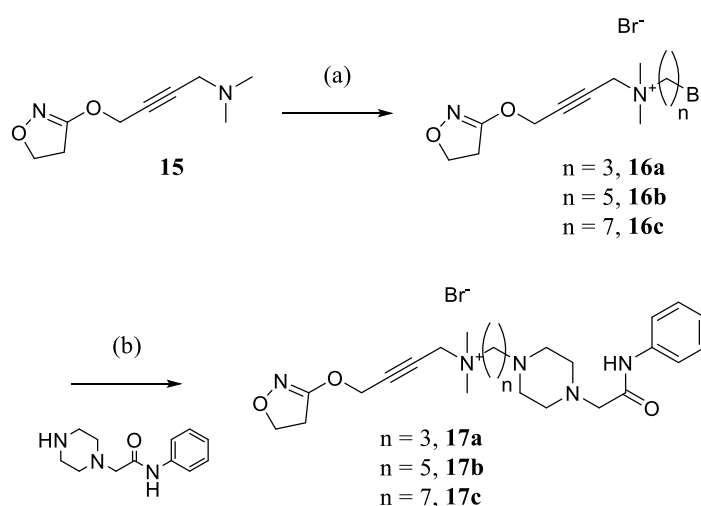
**Scheme 1. Synthesis of McN-A-343 and hybrid ligand derivatives thereof<sup>a</sup>**



<sup>a</sup>Reagents and conditions: (a) 3-chlorophenylisocyanate, TEA, ACN, rt, 16 h, 50%; (b) methyl iodide, TEA, ACN, rt, 16 h, 87 %; (c) *n*-bromo-*N*-phenylalkanamide (Supplementary Information), TEA, ACN, reflux, 16 h, 30 – 44%.

The terminal *N*-phenylamide bearing linkers were synthesized by the method reported in chapter 2, utilizing 2-(6-chloro-1*H*-benzotriazole-1-yl)-1,1,3,3-tetramethylammonium hexafluorophosphate (HCTU) as a coupling reagent to form the *n*-bromo-*N*-phenylalkanamide intermediates (Chapter 2, Supplementary Information). *N*-Quaternisation of McN-A-343-base **13** with the *n*-bromo-*N*-phenylalkanamide intermediates was achieved by combining the reagents with base in ACN and heating to reflux overnight (Scheme 1). Products **14a-c** were then purified by flash column chromatography (FCC) on silica.

**Scheme 2. Synthesis of iperoxo-based hybrid ligands containing structural features of the selective antagonists pirenzepine/ telenzepine<sup>a</sup>**

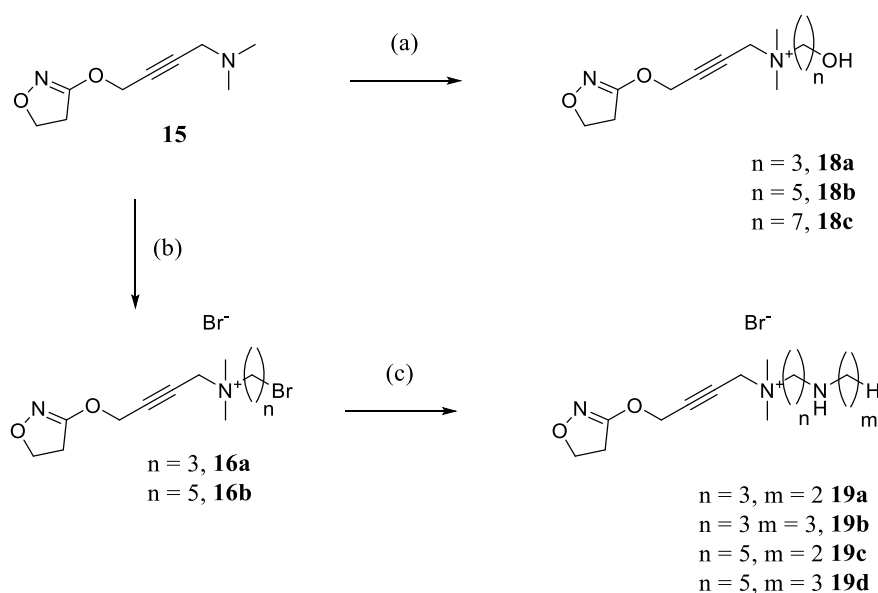


<sup>a</sup>Reagents and conditions: (a) 1,*n*-dibromoalkane, TEA, ACN, rt, 16 h, quantitative (b) *N*-phenyl-2-(piperazin-1-yl)acetamide, TEA, reflux, 16 h, 29 – 46%.

The synthesis of iperoxo-base **15** was carried out as previously reported (Chapter 2, Supplementary Information).<sup>34</sup> The syntheses of the piperizinyllinker based compounds, **17a-c**, were carried out by quaternising iperoxo base with an excess of the appropriate

dibromoalkane (Scheme 2). *N*-Phenyl-2-(piperazin-1-yl)acetamide and the iperoxo-alkylbromides **16a-c** were then combined in ACN with base and heated to reflux overnight to afford the desired products, **17a-c**, that were then isolated by preparative high performance liquid chromatography (HPLC) (Scheme 2). To explore the incorporation of heteroatoms into the linker of our hybrid ligands we synthesized a series of ‘linker-only’ iperoxo-based ligands with either an amine or hydroxyl group, **18a-c** and **19a-d** (Scheme 3). For this ligand series, we chose secondary amines and terminally substituted hydroxyl groups such that in both cases the heteroatom would bear a single hydrogen bond donor, for the sake of comparison of either the nitrogen or oxygen substituent. The linker lengths chosen were all intermediate lengths in the alkyl chain derivatives series (IXO-C<sub>n</sub>, Chapter 2) between the most and least potent, such that we could compare them structurally and pharmacologically to the entire series of alkyl linker derivatives.

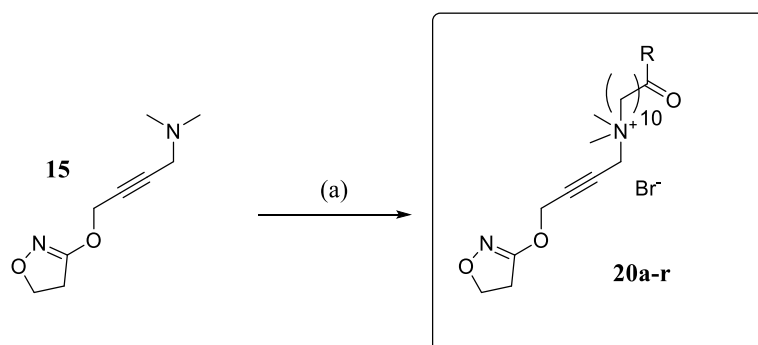
**Scheme 3. Synthesis of NH and OH substituted iperoxo-linker derivatives<sup>a</sup>**



<sup>a</sup>Reagents and conditions: (a) 1-bromoalkanol, TEA, ACN, rt, 16 h, 55 – 67%; (b) 1,n-dibromoalkane, TEA, ACN, rt, 16 h, quantitative; (c) *N*-alkylamine, TEA, reflux, 16 h, 27 – 41%.

Compounds **18a-c** were synthesized by quaternising iperoxo-base, **15**, with 1-bromoalkanols of the appropriate alkyl chain length with TEA as the base (Scheme 3). Compounds **19a-d** were synthesized from the intermediates **16a,b** (Scheme 2) by substituting the terminal bromide with the appropriate *N*-alkylamine, again using TEA as the base (Scheme 3). Finally, we explored the substitution of the phenyl ring of **3** with moieties of differing electron donating/ withdrawing properties, sterics and hydrogen bond forming ability (Figure 6, Scheme 2). The ring substitutions made to compound **3** were intended to maximise the likelihood of forming a specific receptor-ligand binding interaction of the ‘allosteric’ pharmacophore of compound **3** and the M<sub>1</sub> - M<sub>5</sub> mAChRs and to potentially augment its M<sub>4</sub> mAChR selectivity and/ or potency.

**Scheme 4. Synthesis of the phenyl ring substituted derivatives of our previously identified lead compound, iperoxo-based hybrid ligand<sup>a</sup>**



Iteration 1

R = NH(methyl), <b>20a</b>	R = NH(2-methoxyphenyl), <b>20g</b>
R = NH(cyclohexyl) <b>20b</b>	R = NH(3-methoxyphenyl), <b>20h</b>
R = N(methyl)(phenyl), <b>20c</b>	R = NH(4-methoxyphenyl), <b>20i</b>
R = NH(2-fluorophenyl), <b>20d</b>	R = NH(2-trifluoromethylphenyl), <b>20j</b>
R = NH(3-fluorophenyl), <b>20e</b>	R = NH(3-trifluoromethylphenyl), <b>20k</b>
R = NH(4-fluorophenyl), <b>20f</b>	R = NH(4-trifluoromethylphenyl), <b>20l</b>

Iteration 2

R = NH(3,5-bistrifluoromethylphenyl), <b>20m</b>	R = NH(2,5-difluorophenyl), <b>20p</b>
R = NH(3,5-difluorophenyl), <b>20n</b>	R = NH(perfluorophenyl), <b>20q</b>
R = NH(2,6-difluorophenyl), <b>20o</b>	R = NH(3-trifluoromethoxyphenyl), <b>20r</b>

Reagents and conditions: (a) n-bromo-*N*-(substituted phenyl)alkanamide (**21a-h**) (Supplementary Information), TEA, ACN, reflux, 16 h, 22 – 61%.

The intermediate n-bromoalkanamides (**21a-h**) for **20a,e-i,k-l** were synthesized by employing HCTU, as had been used previously for related intermediates (Scheme 4, Supplementary Information). However, for several of the desired n-bromoalkanamide intermediates no product formed with HCTU, 1-[Bis(dimethylamino)methylene]-1*H*-1,2,3-triazolo[4,5-*b*]pyridinium 3-oxide hexafluorophosphate (HATU) or *N,N'*-dicyclohexylcarbodiimide (DCC) coupling reagents. For these n-bromoalkanamide intermediates the acylchloride was performed with thionyl chloride before displacing with the appropriate substituted aniline (or amine), and this gave sufficient yields in all remaining cases.

This method was then employed for the synthesis of **20b-d,j,m-r**. Compounds **20a-r** were synthesized by combining **15** and the n-bromoalkanamides with base in ACN and heating to reflux overnight, and purified by preparative HPLC (Scheme 4).

**Pharmacology.** The McN-A-343-hybrid ligands, **14a-c**, were subjected to concentration-dependent ERK 1/2 phosphorylation assays at the M<sub>1</sub>-M<sub>4</sub> mAChRs. The ERK 1/2 assay was chosen because ERK phosphorylation is a downstream effector of many pathways coupled to the mAChRs, including both G<sub>i</sub> and G<sub>s</sub> G protein activation. Thus, the pERK1/2 assay allows both G<sub>i</sub> and G<sub>s</sub> coupled mAChR subtypes to be evaluated and compared using a single assay type. McN-A-343 and iperoxo displayed potency values consistent with literature values.<sup>29,34</sup> Although several of the derivatives showed some slight pERK 1/2 activity in the time-dependent assays (Supplementary Information), this was not observed in the concentration-dependent assays and was determined to be due to disturbance of the cells by the addition of the ligand solution, and not by activity of the ligand itself. The McN-A-343 hybrid ligands **14a-c** showed no activity at any of the M<sub>1</sub>-M<sub>4</sub> mAChRs above baseline. This is most likely due to the loss of affinity and efficacy (and as a result potency) of the addition of the linker unit (Figure 7). Unfortunately, this observation may suggest that the use of selective partial agonists as the orthosteric pharmacophore of mAChR hybrid ligands may be unviable, as the efficacy of the base orthosteric ligand is typically too low to remain active upon the addition of the (efficacy attenuating) *N*-alkyl linker.

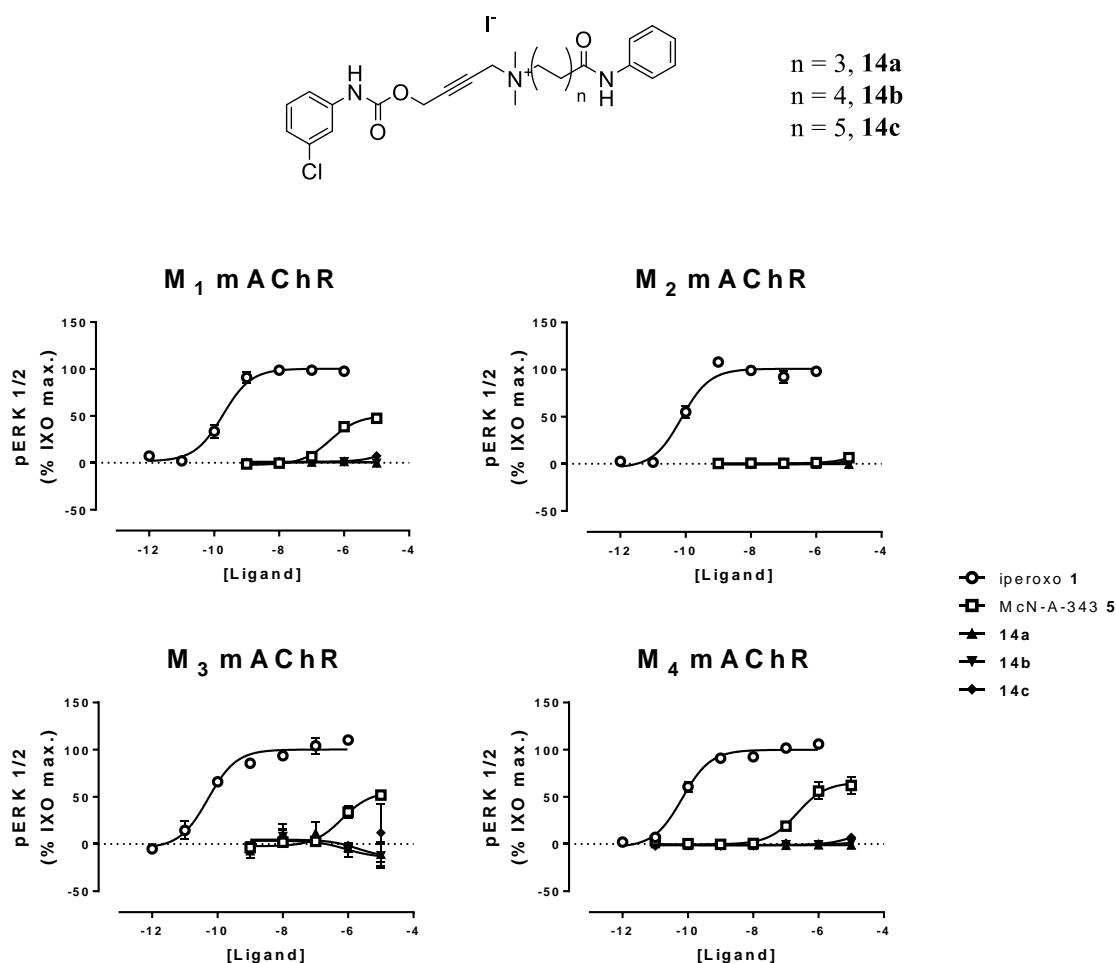


**Figure 7.** Functional response of iperoxo **1**, McN-A-343 **5** and McN-A-343 based hybrid ligands **14a-c** at the M<sub>1</sub>-M<sub>4</sub> mAChRs. Functional response was measured by pERK 1/2 assay in CHO cells expressing the M<sub>3</sub> or M<sub>4</sub> mAChRs. Response was measured at the peak phosphorylation time as determined by time-dependent pERK 1/2 assay (Supplementary Information). Data represent the mean  $\pm$  S. E. of 3 independent experiments performed in duplicate.

We then shifted attention to modifying the hybrid linker, incorporating the hypothesized selective structural motifs of the M<sub>1</sub>/ M<sub>4</sub> mAChR selective antagonists, telenzepine and pirenzepine. We evaluated the piperizynyl linker hybrid ligands **17a-c** by functional assay at the M<sub>3</sub> and M<sub>4</sub> mAChRs, at which the polymethylene *N*-linker hybrid ligands were least and most efficacious, respectively (Figure 8).



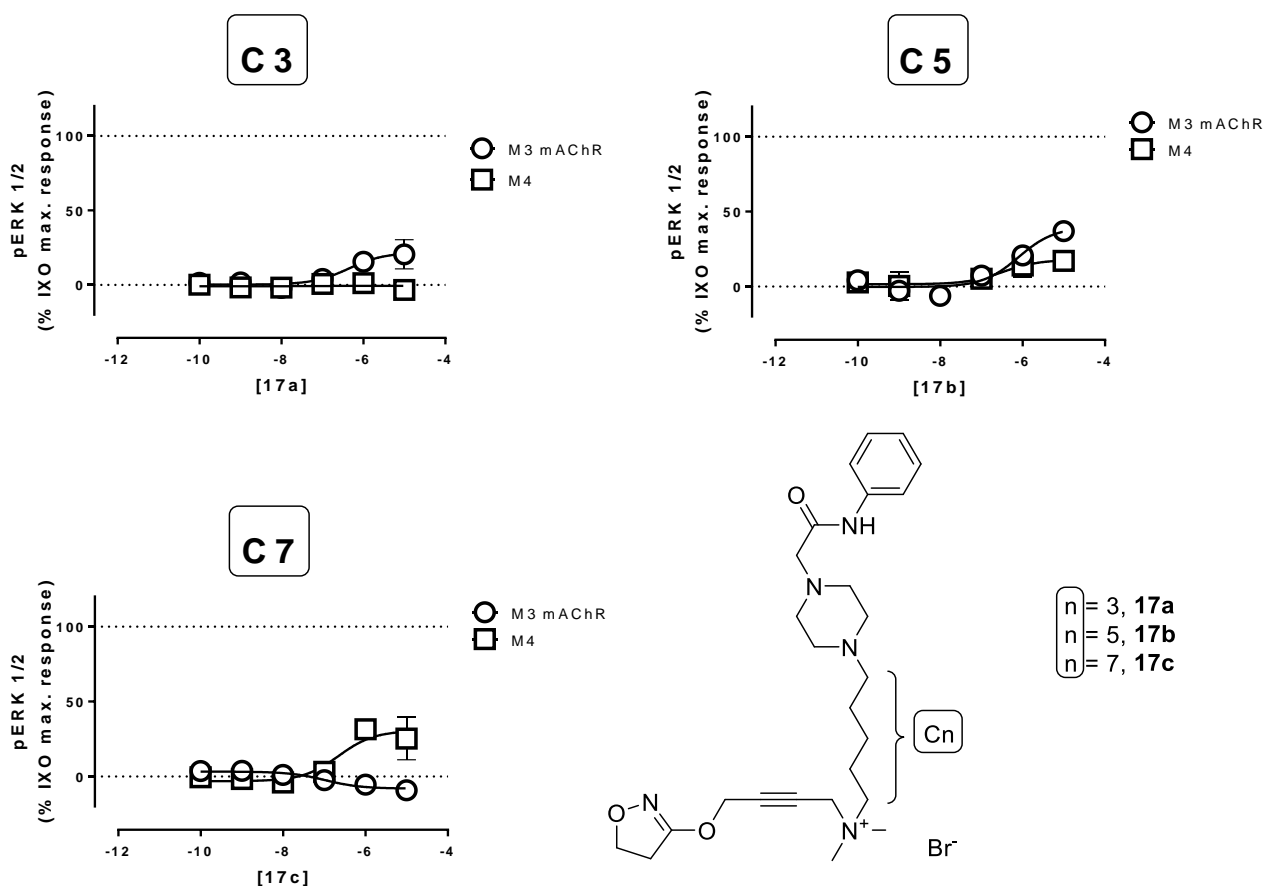
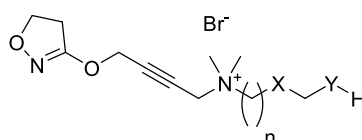


**Figure 8.** Functional response of piperazinyl-linker hybrid ligands **17a** ('C3'), **17b** ('C5') and **17c** ('C7') at the M<sub>3</sub> and M<sub>4</sub> mAChRs. Functional response was measured by pERK 1/2 assay in CHO cells expressing the M<sub>3</sub> or M<sub>4</sub> mAChRs. Response was measured at the peak phosphorylation time as determined by time-dependent pERK 1/2 assays (Supplementary Information). Data represent the mean  $\pm$  S.E. of 3 independent experiments performed in duplicate. S.E. values which are smaller than the symbols used are not shown. Values which appear less than zero are not significantly different from zero by two-way ANOVA.

Substitution of the *N*-linker of our iperoxo **1**-based hybrid ligands with a piperazine moiety yielded compounds with lower potency and/ or reduced M<sub>4</sub> vs. M<sub>3</sub> mAChR selectivity, compared with our most potent and selective polymethylene hybrid ligand, **3**. To investigate this we synthesized several less sterically bulky amine substituted linker derivatives of iperoxo (**1**) as well as several oxygen substituted analogues, to assess the effect of incorporating a hydrogen bond acceptor/ donor functional group into the hybrid ligand *N*-linker. These ligands,

**18a-c** and **19a-d**, were then evaluated by functional assay at the M<sub>3</sub> and M<sub>4</sub> mAChRs, as for **17-a-c** (Table 1).

**Table 1.** Functional data for the NH or OH substituted iperoxo-linker ligands at the M<sub>3</sub> and M<sub>4</sub> mAChRs



Cpd	n	X	Y	mAChR	pEC <sub>50</sub> <sup>a</sup>	E <sub>max</sub> <sup>b</sup>
<b>18a</b>	1	CH <sub>2</sub>	O	M <sub>3</sub>	6.61 ± 0.28	66 ± 9
				M <sub>4</sub>	7.02 ± 0.12	75 ± 4
<b>18b</b>	3	CH <sub>2</sub>	O	M <sub>3</sub>	6.21 ± 0.40	48 ± 12
				M <sub>4</sub>	5.75 ± 0.16	80 ± 8
<b>18c</b>	5	CH <sub>2</sub>	O	M <sub>3</sub>	5.98 ± 0.49	38 ± 13
				M <sub>4</sub>	5.52 ± 0.34	52 ± 12
<b>19a</b>	3	NH	CH <sub>2</sub>	M <sub>3</sub>	7.49 ± 0.21	83 ± 7
				M <sub>4</sub>	7.27 ± 0.11	86 ± 4
<b>19b</b>	3	NH	CH <sub>2</sub> CH <sub>2</sub>	M <sub>3</sub>	7.29 ± 0.23	75 ± 7
				M <sub>4</sub>	5.87 ± 0.21	56 ± 7
<b>19c</b>	5	NH	CH <sub>2</sub>	M <sub>3</sub>	6.85 ± 0.28	59 ± 8
				M <sub>4</sub>	7.19 ± 0.11	87 ± 4
<b>19d</b>	5	NH	CH <sub>2</sub> CH <sub>2</sub>	M <sub>3</sub>	6.11 ± 0.29	67 ± 12
				M <sub>4</sub>	5.80 ± 0.17	71 ± 8

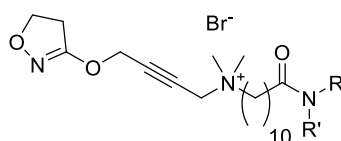
<sup>a</sup>pEC<sub>50</sub> values are the negative logarithm of the concentration of a ligand that was able to elicit 50% the maximum achievable response by that ligand as determined by fitting a 3-parameter concentration-response curve to the data. <sup>b</sup>E<sub>max</sub> values are the maximum response measured by a ligand, as a percentage of the maximum response achievable by the full agonist, iperoxo. Functional response was measured by pERK 1/2 assay in CHO cells expressing the M<sub>3</sub> or M<sub>4</sub> mAChRs. Response was measured at the peak phosphorylation time as determined by time-dependent pERK 1/2 assays (Supplementary Information). Data represent the mean ± S. E. of 3 independent experiments performed in duplicate.

We found that in all evaluated cases, insertion of hydrogen bond acceptor/ donor groups into the *N*-linker of iperoxo **1**-based hybrid ligands was detrimental to the agonism and/ or M<sub>4</sub> mAChR selectivity of the hybrid ligands compared to the polymethylene derivative of equivalent linker length. This intolerance to hydrophilic and/ or bulky substitution in the linker

most likely arises due to the hydrophobic nature of the mAChR vestibule and the fact the vestibule contracts upon receptor activation.<sup>21</sup> This likely explains the poor agonism seen in the piperazinyl linker derivatives, **17a-c**, as well as in **18a-c** and **19a-d**. Given that mAChR hybrid ligands typically have low efficacy compared with their monomeric orthosteric pharmacophore, we considered this property unfavourable and so did not explore *N*-linker substitutions of our hybrid ligands further.

Next, we synthesized and tested two iterations of ring-substituted analogues of **3** in an attempt to further augment or modify the mAChR selectivity and/ or potency of this ligand. The first iteration (compounds **20a-l**) consisted of singly substituted derivatives, designed to maximize the likelihood of forming a specific receptor-ligand interaction (Scheme 4). The second iteration (compounds **20m-r**) included symmetrical derivatives of the most potent ligands, difluoro- substitutions combining the most potent and most selective singly substituted fluoro derivatives, the combining of the potent 3-methoxy and 3-trifluoromethyl into the 3-trifluoromethoxy derivative. The perfluoro derivative, that was intended to invert quadrupole moment of the phenyl ring (compared with the unsubstituted phenyl derivative)<sup>37-38</sup> and, by comparison to **3**, allow us to detect any potential  $\pi$ - $\pi$  aromatic receptor-ligand interactions. The ring substituted derivatives, **20a-r**, were then initially subjected to functional assays at the M<sub>3</sub> and M<sub>4</sub> mAChRs. The most interesting compounds were then evaluated at the remaining M<sub>1</sub>, M<sub>2</sub> and M<sub>5</sub> mAChR subtypes by functional assay and competition radioligand binding to determine their mAChR subtype selectivity at the level of efficacy (Table 2).

**Table 2.** Functional and binding data for the ring substituted hybrid ligands at the M<sub>1</sub>–M<sub>5</sub> mAChRs



Cpd	R	R'	mAChR	pEC <sub>50</sub> <sup>a</sup>	E <sub>max</sub> <sup>b</sup>	pK <sub>i</sub> <sup>c</sup>	<sup>d</sup> Log τ <sub>c</sub>
Iperoxo							
<b>1</b>	n/a	n/a	M <sub>1</sub>	9.46 ± 0.35	100 ± 2	7.62 ± 0.13	1.89 ± 0.10
			M <sub>2</sub>	10.23 ± 0.19	100 ± 4	8.70 ± 0.02	2.02 ± 0.15
			M <sub>3</sub>	9.42 ± 0.31	100 ± 2	6.84 ± 0.14	1.84 ± 0.13
			M <sub>4</sub>	10.43 ± 0.17	100 ± 2	8.18 ± 0.07	2.04 ± 0.12
			M <sub>5</sub>	9.52 ± 0.16	100 ± 4	7.83 ± 0.23	1.67 ± 0.11
<b>3</b>	phenyl	H	M <sub>1</sub>	6.94 ± 0.42	7 ± 2	5.92 ± 0.08	-0.79 ± 0.11
			M <sub>2</sub>	7.72 ± 0.17	73 ± 5	5.62 ± 0.09	1.09 ± 0.13
			M <sub>3</sub>	7.72 ± 0.42	18 ± 3	5.29 ± 0.11	-0.58 ± 0.23
			M <sub>4</sub>	7.66 ± 0.08	74 ± 2	5.62 ± 0.09	1.58 ± 0.09
			M <sub>5</sub>	6.29 ± 0.25	18 ± 2	5.56 ± 0.10	-0.51 ± 0.06
<b>20a</b>	H	CH <sub>3</sub>	M <sub>1</sub>	nd	nd	5.99 ± 0.08	-3
			M <sub>2</sub>	6.84 ± 0.43	40 ± 9	6.04 ± 0.04	1.13 ± 0.47
			M <sub>3</sub>	nd	nd	5.13 ± 0.16	-3
			M <sub>4</sub>	7.51 ± 0.20	57 ± 4	5.50 ± 0.01	1.32 ± 0.03
			M <sub>5</sub>	6.50 ± 0.78	22 ± 10	5.00 ± 0.09	0.17 ± 0.26
<b>20b</b>	cyclohexyl	H	M <sub>3</sub>	nd	nd	-	-
			M <sub>4</sub>	7.56 ± 0.14	57 ± 3	-	-
<b>20c</b>	phenyl	CH <sub>3</sub>	M <sub>3</sub>	nd	nd	-	-
			M <sub>4</sub>	7.49 ± 0.24	43 ± 4	-	-
<b>20d</b>	2-fluorophenyl	H	M <sub>3</sub>	nd	nd	-	-
			M <sub>4</sub>	7.49 ± 0.18	57 ± 4	-	-
<b>20e</b>	3-fluorophenyl	H	M <sub>3</sub>	8.30 ± 0.15	102 ± 5	-	-
			M <sub>4</sub>	8.70 ± 0.11	108 ± 4	-	-
<b>20f</b>	4-fluorophenyl	H	M <sub>3</sub>	7.71 ± 0.28	57 ± 6	-	-
			M <sub>4</sub>	8.42 ± 0.16	75 ± 4	-	-
<b>20g</b>	2-methoxyphenyl	H	M <sub>3</sub>	7.63 ± 0.20	62 ± 4	-	-
			M <sub>4</sub>	8.15 ± 0.13	79 ± 4	-	-
<b>20h</b>	3-methoxyphenyl	H	M <sub>3</sub>	8.29 ± 0.16	74 ± 4	-	-
			M <sub>4</sub>	8.68 ± 0.12	89 ± 3	-	-
<b>20i</b>	4-methoxyphenyl	H	M <sub>3</sub>	7.49 ± 0.47	26 ± 5	-	-
			M <sub>4</sub>	8.24 ± 0.14	75 ± 4	-	-
	2-(trifluoromethyl)						
<b>20j</b>	phenyl	H	M <sub>3</sub>	nd	nd	-	-
			M <sub>4</sub>	7.15 ± 0.20	48 ± 4	-	-

3-(trifluoromethyl)							
20k	phenyl	H	M <sub>3</sub>	8.31 ± 0.19	82 ± 5	-	-
			M <sub>4</sub>	8.71 ± 0.13	92 ± 4	-	-
4-(trifluoromethyl)							
20l	phenyl	H	M <sub>1</sub>	8.50 ± 0.34	58 ± 8	6.56 ± 0.10	1.50 ± 0.67
			M <sub>2</sub>	8.39 ± 0.17	91 ± 5	6.69 ± 0.03	1.63 ± 0.18
			M <sub>3</sub>	8.53 ± 0.16	97 ± 5	6.48 ± 0.27	1.49 ± 0.21
			M <sub>4</sub>	8.89 ± 0.11	97 ± 3	6.21 ± 0.03	2.06 ± 0.23
			M <sub>5</sub>	8.08 ± 0.15	82 ± 5	6.03 ± 0.13	1.39 ± 0.25
3,5-bis(trifluoromethyl)							
20m	phenyl	H	M <sub>1</sub>	nd	nd	7.56 ± 0.39	-3
			M <sub>2</sub>	nd	nd	7.63 ± 0.16	-3
			M <sub>3</sub>	nd	nd	6.93 ± 0.04	-3
			M <sub>4</sub>	nd	nd	7.07 ± 0.22	-3
			M <sub>5</sub>	nd	nd	6.49 ± 0.32	-3
20n	3,5-difluorophenyl	H	M <sub>3</sub>	nd	nd	-	-
			M <sub>4</sub>	7.60 ± 0.18	57 ± 8	-	-
2,6-bis(trifluoromethyl)							
20o	phenyl	H	M <sub>3</sub>	nd	nd	-	-
			M <sub>4</sub>	7.37 ± 0.11	57 ± 3	-	-
20p	2,5-difluorophenyl	H	M <sub>1</sub>	nd	nd	6.42 ± 0.78	-3
			M <sub>2</sub>	nd	nd	6.46 ± 0.15	-3
			M <sub>3</sub>	nd	nd	5.82 ± 0.22	-3
			M <sub>4</sub>	6.87 ± 0.16	39 ± 4	5.90 ± 0.32	0.78 ± 0.22
			M <sub>5</sub>	nd	nd	5.81 ± 0.14	-3
20q	perfluorophenyl	H	M <sub>3</sub>	nd	nd	-	-
			M <sub>4</sub>	7.46 ± 0.10	58 ± 3	-	-
3-(trifluoromethoxy)							
20r	phenyl	H	M <sub>1</sub>	nd	nd	7.05 ± 0.24	-3
			M <sub>2</sub>	7.49 ± 0.26	75 ± 7	6.86 ± 0.05	0.78 ± 0.13
			M <sub>3</sub>	nd	nd	6.32 ± 0.08	-3
			M <sub>4</sub>	7.30 ± 0.43	39 ± 8	6.29 ± 0.23	-0.32 ± 0.13
			M <sub>5</sub>	nd	nd	6.27 ± 0.11	-3

<sup>a</sup>pEC<sub>50</sub> values are the negative logarithm of the concentration of a ligand that was able to elicit 50 % the maximum achievable response by that ligand as determined by fitting a 3-parameter concentration-response curve to the data. <sup>b</sup>E<sub>max</sub> values are the maximum response measured by a ligand, as a percentage of the maximum response achievable by the full agonist, iperexo. Functional response was measured by pERK 1/2 assay in CHO cells expressing the one of the M<sub>1</sub>-M<sub>5</sub> mAChRs. Response was measured at the peak phosphorylation time as determined by time-dependent pERK 1/2 assays (Supplementary Information). <sup>c</sup>pK<sub>i</sub> values are the negative logarithm of the inhibition constant for each ligand, as determined by competition radioligand binding assays with [<sup>3</sup>H]NMS and fitting the data to a one-site inhibition binding model. <sup>d</sup>Log τ<sub>c</sub> is the ligand efficacy (corrected for receptor expression) as determined by fitting the functional ERK 1/2 phosphorylation concentration-response data for each ligand to an operational model of agonism and constraining the model by the measured values of affinity for each ligand at each of the respective mAChR subtype. Instances where no ligand efficacy was observed Log

$\tau_e$  was fixed to -3. Values not measured are denoted '-'. Compounds which gave no determinable response in the specified assay are denoted 'nd'. Data represent the mean  $\pm$  S.E. of 3 independent experiments performed in duplicate.

---

In the first iteration of ligands, **20a-l** the most potent ligand, **20l**, and most M<sub>4</sub> selective ligand, **20a**, were then chosen for measurement of their functional response at the remaining M<sub>1</sub>/M<sub>2</sub>/M<sub>5</sub> mAChRs as well as the affinity at the M<sub>1</sub>-M<sub>5</sub> mAChRs by competition radioligand binding. Although **20l** was highly potent it displayed no selectivity any of the mAChR subtypes. Several derivatives bearing an hydrogen bond (or pseudo hydrogen bond) at the 3- or 4- position (such as **20e,h,k,l**) also displayed high potency at the M<sub>3</sub>/M<sub>4</sub> mAChRs, suggesting that such moieties are favourable to ligand potency at these positions. Compound **20a** was found to possess similar selectivity for the M<sub>2</sub>/M<sub>4</sub>>M<sub>1</sub>/M<sub>3</sub>/M<sub>5</sub> mAChRs to **3**, showing that the phenyl ring is not necessary for potency or selectivity of these ligands, however functionalisation of the ring can affect both properties. Several derivatives, **20b,c,d,j** behaved similarly to the unsubstituted analogue **3** at the M<sub>3</sub> and M<sub>4</sub> mAChRs and were not explored further. Frustratingly, we noted that there appeared to be an inverse relationship between efficacy and selectivity of our first iteration of ligands, **20a-l**. In every case we evaluated, the higher the efficacy of a ligand, the less selective it was. This was also noted previously in chapter 2, where the least efficacious ligands were also the most selective, and similarly the most efficacious ligands possessed little selectivity. The second iteration of ligands, which combined the most potent and most selective substitutions from the first iteration, yielded several interesting compounds. Compound **20m** displayed no measurable activity at the M<sub>1</sub>-M<sub>5</sub> mAChRs and when assessed for binding at the M<sub>1</sub>-M<sub>5</sub> mAChRs, **20m** was shown to completely displace [<sup>3</sup>H]NMS at all M<sub>1</sub>-M<sub>5</sub> mAChR subtypes suggesting it is a non-selective neutral antagonist or weak inverse agonist, showing that ring substitutions of **3** can both

augment or attenuate ligand efficacy significantly. The combination (one of two possible combinations) of the 3-fluoro substitution (that gave a non-selective potent hybrid ligand, **20e**) and the 2-fluoro (the most selective fluoro analogue, **20d**) gave a hybrid ligand that displayed lower potency at the M<sub>4</sub> mAChR than either, **20p**. Despite its relatively lower potency compared other analogues in this set, **20p** displays no activity above baseline at the M<sub>1</sub>-M<sub>3</sub>/M<sub>5</sub> mAChRs, implying that it is selective for the M<sub>4</sub> mAChR, at least with regards to its efficacy in pERK 1/2 signalling *in vitro* (Table 2).

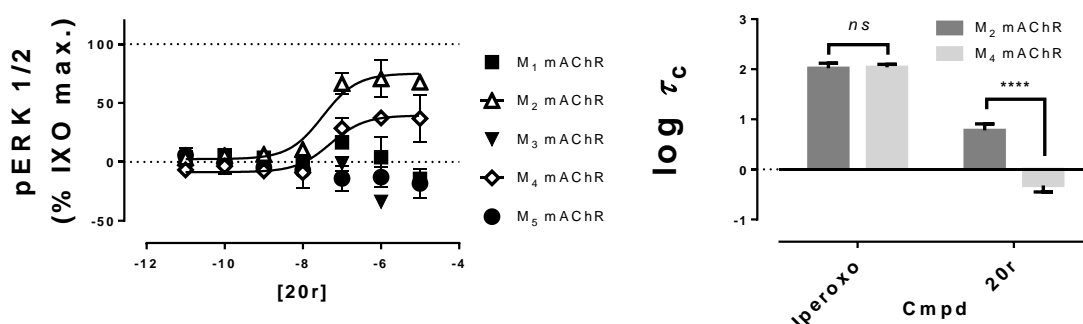


**Figure 9.** (Left) Functional response of **20r** at the M<sub>1</sub>-M<sub>5</sub> mAChRs and (right) efficacy comparison between the M<sub>2</sub> and M<sub>4</sub> mAChRs. Functional response was measured by pERK 1/2 assay in CHO cells expressing the M<sub>1</sub>-M<sub>5</sub> mAChRs. Response was measured at the peak phosphorylation time as determined by time-dependent pERK 1/2 assays (Supplementary Information). Efficacy (Log  $\tau_c$ ) was determined by fitting the functional data and binding data for each ligand to an operational model of agonism (Experimental). Efficacy data was analysed statistically using Bonferroni's multiple comparison test, 2-way ANOVA (*ns* = not significant, \*\*\*\* *p* < 0.001). Data represent the mean  $\pm$  S.E. of 3 independent experiments performed in duplicate. Values which appear less than zero are not significantly different from zero by two-way ANOVA.

Compound **20r** was also particularly interesting. As with many examples in our previous iterations of iperoxo-based hybrid ligands, **20r** displayed no activity above baseline at the M<sub>1</sub>/M<sub>3</sub>/M<sub>5</sub> mAChRs and a partial agonist response at the M<sub>2</sub> and M<sub>4</sub> mAChRs. In contrast to our previous hybrid ligands, **20r** displayed significantly greater efficacy at the M<sub>2</sub> mAChR rather than M<sub>4</sub> mAChRs, making it the first M<sub>2</sub> mAChR selective partial agonist to arise from

our iperoxo **1**-based ligands (Figure 9), at the level of efficacy. Furthermore, all of our previously evaluated iperoxo **1**-based hybrid ligands displayed higher affinity ( $\sim 0.5 - 1$  pK<sub>i</sub> unit) at the M<sub>1</sub> and M<sub>2</sub> mAChRs (compared with the M<sub>3</sub>/ M<sub>4</sub>/ M<sub>5</sub> mAChRs) and attained M<sub>4</sub> mAChR selectivity through efficacy alone. Compound **20r** also displays approximately 10-times higher affinity at the M<sub>1</sub> and M<sub>2</sub> mAChR compared with the M<sub>3</sub>-M<sub>5</sub> mAChRs but in this case, it acts synergistically with its higher efficacy at the M<sub>2</sub> mAChR, resulting in significant M<sub>2</sub>>M<sub>4</sub>>>M<sub>1</sub>/M<sub>3</sub>/M<sub>5</sub> mAChR selectivity at the level of efficacy (Table 2, Figure 9). Unfortunately, as for the singly substituted phenyl ring derivatives, we found that the greater the efficacy of the hybrid ligand the lower the selectivity, and this is the case for both **20p** and **20r**, which had the lowest efficacy values at the M<sub>2</sub> and M<sub>4</sub> mAChRs of any of the ligands tested (which still maintained activity). This apparent interdependence of efficacy and selectivity has limited further optimization of these ligands at this point and, depending on the mechanistic basis for the interdependence, may prove to be an intractable hurdle to designing mAChR hybrid ligands which are both subtype-selective and highly efficacious. However, at this point no mechanistic conclusions can be drawn. Typically, the design of hybrid ligands involves the conjoining of two known ligands in an attempt to engage two discrete binding sites with a single receptor. In this study, we have looked at the conjoining of non-ligand substituents to an orthosteric agonist and shown that these ligands, similar to their biparmacophoric counterparts, can have interesting properties and significant variation in pharmaceutically relevant properties such as efficacy and selectivity.

## ■ CONCLUSIONS

In this chapter, we aimed to optimise the M<sub>2</sub>/M<sub>4</sub> mAChR selective truncated hybrid ligand partial agonists, which we had previously identified (Chapter 2), towards improved



efficacy and M<sub>4</sub> mAChR selectivity. We initially hypothesised that the substitution of iperoxo, **1**, (a non-selective agonist) in our ligands with an M<sub>1</sub>/M<sub>4</sub> mAChR preferring agonist (McN-A-343, **5**) may yield compounds with excellent selectivity for the M<sub>1</sub>/M<sub>4</sub> mAChRs. However, evaluation of our McN-A-343-based hybrid ligands revealed that substitution of the orthosteric pharmacophore with selective partial agonists, such as McN-A-343 (or, likely, xanomeline) may be an unviable route to improving selectivity of mAChR hybrid ligands. We then explored substitutions to the linker, first incorporating a piperazine, a motif commonly found in M<sub>1</sub>/M<sub>4</sub> mAChR selective dibenzodiazepinone-based antagonists. In this case we expected these compounds to gain improved M<sub>1</sub>/M<sub>4</sub> mAChR selectivity at the level of affinity, similar to the parent antagonists from which the piperazine motif was taken. However, these piperazine-linker hybrid ligands displayed reduced efficacy and selectivity as compared with their alkyl chain linked counterparts. Further exploration of the linker SAR, by substituting with a single amine or hydroxyl group demonstrated that hydrogen bond donor/ acceptor groups are poorly tolerated when incorporated into the *N*-linker of iperoxo **1**-based mAChR hybrid ligands. In all of the *N*-linker substituted compounds that we explored we noted a substantial loss of potency, and in several cases a complete loss of selectivity, as compared with the polymethylene *N*-linked derivative of equivalent linker length. Finally, we looked at substituting the phenyl ring of our potent M<sub>2</sub>/ M<sub>4</sub> mAChR selective hybrid ligand **3**, and this yielded several interesting ligands. Substitution of the phenyl ring with hydrogen bond acceptor groups at the 3- and 4-positions generally resulted in an increase in potency, compounds **20e,h,k,l** possessed significantly improved potency over **3** (approximately 10-fold increase). However, as potency was increased, we saw a reduction in M<sub>2</sub>/M<sub>4</sub> mAChR selectivity. Generally, we found the multiple substitutions of the phenyl ring were detrimental to ligand efficacy or gave ligands whose potency was equivalent to the unsubstituted derivative, **3**. However, compound **20p**

showed absolute selectivity at the level of efficacy for the M<sub>4</sub> mAChR, giving no response above baseline at the remaining M<sub>1</sub>-M<sub>3</sub>, M<sub>5</sub> mAChRs under our assay conditions. Additionally, compound **20r** displayed good selectivity for the M<sub>2</sub>>M<sub>4</sub>>>M<sub>1</sub>/M<sub>3</sub>/M<sub>5</sub> mAChR having both higher affinity and efficacy at the M<sub>2</sub> versus the M<sub>4</sub> mAChR. However, as in chapter 2, we have noted difficulties in optimizing both efficacy and selectivity simultaneously. Our results indicate that these two properties may be intrinsically linked in an inverse relationship for these and structurally related hybrid ligands, suggesting that designing a hybrid ligand that is both M<sub>4</sub> mAChR selective and highly efficacious may be impossible. Chapter 4 will focus on understanding the mechanistic basis for the apparent interdependence between efficacy and selectivity of these ligands, to determine the viability of designing a high efficacy M<sub>4</sub> mAChR selective hybrid ligand.

## ■ EXPERIMENTAL SECTION

**Chemistry.** All materials were reagent grade and purchased commercially from Sigma-Aldrich or Matrix Scientific. Anhydrous solvents were obtained from an MBraun MB SPS-800 Solvent Purification System. Analytical thin layer chromatography (TLC) was performed on Silica Gel 60 F254 pre-coated plates (0.25 mm, Merck ART 5554) and visualised using ultraviolet light, iodine, potassium permanganate or ninhydrin as necessary. Silica gel 40–63 micron (Davisil) was used for silica gel flash chromatography. <sup>1</sup>H NMR spectra were recorded on a Brüker Avance 400 MHz Ultrashield Plus spectrometer at 400.13 MHz. Chemical shifts ( $\delta$ ) for all <sup>1</sup>H NMR spectra are reported in parts per million (ppm) using the central peak of the deuterated solvent chemical shift as the reference: MeOD (3.31), CDCl<sub>3</sub> (7.26) and *d*<sub>6</sub>-DMSO (2.50).<sup>39</sup> Each resonance was assigned according to the following convention: chemical shift

( $\delta$ ) (multiplicity, coupling constant(s) in Hz, number of protons). Coupling constants ( $J$ ) are reported to the nearest 0.1 Hz. In reporting the spectral data, the following abbreviations have been used: s, singlet; d, doublet; t, triplet; q, quartet; p, pentet; m, multiplet; br, broad; app, apparent; as well as combinations of these where appropriate.  $^{13}\text{C}$  NMR spectra were recorded at 100.62 MHz using a Bruker Avance 400 MHz Ultrashield Plus spectrometer. Chemical shifts ( $\delta$ ) for all  $^{13}\text{C}$  NMR spectra are reported in parts per million (ppm), using the center peak of the deuterated solvent chemical shift as the reference: MeOD (49.00),  $\text{CDCl}_3$  (77.16) and  $d_6$ -DMSO (39.52).<sup>39</sup> HSQC, HMBC and COSY spectra were obtained using the standard Bruker pulse sequence to assist with structural assignment of the compounds. LC-MS was performed on an Agilent 1200 Series coupled to the 6120 quadrupole mass spectrometer. Elution was also monitored at 254 nm. HRMS analyses were recorded in the specified ion mode using an Agilent 6224 TOF LC-MS coupled to an Agilent 1290 Infinity (Agilent, Palo Alto, CA). Analytical reverse-phase HPLC was performed on a Waters HPLC system using a Phenomenex® Luna C8 (2) 100Å column (150 × 4.6 mm, 5  $\mu\text{m}$ ) and a binary solvent system; solvent A: 0.1% TFA/ $\text{H}_2\text{O}$ ; solvent B: 0.1% TFA/ $\text{CH}_3\text{CN}$ . Isocratic elution was carried out using the following protocol (time, % solvent A, % solvent B): 0 min, 100, 0; 10 min, 20, 80; 11 min, 20, 80; 12 min, 100, 0; 20 min, 100, 0; at a flow rate of 1.0 mL/min monitored at 214 and/ or 254 nm using a Waters 996 Photodiode Array detector. Preparative HPLC was performed using an Agilent 1260 infinity coupled with a binary preparative pump and Agilent 1260 FC-PS fraction collector, using Agilent OpenLAB CDS software (Rev C.01.04) and an Altima 5  $\mu\text{m}$  C8 22 mm × 250 mm column. The following buffers were used: buffer A,  $\text{H}_2\text{O}$ ; buffer B, MeCN, with sample being run at a gradient of 5% buffer B to 100% buffer B over 20 min at a flow rate of 20 mL/min. Characterisation requirements for final compounds were set as:  $^1\text{H}$  NMR,  $^{13}\text{C}$  NMR, LC-MS, HPLC (254 nm and 214 nm) purity >95%.

Compounds **1**, **12** and **15** were synthesised by the methods reported by Kloeckner *et al.* (Chapter 2, Supplementary Information).<sup>34</sup>

**4-((Dimethylamino)but-2-yn-1-yl (3-chlorophenyl)carbamate (6). 12** (1 eq., 212 mg, 1.88 mmol), and TEA (3 eq., 570 mg, 5.64 mmol) were dissolved in dry THF (10 mL) on an ice bath (0 °C). 3-chlorophenyl isocyanate (1.2 eq., 346 mg, 2.25 mmol) was added in one portion and the solution was stirred overnight and allowed to warm to room temperature. The solvent was removed under vacuum and the crude material purified by FCC (eluent EtOAc/MeOH 4:1). Off-white solid; 250.0 mg, 50%. <sup>1</sup>H NMR (MeOD)  $\delta$  9.53 (br s, 1H), 7.58 (t,  $J$  = 2.0 Hz, 1H), 7.30 (ddd,  $J$  = 8.2/2.0/1.0 Hz, 1H), 7.24 (t,  $J$  = 7.8 Hz, 1H), 7.01 (ddd,  $J$  = 7.8/2.0/1.0 Hz, 1H), 4.81 (t,  $J$  = 1.9 Hz, 2H), 3.30 (t,  $J$  = 1.9 Hz, 2H), 2.30 (s, 6H). <sup>13</sup>C NMR (MeOD)  $\delta$  154.7, 141.6, 135.5, 131.1, 123.9, 119.5, 117.8, 82.1, 81.4, 53.6, 48.3, 44.1.  $m/z$  MS (TOF ES<sup>+</sup>) C<sub>13</sub>H<sub>15</sub>ClN<sub>2</sub>O<sub>2</sub> [M+H]<sup>+</sup> calcd, 267.2; found, 267.1. LC-MS:  $t_R$  = 4.64 min.

**4-(((3-Chlorophenyl)carbamoyl)oxy)-*N,N,N*-trimethylbut-2-yn-1-aminium iodide (5). 6** (67 mg, 0.25 mmol) was dissolved in ACN (10 mL). A large excess of iodomethane was added and the solution stirred overnight at room temperature. The solvent was removed under vacuum and the crude material recrystallized from boiling MeOH. White solid; 61.6 mg, 87%. <sup>1</sup>H NMR (*d*<sub>6</sub>-DMSO)  $\delta$  9.65 (br s, 1H), 7.60 (t,  $J$  = 2.0 Hz, 1H), 7.30 (ddd,  $J$  = 8.2/2.0/1.0 Hz, 1H), 7.26 (t,  $J$  = 7.8 Hz, 1H), 7.04 (ddd,  $J$  = 7.8/2.0/1.0 Hz, 1H), 4.91 (t,  $J$  = 1.8 Hz, 2H), 4.44 (t,  $J$  = 1.8 Hz, 2H), 3.25 (s, 9H). <sup>13</sup>C NMR (*d*<sub>6</sub>-DMSO)  $\delta$  154.6, 141.6, 135.6, 131.2, 124.1, 119.5, 117.9, 88.9, 75.3, 57.4, 53.5, 53.3.  $m/z$  MS (TOF ES<sup>+</sup>) C<sub>14</sub>H<sub>18</sub>ClN<sub>2</sub>O<sub>2</sub><sup>+</sup> [M]<sup>+</sup> calcd, 281.1; found, 281.1. LC-MS:  $t_R$  = 4.72 min.

### General procedure for the synthesis of McN-A-343 based hybrid ligands (14a-c)

Compound **6** (250  $\mu\text{mol}$ , 1.0 eq.), *n*-bromo-*N*-phenylalkanamide (250  $\mu\text{mol}$ , 1.0 eq.) (Supplementary Information) and TEA (750  $\mu\text{mol}$ , 3.0 eq.) were dissolved in ACN and heated to reflux with stirring overnight. The solvent was then removed under vacuum and the crude material was purified by FCC (eluent DCM/MeOH 20:1).

***N*-(4-(((3-Chlorophenyl)carbamoyl)oxy)but-2-yn-1-yl)-*N,N*-dimethyl-7-oxo-7-(phenylamino)heptan-1-aminium bromide (14a).** Viscous yellow oil; 156.1 mg, 38%.  $^1\text{H}$  NMR (MeOD)  $\delta$  9.74 (br s, 1H), 9.65 (br s, 1H), 7.62 (t,  $J = 2.1$  Hz, 1H), 7.57-7.53 (m, 2H), 7.32-7.26 (m, 3H), 7.24 (t,  $J = 8.0$  Hz, 1H), 7.08 (tt,  $J = 7.4/1.0$  Hz, 1H), 7.02 (ddd,  $J = 7.8/2.1/1.1$  Hz, 1H), 4.88 (t,  $J = 1.8$  Hz, 2H), 4.38 (t,  $J = 1.8$  Hz, 2H), 3.47-3.39 (m, 2H), 3.17 (s, 6H), 2.37 (t,  $J = 7.4$ , 2H), 1.83-1.74 (m, 2H), 1.67 (p,  $J = 7.3$  Hz, 2H), 1.48-1.34 (m, 4H).  $^{13}\text{C}$  NMR (MeOD)  $\delta$  174.4, 154.6, 141.4, 139.9, 135.6, 131.2, 129.8, 125.1, 124.1, 121.3, 119.4, 117.8, 88.8, 75.3, 65.3, 55.0, 53.3, 51.2, 37.6, 29.5, 26.9, 26.3, 23.4.  $m/z$  MS (TOF ES $^+$ )  $\text{C}_{26}\text{H}_{33}\text{ClN}_3\text{O}_3^+ [\text{M}]^+$  calcd, 470.2; found, 470.2. LC-MS:  $t_{\text{R}} = 5.09$  min.

***N*-(4-(((3-Chlorophenyl)carbamoyl)oxy)but-2-yn-1-yl)-*N,N*-dimethyl-9-oxo-9-(phenylamino)nonan-1-aminium bromide (14b).** Viscous yellow oil; 56.2 mg, 44%.  $^1\text{H}$  NMR (MeOD)  $\delta$  9.73 (br s, 1H), 9.66 (br s, 1H), 7.62 (t,  $J = 2.1$  Hz, 1H), 7.58-7.52 (m, 2H), 7.33-7.26 (m, 3H), 7.24 (t,  $J = 8.0$  Hz, 1H), 7.08 (tt,  $J = 7.4/1.0$  Hz, 1H), 7.03 (ddd,  $J = 7.8/2.1/1.1$  Hz, 1H), 4.88 (t,  $J = 1.8$  Hz, 2H), 4.38 (t,  $J = 1.8$  Hz, 2H), 3.45-3.38 (m, 2H), 3.17 (s, 6H), 2.36 (t,  $J = 7.4$ , 2H), 1.80-1.71 (m, 2H), 1.67 (p,  $J = 7.3$  Hz, 2H), 1.45-1.24 (m, 8H).  $^{13}\text{C}$  NMR (MeOD)  $\delta$  174.7, 154.6, 141.4, 139.9, 135.6, 131.2, 129.8, 125.1, 124.1, 121.3, 119.4, 117.8, 88.8, 75.3, 65.3, 55.0, 53.3, 51.2, 37.9, 30.1, 30.0, 29.9, 27.2, 26.8, 23.6.  $m/z$  MS (TOF ES $^+$ )  $\text{C}_{28}\text{H}_{37}\text{ClN}_3\text{O}_3^+ [\text{M}]^+$  calcd, 498.3; found, 498.2. LC-MS:  $t_{\text{R}} = 5.23$  min.

***N*-(4-(((3-Chlorophenyl)carbamoyl)oxy)but-2-yn-1-yl)-*N,N*-dimethyl-11-oxo-11-(phenylamino)undecan-1-aminium bromide (14c).** Viscous yellow oil; 62.0 mg, 30%. <sup>1</sup>H NMR (MeOD)  $\delta$  9.73 (br s, 1H), 9.66 (br s, 1H), 7.62 (t,  $J$  = 2.1 Hz, 1H), 7.58-7.52 (m, 2H), 7.33-7.26 (m, 3H), 7.24 (t,  $J$  = 8.0 Hz, 1H), 7.08 (tt,  $J$  = 7.4/1.0 Hz, 1H), 7.03 (ddd,  $J$  = 7.8/2.1/1.1 Hz, 1H), 4.88 (t,  $J$  = 1.8 Hz, 2H), 4.38 (t,  $J$  = 1.8 Hz, 2H), 3.45-3.37 (m, 2H), 3.17 (s, 6H), 2.37 (t,  $J$  = 7.4, 2H), 1.81-1.62 (m, 4H), 1.42-1.19 (m, 12H). <sup>13</sup>C NMR (MeOD)  $\delta$  174.7, 154.6, 141.4, 139.9, 135.6, 131.2, 129.8, 125.1, 124.1, 121.3, 119.4, 117.8, 88.8, 75.3, 65.3, 55.0, 53.3, 51.2, 38.0, 30.4, 30.2, 30.1, 30.0, 29.9, 27.3, 26.9, 23.6.  $m/z$  MS (TOF ES<sup>+</sup>) C<sub>30</sub>H<sub>41</sub>ClN<sub>3</sub>O<sub>3</sub><sup>+</sup> [M]<sup>+</sup> calcd, 526.3; found, 526.3. LC-MS:  $t_R$  = 5.38 min.

#### General procedure for the synthesis of piperazinyl-linker hybrid ligands (17a-c)

Compound **15** (1.0 mol, 1.0 eq.), 1,n-dibromoalkane (5.0 mmol, 5.0 eq.) and TEA (3.0 mmol, 3.0 eq.) were dissolved in ACN and stirred overnight at room temperature. The solvent was removed under vacuum and the crude material was washed with hot PE. The crude material, *N*-phenyl-2-(piperazin-1-yl)acetamide (1.2 mmol, 1.2 eq.) and TEA (1.5 mmol, 1.5 eq.) was then dissolved in ACN and stirred overnight at room temperature. The solvent was then removed under vacuum and the crude material was purified by preparative HPLC.

**4-((4,5-Dihydroisoxazol-3-yl)oxy)-*N,N*-dimethyl-*N*-(3-(4-(2-oxo-2-(phenylamino)ethyl)piperazin-1-yl)propyl)but-2-yn-1-aminium bromide (17a).** Viscous yellow oil; 23.8 mg, 35%. <sup>1</sup>H NMR (MeOD)  $\delta$  9.94 (br s, 1H), 7.62-7.53 (m, 2H), 7.32 (ddd,  $J$  = 9.4, 5.6, 2.0 Hz, 2H), 7.13 (ddt,  $J$  = 7.2, 6.1, 1.2 Hz, 1H), 4.92 (t,  $J$  = 1.8 Hz, 2H), 4.44-4.36 (m, 4H), 3.68 (s, 2H), 3.58-3.51 (m, 2H), 3.25-3.16 (m, 10H), 3.08-2.96 (m, 4H), 2.19 (p,  $J$  = 3.8 Hz, 2H), 1.97-1.54 (m, 4H). <sup>13</sup>C NMR (MeOD)  $\delta$  169.4, 162.4, 139.1, 129.9, 125.7, 121.5,

88.5, 76.5, 71.2, 64.9, 61.3, 58.2, 57.9, 55.1, 52.9, 51.1, 33.7, 23.5. *m/z* MS (TOF ES<sup>+</sup>) C<sub>24</sub>H<sub>36</sub>N<sub>5</sub>O<sub>3</sub><sup>+</sup> [M]<sup>+</sup> calcd, 442.3; found, 442.3. LC-MS: *t*<sub>R</sub> = 3.39 min.

***N*-(4-((4,5-Dihydroisoxazol-3-yl)oxy)but-2-yn-1-yl)-*N,N*-dimethyl-5-(4-(2-oxo-2-(phenylamino)ethyl)piperazin-1-yl)pentan-1-aminium bromide (17b).** Viscous yellow oil; 32.9 mg, 46%. <sup>1</sup>H NMR (MeOD) δ 9.73 (br s, 1H), 7.61-7.55 (m, 2H), 7.32 (ddd, *J* = 9.4, 5.6, 2.0 Hz, 2H), 7.13 (ddt, *J* = 7.2, 6.1, 1.2 Hz, 1H), 4.91 (t, *J* = 1.8 Hz, 2H), 4.43-4.33 (m, 4H), 3.53-3.33 (m, 12H), 3.21-3.13 (m, 8H), 3.07-2.87 (m, 4H), 1.97-1.70 (m, 4H), 1.48 (p, *J* = 3.8 Hz, 2H). <sup>13</sup>C NMR (MeOD) δ 169.9, 162.5, 139.1, 129.9, 125.6, 121.5, 87.7, 76.5, 71.2, 65.3, 61.5, 58.2, 57.9, 55.1, 52.9, 51.1, 33.7, 29.6, 24.3, 23.5. *m/z* MS (TOF ES<sup>+</sup>) C<sub>26</sub>H<sub>40</sub>N<sub>5</sub>O<sub>3</sub><sup>+</sup> [M]<sup>+</sup> calcd, 470.3; found, 470.3. LC-MS: *t*<sub>R</sub> = 3.59 min.

***N*-(4-((4,5-Dihydroisoxazol-3-yl)oxy)but-2-yn-1-yl)-*N,N*-dimethyl-7-(4-(2-oxo-2-(phenylamino)ethyl)piperazin-1-yl)heptan-1-aminium bromide (17c).** Viscous yellow oil; 26.8 mg, 29%. <sup>1</sup>H NMR (MeOD) δ 9.74 (br s, 1H), 7.62-7.54 (m, 2H), 7.38-7.27 (m, 2H), 7.13 (tt, *J* = 7.6/ 1.1 Hz, 1H), 4.91 (t, *J* = 1.7 Hz, 2H), 4.44-4.34, 3.69-3.38 (m, 10H), 3.21-3.12 (m, 8H), 3.04-2.94 (m, 4H), 1.84-1.71 (m, 4H), 1.53-1.37 (m, 10H). <sup>13</sup>C NMR (MeOD) δ 169.9, 162.5, 139.1, 129.9, 125.6, 121.5, 87.7, 76.5, 71.2, 65.3, 61.5, 58.2, 57.9, 55.1, 52.9, 51.1, 33.7, 29.6, 27.3, 27.0, 24.9, 23.5. *m/z* MS (TOF ES<sup>+</sup>) C<sub>28</sub>H<sub>44</sub>N<sub>5</sub>O<sub>3</sub><sup>+</sup> [M]<sup>+</sup> calcd, 498.3; found, 498.3. LC-MS: *t*<sub>R</sub> = 3.71 min.

#### **General procedure for the synthesis of OH bearing linker hybrid ligands (18a-c)**

Compound **15** (250 μmol, 1.0 eq.), n-bromo-1-hydroxyalkane (750 μmol, 3.0 eq.) and TEA (750 μmol, 3.0 eq.) were dissolved in ACN (10 mL) and heated to reflux with stirring overnight. The solvent was then removed under vacuum and the crude material was purified by preparative HPLC.

**4-((4,5-Dihydroisoxazol-3-yl)oxy)-N-(3-hydroxypropyl)-N,N-dimethylbut-2-yn-1-aminium bromide (18a).** Viscous white oil; 21.4 mg, 55%.  $^1\text{H}$  NMR (MeOD)  $\delta$  4.91 (t,  $J$  = 1.8 Hz, 2H), 4.46-4.32 (m, 4H), 4.15 (t, 1.9 Hz, 1H), 3.68 (t,  $J$  = 5.8 Hz, 2H), 3.62-3.48 (m, 2H), 3.18 (s, 6H), 3.03 (t,  $J$  = 9.6 Hz, 2H), 2.04-1.92 (m, 2H).  $^{13}\text{C}$  NMR (MeOD)  $\delta$  168.7, 87.8, 76.5, 71.2, 63.6, 59.3, 58.2, 55.3, 51.2, 33.6, 26.9.  $m/z$  MS (TOF ES $^+$ )  $\text{C}_{12}\text{H}_{21}\text{N}_2\text{O}_3^+ [\text{M}]^+$  calcd, 241.1; found, 241.0. LC-MS:  $t_{\text{R}}$  = 1.45 min.

**N-(4-((4,5-Dihydroisoxazol-3-yl)oxy)but-2-yn-1-yl)-5-hydroxy-N,N-dimethylpentan-1-aminium bromide (18b).** Viscous white oil; 31.2mg, 67%.  $^1\text{H}$  NMR (MeOD)  $\delta$  4.91 (t,  $J$  = 1.8 Hz, 2H), 4.47-4.34 (m, 4H), 4.15 (t, 1.9 Hz, 1H), 3.59 (t,  $J$  = 6.3 Hz, 2H), 3.48-3.37 (m, 2H), 3.17 (s, 6H), 3.03 (t,  $J$  = 9.6 Hz, 2H), 1.91-1.74 (m, 2H), 1.72-1.57 (m, 2H), 1.56-1.38 (m, 2H).  $^{13}\text{C}$  NMR (MeOD)  $\delta$  168.7, 87.7, 76.5, 71.2, 65.4, 62.3, 58.2, 55.0, 51.1, 33.6, 32.8, 23.7, 23.4.  $m/z$  MS (TOF ES $^+$ )  $\text{C}_{14}\text{H}_{25}\text{N}_2\text{O}_3^+ [\text{M}]^+$  calcd, 269.2; found, 269.0. LC-MS:  $t_{\text{R}}$  = 1.49 min.

**N-(4-((4,5-Dihydroisoxazol-3-yl)oxy)but-2-yn-1-yl)-7-hydroxy-N,N-dimethylheptan-1-aminium bromide (18c).** Viscous white oil; 37.1 mg, 61%.  $^1\text{H}$  NMR (MeOD)  $\delta$  4.91 (t,  $J$  = 1.8 Hz, 2H), 4.43-4.36 (m, 4H), 4.15 (t, 1.9 Hz, 1H), 3.56 (t,  $J$  = 6.5 Hz, 2H), 3.48-3.37 (m, 2H), 3.16 (s, 6H), 3.03 (t,  $J$  = 9.6 Hz, 2H), 1.84-1.73 (m, 4H), 1.57-1.36 (m, 6H).  $^{13}\text{C}$  NMR (MeOD)  $\delta$  168.7, 87.7, 76.6, 71.2, 65.4, 62.8, 58.2, 55.0, 51.1, 33.6, 33.4, 29.9, 27.2, 26.7, 23.6.  $m/z$  MS (TOF ES $^+$ )  $\text{C}_{16}\text{H}_{29}\text{N}_2\text{O}_3^+ [\text{M}]^+$  calcd, 297.2; found, 297.0. LC-MS:  $t_{\text{R}}$  = 1.68 min.

#### General procedure for the synthesis of NH bearing linker hybrid ligands (19a-d)

Compound **14** (1.0 mmol, 1.0 eq.), 1,n-dibromoalkane (3.0 mmol, 3.0 eq.) and TEA (3.0 mmol, 3.0 eq.) were dissolved in ACN (10 mL) and stirred overnight at room temperature. The solvent was removed under vacuum and the crude material was washed with hot PE. The crude material, *N*-alkylamine (1.5 mmol, 1.5 eq.) and TEA (1.5 mmol, 1.5 eq.) was then dissolved in



ACN (10 mL) and stirred overnight at room temperature. The solvent was then removed under vacuum and the crude material was purified by preparative HPLC.

**4-((4,5-Dihydroisoxazol-3-yl)oxy)-N-(3-(ethylamino)propyl)-N,N-dimethylbut-2-yn-1-aminium bromide (19a).** Viscous yellow oil; 12.2 mg, 38%.  $^1\text{H}$  NMR (MeOD)  $\delta$  4.92 (t,  $J$  = 1.8 Hz, 2H), 4.44-4.37 (m, 4H), 3.60-3.49 (m, 3H), 3.23-3.19 (m, 8H), 3.12 (qd,  $J$  = 6.3, 5.4, 3.1, 2H), 3.05 (t,  $J$  = 9.6 Hz, 2H), 2.22 (p,  $J$  = 5.4 Hz, 2H), 1.34 (t,  $J$  = 7.3 Hz, 3H).  $^{13}\text{C}$  NMR (MeOD)  $\delta$  168.9, 88.2, 76.3, 71.2, 69.4, 61.9, 58.2, 51.4, 44.9, 44.2, 33.7, 21.1, 11.5.  $m/z$  MS (TOF ES $^+$ )  $\text{C}_{14}\text{H}_{26}\text{N}_3\text{O}_2^+ [\text{M}]^+$  calcd, 268.2; found, 268.0. LC-MS:  $t_{\text{R}}$  = 1.34 min.

**4-((4,5-Dihydroisoxazol-3-yl)oxy)-N,N-dimethyl-N-(3-(propylamino)propyl)but-2-yn-1-aminium bromide (19b).** Viscous yellow oil; 14.6 mg, 27%.  $^1\text{H}$  NMR (MeOD)  $\delta$  4.92 (t,  $J$  = 1.8 Hz, 2H), 4.50-4.36 (m, 4H), 3.62-3.48 (m, 3H), 3.20-3.16 (m, 8H), 3.06-3.01 (m, 4H), 2.08-1.93 (m, 2H), 1.63-1.46 (m, 2H), 0.95 (t,  $J$  = 7.4, 3H).  $^{13}\text{C}$  NMR (MeOD)  $\delta$  168.8, 87.7, 76.5, 71.1, 64.9, 58.2, 55.2, 51.2, 48.0, 41.4, 33.8, 32.3, 23.2, 11.5.  $m/z$  MS (TOF ES $^+$ )  $\text{C}_{15}\text{H}_{28}\text{N}_3\text{O}_2^+ [\text{M}]^+$  calcd, 282.2; found, 282.0. LC-MS:  $t_{\text{R}}$  = 1.37 min.

**N-(4-((4,5-Dihydroisoxazol-3-yl)oxy)but-2-yn-1-yl)-5-(ethylamino)-N,N-dimethylpentan-1-aminium bromide (19c).** Viscous yellow oil; 20.0 mg, 40%.  $^1\text{H}$  NMR (MeOD)  $\delta$  4.91 (t,  $J$  = 1.8 Hz, 2H), 4.43-4.37 (m, 4H), 3.48-3.40 (m, 3H), 3.19-3.15 (m, 8H), 3.11-3.00 (m, 4H), 1.90-1.72 (m, 4H), 1.48 (p,  $J$  = 7.7 Hz, 2H), 1.31 (t,  $J$  = 7.3, 3H).  $^{13}\text{C}$  NMR (MeOD)  $\delta$  168.8, 87.8, 76.5, 71.18, 65.0, 58.2, 55.2, 51.2, 48.0, 44.0, 33.7, 26.8, 24.3, 23.2, 11.5.  $m/z$  MS (TOF ES $^+$ )  $\text{C}_{16}\text{H}_{30}\text{N}_3\text{O}_2^+ [\text{M}]^+$  calcd, 296.2; found, 296.0. LC-MS:  $t_{\text{R}}$  = 1.38 min.

**N-(4-((4,5-Dihydroisoxazol-3-yl)oxy)but-2-yn-1-yl)-N,N-dimethyl-5-(propylamino)pentan-1-aminium bromide (19d).** Viscous yellow oil; 12.8 mg, 41%.  $^1\text{H}$  NMR (MeOD)  $\delta$  4.91 (t,  $J$  = 1.8 Hz, 2H), 4.45-4.34 (m, 4H), 3.50-3.37 (m, 3H), 3.20-3.16 (m,

8H), 3.07-2.95 (m, 4H), 1.93-1.64 (m, 6H), 1.50 (p,  $J = 7.7$  Hz, 2H), 1.03 (t,  $J = 7.5$ , 3H).  $^{13}\text{C}$  NMR (MeOD)  $\delta$  168.8, 87.8, 76.5, 71.18, 64.9, 58.2, 55.2, 51.2, 48.0, 44.0, 33.8, 32.3, 26.8, 24.3, 23.2, 11.5.  $m/z$  MS (TOF ES<sup>+</sup>)  $\text{C}_{17}\text{H}_{32}\text{N}_3\text{O}_2^+ [\text{M}]^+$  calcd, 310.3; found, 309.9. LC-MS:  $t_R$  = 1.42 min.

#### **General procedure for the synthesis of ring substituted hybrid ligands (20a,e-i,k-l)**

Compound **15** (250  $\mu\text{mol}$ , 1.0 eq.), n-bromoalkanamide **21a-h** (275  $\mu\text{mol}$ , 1.1 eq.) (Supplementary Information) and TEA (750  $\mu\text{mol}$ , 3.0 eq.) were dissolved in ACN (10 mL) and heated to reflux with stirring overnight. The solvent was then removed under vacuum and the crude material was purified by preparative HPLC.

**General procedure for the synthesis of ring substituted hybrid ligands (20b-d,j,m-r)** 11-Bromoundecanoic acid (650  $\mu\text{mol}$ , 1.0 eq.) was dissolved in DCM (10 mL) with stirring and chilled on an ice bath to 0 °C. Thionyl chloride (1.5 mL) in DCM (10 mL) was then added to the solution dropwise over 1 h. The solution was stirred and allowed to warm to room temperature over 1.5 h. DCM and excess thionyl chloride was then removed from the solution under vacuum. The crude was diluted with toluene (5 mL) and this was removed under vacuum as an azeotropic mixture with residual thionyl chloride. The crude material was then dissolved in DCM (10 mL) and the appropriate amine (1.0 eq.) and TEA (1.5 eq.) were added and the solution stirred overnight at room temperature. The solution was then washed with HCl solution (2M, 10 mL) sat. bicarbonate solution (10 mL), brine (10 mL) and dH<sub>2</sub>O (10 mL), dried over MgSO<sub>4</sub> and the solvent removed under vacuum. The crude material was characterized by LC-MS before combining with **15** (1.0 eq.) and TEA (3.0 eq.) in ACN (10 mL) and heating to reflux with stirring overnight. The solvent was then removed under vacuum and the crude material was purified by preparative HPLC.

***N*-(4-((4,5-Dihydroisoxazol-3-yl)oxy)but-2-yn-1-yl)-*N,N*-dimethyl-11-(methylamino)-11-oxoundecan-1-aminium bromide (20a).** Viscous white oil; 43.6 mg, 45%. <sup>1</sup>H NMR (CDCl<sub>3</sub>) δ 6.33 (q, *J* = 4.0 Hz, 1H), 4.82 (t, *J* = 1.8 Hz, 2H), 4.74 (t, *J* = 1.8 Hz, 2H), 4.43 (t, *J* = 9.6 Hz, 2H), 3.66-3.56 (m, 2H), 3.37 (s, 6H), 3.01 (t, *J* = 9.6 Hz, 2H), 2.81 (d, *J* = 4.3 Hz, 3H), 2.32 (t, *J* = 7.7 Hz, 2H), 1.85-1.56 (m, 4H), 1.47-1.21 (m, 12H). <sup>13</sup>C NMR (CDCl<sub>3</sub>) δ 176.1, 166.9, 86.9, 75.7, 70.2, 64.7, 57.3, 55.1, 50.8, 46.3, 35.9, 33.0, 28.9, 28.8, 28.7, 28.6, 26.7, 26.0, 25.8, 22.8. *m/z* MS (TOF ES<sup>+</sup>) C<sub>21</sub>H<sub>38</sub>N<sub>3</sub>O<sub>3</sub><sup>+</sup> [M]<sup>+</sup> calcd, 380.3; found, 380.3. LC-MS: *t*<sub>R</sub> = 3.39 min.

**11-(Cyclohexylamino)-*N*-(4-((4,5-dihydroisoxazol-3-yl)oxy)but-2-yn-1-yl)-*N,N*-dimethyl-11-oxoundecan-1-aminium bromide (20b).** Viscous white oil; 22.2 mg, 48%. <sup>1</sup>H NMR (MeOD) δ 6.51 (d, *J* = 5.5 Hz, 1H), 4.91 (t, *J* = 1.8 Hz, 2H), 4.43-4.35 (m, 4H), 3.62 (tt, *J* = 10.9/3.9, 1H), 3.46-3.37 (m, 2H), 3.16 (s, 6H), 3.03 (t, *J* = 9.6 Hz, 2H), 2.14 (t, *J* = 7.4 Hz, 2H), 1.89-1.52 (m, 8H), 1.46-1.13 (m, 18H). <sup>13</sup>C NMR (MeOD) δ 175.3, 168.7, 87.7, 76.6, 71.2, 65.5, 58.2, 55.0, 53.8, 51.1, 43.4, 37.2, 33.8, 33.7, 30.4, 30.2, 28.4, 27.4, 27.3, 27.1, 26.7, 26.2, 23.6. *m/z* MS (TOF ES<sup>+</sup>) C<sub>26</sub>H<sub>46</sub>N<sub>3</sub>O<sub>3</sub><sup>+</sup> [M]<sup>+</sup> calcd, 448.4; found, 448.0. LC-MS: *t*<sub>R</sub> = 3.19 min.

***N*-(4-((4,5-Dihydroisoxazol-3-yl)oxy)but-2-yn-1-yl)-*N,N*-dimethyl-11-(methyl(phenyl)amino)-11-oxoundecan-1-aminium bromide (20c).** Viscous white oil; 32.1 mg, 34%. <sup>1</sup>H NMR (MeOD) δ 7.48 (t, *J* = 7.4 Hz, 2H), 7.40 (t, *J* = 7.4 Hz, 1H), 7.27 (d, *J* = 7.0 Hz, 2H), 4.90 (t, *J* = 1.8 Hz, 2H), 4.43-4.35 (m, 4H), 3.45-3.34 (m, 2H), 3.24 (s, 3H), 3.14 (s, 6H), 3.02 (t, *J* = 9.6 Hz, 2H), 2.08 (t, *J* = 7.6 Hz, 2H), 1.82-1.71 (m, 2H), 1.52 (p, *J* = 7.2 Hz, 2H), 1.42-1.13 (m, 12H). <sup>13</sup>C NMR (MeOD) δ 174.1, 168.7, 145.3, 131.0, 129.2, 128.4, 87.7, 76.6, 71.2, 65.5, 58.2, 55.0, 51.1, 37.8, 34.9, 33.7, 30.5, 30.4, 30.3, 30.2, 27.3, 27.2, 26.6, 23.6. *m/z* MS (TOF ES<sup>+</sup>) C<sub>27</sub>H<sub>42</sub>N<sub>3</sub>O<sub>3</sub><sup>+</sup> [M]<sup>+</sup> calcd, 456.3; found, 456.0. LC-MS: *t*<sub>R</sub> = 3.82 min.

***N*-(4-((4,5-Dihydroisoxazol-3-yl)oxy)but-2-yn-1-yl)-11-((2-fluorophenyl)amino)-*N,N*-dimethyl-11-oxoundecan-1-aminium bromide (20d).** Viscous white oil; 42.1 mg, 43%. <sup>1</sup>H NMR (MeOD)  $\delta$  9.58 (br s, 1H), 7.87-7.77 (m, 1H), 7.20-7.10 (m, 3H), 4.90 (t,  $J$  = 1.8 Hz, 2H), 4.42-4.34 (m, 4H), 3.44-3.38 (m, 2H), 3.15 (s, 6H), 3.02 (t,  $J$  = 9.6 Hz, 2H), 2.43 (t,  $J$  = 7.4 Hz, 2H), 1.82-1.65 (m, 4H), 1.47-1.25 (m, 12H). <sup>13</sup>C NMR (MeOD)  $\delta$  178.4, 175.1, 168.7, 156.1 (d,  $J_{CF}$  = 262.4 Hz), 127.1 (d,  $J_{CF}$  = 8.2 Hz), 126.1, 125.3 (d,  $J_{CF}$  = 2.7 Hz), 116.5 (d,  $J_{CF}$  = 13.7 Hz), 87.7, 76.6, 71.2, 65.5, 58.2, 55.0, 51.1, 37.4, 33.7, 30.4, 30.3, 30.2, 30.1, 27.5, 27.2, 26.8, 23.6.  $m/z$  MS (TOF ES<sup>+</sup>) C<sub>26</sub>H<sub>39</sub>FN<sub>3</sub>O<sub>3</sub><sup>+</sup> [M]<sup>+</sup> calcd, 460.3; found, 460.0. LC-MS:  $t_R$  = 3.00 min.

***N*-(4-((4,5-Dihydroisoxazol-3-yl)oxy)but-2-yn-1-yl)-11-((3-fluorophenyl)amino)-*N,N*-dimethyl-11-oxoundecan-1-aminium bromide (20e).** Viscous white oil; 20.1 mg, 61%. <sup>1</sup>H NMR (CDCl<sub>3</sub>)  $\delta$  8.95 (s, 1H), 7.65 (dt,  $J$  = 7.5, 1.6 Hz, 1H), 7.44 (dt,  $J$  = 8.0, 1.5 Hz, 1H), 7.20 (td,  $J$  = 7.5, 4.9 Hz, 1H), 6.73 (tt,  $J$  = 7.4, 1.6 Hz, 1H), 4.84-4.80 (m, 4H), 4.40 (t,  $J$  = 9.6 Hz, 2H), 3.63-3.55 (m, 2H), 3.34 (s, 6H), 2.99 (t,  $J$  = 9.6 Hz, 2H), 2.40 (t,  $J$  = 7.5 Hz, 2H), 1.76-1.62 (m, 4H), 1.36-1.17 (m, 12H). <sup>13</sup>C NMR (CDCl<sub>3</sub>)  $\delta$  172.5, 167.2, 162.4 (d,  $J_{CF}$  = 256.2 Hz), 135.2 (d,  $J_{CF}$  = 7.7 Hz), 129.2 (d,  $J_{CF}$  = 8.0 Hz), 117.0 (d,  $J_{CF}$  = 3.1 Hz), 112.2 (d,  $J_{CF}$  = 19.2 Hz), 108.8 (d,  $J_{CF}$  = 20.1 Hz), 86.7, 75.9, 70.1, 64.6, 57.3, 55.0, 47.3, 37.3, 33.1, 29.1, 28.9, 28.8, 28.7, 28.6, 26.0, 25.6, 22.8.  $m/z$  MS (TOF ES<sup>+</sup>) C<sub>26</sub>H<sub>39</sub>FN<sub>3</sub>O<sub>3</sub><sup>+</sup> [M]<sup>+</sup> calcd, 460.3; found, 460.0. LC-MS:  $t_R$  = 3.11 min.

***N*-(4-((4,5-Dihydroisoxazol-3-yl)oxy)but-2-yn-1-yl)-11-((4-fluorophenyl)amino)-*N,N*-dimethyl-11-oxoundecan-1-aminium bromide (20f).** Viscous white oil; 31.1 mg, 49%. <sup>1</sup>H NMR (CDCl<sub>3</sub>)  $\delta$  8.83 (s, 1H), 7.73-7.64 (m, 2H), 6.98-6.92 (m, 2H), 4.84-4.78 (m, 4H), 4.42 (t,  $J$  = 9.6 Hz, 2H), 3.70-3.58 (m, 2H), 3.37 (s, 6H), 3.00 (t,  $J$  = 9.6 Hz, 2H), 2.45 (t,  $J$  = 7.5 Hz, 2H), 1.76-1.62 (m, 4H), 1.45-1.16 (m, 12H). <sup>13</sup>C NMR (CDCl<sub>3</sub>)  $\delta$  172.5, 166.8, 156.2 (d,

$J_{\text{CF}} = 253.2$  Hz), 135.0 (d,  $J_{\text{CF}} = 2.9$  Hz), 121.8 (d,  $J_{\text{CF}} = 5.5$  Hz) 115.3 (d,  $J_{\text{CF}} = 15.0$  Hz), 86.8, 75.9, 70.2, 64.5, 57.3, 55.0, 47.3, 37.3, 33.1, 29.1, 28.9 28.8, 28.6, 28.5, 26.0, 25.6, 22.8.  $m/z$  MS (TOF ES<sup>+</sup>) C<sub>26</sub>H<sub>39</sub>FN<sub>3</sub>O<sub>3</sub><sup>+</sup> [M]<sup>+</sup> calcd, 460.3; found, 460.0. LC-MS:  $t_{\text{R}} = 3.06$  min.

***N*-(4-((4,5-Dihydroisoxazol-3-yl)oxy)but-2-yn-1-yl)-11-((2-methoxyphenyl)amino)-*N,N*-dimethyl-11-oxoundecan-1-aminium bromide (20g).** Viscous white oil; 22.2 mg, 59%. <sup>1</sup>H NMR (CDCl<sub>3</sub>)  $\delta$  8.30 (dd,  $J = 7.9, 1.6$  Hz, 1H), 7.75 (br s, 1H), 6.99 (td,  $J = 7.8, 1.7$  Hz, 1H), 6.90 (td, 7.8, 1.4 Hz, 1H), 6.84 (dd,  $J = 8.1, 1.4$  Hz, 1H), 4.87-4.76 (m, 4H), 4.38 (t,  $J = 9.6$  Hz, 2H), 3.61-3.51 (m, 2H), 3.39 (s, 6H), 2.97 (t,  $J = 9.6$  Hz, 2H), 2.35 (t,  $J = 7.5$  Hz, 2H), 1.77-1.62 (m, 4H), 1.40-1.19 (m, 12H). <sup>13</sup>C NMR (CDCl<sub>3</sub>)  $\delta$  171.4, 166.8, 147.8, 127.7, 123.6, 121.0, 119.8, 110.0, 86.4, 77.5, 76.0, 70.1, 64.2, 57.3, 55.8, 54.8, 50.6, 38.0, 33.0, 29.3, 29.2, 29.1, 29.0, 26.1, 25.6, 22.9.  $m/z$  MS (TOF ES<sup>+</sup>) C<sub>27</sub>H<sub>42</sub>N<sub>3</sub>O<sub>4</sub><sup>+</sup> [M]<sup>+</sup> calcd, 472.3; found, 472.3. LC-MS:  $t_{\text{R}} = 2.98$  min.

***N*-(4-((4,5-Dihydroisoxazol-3-yl)oxy)but-2-yn-1-yl)-11-((3-methoxyphenyl)amino)-*N,N*-dimethyl-11-oxoundecan-1-aminium bromide (20h).** Viscous white oil; 45.7 mg, 52%. <sup>1</sup>H NMR (CDCl<sub>3</sub>)  $\delta$  8.82 (s, 1H), 7.44 (t,  $J = 2.2$  Hz, 1H), 7.21-7.09 (m, 2H), 6.57 (ddd,  $J = 7.8, 2.6, 1.2$  Hz, 1H), 4.81-4.71 (m, 4H), 4.39 (t,  $J = 9.6$  Hz, 2H), 3.64-3.52 (m, 2H), 3.33 (s, 6H), 2.98 (t,  $J = 9.6$  Hz, 2H), 2.43 (t,  $J = 7.5$  Hz, 2H), 1.75-1.61 (m, 4H), 1.37-1.19 (m, 12H). <sup>13</sup>C NMR (CDCl<sub>3</sub>)  $\delta$  172.6, 166.9, 160.0, 140.2, 129.5, 112.3, 109.6, 105.8, 86.6, 75.9, 70.2, 64.4, 61.4, 57.4, 55.4, 54.9, 50.6, 37.5, 33.0, 28.9, 28.8, 28.7, 28.6, 26.0, 25.6, 22.7.  $m/z$  MS (TOF ES<sup>+</sup>) C<sub>27</sub>H<sub>42</sub>N<sub>3</sub>O<sub>4</sub><sup>+</sup> [M]<sup>+</sup> calcd, 472.3; found, 472.0. LC-MS:  $t_{\text{R}} = 3.02$  min.

***N*-(4-((4,5-Dihydroisoxazol-3-yl)oxy)but-2-yn-1-yl)-11-((4-methoxyphenyl)amino)-*N,N*-dimethyl-11-oxoundecan-1-aminium bromide (20i).** Viscous white oil; 25.1 mg, 36%. <sup>1</sup>H NMR (CDCl<sub>3</sub>)  $\delta$  8.64 (s, 1H), 7.59-7.50 (m, 2H), 6.85-6.75 (m, 2H), 4.84-4.75 (m, 4H),

4.40 (t,  $J = 9.6$  Hz, 2H), 3.63-3.55 (m, 2H), 3.34 (s, 6H), 2.99 (t,  $J = 9.6$  Hz, 2H), 2.40 (t,  $J = 7.5$  Hz, 2H), 1.76-1.62 (m, 4H), 1.38-1.19 (m, 12H).  $^{13}\text{C}$  NMR ( $\text{CDCl}_3$ )  $\delta$  172.2, 156.0, 132.1, 121.9, 114.0, 86.6, 75.9, 70.2, 64.4, 57.4, 55.6, 54.9, 50.6, 37.3, 33.0, 29.0, 28.9, 28.8, 28.7, 28.6, 26.0, 25.7, 22.8.  $m/z$  MS (TOF  $\text{ES}^+$ )  $\text{C}_{27}\text{H}_{42}\text{N}_3\text{O}_4^+ [\text{M}]^+$  calcd, 472.3; found, 472.1. LC-MS:  $t_{\text{R}} = 2.98$  min.

***N*-(4-((4,5-Dihydroisoxazol-3-yl)oxy)but-2-yn-1-yl)-*N,N*-dimethyl-11-oxo-11-((2-(trifluoromethyl)phenyl)amino)undecan-1-aminium bromide (20j).** Viscous white oil; 28.3 mg, 41%.  $^1\text{H}$  NMR (MeOD)  $\delta$  9.57 (br s, 1H), 7.72 (dd,  $J = 7.9, 1.5$  Hz, 1H), 7.64 (td,  $J = 7.7, 1.5$  Hz, 1H), 7.50 (d,  $J = 8.0$  Hz, 1H), 7.45 (t,  $J = 7.7$  Hz, 1H), 4.91 (t,  $J = 1.8$  Hz, 2H), 4.42-4.32 (m, 4H), 3.44-3.35 (m, 2H), 3.15 (s, 6H), 3.02 (t,  $J = 9.6$  Hz, 2H), 2.42 (t,  $J = 7.4$  Hz, 2H), 1.89-1.61 (m, 4H), 1.48-1.23 (m, 12H).  $^{13}\text{C}$  NMR (MeOD)  $\delta$  175.9, 158.1, 136.3, 133.9, 129.8 (q,  $J_{\text{CF}} = 211.7$  Hz), 127.5 (q,  $J_{\text{CF}} = 6.8$  Hz), 126.4, 123.7, 116.9, 92.6, 73.0, 71.9, 65.4, 58.8, 55.3, 53.7, 37.1, 33.9, 30.4, 30.3, 30.2, 30.1, 27.3, 27.2, 26.7, 23.6.  $m/z$  MS (TOF  $\text{ES}^+$ )  $\text{C}_{27}\text{H}_{39}\text{F}_3\text{N}_3\text{O}_3^+ [\text{M}]^+$  calcd, 510.3; found, 509.9. LC-MS:  $t_{\text{R}} = 3.14$  min.

***N*-(4-((4,5-Dihydroisoxazol-3-yl)oxy)but-2-yn-1-yl)-*N,N*-dimethyl-11-oxo-11-((3-(trifluoromethyl)phenyl)amino)undecan-1-aminium bromide (20k).** Viscous white oil; 19.9 mg, 22%.  $^1\text{H}$  NMR ( $\text{CDCl}_3$ )  $\delta$  9.32 (s, 1H), 8.12 (s, 1H), 7.94 (d,  $J = 7.9$  Hz, 1H), 7.37 (t,  $J = 7.9$  Hz, 1H), 7.28 (d,  $J = 7.9$  Hz, 1H), 4.83-4.74 (m, 4H), 4.41 (t,  $J = 9.6$  Hz, 2H), 3.67-3.60 (m, 2H), 3.38 (s, 6H), 3.00 (t,  $J = 9.6$  Hz, 2H), 2.51 (t,  $J = 7.5$  Hz, 2H), 1.81-1.66 (m, 4H), 1.40-1.19 (m, 12H).  $^{13}\text{C}$  NMR ( $\text{CDCl}_3$ )  $\delta$  173.1, 166.9, 139.7, 132.4, 129.7 (q,  $J_{\text{CF}} = 8.2$  Hz), 129.3, 123.7, 118.4 (q,  $J_{\text{CF}} = 239.1$  Hz), 116.6, 86.8, 75.8, 70.2, 64.6, 57.3, 55.0, 47.0, 37.2, 33.0, 29.0, 28.9, 28.8, 28.7, 28.6, 26.0, 25.7, 22.7.  $m/z$  MS (TOF  $\text{ES}^+$ )  $\text{C}_{27}\text{H}_{39}\text{F}_3\text{N}_3\text{O}_3^+ [\text{M}]^+$  calcd, 510.3; found, 510.0. LC-MS:  $t_{\text{R}} = 3.24$  min.

***N*-(4-((4,5-Dihydroisoxazol-3-yl)oxy)but-2-yn-1-yl)-*N,N*-dimethyl-11-oxo-11-((4-(trifluoromethyl)phenyl)amino)undecan-1-aminium bromide (20l).** Viscous white oil; 24.0 mg, 38%. <sup>1</sup>H NMR (CDCl<sub>3</sub>) δ 9.20 (s, 1H), 7.90 (d, *J* = 8.4 Hz, 2H), 7.51 (d, *J* = 8.5 Hz, 2H), 4.86-4.77 (m, 4H), 4.44 (t, *J* = 9.6 Hz, 2H), 3.72-3.64 (m, 2H), 3.37 (s, 6H), 3.01 (t, *J* = 9.6 Hz, 2H), 2.52 (t, *J* = 7.5 Hz, 2H), 2.03-1.67 (m, 4H), 1.43-1.17 (m, 12H). <sup>13</sup>C NMR (CDCl<sub>3</sub>) δ 176.2, 166.9, 143.0, 126.8 (q, *J*<sub>CF</sub> = 3.8 Hz), 126.4 (d, *J*<sub>CF</sub> = 32.7), 125.8 (q, *J*<sub>CF</sub> = 261.9), 120.7, 87.0, 75.8, 70.2, 64.7, 57.3, 55.2, 47.0, 37.2, 33.0, 29.0, 28.9, 28.8, 28.7, 28.6, 26.0, 25.7, 22.7. *m/z* MS (TOF ES<sup>+</sup>) C<sub>27</sub>H<sub>39</sub>F<sub>3</sub>N<sub>3</sub>O<sub>3</sub><sup>+</sup> [M]<sup>+</sup> calcd, 510.3; found, 510.0. LC-MS: *t*<sub>R</sub> = 3.16 min.

**11-((3,5-Bis(trifluoromethyl)phenyl)amino)-*N*-(4-((4,5-dihydroisoxazol-3-yl)oxy)but-2-yn-1-yl)-*N,N*-dimethyl-11-oxoundecan-1-aminium bromide (20m)** Viscous white oil; 23.3 mg, 36%. <sup>1</sup>H NMR (MeOD) δ 10.33 (br s, 1H), 8.23-8.18 (m, 2H), 7.64-7.62 (m, 2H), 4.90 (t, *J* = 1.8 Hz, 2H), 4.42-4.33 (m, 4H), 3.44-3.35 (m, 2H), 3.15 (s, 6H), 3.02 (t, *J* = 9.6 Hz, 2H), 2.42 (t, *J* = 7.4 Hz, 2H), 1.87-1.64 (m, 4H), 1.48-1.28 (m, 12H). <sup>13</sup>C NMR (MeOD) δ 179.1, 168.7, 142.2, 133.2 (q, *J*<sub>CF</sub> = 33.3 Hz), 129.3 (q, *J*<sub>CF</sub> = 267.9 Hz), 120.3 (app t, *J*<sub>CF</sub> = 4.1 Hz), 117.4, 87.7, 76.6, 71.2, 65.5, 58.2, 55.0, 50.6, 38.0, 33.7, 30.4, 30.3, 30.2, 30.1, 27.3, 27.2, 26.5, 23.6. *m/z* MS (TOF ES<sup>+</sup>) C<sub>28</sub>H<sub>38</sub>F<sub>6</sub>N<sub>3</sub>O<sub>3</sub><sup>+</sup> [M]<sup>+</sup> calcd, 578.3; found, 577.9. LC-MS: *t*<sub>R</sub> = 3.21 min.

**11-((3,5-Difluorophenyl)amino)-*N*-(4-((4,5-dihydroisoxazol-3-yl)oxy)but-2-yn-1-yl)-*N,N*-dimethyl-11-oxoundecan-1-aminium bromide (20n).** Viscous white oil; 43.1 mg, 61%. <sup>1</sup>H NMR (MeOD) δ 10.03 (br s, 1H), 7.29-7.20 (m, 2H), 6.64 (tt, *J* = 9.1, 2.3 Hz, 1H), , 4.90 (t, *J* = 1.8 Hz, 2H), 4.42-4.33 (m, 4H), 3.44-3.36 (m, 2H), 3.16 (s, 6H), 3.02 (t, *J* = 9.6 Hz, 2H), 2.37 (t, *J* = 7.4 Hz, 2H), 1.83-1.55 (m, 4H), 1.45-1.29 (m, 12H). <sup>13</sup>C NMR (MeOD) δ 179.6, 169.3, 139.3 (t, *J*<sub>CF</sub> = 2.7 Hz), 101.1 (dd, *J*<sub>CF</sub> = 286.9, 20.5 Hz), 98.5, 94.2, 87.7, 76.6, 71.2,

65.5, 58.2, 55.0, 51.1, 37.4, 33.7, 30.4, 30.3, 30.2, 30.1, 27.5, 27.2, 26.8, 23.6.  $m/z$  MS (TOF ES<sup>+</sup>) C<sub>26</sub>H<sub>38</sub>F<sub>2</sub>N<sub>3</sub>O<sub>3</sub><sup>+</sup> [M]<sup>+</sup> calcd, 478.3; found, 477.9. LC-MS:  $t_R$  = 2.95 min.

**11-((2,6-Difluorophenyl)amino)-*N*-(4-((4,5-dihydroisoxazol-3-yl)oxy)but-2-yn-1-yl)-*N,N*-dimethyl-11-oxoundecan-1-aminium bromide (20o).** Viscous white oil; 27.7 mg, 34%. <sup>1</sup>H NMR (MeOD)  $\delta$  9.67 (br s, 1H), 7.31 (tt,  $J$  = 8.5, 6.2 Hz, 1H), 7.04 (m, 2H), 4.90 (t,  $J$  = 1.8 Hz, 2H), 4.42-4.33 (m, 4H), 3.44-3.36 (m, 2H), 3.16 (s, 6H), 3.02 (t,  $J$  = 9.6 Hz, 2H), 2.43 (t,  $J$  = 7.4 Hz, 2H), 1.88-1.59 (m, 4H), 1.50-1.31 (m, 12H). <sup>13</sup>C NMR (MeOD)  $\delta$  175.3, 168.7, 159.8 (dd,  $J_{CF}$  = 267.5, 8.6 Hz), 129.3 (t,  $J_{CF}$  = 9.9 Hz), 116.7, 112.7 (d,  $J_{CF}$  = 23.9 Hz), 87.7, 76.6, 71.2, 65.5, 58.2, 55.0, 51.0, 36.7, 33.7, 30.4, 30.3, 30.2, 30.1, 30.0, 27.2, 26.8, 23.6.  $m/z$  MS (TOF ES<sup>+</sup>) C<sub>26</sub>H<sub>38</sub>F<sub>2</sub>N<sub>3</sub>O<sub>3</sub><sup>+</sup> [M]<sup>+</sup> calcd, 478.3; found, 478.0. LC-MS:  $t_R$  = 3.08 min.

**11-((2,5-Difluorophenyl)amino)-*N*-(4-((4,5-dihydroisoxazol-3-yl)oxy)but-2-yn-1-yl)-*N,N*-dimethyl-11-oxoundecan-1-aminium bromide (20p).** Viscous white oil; 22.2 mg, 28%. <sup>1</sup>H NMR (CDCl<sub>3</sub>)  $\delta$  8.14 (ddt,  $J$  = 9.9, 6.9, 3.3 Hz, 1H), 7.61 (br s, 1H), 7.01 (ddd,  $J$  = 10.4, 9.0, 4.9 Hz, 1H), 6.70 (ddt,  $J$  = 9.1, 7.3, 3.5 Hz, 1H), 4.81 (t,  $J$  = 1.8 Hz, 2H), 4.45-4.33 (m, 4H), 3.45-3.35 (m, 2H), 3.20 (s, 6H), 3.00 (t,  $J$  = 9.6 Hz, 2H), 2.41 (t,  $J$  = 7.5 Hz, 2H), 1.80-1.56 (m, 4H), 1.43-1.20 (m, 12H). <sup>13</sup>C NMR (CDCl<sub>3</sub>)  $\delta$  171.9, 166.9, 158.7 (d,  $J_{CF}$  = 242.7 Hz), 148.5 (d,  $J_{CF}$  = 238.4 Hz), 127.5 (t,  $J_{CF}$  = 11.9), 115.3 (dd,  $J_{CF}$  = 22.4, 9.6 Hz), 110.1 (d,  $J_{CF}$  = 24.8 Hz), 109.0 (d,  $J_{CF}$  = 30.9 Hz), 87.0, 75.1, 70.2, 64.7, 57.2, 54.9, 50.8, 37.2, 32.9, 29.0, 28.9, 28.8, 28.7, 28.6, 26.0, 25.7, 22.8.  $m/z$  MS (TOF ES<sup>+</sup>) C<sub>26</sub>H<sub>38</sub>F<sub>2</sub>N<sub>3</sub>O<sub>3</sub><sup>+</sup> [M]<sup>+</sup> calcd, 478.3; found, 477.9. LC-MS:  $t_R$  = 3.18 min.

***N*-(4-((4,5-Dihydroisoxazol-3-yl)oxy)but-2-yn-1-yl)-*N,N*-dimethyl-11-oxo-11-((perfluorophenyl)amino)undecan-1-aminium bromide (20q).** Viscous white oil; 34.0 mg, 45%. <sup>1</sup>H NMR (MeOD)  $\delta$  9.95 (br s, 1H), 4.91 (t,  $J$  = 1.8 Hz, 2H), 4.43-4.34 (m, 4H), 3.46-



3.38 (m, 2H), 3.16 (s, 6H), 3.02 (t,  $J = 9.6$  Hz, 2H), 2.46 (t,  $J = 7.3$  Hz, 2H), 1.85-1.61 (m, 4H), 1.49-1.30 (m, 12H).  $^{13}\text{C}$  NMR (MeOD)  $\delta$  175.2, 163.75, 145.5 (d,  $J_{\text{CF}} = 252.1$  Hz), 142.3 (d,  $J_{\text{CF}} = 151.2$  Hz), 137.9, 112.0, 87.7, 76.6, 65.5, 58.2, 55.0, 53.8, 51.1, 36.5, 33.7, 30.4, 30.3, 30.1, 30.0, 27.24, 26.6, 23.6.  $m/z$  MS (TOF ES $^{+}$ )  $\text{C}_{26}\text{H}_{35}\text{F}_5\text{N}_3\text{O}_3^{+}$   $[\text{M}]^{+}$  calcd, 532.3; found, 531.9. LC-MS:  $t_{\text{R}} = 3.22$  min.

***N*-(4-((4,5-Dihydroisoxazol-3-yl)oxy)but-2-yn-1-yl)-*N,N*-dimethyl-11-oxo-11-((3-(trifluoromethoxy)phenyl)amino)undecan-1-aminium bromide (20r).** Viscous white oil; 20.0 mg, 27%.  $^1\text{H}$  NMR (MeOD)  $\delta$  10.00 (br s, 1H), 7.72 (dp,  $J = 3.1, 1.1$  Hz, 1H), 7.44 (ddd,  $J = 8.2, 2.0, 1.1$  Hz, 1H), 7.37 (t,  $J = 8.2$  Hz, 1H), 6.97 (ddt,  $J = 8.1, 2.3, 1.1$  Hz, 1H), 4.90 (t,  $J = 1.8$  Hz, 2H), 4.43-4.34 (m, 4H), 3.44-3.37 (m, 2H), 3.15 (s, 6H), 3.01 (t,  $J = 9.6$  Hz, 2H), 2.38 (t,  $J = 7.5$  Hz, 2H), 1.83-1.62 (m, 4H), 1.46-1.30 (m, 12H).  $^{13}\text{C}$  NMR (MeOD)  $\delta$  174.9, 168.7, 150.7, 141.8, 131.1, 121.9 (q,  $J_{\text{CF}} = 255.5$  Hz), 119.1, 116.9, 113.4, 87.6, 76.6, 71.1, 65.5, 58.2, 55.0, 51.1, 38.0, 33.6, 30.6, 30.5, 30.4, 30.3, 30.2, 27.2, 26.7, 23.6.  $m/z$  MS (TOF ES $^{+}$ )  $\text{C}_{27}\text{H}_{39}\text{F}_3\text{N}_3\text{O}_4^{+}$   $[\text{M}]^{+}$  calcd, 526.3; found, 525.9. LC-MS:  $t_{\text{R}} = 3.19$  min.

**Pharmacology.** *Cell culture.* Flp-In-CHO cells stably expressing human muscarinic  $\text{M}_1$ ,  $\text{M}_2$ ,  $\text{M}_4$ ,  $\text{M}_5$ , or CHO-K1 expressing the  $\text{M}_3$  receptors were cultured at 37 °C in 5%  $\text{CO}_2$  in F-12 (Ham) ( $\text{M}_1$ ) or Dulbecco's modified Eagle media ( $\text{M}_2 - \text{M}_5$ ) supplemented with 10% ( $\text{M}_1$ ) or 5% ( $\text{M}_2 - \text{M}_5$ ) (v/v) FBS.

*ERK 1/2 phosphorylation assay plate preparation.* Cells were seeded into transparent 96-well plates at  $25 \times 10^3$  cells per well and grown for 6 - 8 h. Cells were then washed once with phosphate-buffered saline (PBS) and incubated in serum-free media (180 or 160  $\mu\text{L}$  per well, depending on the intended assay) at 37 °C) for at least 8 h, to allow phosphorylated ERK1/2 levels to subside.

*Concentration-response curves (CRCs).* Cells were plated in 180  $\mu\text{L}$  media per well. A stock solution of acetylcholine ( $10^{-2}$  M) was made up in PBS. Stock solutions of the test ligands ( $10^{-2}$  M) were made up in DMSO. Dilutions of all ligands were made up in FBS-free media at ten times ( $10\times$ ) the required concentration and added to stock plates. Cells were incubated at 37 °C with 20  $\mu\text{L}$  per well until peak phosphorylation occurred at which point the assay was terminated.

*Assay termination and data collection.* Agonist-stimulated ERK1/2 phosphorylation was terminated by the removal of drugs and the addition of 100  $\mu\text{L}$  p/well of *SureFire*<sup>TM</sup> lysis buffer. The cell lysates were agitated for 5-10 min. Following agitation, 10  $\mu\text{L}$  of cell lysates were transferred into a 384-well white opaque Optiplat<sup>TM</sup>, followed by addition of 8.3  $\mu\text{L}$  of a solution of reaction buffer / activation buffer / acceptor beads / donor beads in a ratio of 60/10/0.3/0.3 (v/ v/ v/ v) under green light conditions. The plates were then incubated at 37 °C in the dark for 1 h and fluorescence was measured on a Envision<sup>TM</sup> plate reader (PerkinElmer) using standard settings.

*Radioligand equilibrium whole cell binding assay plate preparation.* Cells were seeded into white opaque Isoplates<sup>TM</sup> at  $10 \times 10^3$  cells per well and then grown at 37 °C for 20-24 h. Cells were then washed twice with 50  $\mu\text{L}$  of cold HEPES-buffered saline, then 140 or 160  $\mu\text{L}$  of cold HEPES-buffered saline was added per well.

*Saturation binding assay protocol with [<sup>3</sup>H]NMS.* Stock solutions of [<sup>3</sup>H]NMS ( $10^{-2}$  M) were made up in cold HEPES-buffered saline. Dilutions of [<sup>3</sup>H]NMS were made up in cold HEPES-buffered saline at ten times ( $10\times$ ) the required concentration and added to stock plates on ice. Cells were equilibrated at 25 °C for 4 h. The  $K_d$  values for [<sup>3</sup>H]NMS at the M<sub>1</sub>-M<sub>5</sub> mAChR subtypes were found to be as follows: M<sub>1</sub> mAChR:  $0.06 \pm 0.01$  nM, M<sub>2</sub> mAChR: 0.11

$\pm 0.02$  nM, M<sub>3</sub> mAChR:  $0.19 \pm 0.12$  nM, M<sub>4</sub> mAChR:  $0.12 \pm 0.03$  nM, M<sub>5</sub> mAChR:  $0.11 \pm 0.07$  nM.

*Orthosteric competition binding assay protocol.* Stock solutions of each ligand ( $10^{-2}$  M) were made up in cold HEPES-buffered saline. Dilutions of all ligands were made up in cold HEPES-buffered saline at ten times ( $10\times$ ) the required concentration and added to stock plates on ice. Cells were equilibrated at 25 °C for 4 h with 20  $\mu$ L of a single interacting ligand and 20  $\mu$ L of 1 nM [<sup>3</sup>H]NMS (total volume 200  $\mu$ L per well).

*Assay termination and data collection.* Assays were terminated by media removal of the assay buffer and by washing twice with 50  $\mu$ L 0.9% NaCl solution. Microscint-20 scintillation liquid (100  $\mu$ L per well) was then added to each well and the plates covered. The levels of remaining bound radioligand, were measured in counts per minute (cpm) on the Microbeta2™ LumiJET 2460 microplate counter (PerkinElmer).

*Data analysis.* All data analysis was managed using Prism 6 software (GraphPad Software, San Diego, CA).

Whole cell equilibrium competition radioligand binding experiments were fitted to a one-site competition binding equation (1) to estimate the  $pK_i$  for each ligand. The equation assumes that there is only one-site the ligands bind to and that the binding is reversible and at equilibrium:

$$Y = bottom + \frac{top - bottom}{1 + 10^{[I] - \log(10^{K_i(1 + \frac{[A]}{K_A})})}} \quad (1)$$

where Y is the percentage (vehicle control) binding, top and bottom are the total and non-specific binding, respectively. [A] and [I] are the concentrations of [<sup>3</sup>H]NMS, and competing “cold” ligand respectively,  $K_A$  and  $K_i$  are the equilibrium dissociation constants of [<sup>3</sup>H]NMS

and the “cold” ligand, respectively. The efficacy ( $\tau$ ) of several ligands was determined by fitting the functional data to an operational model of agonism (2):

$$Y = \frac{E_{max}-Basal}{1+(\frac{10^{\log K_A+10[L]}}{10^{\log \tau+[L]}})^n} \quad (2)$$

where Y is the measured response,  $E_{max}$  and basal are the top and bottom asymptotes of the curve, respectively,  $K_A$  equilibrium dissociation constant for the ligand being tested, [L] is the concentration of ligand in solution,  $\tau$  is the efficacy of the ligand being tested and n is the transducer slope. The efficacy values were then normalised to the M<sub>4</sub> mAChR values, to give the ‘corrected efficacy’ ( $\tau_c$ ), to account for the varying receptor expression in each cell line used by the following equation:

$$\log \tau_c = \log \tau - \log\left(\frac{B_{max_{Mx}}}{B_{max_{M4}}}\right) \quad (3)$$

where  $\tau_c$  is the corrected efficacy,  $\tau$  is the measured efficacy (as determined by equation 2),  $B_{max}$  is the maximum counts recorded when the mAChR in question is incubated with a saturating concentration of [<sup>3</sup>H]NMS, at mAChR M<sub>x</sub>, where x gives the subtype in question, compared to the M<sub>4</sub> mAChR.

## ■ REFERENCES

- (1) Overington, J. P.; Al-Lazikani, B.; Hopkins, A. L., How many drug targets are there? *Nat. Rev. Drug Discov.* **2006**, *5*, 993-6.
- (2) Sriram, K.; Insel, P. A. GPCRs as targets for approved drugs: How many targets and how many drugs? *Mol. Pharmacol.* **2018**, *96*, 251-58.
- (3) Santos, R.; Ursu, O.; Gaulton, A.; Bento, A. P.; Donadi, R. S.; Bologa, C. G.; Karlsson, A.; Al-Lazikani, B.; Hersey, A.; Oprea, T. I.; Overington, J. P., A comprehensive map of molecular drug targets. *Nat. Rev. Drug Discov.* **2016**, *16*, 19-34.
- (4) Zhou, X. E.; Melcher, K.; Xu, H. E., Structure and activation of rhodopsin. *Acta. Pharmacol. Sin.* **2012**, *33*, 291-9.
- (5) Shonberg, J.; Kling, R. C.; Gmeiner, P.; Löber, S., GPCR crystal structures: Medicinal chemistry in the pocket. *Bioorg. Med. Chem.* **2015**, *23*, 3880-906.

- (6) Christopoulos, A. Allosteric binding sites on cell-surface receptors: novel targets for drug discovery. *Nat. Rev. Drug Discov.* **2002**, *1*, 198-210.
- (7) Mohr, K.; Tränkle, C.; Kostenis, E.; Barocelli, E.; De Amici, M.; Holzgrabe, U., Rational design of dualsteric GPCR ligands: quests and promise. *Br J Pharmacol.* **2010**, *159* (5), 997-1008.
- (8) Lane, R. J.; Sexton, P. M.; Christopoulos, A. Bridging the gap: bitopic ligands of G-protein-coupled receptors. *Trends Pharmacol. Sci.* **2013**, *34*, 59-66.
- (9) Valant, C.; Lane, R. J.; Sexton, P. M.; Christopoulos, A., The best of both worlds? Bitopic orthosteric/allosteric ligands of G protein-coupled receptors. *Annu. Rev. Pharmacol. Toxicol.* **2012**, *52*, 153-78.
- (10) Greig, N. H.; Reale, M.; Tata, A. M., New pharmacological approaches to the cholinergic system: an overview on muscarinic receptor ligands and cholinesterase inhibitors. *Recent Pat CNS Drug Discov.* **2013**, *8* (2), 123-41.
- (11) Alagha, K.; Palot, A.; Sofalvi, T.; Pahus, L.; Gouitaa, M.; Tummino, C.; Martinez, S.; Charpin, D.; Bourdin, A.; Chanez, P., Long-acting muscarinic receptor antagonists for the treatment of chronic airway diseases. *Ther Adv Chronic Dis.* **2014**, *5*, 85-98.
- (12) Langmead, C. J.; Watson, J.; Reavill, C., Muscarinic acetylcholine receptors as CNS drug targets. *Pharmacol Ther* **2008**, *117* (2), 232-243.
- (13) Bodick, N. C.; Offen, W. W.; Levey, A. I.; Cutler, N. R.; Gauthier, S. C.; Satlin, A.; Shannon, H. E.; Tollefson, G. D.; Rasmussen, K.; Bymaster, F. P.; Hurley, D. J.; Potter, W. Z.; Paul, S. M.; Effects of xanomeline, a selective muscarinic receptor agonist, on cognitive function and behavioral symptoms in Alzheimer's disease. *Arch. Neurol.* **1997**, *54*, 465-73.
- (14) Bodick, N. C.; Offen, W. W.; Shannon, H. E.; Satterwhite, J.; Lucas, R.; van Lier, R.; Paul, S. M. The selective muscarinic agonist xanomeline improves both the cognitive deficits and behavioral symptoms of Alzheimer disease. *Alzheimer Dis. Assoc. Disord.* **1997**, *11 Suppl 4*, S16-22.
- (15) Mirza, N. R.; Peters, D.; Sparks, R. G., Xanomeline and the Antipsychotic Potential of Muscarinic Receptor Subtype Selective Agonists. *CNS Drug Rev* **2003**, *9* (2), 159-186.
- (16) Shekhar, A.; Potter, W.; Lienemann, J.; Sundblad, K.; Lightfoot, J.; Herrera, J.; Unverzagt, F.; Bymaster, F.; Felder, C. Efficacy of xanomeline, a selective muscarinic agonist, in treating schizophrenia: a double-blind, placebo controlled study, *ACNP 40th Annual Meeting*, **2001**; 9-13.
- (17) Shannon, H. E.; Rasmussen, K.; Bymaster, F. P.; Hart, J. C.; Peters, S. C.; Swedberg, M. D. B.; Jeppesen, L.; Sheardown, M. J.; Sauerberg, P.; Fink-Jensen, A., Xanomeline, an M1/M4 preferring muscarinic cholinergic receptor agonist, produces antipsychotic-like activity in rats and mice. *Schizophr Res* **2000**, *42* (3), 249-259.
- (18) Andersen, M. B.; Fink-Jensen, A.; Peacock, L.; Gerlach, J.; Bymaster, F.; Lundbæk, J. A.; Werge, T. The Muscarinic M1/M4 Receptor Agonist Xanomeline Exhibits Antipsychotic-Like Activity in Cebus apella Monkeys. *Neuropsychopharmacology* **2003**, *28*, 1168-75.
- (19) Shekhar, A.; Potter, W. Z.; Lightfoot, J.; Lienemann, J.; Dubé, S.; Mallinckrodt, C.; Bymaster, F. P.; McKinzie, D. L.; Felder, C. C. Selective Muscarinic Receptor Agonist Xanomeline as a Novel Treatment Approach for Schizophrenia. *Am. J. Psychiatry* **2008**, *165*, 1033-9.
- (20) Haga, K.; Kruse, A. C.; Asada, H.; Yurugi-Kobayashi, T.; Shiroishi, M.; Zhang, C.; Weis, W. I.; Okada, T.; Kobilka, B. K.; Haga, T.; Kobayashi, T., Structure of the human M2 muscarinic acetylcholine receptor bound to an antagonist. *Nature* **2012**, *482*, 547.
- (21) Kruse, A. C.; Ring, A. M.; Manglik, A.; Hu, J.; Hu, K.; Eitel, K.; Hubner, H.; Pardon, E.; Valant, C.; Sexton, P. M.; Christopoulos, A.; Felder, C. C.; Gmeiner, P.; Steyaert, J.; Weis, W.

- I.; Garcia, K. C.; Wess, J.; Kobilka, B. K. Activation and allosteric modulation of a muscarinic acetylcholine receptor. *Nature* **2013**, *504*, 101-6.
- (22) Thal, D. M.; Sun, B.; Feng, D.; Nawaratne, V.; Leach, K.; Felder, C. C.; Bures, M. G.; Evans, D. A.; Weis, W. I.; Bachhawat, P.; Kobilka, T. S.; Sexton, P. M.; Kobilka, B. K.; Christopoulos, A. Crystal structures of the M1 and M4 muscarinic acetylcholine receptors. *Nature* **2016**, *531*, 335-40.
- (23) Kruse, A. C.; Hu, J.; Pan, A. C.; Arlow, D. H.; Rosenbaum, D. M.; Rosemond, E.; Green, H. F.; Liu, T.; Chae, P. S.; Dror, R. O.; Shaw, D. E.; Weis, W. I.; Wess, J.; Kobilka, B. K., Structure and dynamics of the M3 muscarinic acetylcholine receptor. *Nature* **2012**, *482*, 552-6.
- (24) Matera, C.; Flammini, L.; Quadri, M.; Vivo, V.; Ballabeni, V.; Holzgrabe, U.; Mohr, K.; De Amici, M.; Barocelli, E.; Bertoni, S.; Dallanoce, C., Bis(ammonio)alkane-type agonists of muscarinic acetylcholine receptors: Synthesis, in vitro functional characterization, and in vivo evaluation of their analgesic activity. *Eur. J. Med. Chem.* **2014**, *75*, 222-32.
- (25) Bock, A.; Merten, N.; Schrage, R.; Dallanoce, C.; Bätz, J.; Klöckner, J.; Schmitz, J.; Matera, C.; Simon, K.; Kebig, A.; Peters, L.; Müller, A.; Schrobang-Ley, J.; Tränkle, C.; Hoffmann, C.; De Amici, M.; Holzgrabe, U.; Kostenis, E.; Mohr, K., The allosteric vestibule of a seven transmembrane helical receptor controls G-protein coupling. *Nat. Commun.* **2012**, *3*, 1044.
- (26) Schmitz, J.; van der May, D.; Bermudez, M.; Klöckner, J.; Schrage, R.; Kostenis, E.; Tränkle, C.; Wolber, G.; Mohr, K.; Holzgrabe, U. Dualsteric Muscarinic Antagonists—Orthosteric Binding Pose Controls Allosteric Subtype Selectivity. *J. Med. Chem.* **2014**, *57*, 6739–50.
- (27) Disingrini, T.; Muth, M.; Dallanoce, C.; Barocelli, E.; Bertoni, S.; Kellershohn, K.; Mohr, K.; De Amici, M.; Holzgrabe, U. Design, Synthesis, and Action of Oxotremorine-Related Hybrid-Type Allosteric Modulators of Muscarinic Acetylcholine Receptors. *J. Med. Chem.* **2006**, *49*, 366-72.
- (28) Valant, C.; Gregory, K. J.; Hall, N. E.; Scammells, P. J.; Lew, M. J.; Sexton, P. M.; Christopoulos, A. A Novel Mechanism of G Protein-coupled Receptor Functional Selectivity: Muscarinic partial agonist McN-A-343 as a bitopic orthosteric/allosteric ligand. *J. Biol. Chem.* **2008**, *283*, 29312–21.
- (29) Mitchelson, F. J. The pharmacology of McN-A-343. *Pharmacol. Ther.* **2012**, *135*, 216-45.
- (30) Micheletti, R.; Schiavone, A., Functional determination of McN-A-343 affinity for M1 muscarinic receptors. *J. Pharmacol. Exp. Ther.* **1990**, *253*, 310-4.
- (31) She, X.; Pegoli, A.; Mayr, J.; Hübner, H.; Bernhardt, G.; Gmeiner, P.; Keller, M., Heterodimerization of Dibenzodiazepinone-Type Muscarinic Acetylcholine Receptor Ligands Leads to Increased M2R Affinity and Selectivity. *ACS Omega* **2017**, *2*, 6741-54.
- (32) Tränkle, C.; Andresen, I.; Lambrecht, G.; Mohr, K., M2 receptor binding of the selective antagonist AF-DX 384: possible involvement of the common allosteric site. *Mol. Pharmacol.* **1998**, *53*, 304-12.
- (33) Bermudez, M.; Bock, A.; Krebs, F.; Holzgrabe, U.; Mohr, K.; Lohse, M. J.; Wolber, G. Ligand-Specific Restriction of Extracellular Conformational Dynamics Constrains Signaling of the M2 Muscarinic Receptor. *ACS Chem. Biol.* **2017**, *12*, 1743-48.
- (34) Klöckner, J.; Schmitz, J.; Holzgrabe, U., Convergent, short synthesis of the muscarinic superagonist iperovo. *Tetrahedron Lett.* **2010**, *51*, 3470-2.

- (35) Mellin, C.; Vargas, H. M.; Ringdahl, B., Dimethylsulfonium analogs of the muscarinic agent McN-A-343: [4-[[N-(3- or 4-halophenyl)carbamoyl]oxy]-2-butynyl]dimethylsulfonium perchlorates. *J. Med. Chem.* **1989**, *32*, 1590-3.
- (36) Ringdahl, B.; Mellin, C.; Ehlert, F. J.; Roch, M.; Rice, K. M.; Jenden, D. J., Tertiary (2-haloethyl)amine derivatives of the muscarinic agent McN-A-343, [4-[[N-(3-chlorophenyl)carbamoyl]oxy]-2-butynyl]trimethylammonium chloride. *J. Med. Chem.* **1990**, *33*, 281-6.
- (37) Battaglia, M. R.; Buckingham, A. D.; Williams, J. H., The electric quadrupole moments of benzene and hexafluorobenzene. *Chem. Phys. Lett.* **1981**, *78*, 421-3.
- (38) Tsuzuki, S.; Uchimaru, T.; Mikami, M., Intermolecular Interaction between Hexafluorobenzene and Benzene: Ab Initio Calculations Including CCSD(T) Level Electron Correlation Correction. *J. Phys. Chem. A.* **2006**, *110*, 2027-33.
- (39) Gottlieb, H. E.; Kotlyar, V.; Nudelman, A. NMR Chemical Shifts of Common Laboratory Solvents as Trace Impurities. *J. Org. Chem.* **1997**, *62*, 7512-5.

# Chapter Four



## **Declaration of Contributions for Chapter Four**

All of the pharmacological assaying/ evaluation of the ligands in this chapter was performed by myself, including all assay design and analysis. The *in silico* docking work was also performed by myself. The cloned hM<sub>1</sub>-M<sub>5</sub> muscarinic acetylcholine cell lines used in this work were provided by the laboratory of Dr. Arthur Christopoulos. General guidance in the pharmacological analysis was also provided by Dr. Arthur Christopoulos and Dr. Celine Valant.

# Investigation into the Molecular Mechanism of Efficacy and Selectivity of Iperoxo-Based Muscarinic Acetylcholine Receptor Hybrid Ligands

**ABSTRACT:** In chapter 2 and 3, while attempting to optimise a series of *N*-alkyl iperoxo derived muscarinic acetylcholine receptor (mAChR) hybrid ligands for potency and M<sub>2</sub>/ M<sub>4</sub> mAChR selectivity, we identified an apparent inverse correlation between the two properties which limited further optimisation. To investigate this apparent interdependence of efficacy and M<sub>2</sub>/M<sub>4</sub> mAChR selectivity we have investigated the effect of interacting the hybrid ligands with the allosteric potentiator, LY2119620, as well as the effect of key orthosteric and allosteric mutations on the hybrid ligand pharmacology. The experimental results were then contextualized with *in silico* docking to give a binding model that is consistent with the observed data and which explains the observed interdependence of efficacy and M<sub>2</sub>/M<sub>4</sub> mAChR selectivity. Interaction binding data showed a strong correlation between the induced potentiation of binding affinity and the selectivity of the hybrid ligands, possibly suggesting that binding conformation plays a direct role in selectivity or that the linker interferes with allosteric-orthosteric cooperativity. We found no evidence that any of our hybrid ligands made a direct interaction with the allosteric site of the M<sub>2</sub> or M<sub>4</sub> mAChRs. However, efficacy of the more selective ligands (e.g. IXO-C10) was found to increase upon allosteric mutation with no change in binding affinity relative to their respective wild-type receptors, confirming our hypothesis that these ligands obstruct the allosteric site rather than interfere with cooperativity. Additionally, the affinities of the hybrid ligands were found to be unaffected by the M<sub>2</sub> mAChR orthosteric mutation Y426F<sup>7,39</sup>, suggesting that Y426<sup>7,39</sup> is perturbed by the *N*-linker of our hybrid ligands in the wild-type M<sub>2</sub> mAChR, and this is supported by molecular docking

models. Together our results suggest that the linker and terminal substituent of our hybrid ligands can adopt two conformations at each of the M<sub>1</sub>-M<sub>5</sub> mAChR subtypes, dependent on the ligand linker length and/ or substituent. One conformation in which the linker and terminal substituent of the hybrid ligands obstructs the allosteric site and attenuates efficacy and a second conformation which does not obstruct the allosteric site, and which results in a non-selective maintenance of efficacy relative to the orthosteric ligand, iperoxo.

## ■ INTRODUCTION

G protein-coupled receptors (GPCRs) are a class of ~800 membrane bound receptor proteins that mediate a wide range of physiological processes in the central and peripheral nervous system of the human body, and hence many GPCRs are of pharmaceutical interest for the treatment of various diseases.<sup>1-2</sup> The muscarinic acetylcholine receptors (mAChRs) are one such sub-family of GPCRs which historically, and up to the present, have received significant attention from both academia and industry, due to the roles that each of the five subtypes (M<sub>1</sub>-M<sub>5</sub> mAChRs) plays in the smooth muscle contractility in the lungs, heart, eyes, bladder, and other organs.<sup>3-6</sup> For instance, antagonists targeting the M<sub>2</sub> and M<sub>3</sub> mAChRs have successfully been developed in the past, but generally possess significant off-target side effects due to action at related mAChR subtypes.<sup>7-9</sup> For several decades, significant research efforts have been directed towards the development of agonists for the M<sub>1</sub> and M<sub>4</sub> mAChRs due to their involvement in the progression of Alzheimer's disease and schizophrenia, respectively.<sup>10-12</sup>

However although the most recent M<sub>1</sub>/ M<sub>4</sub> mAChR preferring clinical candidate, xanomeline (**1**) (Figure 1), showed promising results in treating both disorders in phase 2 trials, it was not progressed further at the time due to intolerable off-target cholinergic side effects.<sup>10-</sup>

<sup>11</sup> More recently a new formulation of xanomeline (**1**) in combination with a peripherally

restricted muscarinic antagonist has re-entered clinical trials in an attempt to limit its peripheral side effects, however this combination therapy approach may give rise to new drug-drug interactions and is far from an ideal solution to achieving mAChR subtype selectivity.<sup>13</sup>

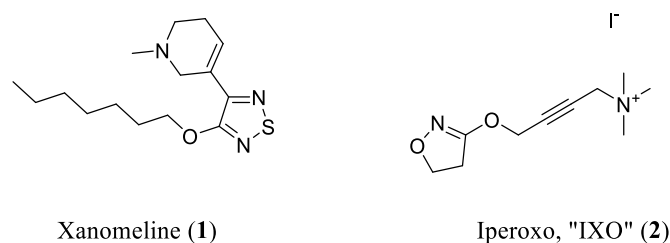


**Figure 1.** Structures of the M<sub>1</sub>/ M<sub>4</sub> mAChR preferring partial agonist, xanomeline (**1**), and non-selective full agonist, iperoxo iodide (or “IXO”) (**2**).

The inherent lack of subtype selectivity is common to many GPCR ligands, and arises due to the high degree of amino acid conservation observed between the endogenous ligand binding sites (orthosteric sites) of subtypes within GPCR sub-families.<sup>14</sup> Previously in chapters 2 and 3 we explored the structure-activity relationship (SAR) surrounding agonist-based hybrid ligands, with regards to their efficacy and M<sub>2</sub>/M<sub>4</sub> mAChR selectivity.

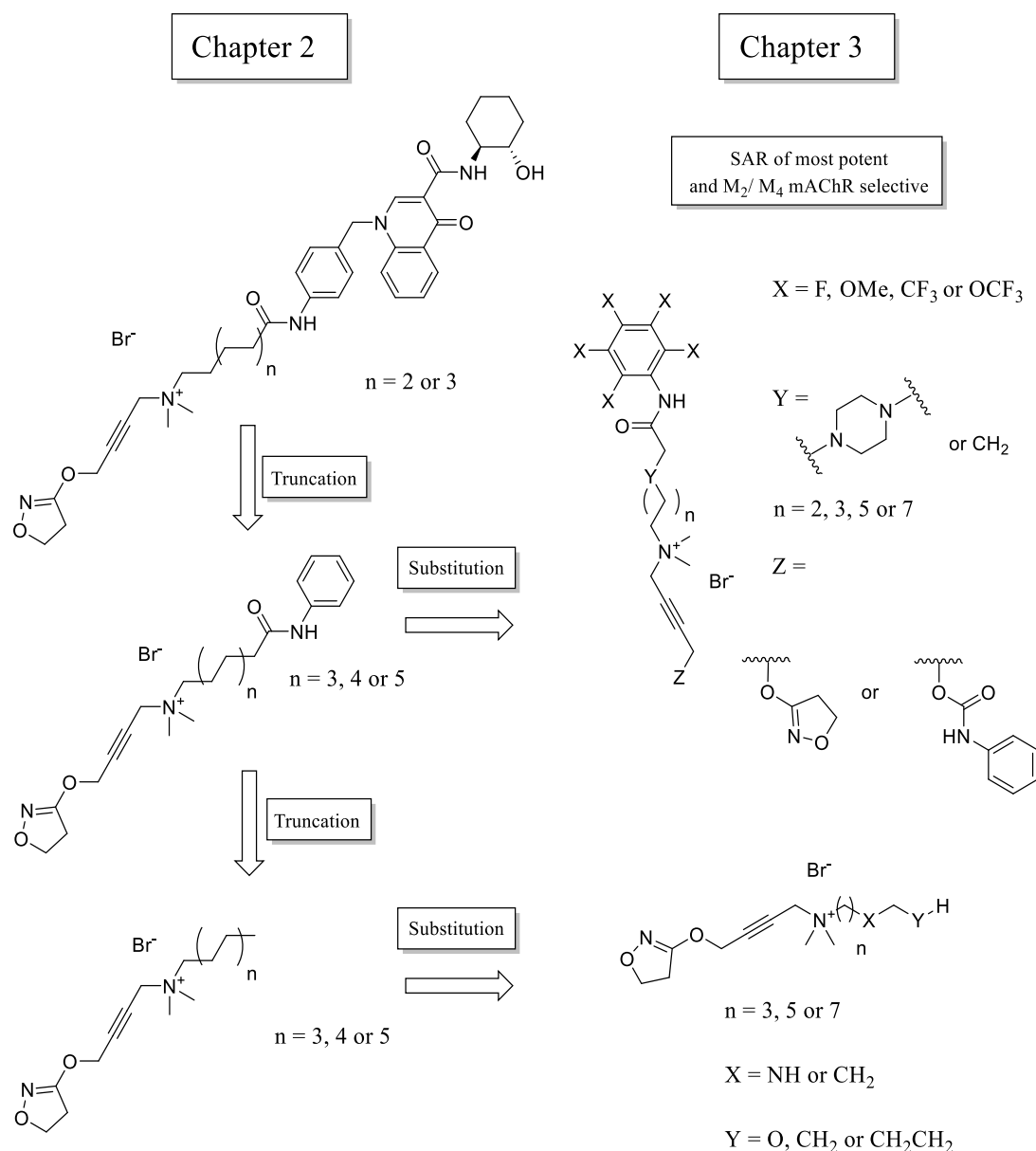
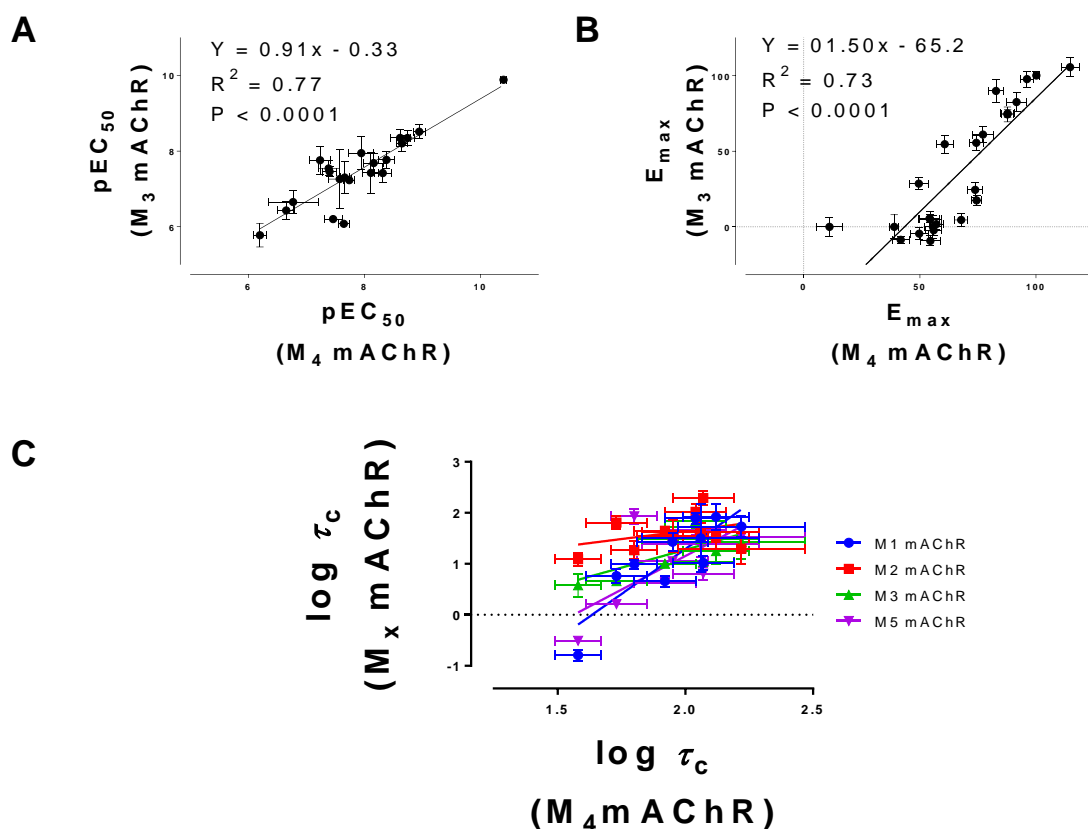


**Figure 2.** Summary of the chemical space explored surrounding agonist-based mAChR hybrid ligands and truncated hybrid ligands with regards to efficacy and mAChR subtype selectivity, detailed in chapters 2 and 3.

Similar to other agonist-based mAChR hybrid ligands reported in the literature, most possess moderate to good M<sub>2</sub>/M<sub>4</sub> mAChR selectivity and an ‘optimal’ linker length, at which efficacy is highest, similar to putative ‘bitopic’ ligands.<sup>15-20</sup> However, structurally these hybrid ligands do not retain an allosteric pharmacophore as a substituent at all (Figure 2), ruling out a bitopic mechanism as their mode of action. A key example of this being *N*-decyl iperoxo (IXO-

C10), which retains good M<sub>2</sub>/M<sub>4</sub> mAChR selectivity and moderate potency, without any allosteric pharmacophore (Chapter 2). When the efficacy of these hybrid ligands was higher (such as at ‘optimal’ linker lengths) we found that the M<sub>2</sub>/M<sub>4</sub> mAChR selectivity was significantly attenuated or abolished. Analysis of our entire set of hybrid ligands revealed an apparent linear relationship between their potency and maximum response between the M<sub>3</sub> mAChR (at which ligand efficacy was typically lowest) and M<sub>4</sub> mAChR (at which ligand efficacy was typically highest). Further analysis of a representative subset of our hybrid ligands across all M<sub>1</sub>-M<sub>5</sub> mAChR subtypes also shows that M<sub>1</sub>, M<sub>3</sub> and M<sub>5</sub> (but not M<sub>2</sub>) mAChR ligand efficacy correlates with M<sub>4</sub> mAChR ligand efficacy, implying that M<sub>2</sub>/M<sub>4</sub> mAChR selectivity correlates inversely with ligand efficacy at the M<sub>2</sub>/M<sub>4</sub> mAChRs (Figure 3).



mAChR	M1	M2	M3	M5
Equation	$Y = 3.532 \cdot X - 5.773$	$Y = 0.6324 \cdot X + 0.3795$	$Y = 1.404 \cdot X - 1.532$	$Y = 2.635 \cdot X - 4.117$
R squared	0.7346	0.1181	0.4934	0.4742
P value	0.0015	0.3309	0.0235	0.0277

**Figure 3.** (A) Potency and (B) maximum response at the M<sub>3</sub> versus M<sub>4</sub> mAChRs for all of the hybrid ligands evaluated in chapters 2 and 3. (C) Plot of the hybrid ligand efficacy at the M<sub>1</sub>-M<sub>3</sub>, M<sub>5</sub> mAChRs versus the M<sub>4</sub> mAChR. pEC<sub>50</sub> values are the negative logarithm of the concentration of a ligand that was able to elicit 50 % the maximum achievable response by that ligand as determined by fitting a 3-parameter concentration-response curve to the ERK 1/2 phosphorylation concentration-response data. E<sub>max</sub> values are the maximum response measured by each ligand, as a percentage of the maximum response achievable by the full agonist, iperoxo (2). Log  $\tau_c$  is the ligand efficacy, corrected for receptor expression (determined by radioligand binding assays), as determined by fitting the functional data for each ligand to an operational model of agonism and constraining the model by the measured values of affinity for each ligand at each of the respective mAChR subtype. Each value in the x and y direction represents the mean  $\pm$  S.E. of at least 3 independent experiments performed in duplicate. Linear slopes and intercepts were calculated using least squares regression to find a line of best fit.

There have been proposed several binding models to explain the observed pharmacology of various mAChR hybrid ligands, which are structurally related to our hybrid ligands.<sup>19-21</sup> These include bitopic binding, alternating allosteric-orthosteric binding, mechanisms in which two ligands bind to the receptor, and others.<sup>17</sup> Given that our hybrid ligands fully displace the radioligand [<sup>3</sup>H]*N*-methylscopolamine ([<sup>3</sup>H]NMS) in equilibrium binding assays (Chapter 2 and 3) and that they lack of an allosteric pharmacophore as a substituent, we expected that these ligands bound predominantly orthosterically, and that the pharmacology of these ligands would be very similar, regardless of the terminal ‘allosteric’ substituent. However, we found that substitution of the terminal ‘allosteric’ substituent could significantly modify the efficacy and selectivity of these ligands (Figure 4). The M<sub>2</sub>/M<sub>4</sub> mAChR selectivity of some the hybrid ligands is well explained by the model proposed by Bermudez *et al.*, in which the linker moiety sterically disrupts/ obstructs the allosteric vestibule resulting in attenuation in coupling to G<sub>q</sub> versus G<sub>i</sub> G proteins, and hence resulting in M<sub>2</sub>/M<sub>4</sub> mAChR selectivity.<sup>20</sup> However this model could not explain why some hybrid ligands also display an ‘optimal’ linker length (at which efficacy is highest) similar to putative bitopic hybrid ligands,<sup>15, 18, 22-23</sup> despite lacking an allosteric pharmacophore with which to make a bitopic receptor-ligand interaction. Furthermore, this model suggests that significant differences between the efficacy at the M<sub>2</sub> and M<sub>4</sub> mAChRs should not be possible, however in several of our hybrid ligands a significant difference in efficacy (i.e. selectivity) between the two G<sub>i</sub> coupled (M<sub>2</sub> and M<sub>4</sub>) mAChRs was observed (Figure 4).



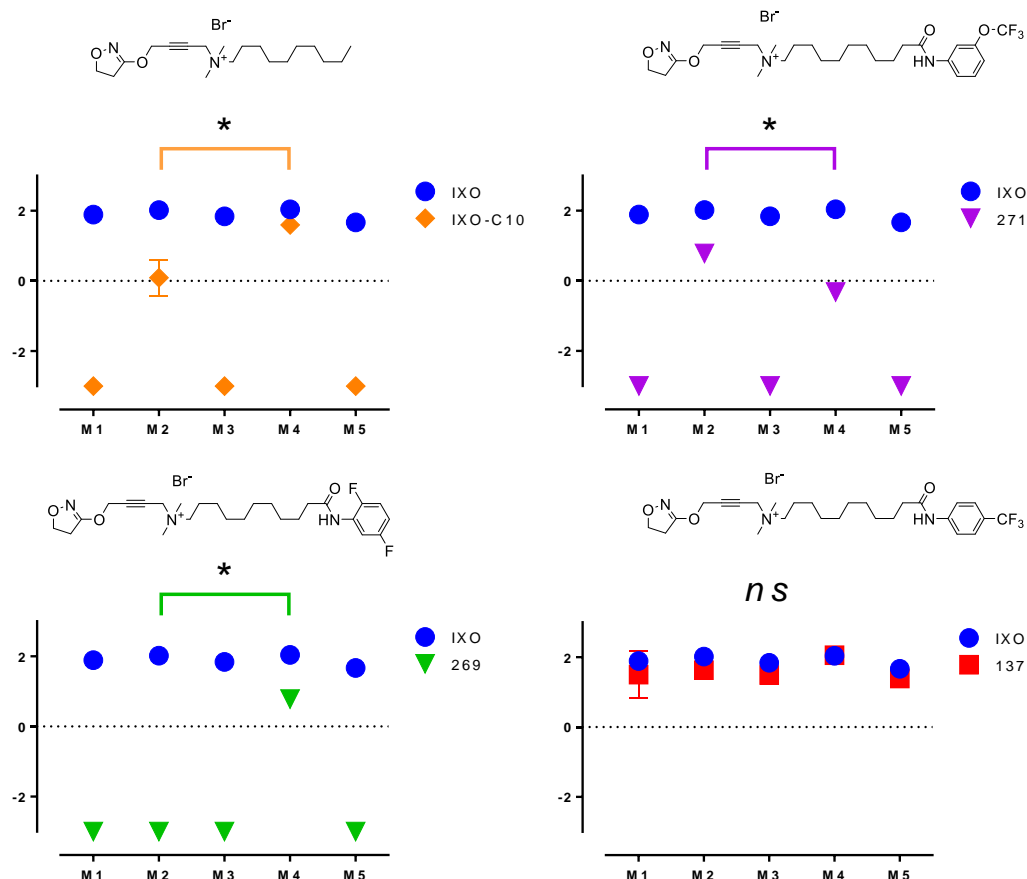


**Figure 4.** Plots of efficacy versus mAChR subtype for ligands evaluated in chapters 2 and 3 that could not be explained by currently proposed models of mAChR hybrid ligand binding. (A) Shows ligands with significant efficacy selectivity for the M<sub>4</sub> mAChR, (B) shows the ligand with significant selectivity for the M<sub>2</sub> mAChR, and (C) shows a higher efficacy, non-selective ligand sharing structural similarities to other selective hybrid ligands. Log  $\tau_c$  is the ligand efficacy, corrected for receptor expression (determined by radioligand binding assays), as determined by fitting the functional ERK 1/2 phosphorylation concentration-response data for each ligand to an operational model of agonism and constraining the model by the measured values of affinity for each ligand at each of the M<sub>1</sub>-M<sub>5</sub> mAChR subtypes. Data was statistically analysed using Bonferroni's multiple comparison test, 2-way ANOVA (*ns* = not significant, \* *p* < 0.05). Each data point represents the mean  $\pm$  S.E. of 3 independent experiments performed in duplicate.

The model proposed by Bermudez *et al.*<sup>20</sup> also does not account for why some hybrid ligands displayed comparatively higher efficacy across the M<sub>1</sub>-M<sub>5</sub> mAChR subtypes and no M<sub>2</sub>/M<sub>4</sub> mAChR selectivity, despite sharing many common structural features with hybrid

ligands that did (Figure 4, C). To better understand the molecular mechanism that determines the efficacy and selectivity in our hybrid ligands, we chose several representative ligands from our SAR studies in chapter 2 and 3 (Figure 5).

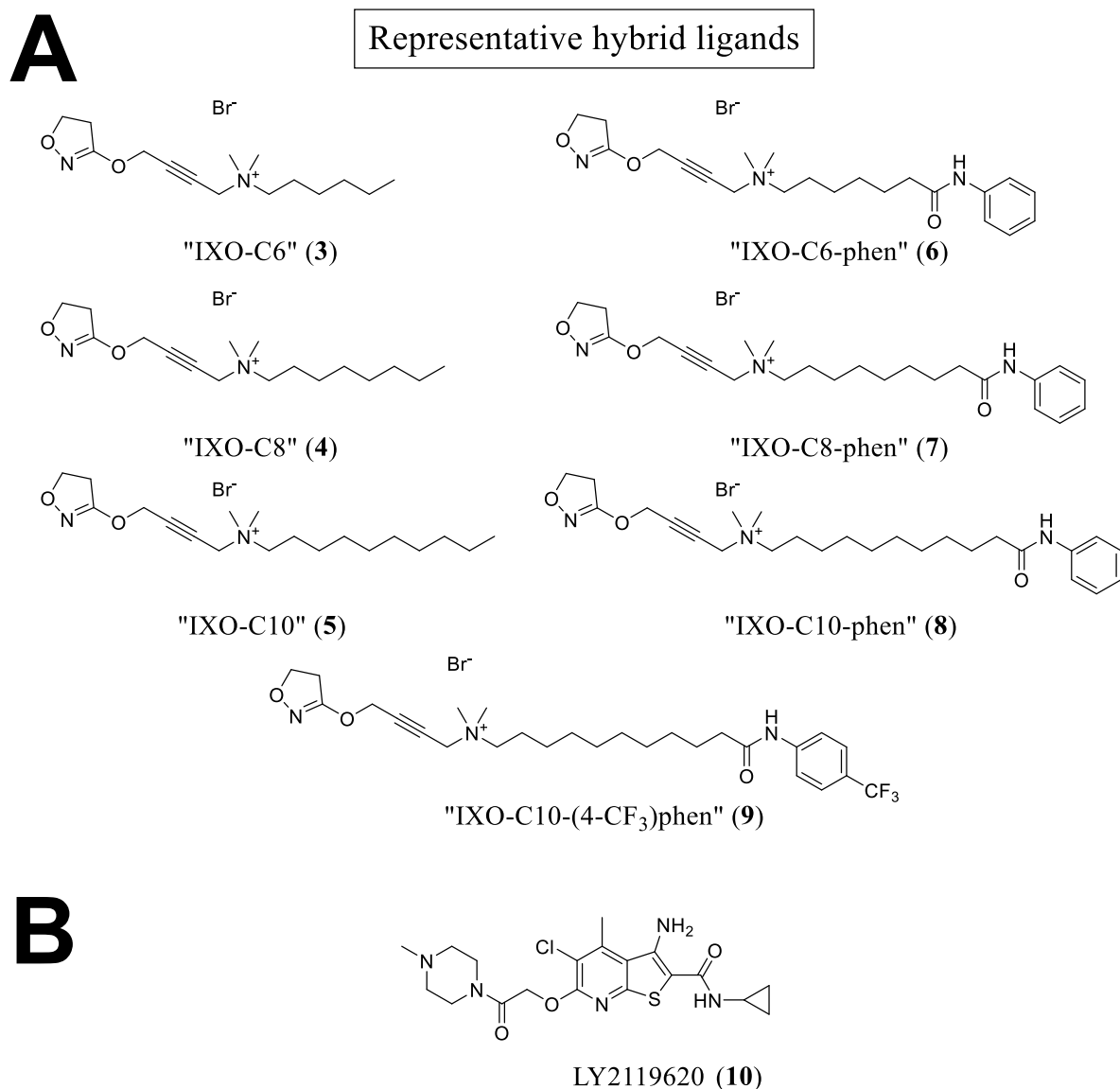


**Figure 5.** Chemical structures of (A) the representative hybrid ligands chosen for mechanistic evaluation from chapters 2 and 3 and (B) the M<sub>2</sub>/M<sub>4</sub> selective PAM, LY2119620 (10).

The goal was to select a subset of our hybrid ligands which would best represent our entire series of hybrid ligands, in terms of chemical structure, efficacy and selectivity. IXO-C6 (3), IXO-C8 (4) and IXO-C10 (5) were chosen because these ligands demonstrated a simple relationship between linker length and efficacy/ selectivity, with their efficacy decreasing and selectivity increasing as linker length increased. IXO-C6 (3) showed good efficacy relative to iperoxo (2) and no selectivity, while IXO-C10 (5) showed excellent selectivity and significantly lower efficacy across the mAChR subtypes compared to iperoxo (2) with IXO-C8 (4) being intermediate to the other two. Structurally these IXO-Cn ligands also represented the simplest cases of iperoxo-based hybrid ligands and in that sense, could act as a control for other linker lengths of hybrid ligands in our subset. IXO-C6-phen (6), IXO-C8-phen (7) and IXO-C10-phen (8) were chosen because they displayed an optimal linker length at IXO-C8-phen (7) at which selectivity was lowest and efficacy across the mAChR subtypes was highest, similar to ours and others' hybrid ligands, and it was hoped that analysis of these compounds would allow us to understand why this optimal linker length phenomenon occurs. IXO-C10-(4-CF<sub>3</sub>)phen (9) was chosen because although it is almost identical to IXO-C10-phen (8) in terms of its structure, its efficacy and selectivity are essentially diametrically opposed (Figure 4), and we believed that comparison of IXO-C10-phen (8) and IXO-C10(4-CF<sub>3</sub>)phen (9) would yield the greatest insight into the differences between their mechanism of action. We then evaluated the representative hybrid ligands in binding, functional and interaction assays with the well-characterized positive allosteric modulator (PAM) LY2119620 (10) (Figure 5) at wild-type (wt) M<sub>2</sub> and M<sub>4</sub> mAChRs to determine whether these ligands invariably obstructed the allosteric site, as suggested by the Bermudez *et al.* model. Then, we investigated the effects of a specific mutation of a residue located in the ECL2 of the receptors (M<sub>2</sub> mAChR - Y177A<sup>ECL2</sup>, M<sub>4</sub> mAChR - F186A<sup>ECL2</sup>) of the M<sub>2</sub> and M<sub>4</sub> mAChRs, that are essential for allosteric ligand

binding, to confirm a lack of allosteric mode of action of these ligands, as in models proposed by Bock *et al.*, for structurally related hybrid ligands to our own.<sup>21, 24</sup> We then performed molecular docking of the hybrid ligands which suggested that the conserved orthosteric tyrosine Y<sup>7.39</sup>, located at the interface between the orthosteric and the allosteric sites, was highly perturbed in the binding modes of all hybrid ligands at both the M<sub>2</sub> and M<sub>4</sub> mAChRs. Previously, crystallographic data has shown the importance of this residue to mAChR agonist binding and function, including the importance of the 4-hydroxyl group of Y<sup>7.39</sup> which in the iperoxo (**2**)-bound crystal structure of the M<sub>2</sub> mAChR forms hydrogen bonds with two other conserved orthosteric tyrosine Y<sup>3.34</sup> and Y<sup>6.51</sup>.<sup>25</sup> Consequently, we decided to explore further the role of Y<sup>7.39</sup> by studying a specific mutant (Y429<sup>7.39</sup>F) , lacking the key 4-hydroxyl group, at the M<sub>2</sub> mAChR, the receptor for which we have the largest amount of structural data, in binding, functional and interaction binding studies to assess its effect on the hybrid ligands. Finally, combining molecular pharmacology, mutagenesis and molecular docking data, we propose a binding model that is consistent with all of the collected data, here and in chapters 2 and 3, and which explains the apparent inverse correlation between mAChR hybrid ligand efficacy and M<sub>2</sub>/ M<sub>4</sub> mAChR selectivity, and gives a plausible explanation for why some of these ligands display significantly greater M<sub>2</sub> or greater M<sub>4</sub> mAChR selectivity at the level of efficacy.

## ■ RESULTS AND DISCUSSION

**Interaction binding study of hybrid ligands with LY2119620 (**10**).** To assess whether the hybrid ligands obstructed the allosteric site, similar to previously reported agonist-based mAChR hybrid ligands,<sup>20</sup> we performed [<sup>3</sup>H]NMS competition binding interaction assays on our set of representative hybrid ligands (Figure 5). We chose the M<sub>2</sub>/M<sub>4</sub> mAChR selective

positive allosteric modulator (PAM) LY2119620 (**10**) (Figure 5) because crystallographic data has previously revealed precisely its binding mode in complex with the agonist iperoxo (**2**) and the active state M<sub>2</sub> mAChR.<sup>25</sup> As such, comparison of the LY2119620 (**10**) interaction binding data for the iperoxo-based hybrid ligands, to the published M<sub>2</sub> mAChR LY2119620 (**10**)/ iperoxo (**2**)-bound structural data<sup>25</sup> allowed us to rule out an allosteric obstruction as the mechanism for several ligands (Figure 6).

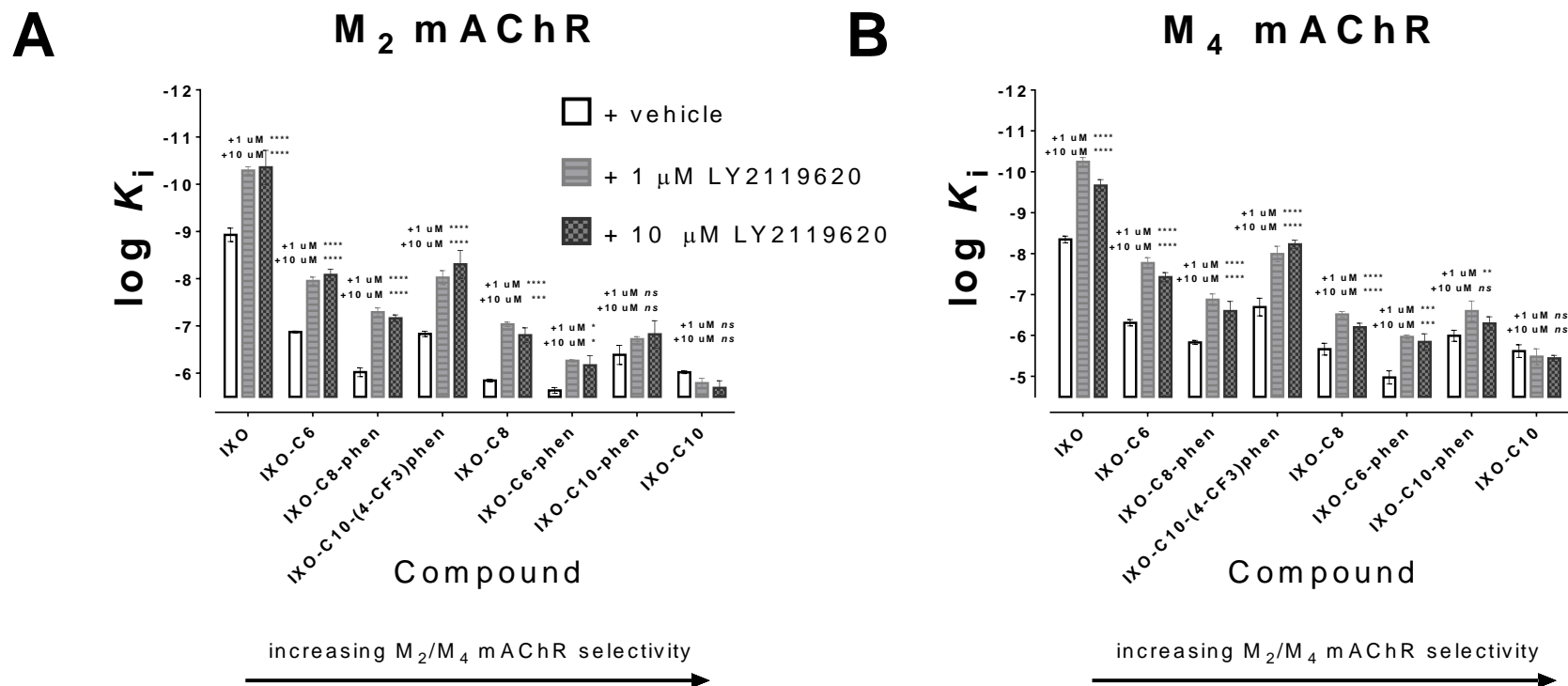


**Figure 6.** Radioligand interaction binding assays measuring the change in affinity of ligands the representative hybrid ligands in the absence or presence of 1 or 10  $\mu$ M of LY2119620 (**10**) at the (A) M<sub>2</sub> and (B) M<sub>4</sub> mAChRs. Binding was measured in whole-cell assays on Flp-In-CHO cells expressing the appropriate M<sub>1</sub>-M<sub>5</sub> mAChR subtype, by competing each ligand with a  $K_d$  concentration of [<sup>3</sup>H]NMS, as determined by saturation binding assays, in the presence of 1  $\mu$ M or 10  $\mu$ M of the M<sub>2</sub>/ M<sub>4</sub> mAChRs selective PAM, LY2119620 (**10**). Data was statistically analysed using Bonferroni's multiple comparison test, 2-way ANOVA (*ns* = not significant \*  $p < 0.05$ , \*\*  $p \leq 0.01$ , \*\*\*  $p \leq 0.001$ , \*\*\*\*  $p \leq 0.0001$ ). Each data point represents the mean  $\pm$  S.E. of 3 independent experiments, performed in duplicate.

The most M<sub>2</sub>/M<sub>4</sub> mAChR selective ligand, IXO-C10 (**5**) was not significantly potentiated by LY2119620 (**10**) at either of the M<sub>2</sub> and M<sub>4</sub> mAChRs showing no statistically significant change in affinity with even saturating concentrations of LY2119620 (**10**) (Figure 6), suggesting that the linker sterically interferes with the binding of LY2119620 (**10**) to the allosteric site, or interferes with allosteric-orthosteric cooperativity. In contrast, the non-selective hybrid ligands, IXO-C6 (**3**), IXO-C8-phen (**7**) and IXO-C10-(4-CF<sub>3</sub>)phen (**9**) were significantly potentiated in the presence of 1 and 10  $\mu$ M LY2119620 (**10**) (Figure 6), demonstrating that they do not occupy the allosteric site of the M<sub>2</sub> and M<sub>4</sub> mAChRs under equilibrium conditions. This data provides a preliminary explanation for the lack of selectivity of these ligands as they do not obstruct the allosteric site and hence possess no G<sub>i</sub> bias (and hence no M<sub>2</sub>/M<sub>4</sub> mAChR selectivity) as in the model by Bermudez *et al.*<sup>20</sup> Interestingly, the ligands with intermediate selectivity, IXO-C6-phen (**6**) and IXO-C10-phen (**8**) also displayed less significant potentiation of affinity by LY2119620 (**10**). This result could be interpreted in two ways as, either the hybrid ligands have attenuated cooperativity with LY2119620 (**10**) or they bind to the M<sub>2</sub> and M<sub>4</sub> mAChRs in different proportions of binding conformations, one which obstructs LY2119620 (**10**) binding and one which does not. To further investigate the apparent relationship between selectivity and potentiation by LY2119620 (**10**) we plotted the ratio of efficacy values (i.e. selectivity) relative to the M<sub>2</sub> or M<sub>4</sub> mAChRs for each of the hybrid ligands against the change in affinity in the presence of 1 or 10  $\mu$ M LY2119620 (**10**) at the respective M<sub>2</sub> or M<sub>4</sub> mAChRs (Figure 7).

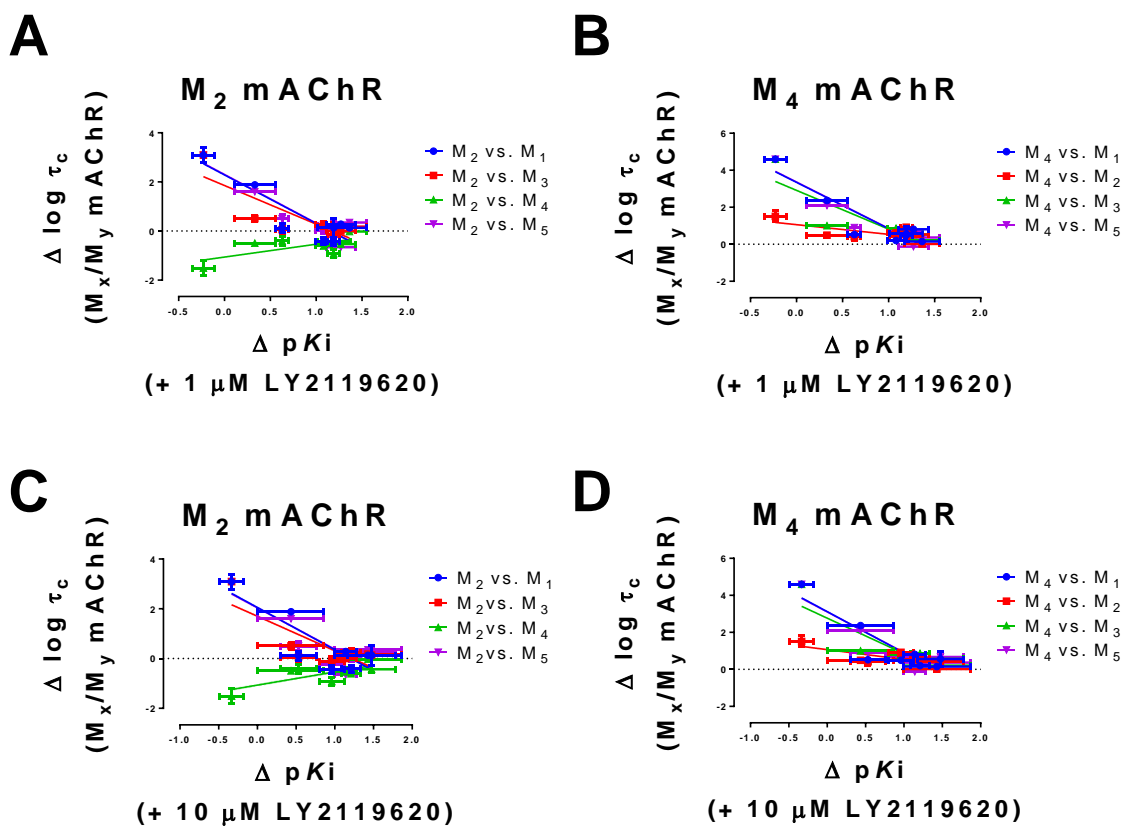


**Figure 7.** (A-D) Selectivity of the hybrid ligands versus change in affinity in the presence of (A-B) 1  $\mu\text{M}$  or (C-D) 10  $\mu\text{M}$  LY2119620 (**10**) at the (A, C)  $M_2$  and (B, D)  $M_4$  mAChRs. Selectivity ( $\Delta \log \tau_c$ ) is quantitated as the logarithm of the ratio of the efficacy at the mAChR subtype in question divided by the efficacy at either the  $M_2$  or the  $M_4$  mAChRs, respectively. Change in affinity in the presence of LY2119620 (**10**) ( $\Delta pK_i$ ) is quantitated as the difference between the negative logarithms of the measured inhibition constants for each ligand in the presence of 1 or 10  $\mu\text{M}$  LY2119620 (**10**) versus in the absence of LY2119620 (**10**). Linear slopes and intercepts were calculated using least squares regression to find a line of best fit in the GraphPad 7 software. Each value in the  $x$  and  $y$  direction represents the mean  $\pm$  S.E. of at least 3 independent experiments performed in duplicate.



**Table 1.** Linear regression analysis of hybrid ligand selectivity versus potentiation by LY2119620 (**10**) at the M<sub>2</sub> and M<sub>4</sub> mAChRs

mAChR <sup>a</sup>	wt M <sub>2</sub> mAChR				wt M <sub>4</sub> mAChR			
versus mAChR <sup>b</sup>	M <sub>1</sub>	M <sub>3</sub>	M <sub>4</sub>	M <sub>5</sub>	M <sub>1</sub>	M <sub>2</sub>	M <sub>3</sub>	M <sub>5</sub>
LY2119620 <sup>c</sup>	+ 1 $\mu$ M	+ 1 $\mu$ M	+ 1 $\mu$ M	+ 1 $\mu$ M	+ 1 $\mu$ M	+ 1 $\mu$ M	+ 1 $\mu$ M	+ 1 $\mu$ M
Equation <sup>d</sup> Y =	-1.98x + 2.29	-1.57x + 1.85	0.52x - 1.06	-1.98x + 2.31	-2.50x + 3.35	-0.52x + 1.06	-2.09x + 2.91	-2.50x + 3.37
R <sup>2</sup> value <sup>e</sup>	0.81	0.70	0.45	0.87	0.83	0.45	0.68	0.88
P value <sup>f</sup>	0.0024	0.010	0.070	0.00080	0.0016	0.070	0.012	0.00060
mAChR <sup>a</sup>	wt M <sub>2</sub> mAChR				wt M <sub>4</sub> mAChR			
versus mAChR <sup>b</sup>	M <sub>1</sub>	M <sub>3</sub>	M <sub>4</sub>	M <sub>5</sub>	M <sub>1</sub>	M <sub>2</sub>	M <sub>3</sub>	M <sub>5</sub>
LY2119620 <sup>c</sup>	+ 10 $\mu$ M	+ 10 $\mu$ M	+ 10 $\mu$ M	+ 10 $\mu$ M	+ 10 $\mu$ M	+ 10 $\mu$ M	+ 10 $\mu$ M	+ 10 $\mu$ M
Equation <sup>d</sup> Y =	-1.70x + 2.05	-1.39x + 1.70	0.53x - 1.07	-1.66x + 2.04	-2.23x + 3.12	-0.53x + 1.07	-1.92x + 2.77	-2.20x + 3.11
R <sup>2</sup> value <sup>e</sup>	0.71	0.64	0.55	0.73	0.79	0.55	0.68	0.80
P value <sup>f</sup>	0.0087	0.017	0.037	0.0073	0.0033	0.037	0.012	0.0027

<sup>a</sup>Muscarinic acetylcholine receptor subtype in question at which interaction assays with LY2119620 (**10**) were performed. <sup>b</sup>Muscarinic acetylcholine receptor which is being compared in terms of difference in efficacy (i.e. selectivity). <sup>c</sup>Concentration of the allosteric potentiator LY2119620 (**10**) used in the experimental protocol. <sup>d</sup>Equation of line of best fit in terms of 'Y', the efficacy (log  $\tau_c$ ) of the hybrid ligand in question, and 'x' the change in affinity ( $\Delta pK_i$ ) of that hybrid ligand in the presence of the specified concentration of LY2119620 (**10**). <sup>e</sup>R<sup>2</sup> is the square of the coefficient of determination which is the ratio of variation in 'Y' which is explained by variation in 'x', divided by the total variation. <sup>f</sup>P value is the probability of the null hypothesis, which is that the coefficient of the slopes is equal to zero. Slopes and associated values were determined by least-squares linear regression using the GraphPad 7 software. Each data point represents the mean  $\pm$  S.E. of 3 independent experiments performed in duplicate, for both the x and y dimensions.

Plotting the ratio of efficacies (i.e. selectivity) versus change in affinity (i.e. potentiation) in the presence of LY2119620 (**10**) at the M<sub>2</sub> and M<sub>4</sub> mAChRs reveals correlations between the two properties at both subtypes (Figure 7). This correlation is significant when comparing any of the mAChR subtypes, except for between the M<sub>2</sub> versus the M<sub>4</sub> mAChRs at 1  $\mu$ M LY2119620 (**10**), although the correlation is near-significant at this concentration ( $p = 0.07$ ) (Table 1). At the higher concentration of 10  $\mu$ M LY2119620 (**10**) the correlation between potentiation and selectivity is significant ( $p = 0.0027$ ) (Table 1) between the M<sub>2</sub> versus the M<sub>4</sub> mAChRs, potentially suggesting differences in hybrid ligand binding conformation or cooperativity between these two subtypes. It should be noted that although the correlation between selectivity and potentiation was statistically significant at 10  $\mu$ M LY2119620 (**10**) between the M<sub>2</sub> and M<sub>4</sub> mAChRs the coefficient of determination ( $R^2$  value) was lower than when comparing the M<sub>2</sub> and M<sub>4</sub> mAChR to the other M<sub>1</sub>, M<sub>3</sub> and M<sub>5</sub> mAChRs (Table 1), suggesting that there may be other contributing factors which influence the relationship. The significant difference in potentiation by LY2119620 (**10**) at 10  $\mu$ M between the M<sub>2</sub> and M<sub>4</sub> mAChRs, assuming it does not arise from attenuated cooperativity, implies a difference in proportions of different populations of binding conformations for some of these hybrid ligands between these two subtypes, under assay conditions. In that specific case, this difference in the proportions of conformations may in turn explain the differences in efficacy observed between the M<sub>2</sub> and M<sub>4</sub> mAChRs for IXO-C10 (**5**) and other the hybrid ligands which distinguish between the M<sub>2</sub> and M<sub>4</sub> mAChRs (Figure 4). As previously noted, the properties of efficacy and selectivity of the hybrid ligands show a correlation when plotted against one another (Figure 3). Having shown that potentiation by LY2119620 (**10**) correlates with selectivity (Figure

7, Table 1) we wanted to know whether efficacy also correlated with potentiation by LY2119620 (10), such as to show the interdependence of all three properties, efficacy, selectivity and potentiation by LY2119620 (10). To investigate this we plotted the efficacy versus potentiation by LY2119620 (10) at the M<sub>2</sub> and M<sub>4</sub> mAChRs, respectively and again analysed the data by linear regression (Figure 8, Table 2).

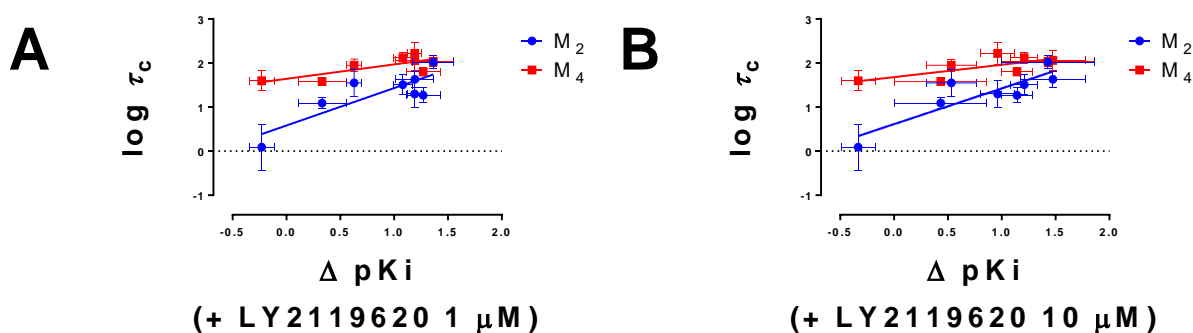


**Figure 8.** Efficacy of the hybrid ligands (log  $\tau_c$ ) versus change in affinity ( $\Delta pK_i$ ) in the presence of (A) 1  $\mu$ M or (B) 10  $\mu$ M LY2119620 (10) at the M<sub>2</sub> and M<sub>4</sub> mAChRs. Change in affinity in the presence of LY2119620 (10) ( $\Delta pK_i$ ) is quantitated as the difference between the negative logarithms of the measured inhibition constants for each ligand in the presence of 1 or 10  $\mu$ M LY2119620 (10) versus in the absence of LY2119620 (10). Linear slopes and intercepts were calculated using least squares regression to find a line of best fit. Each value in the  $x$  and  $y$  direction represents the mean  $\pm$  S.E. of at least 3 independent experiments performed in duplicate.

**Table 2.** Linear regression analysis of hybrid ligand efficacy versus change in affinity in the presence of LY2119620 (**10**) at the M<sub>2</sub> and M<sub>4</sub> mAChRs

mAChR <sup>a</sup>	wt M <sub>2</sub> mAChR		wt M <sub>4</sub> mAChR	
	+ 1 $\mu$ M	+ 10 $\mu$ M	+ 1 $\mu$ M	+ 10 $\mu$ M
LY2119620 <sup>b</sup>				
Equation <sup>c</sup>	Y = 0.85x + 0.58	Y = 0.81x + 0.61	Y = 0.33x + 1.64	Y = 0.2809x + 1.68
R <sup>2</sup> value <sup>d</sup>	0.71	0.77	0.60	0.52
P value <sup>e</sup>	0.0085	0.0042	0.025	0.043

<sup>a</sup>Muscarinic acetylcholine receptor subtype in question. <sup>b</sup>Concentration of the allosteric potentiator LY2119620 (**10**) used in the experimental protocol. <sup>c</sup>Equation of line of best fit in terms of ‘Y’, the efficacy (log  $\tau_c$ ) of the hybrid ligand in question, and ‘x’ the change in affinity ( $\Delta$  pK<sub>i</sub>) of that hybrid ligand in the presence of the specified concentration of LY2119620 (**10**). <sup>d</sup>R<sup>2</sup> is the square of the coefficient of determination which is the ratio of variation in ‘Y’ which is explained by variation in ‘x’, divided by the total variation. <sup>e</sup>P value is the probability of the null hypothesis, which is that the coefficient of the slope is equal to zero. Slopes and associated values were determined by least-squares linear regression using the GraphPad 7 software. Each data point represents the mean  $\pm$  S.E. of 3 independent experiments performed in duplicate, for both the x and y dimensions.

Our analysis showed that there was indeed a significant correlation between efficacy at the M<sub>2</sub> ( $p < 0.01$ ) and M<sub>4</sub> ( $p < 0.05$ ) mAChRs and potentiation by LY2119620 (**10**) at both 1 and 10  $\mu$ M (Table 2). The coefficient of determination (R<sup>2</sup> value) at the M<sub>2</sub> mAChR is higher than at the M<sub>4</sub> mAChR suggesting that potentiation by LY2119620 (**10**) explains differences in efficacy better at the M<sub>2</sub> mAChR than at the M<sub>4</sub> mAChR for the hybrid ligands. Again, assuming that the differences in potentiation by LY2119620 (**10**) imply differences in binding conformation of the hybrid ligands then this suggests that the differences in coefficient of determination (R<sup>2</sup> value) between the M<sub>2</sub> and M<sub>4</sub> mAChRs (Table 2) may suggest that binding conformation plays a more significant role in determining efficacy at the M<sub>2</sub> than at the M<sub>4</sub> mAChR. This in turn may elude to why some of the hybrid ligands display selectivity between these two mAChR subtypes (Figure 4).

**Evaluation of hybrid ligands at allosterically impaired mutant mAChRs.** As previously mentioned, several models of bitopic mAChR ligand binding indicate that these ligands may adopt a secondary, purely allosteric, binding mode.<sup>16-17, 21, 26</sup> To evaluate the potential for “pure” allosteric binding modes of the hybrid ligands we evaluated these ligands by concentration-response curves in pERK 1/2 assays and competition radioligand binding with [<sup>3</sup>H]NMS at the mutant Y177A<sup>ECL2</sup> M<sub>2</sub> mAChR and F186A<sup>ECL2</sup> M<sub>4</sub> mAChR. These mutants were chosen because the Y177<sup>ECL2</sup> residue in the M<sub>2</sub> mAChR and the homologous F186<sup>ECL2</sup> residue in the M<sub>4</sub> mAChR are central to the mAChR allosteric site and integral to the binding of allosteric ligands, such as LY2119620 (**10**), in those subtypes.<sup>25, 27</sup> We first of all wished to ascertain whether our hybrid ligands lost affinity upon impairment of the allosteric site, which would indicate that they engage the receptor in a “pure” allosteric binding mode. Secondly we wished to know whether the efficacy of the selective hybrid ligands increased upon mutation of the allosteric site, which has been previously used as an indication that similar hybrid ligands conformationally restrict the allosteric site, resulting in the M<sub>2</sub>/M<sub>4</sub> mAChR selectivity.<sup>20</sup> In doing so we could confirm our hypothesis that these ligands obstruct the binding of LY2119620 (**10**), rather than interfere with allosteric-orthosteric cooperativity, which would in turn imply that our interaction binding data was indicative of the binding conformation of the hybrid ligands.

**Table 3.** Functional and binding data for the hybrid ligands at the wt M<sub>2</sub>, Y177A<sup>ECL2</sup> M<sub>2</sub>, M<sub>4</sub> (3xHA) and F186A<sup>ECL2</sup> M<sub>4</sub> mAChRs

Cpd	wt M <sub>2</sub> mAChR				Y177A <sup>ECL2</sup> M <sub>2</sub> mAChR			
	pEC <sub>50</sub> <sup>a</sup>	E <sub>max</sub> <sup>b</sup>	pK <sub>i</sub> <sup>c</sup>	Log τ <sub>c</sub> <sup>d</sup>	pEC <sub>50</sub> <sup>a</sup>	E <sub>max</sub> <sup>b</sup>	pK <sub>i</sub> <sup>c</sup>	Log τ <sub>c</sub> <sup>d</sup>
<b>iperoxo</b>	10.23 ± 0.19	100 ± 4	8.70 ± 0.02	2.02 ± 0.15	10.15 ± 0.08	100 ± 2	8.76 ± 0.03	1.70 ± 0.14
<b>IXO-C8</b>	7.23 ± 0.28	62 ± 6	5.93 ± 0.22	1.33 ± 0.20	8.30 ± 0.19	56 ± 4	6.35 ± 0.02	1.79 ± 0.16
<b>IXO-C10</b>	6.36 ± 0.22	38 ± 7	6.33 ± 0.38	0.33 ± 0.15	7.77 ± 0.28	36 ± 4	6.06 ± 0.05	1.56 ± 0.16*
<b>IXO-C10-phen</b>	7.72 ± 0.20	73 ± 5	6.21 ± 0.14	0.99 ± 0.17	8.66 ± 0.36	59 ± 4	6.87 ± 0.04	2.10 ± 0.16*
<b>IXO-C10-(4-CF<sub>3</sub>)phen</b>	8.39 ± 0.17	91 ± 5	6.69 ± 0.03	1.63 ± 0.18	8.52 ± 0.31	49 ± 4*	7.23 ± 0.01	2.03 ± 0.18
	wt M <sub>4</sub> mAChR (3xHA)				F186A <sup>ECL2</sup> M <sub>4</sub> mAChR (3xHA)			
	pEC <sub>50</sub> <sup>a</sup>	E <sub>max</sub> <sup>b</sup>	pK <sub>i</sub> <sup>c</sup>	Log τ <sub>c</sub> <sup>d</sup>	pEC <sub>50</sub> <sup>a</sup>	E <sub>max</sub> <sup>b</sup>	pK <sub>i</sub> <sup>c</sup>	Log τ <sub>c</sub> <sup>d</sup>
<b>iperoxo</b>	10.23 ± 0.13	100 ± 4	8.42 ± 0.32	2.19 ± 0.11	9.74 ± 0.17	100 ± 5	8.34 ± 0.28	2.26 ± 0.13
<b>IXO-C8</b>	6.91 ± 0.29	43 ± 5	6.01 ± 0.08	1.08 ± 0.08	7.30 ± 0.30	37 ± 4	6.02 ± 0.34	1.89 ± 0.12*
<b>IXO-C10</b>	6.77 ± 0.70	6 ± 4	5.83 ± 0.18	0.11 ± 0.24	7.19 ± 0.42	23 ± 4*	5.97 ± 0.20	1.55 ± 0.18*
<b>IXO-C10-phen</b>	7.08 ± 0.47	35 ± 7	6.34 ± 0.28	0.82 ± 0.11	7.48 ± 0.34	34 ± 4	6.33 ± 0.60	1.34 ± 0.13
<b>IXO-C10-(4-CF<sub>3</sub>)phen</b>	7.91 ± 0.38	66 ± 8	7.14 ± 0.15	1.41 ± 0.12	7.91 ± 0.34	43 ± 5*	6.63 ± 0.37	1.66 ± 0.10

<sup>a</sup>pEC<sub>50</sub> values are the negative logarithm of the concentration of a ligand that was able to elicit 50 % the maximum achievable response by that ligand as determined by fitting a 3-parameter concentration-response curve to the ERK 1/2 phosphorylation functional data. <sup>b</sup>E<sub>max</sub> values are the maximum response measured by a ligand, as a percentage of the maximum response achievable by the full agonist, iperoxo (2). <sup>c</sup>pK<sub>i</sub> values are the negative logarithm of the inhibition constant for each ligand, as determined by competition radioligand binding assays with [<sup>3</sup>H]NMS and fitting the data to a one-site inhibition binding model. <sup>d</sup>Log τ<sub>c</sub> is the ligand efficacy, corrected for receptor expression, as determined by fitting the functional data for each ligand to an operational model of agonism and constraining the model by the measured values of affinity for each ligand at each mutant or wt mAChR subtype. Data was statistically analysed using Bonferroni's multiple comparison test, 2-way ANOVA (*ns* = not significant \* *p* < 0.05, \*\* *p* ≤ 0.01, \*\*\* *p* ≤ 0.001, \*\*\*\* *p* ≤ 0.0001). Data represent the mean ± S.E. of 3 independent experiments performed in duplicate.

We found no significant difference in the affinity of iperoxo (**2**) or any of the hybrid ligands at either the Y177A<sup>ECL2</sup> M<sub>2</sub> mAChR versus wt M<sub>2</sub> mAChR or F186A<sup>ECL2</sup> M<sub>4</sub> mAChR (3xHA tagged) versus wt M<sub>4</sub> mAChR (3xHA tagged). This lack of change in affinity for our hybrid ligands in the allosterically impaired mutant M<sub>2</sub> and M<sub>4</sub> mAChRs confirms that a “pure” allosteric binding mode for these ligands is not the cause of their selectivity, nor is it the reason why potentiation by LY2119620 (**10**) is attenuated in the more selective ligands (Table 3). The hybrid ligands displayed no significant difference in potency at the mutant Y177A<sup>ECL2</sup> and F186A<sup>ECL2</sup> mAChRs versus their equivalent wild type receptor (Table 3). However, particularly for the most selective ligand, IXO-C10, these ligands did display higher efficacy at both the Y177A<sup>ECL2</sup> and F186A<sup>ECL2</sup> mutants which is significant or near-significant in all cases (Table 3, Figure 9). This increase in efficacy is explained by the model proposed by Bermudez *et al.*<sup>20</sup> which proposes that the increased space in the allosteric vestibule, upon mutation of the tyrosine (Y177<sup>ECL2</sup> in the M<sub>2</sub> mAChR) or the corresponding phenylalanine (F186<sup>ECL2</sup> in the M<sub>4</sub> mAChR) to the less sterically bulky alanine mutants, limits the conformational restriction of the allosteric site, which is responsible for a G<sub>i</sub>-biased attenuation in efficacy.

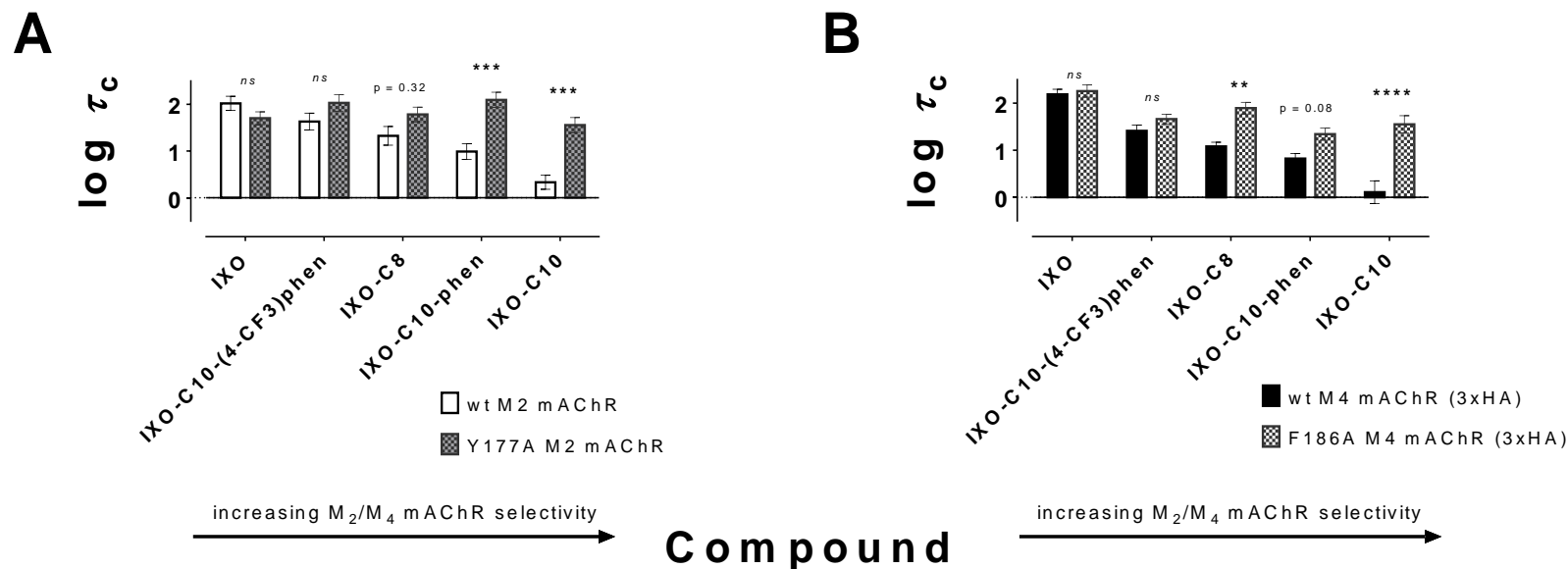


**Figure 9.** Comparison of the change in ligand efficacy upon mutation of core allosteric residue within ECL2 of the mutant M<sub>2</sub> and M<sub>4</sub> mAChRs, (A) Y177A<sup>ECL2</sup> and (B) F186A<sup>ECL2</sup>. Log  $\tau_c$  is the ligand efficacy, corrected for receptor expression, as determined by fitting the functional ERK 1/2 phosphorylation concentration-response data for each ligand to an operational model of agonism and constraining the model by the measured values of affinity for each ligand at each mutant or wt mAChR subtype. Compounds are arranged from left to right, on the x-axis in order of increasing selectivity for the M<sub>2</sub>/M<sub>4</sub> mAChR to illustrate the apparent effect that the Y177A<sup>ECL2</sup> and F186A<sup>ECL2</sup> mutation has on the efficacy hybrid ligands with respect to their M<sub>2</sub>/M<sub>4</sub> mAChR selectivity. Data was statistically analysed using Bonferroni's multiple comparison test, 2-way ANOVA (*ns* = not significant \*  $p < 0.05$ , \*\*  $p \leq 0.01$ , \*\*\*  $p \leq 0.001$ , \*\*\*\*  $p \leq 0.0001$ ). Each data point represents the mean  $\pm$  S.E. of 3 independent experiments, performed in duplicate.



This result confirms our hypothesis that in some binding conformations these hybrid ligands obstruct the allosteric site rather than attenuate cooperativity with LY2119620 (**10**). The hybrid ligands with intermediate selectivity, IXO-C8 (**4**) and IXO-C10-phen (**8**) as in the interaction study, gave apparently intermediary results to least and most M<sub>2</sub>/M<sub>4</sub> mAChR selective ligands, iperoxo (**2**) and IXO-C10 (**5**), respectively, particularly at the M<sub>4</sub> mAChR. Specifically, IXO-C8 (**4**) and IXO-C10-phen (**8**) showed a significant or near-significant increase in efficacy at the allosteric mutants, Y177A<sup>ECL2</sup> F186A<sup>ECL2</sup>, when compared to their wild-type equivalent M<sub>2</sub> mAChR and M<sub>4</sub> mAChRs, respectively (Figure 9). These observations are consistent with the interaction binding data at the M<sub>2</sub> and M<sub>4</sub> mAChRs and further suggest that these ligands may be able to adopt different proportions of two conformations.

**Docking study of hybrid ligands at the M<sub>2</sub> and M<sub>4</sub> mAChRs.** To examine the binding modes of the hybrid ligands in more detail, we employed molecular docking of the aforementioned hybrid ligands at the active (PDB=4MQS), active (PDB=4MQT) and inactive (PDB=3UON) M<sub>2</sub> mAChR and inactive (PDB=5DSG) M<sub>4</sub> mAChR crystal structures and excluding poses based on our experimental findings.<sup>25, 27-28</sup> The criteria for an acceptable pose was defined as follows; the orthosteric pharmacophore adopted a comparable pose to crystallographic pose of iperoxo (**2**) at the M<sub>2</sub> mAChR (PDB=4MQS/4MQT); for the non-selective hybrid ligands, IXO-C6 (**3**), IXO-C8-phen (**7**) and IXO-C10-(4-CF<sub>3</sub>)phen (**9**), poses that overlapped with the crystallographic LY2119620 (**10**) pose were excluded based on our interaction binding data (Figure 6); and for the M<sub>2</sub>/M<sub>4</sub> mAChR selective ligand, IXO-C10 (**5**), poses engaging Y177<sup>ECL2</sup> (M<sub>2</sub> mAChR) or F186<sup>ECL2</sup> (M<sub>4</sub> mAChR) directly were excluded based on mutagenesis data (Table 3, Figure 9) and

poses not overlapping the LY2119620 (**10**) binding site were excluded based on interaction data (Figure 6).

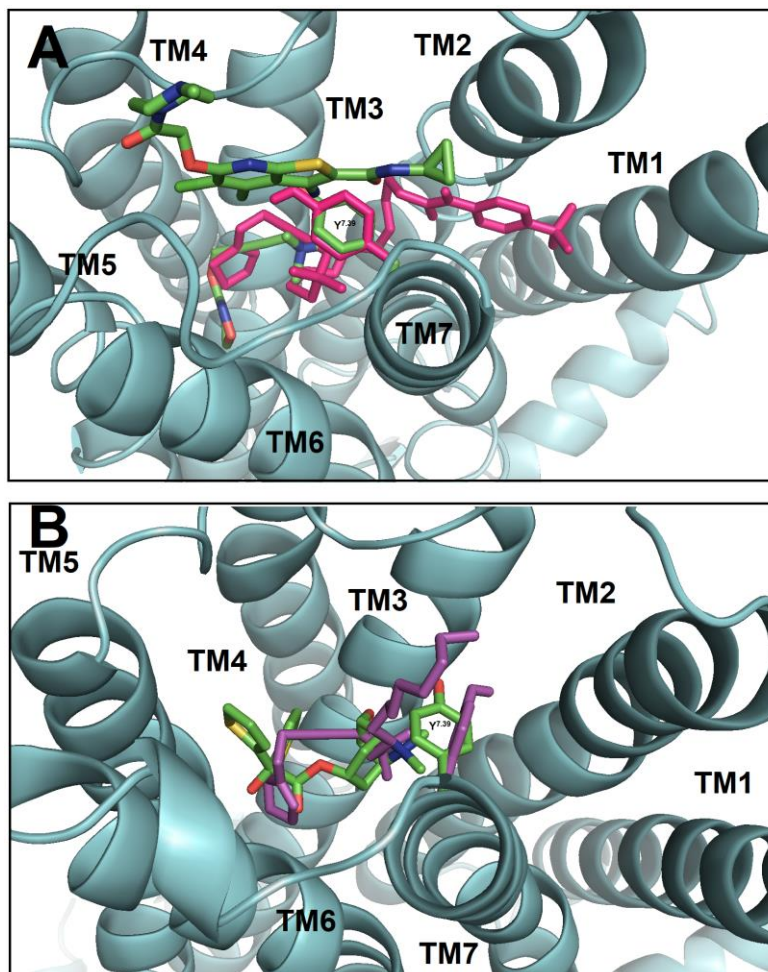


**Figure 10.** Docked poses for highest efficacy, IXO-C10-(4-CF<sub>3</sub>)phen (**9**), and most selective, IXO-C10 (**5**), hybrid ligands, showing a significant difference in the pose of the orthosteric residue, Y<sup>7.39</sup>. (A) shows an example pose of IXO-C10-(4-CF<sub>3</sub>)phen (**9**) and Y426<sup>7.39</sup> in pink, docked into the LY2119620 (**10**) / iperoxo (**2**) bound, active state M<sub>2</sub> mACHR (PDB=4MQT). The crystallographic data for residue Y426<sup>7.39</sup> and ligands LY2119620 (**10**) and iperoxo (**2**) is shown with carbon as green, oxygen as red, nitrogen as blue, sulfur as yellow and chlorine as light green. (B) Shows an example pose of IXO-C10 (**5**) and Y439<sup>7.39</sup> in purple, docked into the tiotropium-bound, inactive state M<sub>4</sub> mACHR (PDB=5DSG). The crystallographic data for residue Y439<sup>7.39</sup> and ligand tiotropium is shown with carbon as green, oxygen as red, nitrogen as blue and sulfur as yellow. Both receptors are viewed from the extracellular space, down towards the orthosteric site, and the transmembrane helices are labelled 'TM1-7' for orientation.

The most significant difference between the poses for the hybrid ligands, besides those specified in the criteria, was the deviation of orthosteric residue Y426<sup>7,39</sup> (M<sub>2</sub> mAChR) or the homologous Y439<sup>7,39</sup> (M<sub>4</sub> mAChR) in the poses for IXO-C10 (**5**) from its crystallographic orientation (Figure 10).<sup>25, 27-28</sup> The 4-hydroxyl group within Y426<sup>7,39</sup> forms hydrogen bonding interactions with other orthosteric residues (Y104<sup>3,33</sup> and Y403<sup>6,51</sup>) (via their 4-hydroxyl groups) upon receptor activation, and the importance of this interaction for mAChR agonism has been demonstrated crystallographically.<sup>25</sup> Y426<sup>7,39</sup> forms part of the ‘tyrosine lid’ that occludes the orthosteric binding site from the extracellular domain in the mAChRs. This residue is essential to M<sub>2</sub> mAChR agonist binding and function, and the Y426A<sup>7,39</sup> mutant loses agonist binding and response.<sup>29</sup> However the Y426F<sup>7,39</sup> mutant M<sub>2</sub> mAChR exhibits some, albeit weaker, response to agonists, demonstrating the importance of the 4-hydroxyl group in stabilizing an active receptor state in the mAChRs.<sup>25</sup>

**Evaluation of truncated and substituted truncated hybrid ligands at an orthosterically impaired mutant receptor.** To examine the role of Y426<sup>7,39</sup> in more detail we subjected IXO-C8 (**4**), IXO-C10 (**5**), IXO-C10-phen (**8**) and IXO-C10-(4-CF<sub>3</sub>)phen (**9**) to evaluation by concentration-response curve pERK 1/2 assay and competition radioligand binding with [<sup>3</sup>H]NMS at the mutant Y426F<sup>7,39</sup> M<sub>2</sub> mAChR, to evaluate whether this residue was important to the binding and function of our hybrid ligands, as it is for prototypical orthosteric agonists. We also evaluated each ligand in the presence of 10  $\mu$ M LY2119620 (**10**), as we had previously done for the wild-type M<sub>2</sub> mAChR, to ascertain whether the hybrid ligands adopted a comparable binding mode in the Y426F<sup>7,39</sup> and wild-type M<sub>2</sub> mAChR.

**Table 4.** Functional, binding and interaction-binding data for ligands hybrid ligands at the Y426F<sup>7,39</sup> mutant M<sub>2</sub> mAChR

Cpd	Y426F <sup>7,39</sup> M <sub>2</sub> mAChR				+ LY2119620 (10 $\mu$ M)
	pEC <sub>50</sub> <sup>a</sup>	E <sub>max</sub> <sup>b</sup>	pK <sub>i</sub> <sup>c</sup>	Log $\tau_c$ <sup>d</sup>	$\Delta$ pK <sub>i</sub> <sup>e</sup>
ACh	5.13 $\pm$ 0.10*	108 $\pm$ 3	4.19 $\pm$ 0.24*	0.79 $\pm$ 0.07*	3.14 $\pm$ 0.32*†
iperoxo	7.82 $\pm$ 0.10*	100 $\pm$ 3	7.31 $\pm$ 0.21*	0.67 $\pm$ 0.08*	2.73 $\pm$ 0.36*†
IXO-C8	6.06 $\pm$ 0.17*	72 $\pm$ 2	6.20 $\pm$ 0.09	0.11 $\pm$ 0.05*	0.77 $\pm$ 0.14
IXO-C10	5.97 $\pm$ 0.14	86 $\pm$ 3	6.46 $\pm$ 0.05	0.17 $\pm$ 0.06	-0.34 $\pm$ 0.07
IXO-C10-phen	7.30 $\pm$ 0.21	57 $\pm$ 3	6.75 $\pm$ 0.12	0.53 $\pm$ 0.06	-0.14 $\pm$ 0.21
IXO-C10-(4-CF <sub>3</sub> )phen	7.35 $\pm$ 0.18*	65 $\pm$ 4	7.08 $\pm$ 0.15	0.07 $\pm$ 0.05*	1.85 $\pm$ 0.15†

<sup>a</sup>pEC<sub>50</sub> values are the negative logarithm of the concentration of a ligand that was able to elicit 50 % the maximum achievable response by that ligand as determined by fitting a 3-parameter concentration-response curve to the data. <sup>b</sup>E<sub>max</sub> values are the maximum response measured by a ligand, as a percentage of the maximum response achievable by the full agonist, iperoxo (**2**). <sup>c</sup>pK<sub>i</sub> values are the negative logarithm of the inhibition constant for each ligand, as determined by competition radioligand binding assays with [<sup>3</sup>H]NMS and fitting the data to a one-site inhibition binding model. <sup>d</sup>Log  $\tau_c$  is the ligand efficacy, corrected for receptor expression, as determined by fitting the functional ERK 1/2 phosphorylation concentration-response data for each ligand to an operational model of agonism and constraining the model by the measured values of affinity for each ligand at each mutant or wt mAChR subtype. <sup>e</sup> $\Delta$  pK<sub>i</sub> values represent the change in affinity in the presence of 10  $\mu$ M LY2119620 (**10**) versus vehicle control. \* indicates that the value is significantly different from the wt M<sub>2</sub> mAChR, and † indicates that the value is significantly different from the vehicle control. Data was statistically analysed using Bonferroni's multiple comparison test, 2-way ANOVA (both \* and † indicate  $p < 0.05$ ). Data represent the mean  $\pm$  S.E. of 3 independent experiments performed in duplicate.

Although orthosteric agonists acetylcholine (ACh) and iperoxo (**2**) both displayed a significant decrease in affinity upon mutation Y426F<sup>7.39</sup>, the hybrid ligands maintained affinity relative to the wild-type M<sub>2</sub> mAChR, suggesting that Y426<sup>7.39</sup> is already perturbed by the binding of all of the hybrid ligands at the wild-type M<sub>2</sub> mAChR, and cannot be further altered in the Y426F<sup>7.39</sup> mutant. The non-selective ligands, ACh, iperoxo (**2**) and IXO-C10-(4-CF<sub>3</sub>)phen (**9**), and the intermediate selectivity hybrid ligand, IXO-C8 (**4**), suffered a significant loss of efficacy, while efficacy was approximately maintained in the more selective ligands, IXO-C10 (**5**) and IXO-C10-phen (**8**). In the presence of a saturating concentration of LY2119620 (**10**) in equilibrium binding assays iperoxo (**2**) and all of the evaluated hybrid ligands gave similar results to the wild-type M<sub>2</sub> mAChR (Figure 6, Table 4), suggesting that their binding conformation is similar in both the Y426F<sup>7.39</sup> and wild-type M<sub>2</sub> mAChRs.

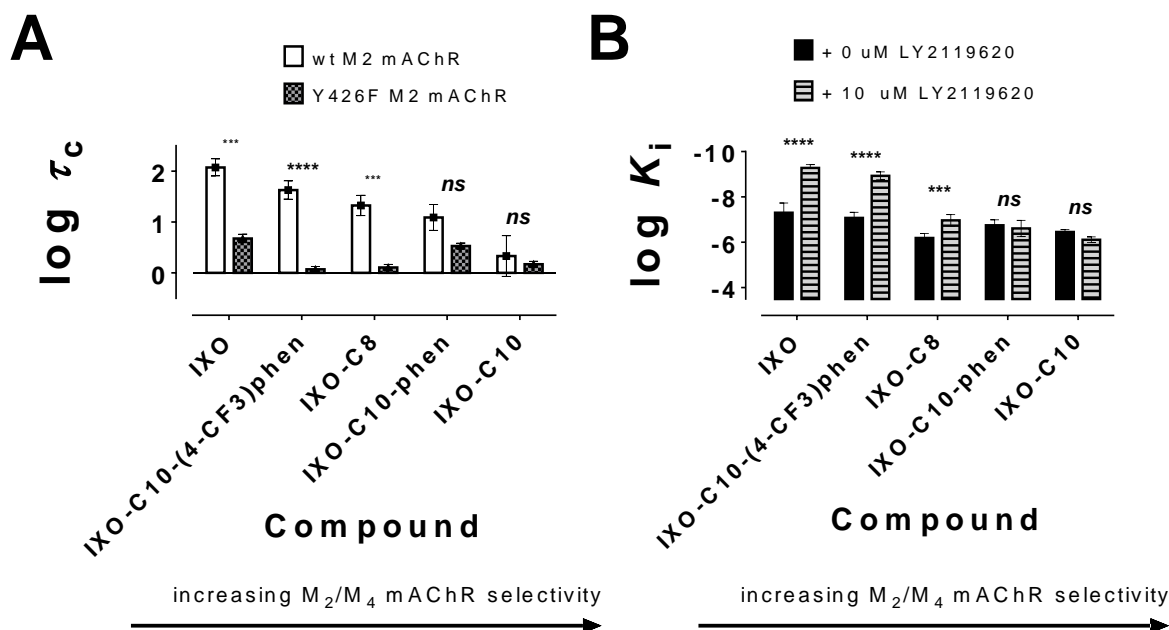


**Figure 11.** (A) Efficacy of the hybrid ligands at the wt M<sub>2</sub> and mutant Y426F M<sub>2</sub> mAChRs in pERK 1/2 assay, and (B) radioligand interaction binding assays of hybrid ligands with 10  $\mu$ M or vehicle control of the PAM LY2119620 (**10**) at the mutant Y426F M<sub>2</sub> mAChR. Binding was measured in whole-cell assays on Flp-In-CHO cells expressing either the M<sub>2</sub> or M<sub>4</sub> mAChRs by competing increasing concentrations of each ligand with a  $K_d$  concentration of [<sup>3</sup>H]NMS, as determined by saturation binding assays. Log  $\tau_c$  is the ligand efficacy, corrected for receptor expression, as determined by fitting the functional ERK 1/2 phosphorylation concentration-response curve data for each ligand to an operational model of agonism and constraining the model by the measured values of affinity for each ligand at each of the respective mAChR subtype or mutant. Compounds are arranged from left to right, on the x-axis in order of increasing preference for the M<sub>4</sub> mAChR, to illustrate the apparent effect that the Y426F mutation at the M<sub>2</sub> mAChR has on the efficacy of hybrid ligand with respect to its M<sub>2</sub>/M<sub>4</sub> mAChR selectivity. Data was statistically analysed using Bonferroni's multiple comparison test, 2-way ANOVA (*ns* = not significant \*  $p < 0.05$ , \*\*  $p < 0.01$ , \*\*\*  $p < 0.001$ , \*\*\*\*  $p < 0.0001$ ). Each data point represents the mean  $\pm$  S.E. of 3 independent experiments, performed in duplicate.

With the loss of the 4-hydroxyl group in the Y426F<sup>7,39</sup> M<sub>2</sub> mAChR mutant the hydrogen bonding interactions with Y104<sup>3,33</sup> and Y403<sup>6,51</sup> are no longer possible, significantly decreasing in efficacy of iperoxo (**2**). In the case of IXO-C10-(4-CF<sub>3</sub>)phen (**9**) the docking results suggest that this interaction should still be possible in the wild-type M<sub>2</sub> mAChR (Figure 10), and consistent with our modelling studies, excitingly this the loss of the 4-hydroxyl in the Y426F M<sub>2</sub> mAChR causes a similar significant decrease in efficacy to that seen for iperoxo (**2**) (Figure

11). The more selective M<sub>2</sub>/M<sub>4</sub> mAChR ligands, IXO-C10 (**5**) and IXO-C10-phen (**8**), however displayed no significant change in efficacy compared with the wild-type M<sub>2</sub> mAChR (Figure 11). In the docked poses of IXO-C10 (**5**) and IXO-C10-phen (**8**) that fit the aforementioned experimentally determined criteria, Y426<sup>7,39</sup> is highly perturbed, compared with the crystallographic pose, forced outwards towards TM2 by the *N*-alkyl linker, and making the formation of hydrogen bonds with Y104<sup>3,33</sup> and Y403<sup>6,51</sup> impossible (Figure 10). In agreement with our molecular modelling studies, the loss of this 4-hydroxyl in the Y426F<sup>7,39</sup> mutant has little to no effect on the efficacy of the more selective ligands, IXO-C10 (**5**) and IXO-C10-phen (**8**). We believe that this is because, in their dominant binding mode, Y426<sup>7,39</sup> is displaced from its crystallographic conformation, and cannot form the hydrogen bonds with Y104<sup>3,33</sup> and Y403<sup>6,51</sup>, that are key to M<sub>2</sub> mAChR activation.<sup>25</sup>

## ■ CONCLUSIONS

Our results suggest that the ‘allosteric’ substituent and linker of the hybrid ligands can adopt two binding modes, while the orthosteric pharmacophore retains a pose homologous to the one observed crystallographically. One of these conformations apparently disrupts the active state structure of the ‘typical’ allosteric site (between ECL2 and TM6/7), and results in attenuation of ligand efficacy in a (presumably) G<sub>i</sub> biased manner, as has been previously reported for structurally related mAChR hybrid ligands.<sup>20</sup> However interaction binding, mutagenesis and molecular modelling studies performed herein suggest a second binding conformation, outside of the ‘typical’ allosteric site, that promotes the non-selective maintenance of efficacy (relative to the orthosteric pharmacophore, iperoxo (**2**)) across the M<sub>1</sub>-M<sub>5</sub> mAChR subtypes. In light of this, the linear relationship between selectivity and potentiation by LY2119620 (**10**) at the M<sub>2</sub> and M<sub>4</sub> mAChRs for the evaluated hybrid ligands is likely indicative of the proportion of bound ligands in the conformation that obstructs the

allosteric site versus the one which does not. The efficacy of all of these ligands appears to be, in part, determined by the proportions of the populations of these two binding modes at the different M<sub>1</sub>-M<sub>5</sub> mAChR subtypes, and this model gives an explanation for the linear relationship between efficacy and selectivity for our hybrid ligands observed in chapters 2 and 3. Our results suggest that this may even extend to differences in hybrid ligand efficacy between the M<sub>2</sub> and M<sub>4</sub> mAChRs, and potentially offers an explanation for our identified examples of hybrid ligands which show greater selectivity for either the M<sub>2</sub> or M<sub>4</sub> mAChR (Figure 4). We propose that the dominant binding conformation of these M<sub>2</sub> or M<sub>4</sub> mAChR preferring hybrid ligands obstructs the allosteric site (resulting in G<sub>i</sub> biased efficacy attenuation), and then it is subtle differences in the population size of ligands bound in the alternative conformation (which allows similar efficacy to iperoxo (**2**)) which results in significant differences in the efficacy at the M<sub>2</sub> or M<sub>4</sub> mAChRs. Since these proportions are apparently not equal at the M<sub>2</sub> versus M<sub>4</sub> mAChRs, this would explain why their efficacy values are also not equal, (i.e. they possess M<sub>2</sub> or M<sub>4</sub> mAChR subtype selectivity) (Figure 12).



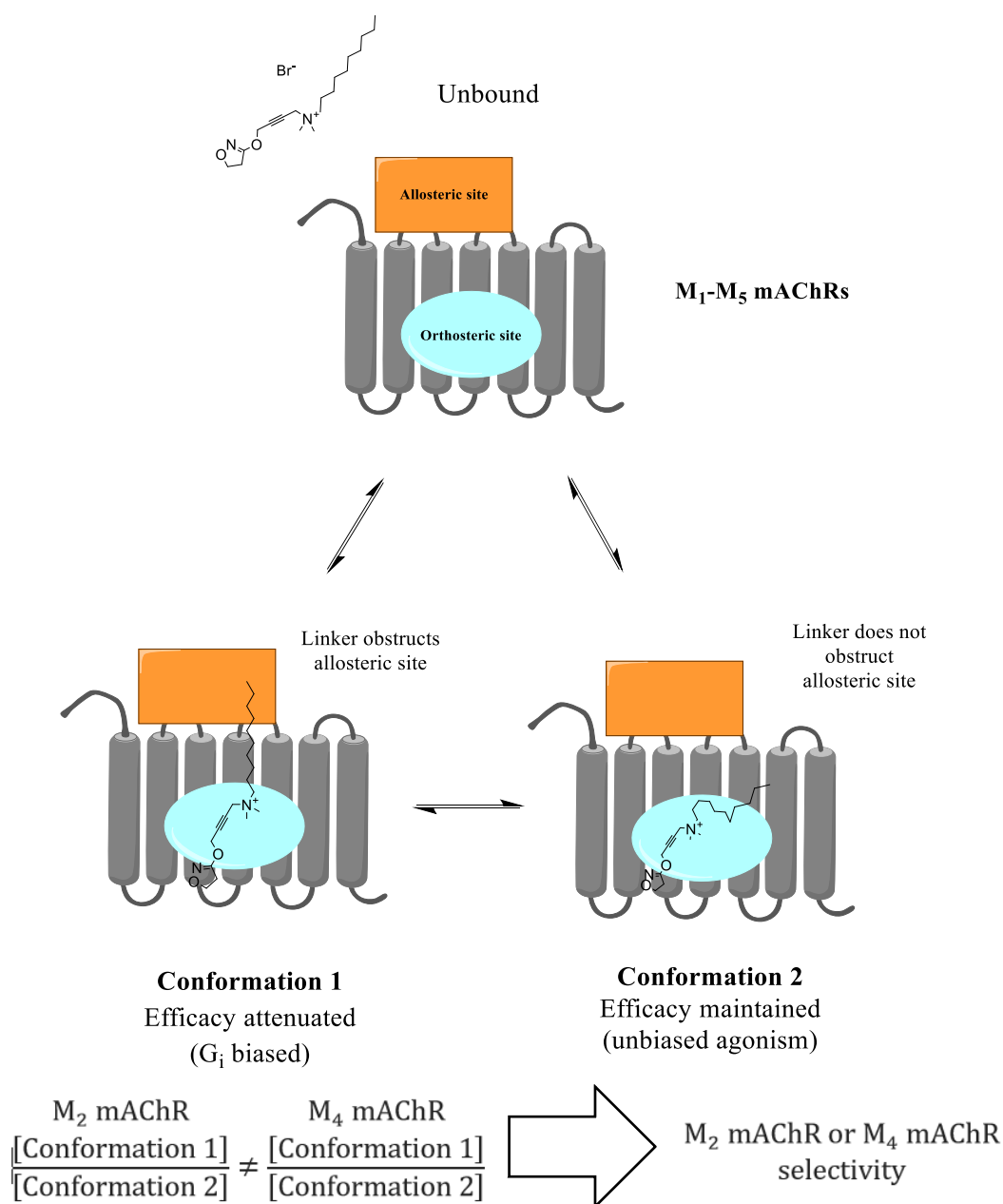


**Figure 12.** Proposed mechanism of binding for hybrid ligands in which different proportions of binding conformations can induce differences in the efficacy at the M<sub>2</sub> and M<sub>4</sub> mAChRs.

Future work will involve further interaction binding studies, examining the binding modes of the other M<sub>2</sub> or M<sub>4</sub> mAChR selective hybrid ligands, as well as measuring the G<sub>i</sub> bias of these ligands, to examine whether their binding and functional outputs are consistent with the model we have proposed here. We hope that application of this model can be used to optimise the selectivity of mAChR hybrid ligands to ultimately aid in the design of a M<sub>4</sub>

mAChR selective partial agonist for the treatment of cognitive disorders, such as schizophrenia.

## ■ EXPERIMENTAL SECTION

**Pharmacology.** *Cell culture.* Flp-In-CHO cells stably expressing human muscarinic M<sub>1</sub>, M<sub>2</sub>, M<sub>4</sub>, M<sub>5</sub>, or CHO-K<sub>1</sub> expressing the M<sub>3</sub> receptors were cultured at 37 °C in 5% CO<sub>2</sub> in F-12 (Ham) (M<sub>1</sub>) or Dulbecco's modified Eagle media (M<sub>2</sub> – M<sub>5</sub>) supplemented with 10% (M<sub>1</sub>) or 5% (M<sub>2</sub> – M<sub>5</sub>) (v/v) FBS.

*ERK 1/2 phosphorylation assay plate preparation.* Cells were seeded into transparent 96-well plates at  $25 \times 10^4$  cells per well and grown for 6 - 8 h. Cells were then washed once with phosphate-buffered saline (PBS) and incubated in serum-free media (180 or 160 µL per well, depending on the intended assay) at 37 °C) for at least 8 h, to allow phosphorylated ERK1/2 levels to subside.

*Concentration-response curves (CRCs).* Cells were plated in 180 µL media per well. A stock solution of acetylcholine ( $10^{-2}$  M) was made up in PBS. Stock solutions of the test ligands ( $10^{-2}$  M) were made up in DMSO. Dilutions of all ligands were made up in FBS-free media at ten times (10×) the required concentration and added to stock plates. Cells were incubated at 37 °C with 20 µL per well until peak phosphorylation occurred at which point the assay was terminated.

*Allosteric-orthosteric ligand interaction assays.* As for CRCs, except that cells were plated in 160 µL media per well. The allosteric ligand (20 µL) and orthosteric ligands (20 µL) were added successively.

*Assay termination and data collection.* Agonist-stimulated ERK1/2 phosphorylation was terminated by the removal of drugs and the addition of 100 µL p/well of SureFire™ lysis buffer. The cell lysates were agitated for 5-10 min. Following agitation, 10 µL of cell lysates

were transferred into a 384-well white opaque Optiplate™, followed by addition of 8.3 µL of a solution of reaction buffer / activation buffer / acceptor beads / donor beads in a ratio of 60/10/0.3/0.3 (v/ v/ v/ v) under green light conditions. The plates were then incubated at 37 °C in the dark for 1 h and fluorescence was measured on a Envision™ plate reader (PerkinElmer) using standard settings.

*Radioligand equilibrium whole cell binding assay plate preparation.* Cells were seeded into white opaque Isoplates™ at 10 000 cells per well and then grown at 37 °C for 20-24 h. Cells were then washed twice with 50 µL of cold HEPES-buffered saline, then 140 or 160 µL of cold HEPES-buffered saline was added per well.

*Saturation binding assay protocol with [<sup>3</sup>H]NMS.* Stock solutions of [<sup>3</sup>H]NMS (10<sup>-2</sup> M) were made up in cold HEPES-buffered saline. Dilutions of [<sup>3</sup>H]NMS were made up in cold HEPES-buffered saline at ten times (10×) the required concentration and added to stock plates on ice. Cells were equilibrated at 25 °C for 4 h. The *K<sub>d</sub>* values for [<sup>3</sup>H]NMS at the M<sub>1</sub>-M<sub>5</sub> mAChR subtypes were found to be as follows: M<sub>1</sub> mAChR: 0.06 ± 0.01 nM, M<sub>2</sub> mAChR: 0.11 ± 0.02 nM, M<sub>3</sub> mAChR: 0.19 ± 0.12 nM, M<sub>4</sub> mAChR: 0.12 ± 0.03 nM, M<sub>5</sub> mAChR: 0.11 ± 0.07 nM, Y426F M<sub>2</sub> mAChR: 0.51 ± 0.10 nM, Y177A M<sub>2</sub> mAChR: 0.11 ± 0.02 nM, M<sub>4</sub> mAChR (3xHA): 0.04 ± 0.01 nM, F186A M<sub>4</sub> mAChR (3xHA): 0.11 ± 0.11 nM.

*Orthosteric competition binding assay protocol.* Stock solutions of each ligand (10<sup>-2</sup> M) were made up in cold HEPES-buffered saline. Dilutions of all ligands were made up in cold HEPES-buffered saline at ten times (10×) the required concentration and added to stock plates on ice. Cells were equilibrated at 25 °C for 4 h with 20 µL of a single interacting ligand and 20 µL of 1 nM [<sup>3</sup>H]NMS (total volume 200 µL per well).

*Allosteric interaction assay protocol.* Stock solutions of each orthosteric ligand (10<sup>-2</sup> M) were made up in cold HEPES-buffered saline. Stock solutions of the interacting allosteric ligands of choice (10<sup>-2</sup> M) were made up in DMSO. Dilutions of all ligands were made up in

cold HEPES-buffered saline at ten times (10×) the required concentration and added to stock plates. Cells were equilibrated at 4 °C for 4 h with 20 µL of ACh, 20 µL of a single interacting allosteric ligand and 20 µL of 1 nM [<sup>3</sup>H]NMS (total volume 200 µL per well).

*Assay termination and data collection.* Assays were terminated by media removal of the assay buffer and by washing twice with 50 µL 0.9% NaCl solution. Microscint-20 scintillation liquid (100 µL per well) was then added to each well and the plates covered. The levels of remaining bound radioligand, were measured in counts per minute (cpm) on the Microbeta2™ LumiJET 2460 microplate counter (PerkinElmer).

*Data analysis.* All data analysis was managed using Prism 6 software (GraphPad Software, San Diego, CA). Experiments measuring radioligand equilibrium whole cell binding interactions were fitted to the allosteric ternary complex model (1):

$$Y = \frac{[A]}{[A] + \left( \frac{K_A K_B}{(\alpha' [B] + K_B)} \right) \left( 1 + \frac{[I]}{K_I} + \frac{[B]}{K_B} + \frac{\alpha [I][B]}{K_I K_B} \right)} \quad (1)$$

where Y is the percentage (vehicle control) specific binding, [A], [B] and [I] are the concentrations of [<sup>3</sup>H]NMS, **3**, and **1** respectively,  $K_A$  and  $K_B$  are the equilibrium dissociation constants of [<sup>3</sup>H]NMS and the allosteric ligand, respectively,  $K_i$  is the equilibrium dissociation constant of **1**, and  $\alpha$  and  $\alpha'$  are the cooperativities between the allosteric ligand and [<sup>3</sup>H]NMS or **1**, respectively. Values of  $\alpha$  (or  $\alpha'$ ) > 1 denote positive cooperativity; values < 1 denote negative cooperativity, and values = 1 denote neutral cooperativity. Functional orthosteric and allosteric agonist concentration-response curves were fitted via nonlinear regression to the three-parameter logistic function (2):

$$E = basal + \frac{E_{max} - basal}{1 + 10^{-pEC_{50} - \log[A]}} \quad (2)$$

where E is response,  $E_{max}$  and basal are the top and bottom asymptotes of the curve, respectively,  $\log [A]$  is the logarithm of the agonist concentration, and  $pEC_{50}$  is the negative logarithm of the agonist concentration that gives a response halfway between  $E_{max}$  and basal.

Functional experiments measuring the interactions between **1** and **3** were fitted to the operational model of allosterism (3) to derive functional estimates of modulator affinity, cooperativity, and efficacy.

$$E = \frac{E_{max}(\tau_A[A](K_B + \alpha\beta[B]) + \tau_B[B]K_A)^n}{([A]K_B + K_A K_B + [B]K_A + \alpha[A][B])^n + (\tau_A[A](K_B + \alpha\beta[B]) + \tau_B[B]K_A)^n} \quad (3)$$

where  $E_{max}$  is the maximum attainable system response for the pathway under investigation; [A] and [B] are the concentrations of orthosteric and allosteric ligands, respectively;  $K_A$  and  $K_B$  are the equilibrium dissociation constants of the orthosteric and allosteric ligands, respectively;  $\tau_A$  and  $\tau_B$  are the operational measures of orthosteric and allosteric ligand efficacy (which incorporate both signal efficiency and receptor density), respectively;  $n$  is a transducer slope factor linking occupancy to response;  $\alpha$  is the binding cooperativity parameter between the orthosteric and allosteric ligand;  $\beta$  denotes the magnitude of the allosteric effect of the modulator on the efficacy of the orthosteric agonist. The equilibrium dissociation constant of BQCA-derivative was fixed to that determined from the competition binding experiments.

Whole cell equilibrium competition radioligand binding experiments were fitted to a one-site competition binding equation (4) to estimate the  $pK_i$  for each ligand. The equation assumes that there is only one-site the ligands bind to and that the binding is reversible and at equilibrium:

$$Y = bottom + \frac{top - bottom}{1 + 10^{[I] - \log(10^{K_i(1 + \frac{[A]}{K_A})})}} \quad (4)$$

where  $Y$  is the percentage (vehicle control) binding, top and bottom are the total and non-specific binding, respectively. [A] and [I] are the concentrations of [ $^3H$ ]NMS, and competing “cold” ligand respectively,  $K_A$  and  $K_i$  are the equilibrium dissociation constants of [ $^3H$ ]NMS and the “cold” ligand, respectively. The efficacy ( $\tau$ ) of several ligands was determined by fitting the functional data to an operational model of agonism:

$$Y = \frac{E_{max} - Basal}{1 + (\frac{10^{\log K_A + 10[L]}}{10^{\log \tau + [L]}})^n} \quad (5)$$

where Y is the measured response,  $E_{\max}$  and basal are the top and bottom asymptotes of the curve, respectively,  $K_A$  equilibrium dissociation constant for the ligand being tested, [L] is the concentration of ligand in solution,  $\tau$  is the efficacy of the ligand being tested and n is the transducer slope. The efficacy values were then normalised to the M<sub>4</sub> mAChR values, to give the ‘corrected efficacy’ ( $\tau_c$ ), to account for the varying receptor expression in each cell line used by the following equation:

$$\log \tau_c = \log \tau - \log \left( \frac{B_{\max Mx}}{B_{\max M4}} \right) \quad (6)$$

where  $\tau_c$  is the corrected efficacy,  $\tau$  is the measured efficacy (as determined by equation 5), Bmax is the maximum counts recorded when the mAChR in question is incubated with a saturating concentration of [<sup>3</sup>H]NMS, at mAChR M<sub>x</sub>, where x gives the subtype in question, compared to the M<sub>4</sub> mAChR.

## ■ REFERENCES

- (1) Insel, P. A.; Snead, A.; Murray, F.; Zhang, L.; Yokouchi, H.; Katakia, T.; Kwon, O.; Dimucci, D.; Wilderman, A., GPCR expression in tissues and cells: are the optimal receptors being used as drug targets? *Br. J. Pharmacol.* **2012**, *165*, 1613-6.
- (2) Sriram, K.; Insel, P. A. GPCRs as targets for approved drugs: How many targets and how many drugs? *Mol. Pharmacol.* **2018**, *96*, 251-58.
- (3) Brodde, O. E.; Michel, M. C., Adrenergic and muscarinic receptors in the human heart. *Pharmacol. Rev.* **1999**, *51*, 651-90.
- (4) Eglen, R. M.; Hegde, S. S.; Watson, N., Muscarinic receptor subtypes and smooth muscle function. *Pharmacol. Rev.* **1996**, *48*, 531-65.
- (5) Gautam, D.; Gavrilova, O.; Jeon, J.; Pack, S.; Jou, W.; Cui, Y.; Li, J. H.; Wess, J., Beneficial metabolic effects of M3 muscarinic acetylcholine receptor deficiency. *Cell Metab.* **2006**, *4*, 363-75.
- (6) Wess, J., Muscarinic acetylcholine receptor knockout mice: novel phenotypes and clinical implications. *Annu. Rev. Pharmacol. Toxicol.* **2004**, *44*, 423-50.
- (7) Wallis, R. M.; Napier, C. M., Muscarinic antagonists in development for disorders of smooth muscle function. *Life Sci.* **1999**, *64*, 395-401.
- (8) Chapple, C. R., Muscarinic receptor antagonists in the treatment of overactive bladder. *Urology* **2000**, *55* (5A Supplement 1), 33-46.
- (9) Alabaster, V. A. Discovery & development of selective M3 antagonists for clinical use. *Life sciences* **1997**, *60*, 1053-60.
- (10) Bodick, N. C.; Offen, W. W.; Levey, A. I.; Cutler, N. R.; Gauthier, S. C.; Satlin, A.; Shannon, H. E.; Tollefson, G. D.; Rasmussen, K.; Bymaster, F. P.; Hurley, D. J.; Potter, W. Z.;

- Paul, S. M.; Effects of xanomeline, a selective muscarinic receptor agonist, on cognitive function and behavioral symptoms in Alzheimer's disease. *Arch. Neurol.* **1997**, *54*, 465-73.
- (11) Bodick, N. C.; Offen, W. W.; Shannon, H. E.; Satterwhite, J.; Lucas, R.; van Lier, R.; Paul, S. M. The selective muscarinic agonist xanomeline improves both the cognitive deficits and behavioral symptoms of Alzheimer disease. *Alzheimer Dis. Assoc. Disord.* **1997**, *11 Suppl 4*, S16-22.
- (12) Nathan, P. J.; Watson, J.; Lund, J.; Davies, C. H.; Peters, G.; Dodds, C. M.; Swirski, B.; Lawrence, P.; Bentley, G. D.; O'Neill, B. V.; Robertson, J.; Watson, S.; Jones, G. A.; Maruff, P.; Croft, R. J.; Laruelle, M.; Bullmore, E. T., The potent M1 receptor allosteric agonist GSK1034702 improves episodic memory in humans in the nicotine abstinence model of cognitive dysfunction. *Int. J. Neuropsychopharmacol.* **2013**, *16*, 721-31.
- (13) KarTX clinical trial. <https://clinicaltrials.gov/ct2/show/study/NCT03697252>.
- (14) Gregory, K. J.; Sexton, P. M.; Christopoulos, A., Allosteric Modulation of Muscarinic Acetylcholine Receptors. *Curr. Neuropharmacol.* **2007**, *5*, 157-67.
- (15) Disingrini, T.; Muth, M.; Dallanoce, C.; Barocelli, E.; Bertoni, S.; Kellershohn, K.; Mohr, K.; De Amici, M.; Holzgrabe, U. Design, Synthesis, and Action of Oxotremorine-Related Hybrid-Type Allosteric Modulators of Muscarinic Acetylcholine Receptors. *J. Med. Chem.* **2006**, *49*, 366-72.
- (16) Valant, C.; Robert Lane, J.; Sexton, P. M.; Christopoulos, A. The best of both worlds? Bitopic orthosteric/allosteric ligands of G protein-coupled receptors. *Annu. Rev. Pharmacol. Toxicol.* **2012**, *52*, 153-78.
- (17) Lane, R. J.; Sexton, P. M.; Christopoulos, A. Bridging the gap: bitopic ligands of G-protein-coupled receptors. *Trends Pharmacol. Sci.* **2013**, *34*, 59-66.
- (18) Messerer, R.; Kauk, M.; Volpato, D.; Alonso Canizal, M. C.; Klockner, J.; Zabel, U.; Nuber, S.; Hoffmann, C. FRET Studies of Quinolone-Based Bitopic Ligands and Their Structural Analogues at the Muscarinic M1 Receptor. *ACS Chem. Biol.* **2017**, *12*, 833-43.
- (19) Schmitz, J.; van der May, D.; Bermudez, M.; Klöckner, J.; Schrage, R.; Kostenis, E.; Tränkle, C.; Wolber, G.; Mohr, K.; Holzgrabe, U. Dualsteric Muscarinic Antagonists—Orthosteric Binding Pose Controls Allosteric Subtype Selectivity. *J. Med. Chem.* **2014**, *57*, 6739–50.
- (20) Bermudez, M.; Bock, A.; Krebs, F.; Holzgrabe, U.; Mohr, K.; Lohse, M. J.; Wolber, G. Ligand-Specific Restriction of Extracellular Conformational Dynamics Constrains Signaling of the M2 Muscarinic Receptor. *ACS Chem. Biol.* **2017**, *12*, 1743-48.
- (21) Bock, A.; Bermudez, M.; Krebs, F.; Matera, C.; Chirinda, B.; Sydow, D.; Dallanoce, C.; Holzgrabe, U.; De Amici, M.; Lohse, M. J.; Wolber, G.; Mohr, K. Ligand Binding Ensembles Determine Graded Agonist Efficacies at a G Protein-coupled Receptor. *J. Biol. Chem.* **2016**, *291*, 16375-89.
- (22) Steinfeld, T.; Mammen, M.; Smith, J. A.; Wilson, R. D.; Jasper, J. R. A Novel Multivalent Ligand That Bridges the Allosteric and Orthosteric Binding Sites of the M2 Muscarinic Receptor. *Mol. Pharmacol.* **2007**, *72*, 291-302.
- (23) Steinfeld, T.; Hughes, A. D.; Klein, U.; Smith, J. A.; Mammen, M. THRX-198321 Is a Bifunctional Muscarinic Receptor Antagonist and beta-2-Adrenoceptor Agonist (MABA) That Binds in a Bimodal and Multivalent Manner *Mol. Pharmacol.* **2010**, *79*, 389–99.
- (24) Bock, A.; Chirinda, B.; Krebs, F.; Messerer, R.; Bätz, J.; Muth, M.; Dallanoce, C.; Klighenthal, D.; Tränkle, C.; Hoffmann, C.; De Amici, M.; Holzgrabe, U.; Kostenis, E.; Mohr, K. Dynamic ligand binding dictates partial agonism at a g protein-coupled receptor. *Nat. Chem. Biol.* **2014**, *10*, 18-20.
- (25) Kruse, A. C.; Ring, A. M.; Manglik, A.; Hu, J.; Hu, K.; Eitel, K.; Hubner, H.; Pardon, E.; Valant, C.; Sexton, P. M.; Christopoulos, A.; Felder, C. C.; Gmeiner, P.; Steyaert, J.; Weis, W.

- I.; Garcia, K. C.; Wess, J.; Kobilka, B. K. Activation and allosteric modulation of a muscarinic acetylcholine receptor. *Nature* **2013**, *504*, 101-6.
- (26) Valant, C.; Gregory, K. J.; Hall, N. E.; Scammells, P. J.; Lew, M. J.; Sexton, P. M.; Christopoulos, A. A Novel Mechanism of G Protein-coupled Receptor Functional Selectivity: Muscarinic partial agonist McN-A-343 as a bitopic orthosteric/allosteric ligand. *J. Biol. Chem.* **2008**, *283*, 29312–21.
- (27) Thal, D. M.; Sun, B.; Feng, D.; Nawaratne, V.; Leach, K.; Felder, C. C.; Bures, M. G.; Evans, D. A.; Weis, W. I.; Bachhawat, P.; Kobilka, T. S.; Sexton, P. M.; Kobilka, B. K.; Christopoulos, A. Crystal structures of the M1 and M4 muscarinic acetylcholine receptors. *Nature* **2016**, *531*, 335-40.
- (28) Haga, K.; Kruse, A. C.; Asada, H.; Yurugi-Kobayashi, T.; Shiroishi, M.; Zhang, C.; Weis, W. I.; Okada, T.; Kobilka, B. K.; Haga, T.; Kobayashi, T., Structure of the human M2 muscarinic acetylcholine receptor bound to an antagonist. *Nature* **2012**, *482*, 547-51.
- (29) Chaim, Y. B.; Bochnik, S.; Parnas, I.; Parnas, H., Voltage Affects the Dissociation Rate Constant of the m2 Muscarinic Receptor. *PLoS One* **2013**, *8*, e74354.



# Chapter Five

## **Declaration of Contributions for Chapter Five**

The initial concept of the fluorophore-tagged ligand in this chapter is attributed to Dr. Celine Valant. The specific design and synthesis of the molecules in this chapter was performed by myself. Pharmacological characterisation of the final fluorophore-tagged ligand was performed by Olivia Mastromihalis, Vi Pham and Jordan Arthur Michaelis, and the generation of the GFP-tagged M<sub>2</sub> muscarinic acetylcholine receptor expressing cell line was performed by Dr. Emma van der Westhuizen and Geoff Thompson.

# Design, Synthesis and Evaluation of a Fluorophore-tagged Muscarinic Acetylcholine Receptor Allosteric Probe

**ABSTRACT:** The muscarinic acetylcholine receptors (mAChRs) have received significant attention from both academia and industry for the treatment of numerous diseases, most recently targeting the allosteric sites of the M<sub>1</sub> and M<sub>4</sub> mAChRs for the treatment of impairment of memory and cognition in Alzheimer's disease and schizophrenia. The evaluation of ligand affinity is often fundamental in the characterization and optimization of new ligands, and the process of measuring ligand affinity typically involves competing increasing concentrations of an unlabeled test ligand against a labeled probe ligand (at a fixed  $K_d$  concentration) and measuring the change in the amount of bound probe as a function of the concentration of unlabeled test ligand. However, at the current time there is a lack of probes targeting the allosteric sites of the mAChRs. There have been several radiolabelled probes which have been successfully produced targeting the mAChRs allosteric sites. However due to radioactive hazards, waste and their limited affinity (requiring high concentrations of probe) the applications of these probes are limited to low-throughput assay setups. To overcome these issues in measuring muscarinic acetylcholine receptor (mAChR) allosteric ligand affinity we have designed, synthesized and evaluated a novel fluorescently tagged mAChR allosteric probe. The probe that we have produced, C<sub>7/3</sub>-phth-Lissamine B, is derived from the mAChR negative allosteric modulator (NAM) C<sub>7/3</sub>-phth, and we have exploited the flexible SAR surrounding the phthalimido ring motif of C<sub>7/3</sub>-phth to install the fluorophore (Lissamine B) directly into the pharmacophore of the parent ligand. C<sub>7/3</sub>-phth-Lissamine B shows comparable affinity to its unlabeled derivative in both radioligand binding assays and in FRET based assays. Furthermore, C<sub>7/3</sub>-phth-Lissamine B competes with, and shows comparable allosteric pharmacology when interacting with [<sup>3</sup>H]NMS, to the parent ligand C<sub>7/3</sub>-phth, at the eGFP-

tagged M<sub>2</sub> mAChR, suggesting both ligands share a common allosteric mode of action. This probe allows for the direct determination of allosteric ligand affinity by FRET-based competition binding assays, which could in principal be scaled to allow for its use in a high-throughput assay setup. Additional to its advantages in safety and waste production over similar radiolabelled probes, this fluorescently tagged mAChR allosteric probe can be used for real-time imaging studies using confocal microscopy techniques, allowing for the studying of mAChR trafficking and localization in the presence of the probe.

## ■ INTRODUCTION

The muscarinic acetylcholine receptors (mAChRs) are currently being actively pursued as potential targets for the treatment of several diseases, including Alzheimer's and schizophrenia.<sup>1-4</sup> The targeting of allosteric site of the mAChRs has gained popularity in recent decades due to the advantages that allosteric ligands have in terms of selectivity and their functioning depending on the presence of endogenous tone over more conventional 'orthosteric' ligands, which bind to the endogenous ligand binding site.<sup>5-6</sup> In most drug discovery efforts determination of ligand affinity is important for structural optimization. For orthosteric ligands this is typically done by competing an unlabeled test ligand against a fixed concentration of a labelled probe (typically radiolabelled) and fitting the data to a law of mass action based binding model to estimate affinity.<sup>7-9</sup> However using an orthosteric probe for estimating this parameter in allosteric ligands is more complex, requiring a three ligand 'interaction assay' system under equilibrium conditions, or measurement of the change in dissociation rate of a radioligand in the presence of increasing concentrations of an allosteric test ligand under non-equilibrium conditions, to estimate the allosteric ligand affinity with reasonable error.<sup>9-12</sup> Aside from being inefficient, these methods are limited as they rely upon the cooperativity between the competing orthosteric ligand and allosteric test ligand, meaning

that affinity cannot be determined for neutral allosteric ligands (NALs) or at receptor subtypes where the allosteric test ligand and competing orthosteric ligand have no measurable cooperativity, but may still bind simultaneously. To address this, two groups have developed tritium radiolabelled derivatives of mAChR allosteric ligands, [ $^3\text{H}$ ]LY2119620 and [ $^3\text{H}$ ]dimethyl-W84 (Figure 1).<sup>13-14</sup>

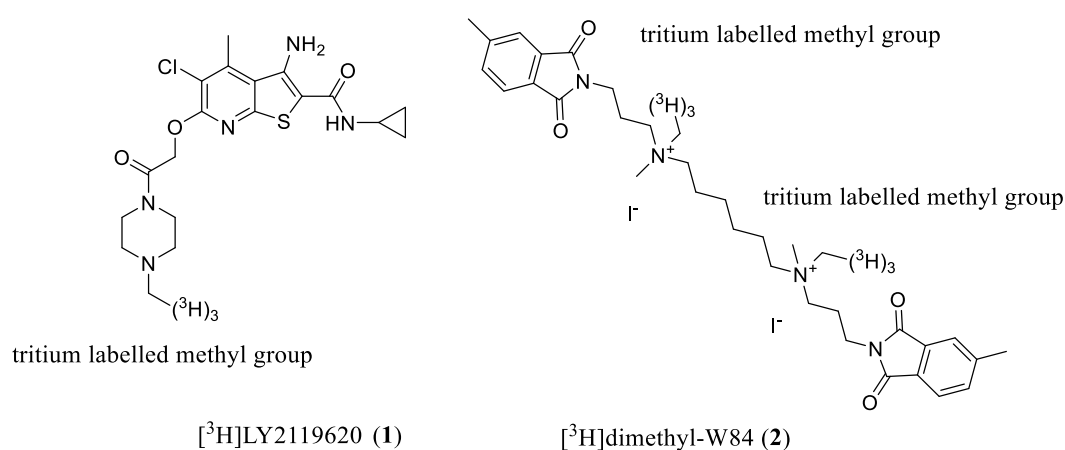


**Figure 1.** Chemical structure of the  $\text{M}_2/\text{M}_4$  mAChR selective allosteric modulator, [ $^3\text{H}$ ]LY2119620 (**1**) and mAChR NAM [ $^3\text{H}$ ]dimethyl-W84 (**2**).

These probes carry several advantages which are common to tritium labelled probes including that they are chemically identical to their unlabeled parent compounds, meaning that rigorous validation of the probe pharmacology is unnecessary. Additionally, as for all tritium labelled probes, their output signals are stable for a longer period relative to common assay durations, due to the relatively long half-life of tritium. Despite this, these probes also have several limitations. For example [ $^3\text{H}$ ]LY2119620 (**1**) was found to have affinity only for the  $\text{M}_2$  and  $\text{M}_4$  mAChRs,<sup>15</sup> making it unsuitable for measuring ligand affinity at the remaining  $\text{M}_1$ ,  $\text{M}_3$  and  $\text{M}_5$  mAChR subtypes. [ $^3\text{H}$ ]Dimethyl-W84 (**2**) does not share this issue, having reasonable affinity at all  $\text{M}_1$ - $\text{M}_5$  mAChR subtypes, making it more broadly applicable as a tool molecule.<sup>14, 16</sup> However for both [ $^3\text{H}$ ]LY2119620 (**1**) and [ $^3\text{H}$ ]dimethyl-W84 (**2**), as with all radioligands, radioactive hazards and waste are associated with their use. Compounding the

problem is the relatively low affinity of allosteric probes as compared with orthosteric probes commonly used at the mAChRs, requiring concentrations approximately 100 to 1000-fold greater and hence resulting in a similar relative increase in radioactive hazards, waste and the cost of each assay. Despite these issues these probes are valuable tools for measuring ligand allosteric affinity at the mAChRs in a low-throughput assay setup. However, the use of both [<sup>3</sup>H]LY2119620 (**1**) and [<sup>3</sup>H]dimethyl-W84 (**2**) becomes less practical as desired throughput increases. More recently, another tritium-labelled allosteric probe, [<sup>3</sup>H]PT-1284 has been developed which targets the M<sub>1</sub> mAChR. However this probe suffers from the same disadvantages as [<sup>3</sup>H]LY2119620 (**1**) and [<sup>3</sup>H]dimethyl-W84 (**2**) as it is relatively low affinity compared with orthosteric ligands and has selectivity for the M<sub>1</sub> mAChR, limiting its applicability to that receptor subtype, and further demonstrates that these issues are essentially intrinsic to tritium labelled allosteric probes.<sup>17</sup> Fluorescently tagged probes offer attractive solutions to several of these issues as they have none of the associated radioactive hazards and are hence significantly more practical in larger scale assay formats. Fluorescence probes (when used in conjunction with a fluorescently tagged receptor) can also be used to image ligand binding directly in real-time, giving important information about receptor internalization and binding kinetics from a single assay. However, unlike tritium labelled probes, fluorescently tagged probes are generally not chemically identical to their parent ligand and hence must be chemically optimised and thoroughly characterised pharmacologically to ensure that they retain the desired pharmacological properties for the intended application.<sup>18</sup> Fluorescent probes can be prone to photo-bleaching, in some cases on timescales comparable to assay times, resulting in signal-drift, however this may be mitigated by the choice of a more stable fluorophore tag.<sup>19</sup> There have been several fluorescently tagged probes which have been reported for the mAChRs which bind either orthosterically or bitopically (Figure 2).

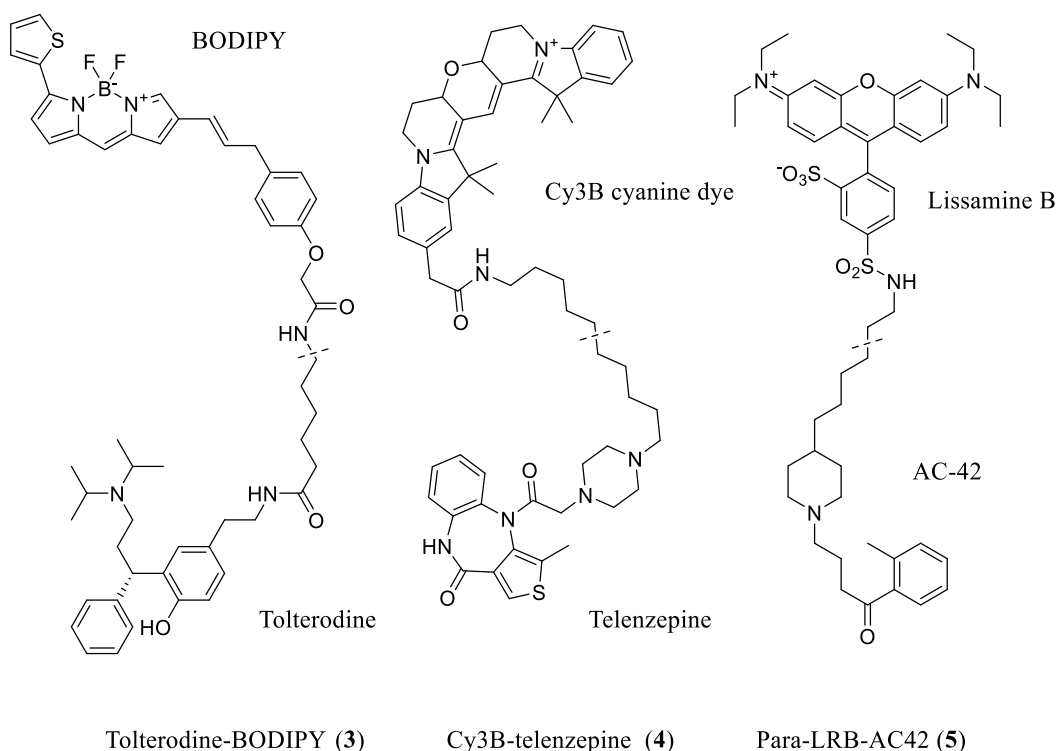


**Figure 2.** Chemical structures of fluorescent tracer ligands targeting the mAChRs; tolterodine-BODIPY (3), Cy3B-telenzepine (4) and para-LRB-AC42 (5).

Tolterodine-BODIPY (3) was designed for use in receptor occupancy studies of the mAChRs orthosteric sites and has potential applications in high-throughput screening (HTS).<sup>20</sup> The BODIPY-based fluorophore used in tolterodine-BODIPY (3) comes in a range of absorption/ emission wavelengths which could have potentially been suitable for our application, however these fluorophores are very expensive compared with other near-infrared fluorophores which were similarly suitable, making a BODIPY fluorophore a less attractive choice for our fluorescent probe. Cy3B-telenzepine (4) was developed to address questions relating to the existence and function of receptor dimers in the mAChRs. Ultimately, Cy3B-telenzepine (4) was used to demonstrate that approximately 30% of the M<sub>1</sub> mAChRs existed as dimers, and this study illustrates the versatility of applications of such fluorophore-tagged ligands.<sup>21</sup> However the fluorophore used Cy3B (and other cyanine-based dyes) do not possess the appropriate near-infrared absorption/ emission wavelengths for our use here.

Para-LRB-AC42 (**5**) was developed to address questions relating to the ambiguous orthosteric/ allosteric pharmacology of the base pharmacophore AC-42, again highlighting the wide range of applications of fluorophore-tagged ligands.<sup>22</sup> However Para-LRB-AC42 (**5**) was found to directly compete with allosteric modulator gallamine at the M<sub>1</sub> mAChR, but not with other allosteric ligands including WIN 51,708 and *N*-desmethylozapine, suggesting that the interesting molecular pharmacology of the probe may make it unsuitable as a general purpose mAChR allosteric probe. The fluorophore used in Para-LRB-AC42 (**5**), Lissamine B, possesses suitable absorption/ emission wavelengths, as well as having good photostability and chemical stability for our intended application here and was strongly considered as a candidate fluorophore. Another fluorophore we considered was Texas Red, which has suitable absorption/ emission wavelengths, but is again considerably more expensive than, for example, Lissamine B which also has suitable properties for our application. Herein we detail the design, synthesis and evaluation of a novel fluorophore-tagged allosteric modulator probe for the M<sub>1</sub>-M<sub>5</sub> mAChR subtypes. The goals of our design were as follows; a probe that was synthetically accessible from commonly available reagents, had potential applications in fluorescence resonance energy transfer (FRET), bioluminescence resonance energy transfer (BRET) and fluorescence polarimetry (FP), and which had suitable affinity at the allosteric site of the M<sub>1</sub>-M<sub>5</sub> mAChRs for use at all five subtypes. As a detection method we chose FRET, using the ligand in conjunction with an N-terminus enhanced green-fluorescent protein (eGFP) tagged M<sub>2</sub> mAChR as a proof of concept assay system, due the high sensitivity achievable, ability to image receptor-ligand binding and receptor trafficking in real-time, and the potential to adapt the method for HTS.<sup>23</sup> The N-terminus of the M<sub>2</sub> mAChR is an ideal location for the eGFP tag, giving an ideal distance between the allosteric site and eGFP that is within the Förster radius (3-6 nm), while additionally minimizing the likelihood of interfering with the structure and function of the M<sub>2</sub> mAChR.<sup>24-25</sup> We chose C<sub>7/3</sub>-phth (**6**), a mAChR NAM belonging to a class



of well-studied bis(ammonio)alkane-type ligands as the allosteric parent ligand for our probe for several reasons (Figure 3).

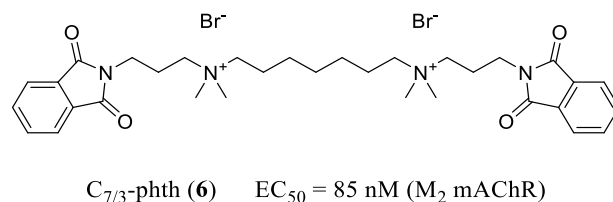


**Figure 3.** Chemical structure of our parent ligand for our mAChR allosteric probe design,  $C_{7/3}$ -phth (**6**).

Firstly,  $C_{7/3}$ -phth (**6**) binds to all five mAChR subtypes with similar affinity, unlike for example LY2119620 (**1**), which only has affinity for the  $M_2$  and  $M_4$  mAChRs.<sup>13,26</sup> Importantly,  $C_{7/3}$ -phth (**6**) is synthetically accessible from commonly available starting materials, such that our probe could be cheaply reproduced by other groups to increase the broadness of its applicability.  $C_{7/3}$ -phth also displays good flexibility in its structure-activity relationship (SAR) surrounding the terminal ring motifs,<sup>27</sup> which was important to our design approach to allow for the installation of the fluorophore tag directly into the ligand pharmacophore. As examples of this flexibility, CHIN 3/6 (**8**), naphmethonium (**9**), compound **10** and compound **11** illustrate how significant modification the aromatic ring motifs (and changes in linker length) gives ligands with comparable allosteric potency to the parent ligand,  $C_{7/3}$ -phth (Figure 4).<sup>27-29</sup> In particular these compounds **8-11** (Figure 4) demonstrate that a significant increase in steric bulk by substituting the phthalimido group with other larger aromatic groups is tolerated, suggesting that this region of the molecule could possibly be substituted for a similarly bulky, aromatic fluorophore without significant loss of allosteric potency. Additionally, although  $C_{7/3}$ -phth (**6**) is a homobivalent ligand, structurally related hybrid ligands show that being homobivalent is not a necessity for it possessing allosteric properties.<sup>30</sup>

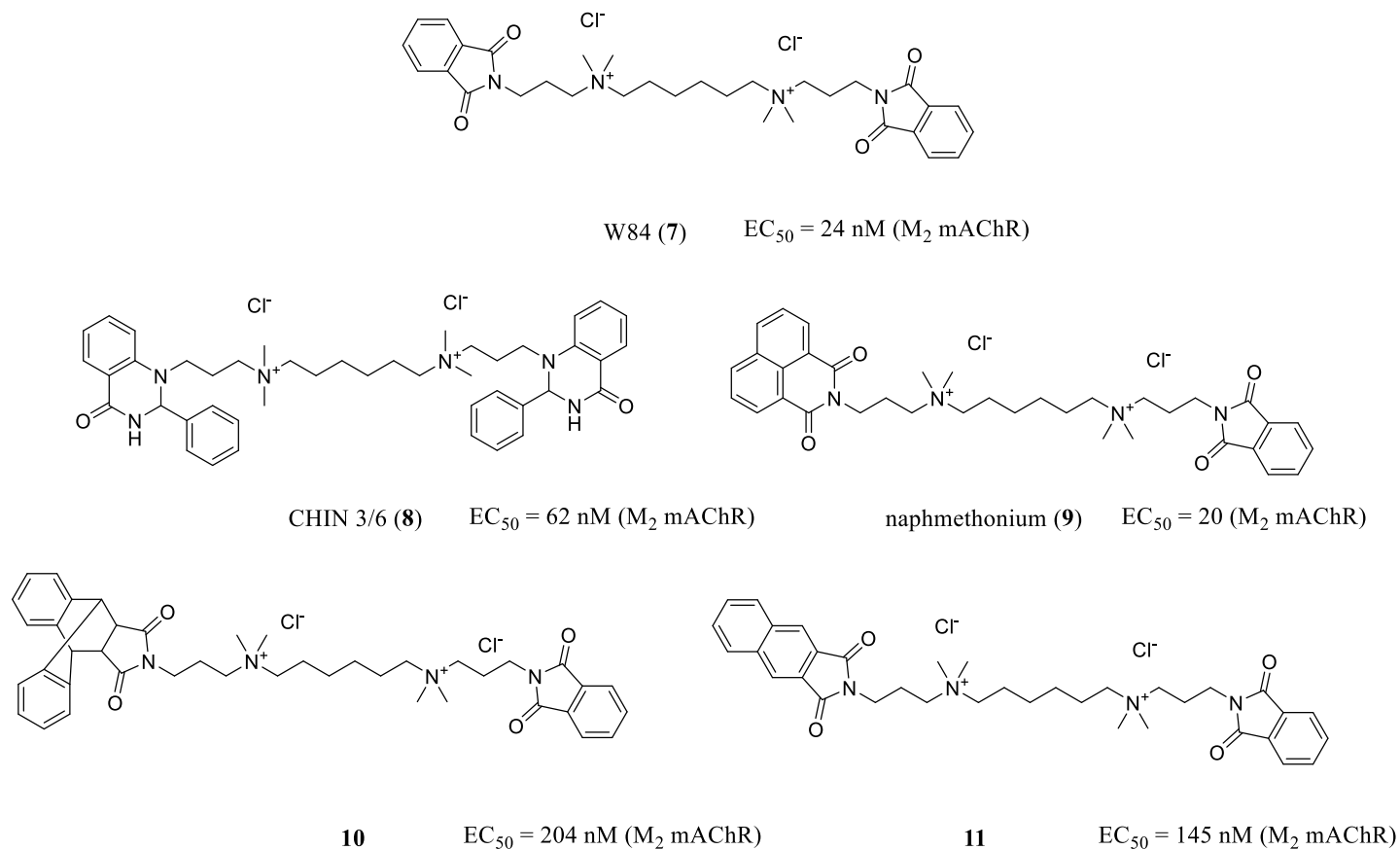
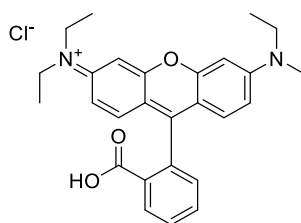


**Figure 4.** Chemical structures of compounds structurally related to C<sub>7/3</sub>-phth (6) showing the flexibility in the phthalimido ring SAR, W84 (7), CHIN 3/6 (8), naphmethonium (9), compound 10 and compound 11.  $EC_{50}$  is the allosteric potency for inhibition of the dissociation rate of [<sup>3</sup>H]NMS at the M<sub>2</sub> mAChR.<sup>27, 31-32</sup>

Another advantage of using C<sub>7/3</sub>-phth (**6**) was that it has been well characterized pharmacologically in the literature,<sup>26</sup> giving a good basis for comparison and understanding of the molecular pharmacology of our resultant C<sub>7/3</sub>-phth-based fluorescent probe. As a proof of concept design for the probe we chose the fluorophore Rhodamine B (**12**) (Figure 5) because its absorption/emission spectra are appropriate for use with eGFP-tagged receptor in FRET assays. Additionally, Rhodamine B (**12**) possesses a carboxyl group for use as a convenient attachment point to the ligand and is cheap/ readily available, and is even easily synthetically accessible from commonly available reagents.<sup>33</sup>



Rhodamine B (**12**)

**Figure 5.** Chemical structures of Rhodamine B (**12**).

High photostability and quantum yield have been noted as common in Rhodamine-based probes,<sup>34</sup> and so we deemed this fluorophore ideal for our initial proof of concept probe design. In principle, the probe was intended to be suitably versatile such that it would have potential applications in BRET and FP based assays, provided it binds allosterically to the target mAChRs with suitable affinity. One important consideration in fluorophore-tagged probe design is the attachment point of the fluorophore, the chemical structure of the linker, and length of the linker used to attach the fluorophore, all of which can dramatically affect the resultant probes physiochemical, binding and/ or other pharmacological properties.<sup>35</sup> Given the already ‘linker-

like' structure of C<sub>7/3</sub>-phth (**6**) and the demonstrated flexibility of the SAR surrounding the ring motif in structurally related analogues,<sup>36</sup> we proposed a design that incorporated the fluorophore directly into the ligand (Figure 6).

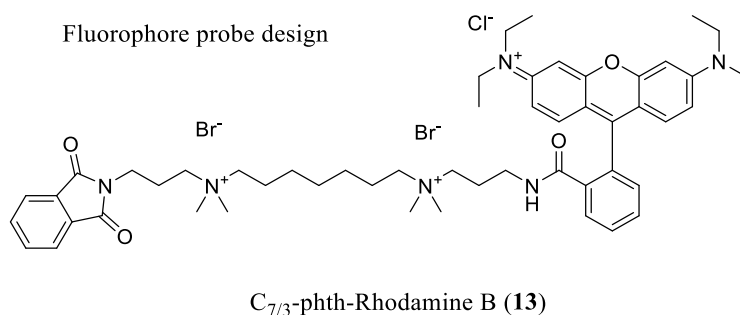


**Figure 6.** Chemical structures of our initial design of our proposed C<sub>7/3</sub>-phth based, Rhodamine B tagged mAChR allosteric probe C<sub>7/3</sub>-phth-Rhodamine B (**13**)

Incorporation of the fluorophore directly into the ligand without the addition of a linker carries the advantage that the resultant pharmacology of the probe should closely resemble that of the base ligand, limiting the potential for unexpected pharmacological properties of the probe which may limit its potential applications. The absence of a hydrophobic linker also helps to limit the hydrophobicity of the final probe, improving its solubility in aqueous assay solutions and limiting non-specific binding which can interfere with measurements made using the probe.<sup>18</sup> This approach has been successfully employed by Petrov *et al.* in the design of their CB2 cannabinoid receptor probe.<sup>37</sup> The group had previously noted flexibility in the SAR surrounding the hydrazone substituent of their base ligand, compound **14**, and managed to successfully incorporate a fluorescent 7-nitrobenzoxadiazole moiety into the ligand at this point, resulting in the probe NMP6 (**15**), which maintains good affinity and physiochemical properties relative to the parent compound (Figure 7).<sup>37-38</sup>

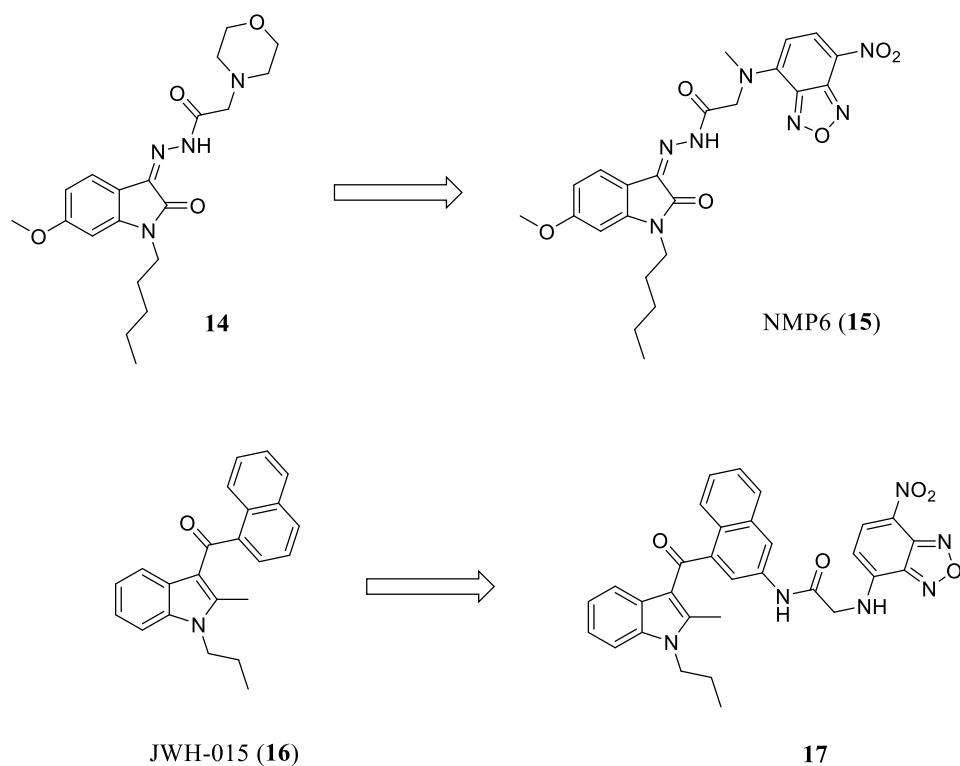


**Figure 7.** Chemical structures CB2 cannabinoid receptor ligands, compound **14** and JWH-015 (**16**) and probes derived from these ligands with the 7-nitrobenzoxadiazole fluorophore incorporated into the pharmacophore, NMP6 (**15**) and compound **17**.

However, in a similar study, looking to incorporate the same 7-nitrobenzoxadiazole moiety into the CB2 cannabinoid receptor agonist, JWH-015 (**16**), without the addition of a significant length linker, the resultant ligand exhibited a complete loss of both affinity and efficacy at the CB2 cannabinoid receptor upon addition of the fluorescent tag.<sup>39</sup> These studies highlight the importance of understanding the SAR of the base pharmacophore when designing a fluorescent probe, and illustrate that the strategy of incorporating the fluorophore directly into the pharmacophore of a ligand without the addition of a significant length linker to space the functional moieties is one of ‘high-risk/ high-reward’.

## ■ RESULTS AND DISCUSSION

**Chemistry.** Our planned synthetic approach was to utilize chemistry that had already been established for the synthesis of  $C_{7/3}$ -phth based hybrid ligands,<sup>30</sup> substituting a suitably derivatised analogue of Rhodamine B for the orthosteric pharmacophore of those hybrid ligands in the final step of the synthesis to obtain our desired fluorophore probe (Figure 8).

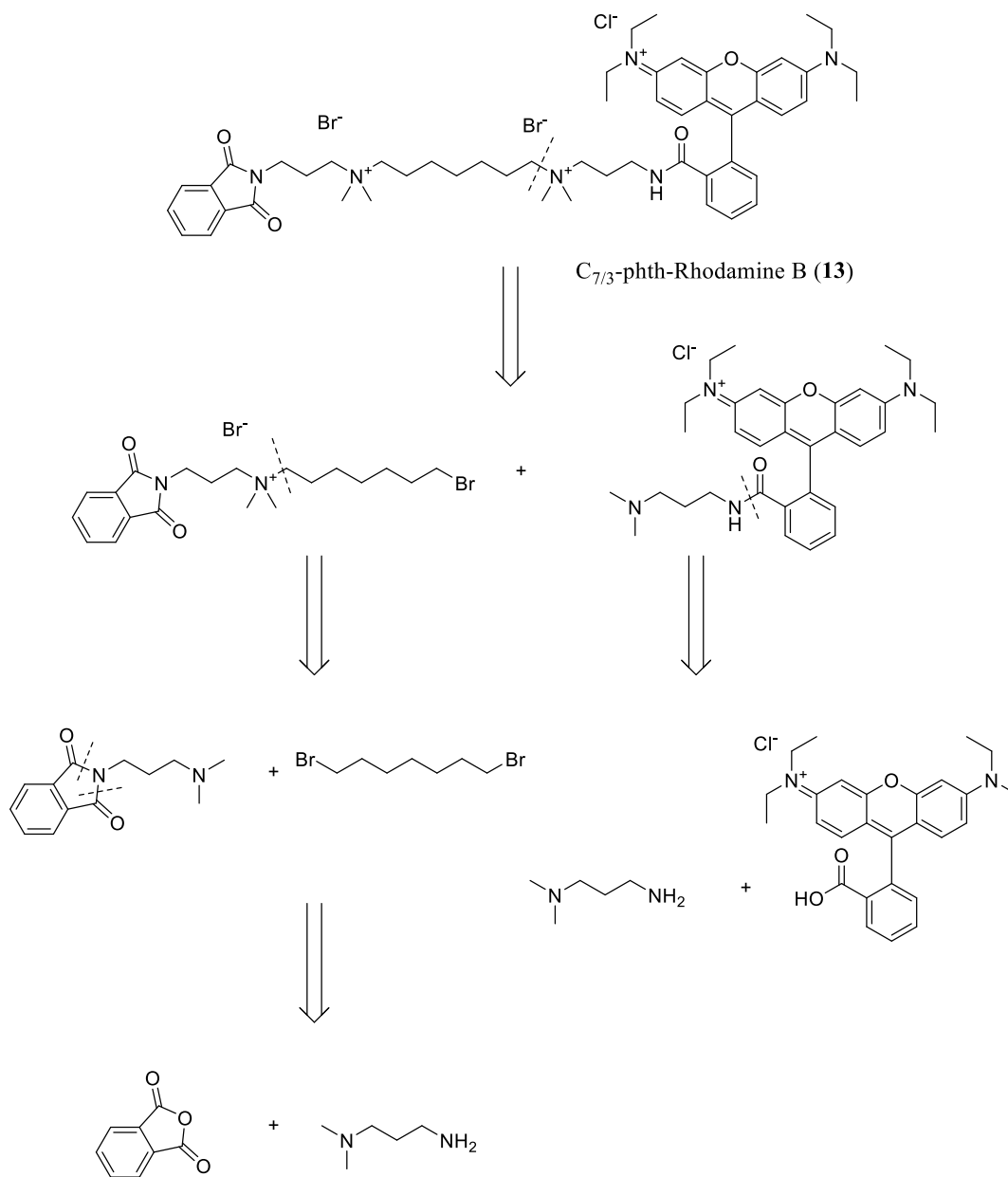
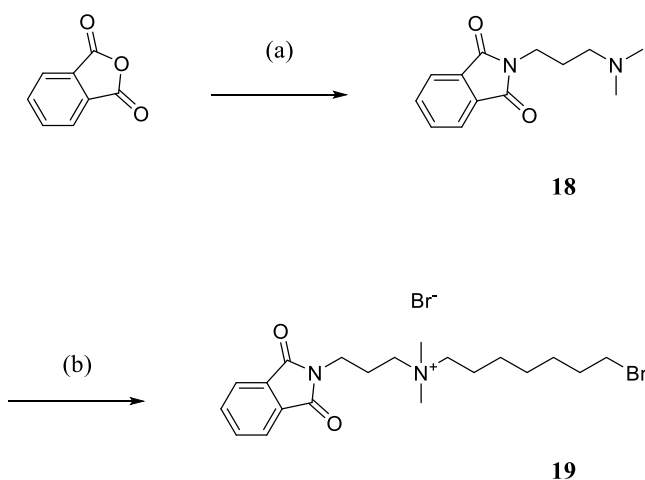


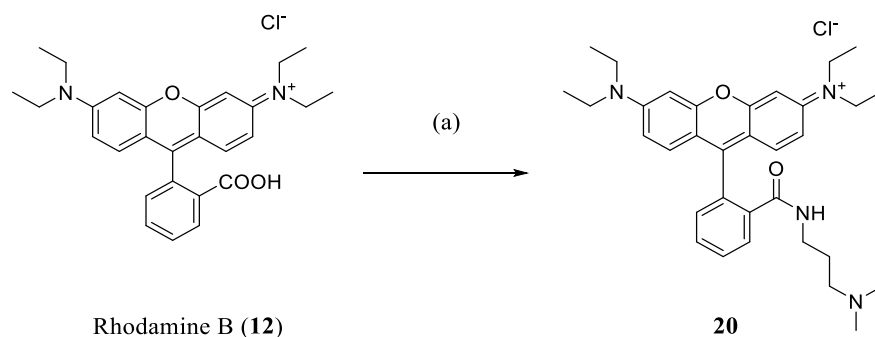
**Figure 8.** Retrosynthetic analysis of the target compound,  $C_{7/3}$ -phth-Rhodamine B (**13**).

Typically, the addition of the fluorophore is done in the final step of synthesis for probes such as this one. However, as previously mentioned, we wished to employ the well-established chemistry for related compounds to C<sub>7/3</sub>-phth (**6**) (which involves the *N*-quaternisation in the final step) to increase the likelihood of our synthesis being successful. Additionally the alternative route would require initially protecting *N*<sup>1</sup>,*N*<sup>1</sup>-dimethylpropane-1,3-diamine with Boc anhydride and subsequently deprotecting it once it was installed onto our intermediate compound, increasing the complexity of the synthesis, lowering the overall yields and limiting the ease of reproducibility of the synthesis of our probe. We synthesized compound **18** by refluxing 4 molar equivalents of phthalic anhydride and *N*<sup>1</sup>,*N*<sup>1</sup>-dimethylpropane-1,3-diamine in AcOH for 24 hours, and purifying the resultant crude mixture by flash column chromatography (FCC) on silica. Subsequently, compound **19** was synthesized according to the method described previously,<sup>27, 30, 40-41</sup> noting comparable yields, and again being purified by FCC on silica.



**Scheme 1.** Reagents and conditions: (a) *N*<sup>1</sup>,*N*<sup>1</sup>-dimethylpropane-1,3-diamine, AcOH, reflux, 24 h, 86%; (b) 1,7-dibromoheptane (neat, excess), reflux, 16 h, 67%.

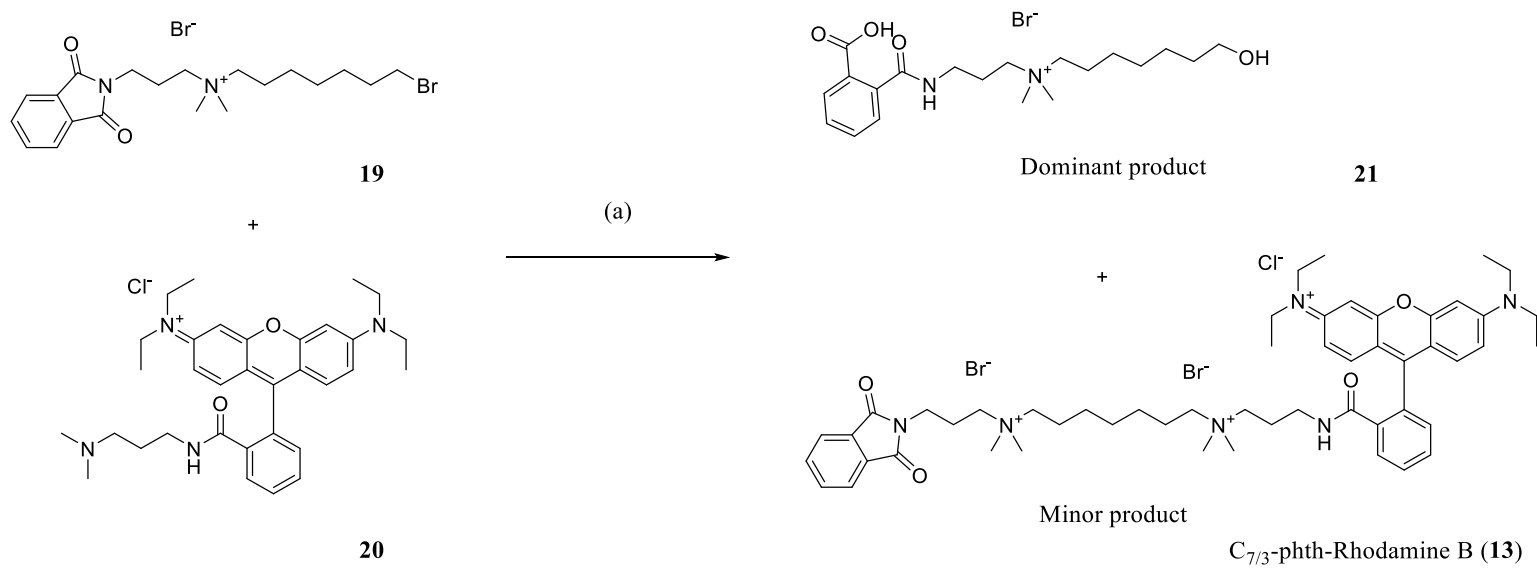
To derivatise Rhodamine B (**12**) such that it could be incorporated into our fluorophore probe via a simple substitution reaction, we synthesized compound **20** by combining *N*<sup>1</sup>,*N*<sup>1</sup>-dimethylpropane-1,3-diamine and Rhodamine B (**12**) and forming the amide using 2-(6-chloro-1-*H*-benzotriazole-1-yl)-1,1,3,3-tetramethylaminium hexafluorophosphate (HCTU) amide coupling reagent under standard conditions (Scheme 2). The crude organic mixture, containing compound **20**, was washed repeatedly with water and saturated NaHCO<sub>3</sub> solution and then separated by FCC on silica to give material of suitable purity for the following steps in the synthesis, and in moderate yields.



**Scheme 2.** Reagents and conditions: (a) *N*<sup>1</sup>,*N*<sup>1</sup>-dimethylpropane-1,3-diamine, HCTU, DIPEA, DCM:DMF (1:1), room temperature, 24 h, 46%.

The first attempt at a synthesis of C<sub>7/3</sub>-phth-Rhodamine B (**13**) was in AR grade ACN with catalytic amounts of DIPEA as the base. The procedure involved increasing the temperature from room temperature to 110 °C incrementally over 48 h, until material with a mass-to-charge ratio (*m/z*) consistent with our product, C<sub>7/3</sub>-phth-Rhodamine B (**13**), was detectable by LC-MS. Although ultimately such a species was detected by LC-MS, the yields were very low, and effective separation by FCC on silica proved to be challenging due to the large number of byproducts formed in the reaction (Scheme 3).





**Scheme 3.** Reagents and conditions: (a) DIPEA, AR grade ACN, 25 → 110 °C, 48 h, 5%.

The dominant byproduct gave a  $m/z$  ratio consistent with the fully hydrolysed starting material, compound **21**. It was thought that this hydrolysis occurred due to the presence of water in the reaction mixture in the AR grade ACN used, and the high temperatures required to promote a reaction (Scheme 3). The purified product **13** exhibited no obvious fluorescence and was a nearly clear oil (faintly pink), instead of the expected deep red of the fluorophore starting materials, Rhodamine B (**12**) and compound **20**. Analysis by  $^1\text{H}$  NMR revealed that the amide NH proton was not detected, suggesting that (as with some other Rhodamine based probes<sup>42-43</sup>) this derivative may convert to a spirolactam form under solvated conditions, which is colourless. Heating the colourless product, C<sub>7/3</sub>-phth-Rhodamine B (**13**), in concentrated hydrochloric acid solution (32% HCl w/w) produced a red precipitate which was separated by filtration, and returned to colourless upon dissolution in MeOH. We expect that the red precipitate and colourless appearances of the material (upon dissolution in MeOH) are the ring opened (amide) and ring closed (spirolactam) derivatives of our desired product, respectively (Figure 9).

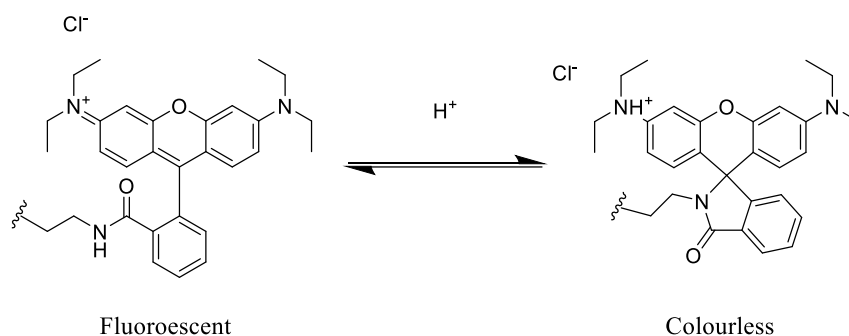


**Figure 9.** Equilibrium reaction showing the proposed ring-opened (fluorescent) and spirolactam (colourless) forms of compound **13**.

This raises the question as to why compound **20** did not similarly lose fluorescence upon addition of the linker moiety. One possible explanation is that in compound **13** the nearby quaternised amine has an electron withdrawing effect on the amide nitrogen, stabilizing the deprotonated state and facilitating cyclisation of the spirolactone. Alternatively, the presence

of the positive charge in the quaternary compound **13** stabilises the negatively charged deprotonated amide, which again facilitates cyclisation. To overcome this issue, we redesigned the ligand to incorporate a Rhodamine-based fluorophore which is attached at the 4-position of its phenyl ring, Lissamine B (**22**), excluding the formation of the spirolactam (Figure 10). The only noteworthy drawback of this solution is that Lissamine B (**22**) is approximately 10 times more expensive than Rhodamine B (**12**). However as with Rhodamine B (**12**), Lissamine B shows good spectral overlap with the eGFP protein, and so is practically a good alternative.<sup>22</sup> An alternative solution, in which the cheaper and more commonly available Rhodamine B (**12**) may still be used, is to make the *N*-methylated derivative, compound **24**, which would also preclude spirolacem formation, and this could be explored in future work (Figure 10).

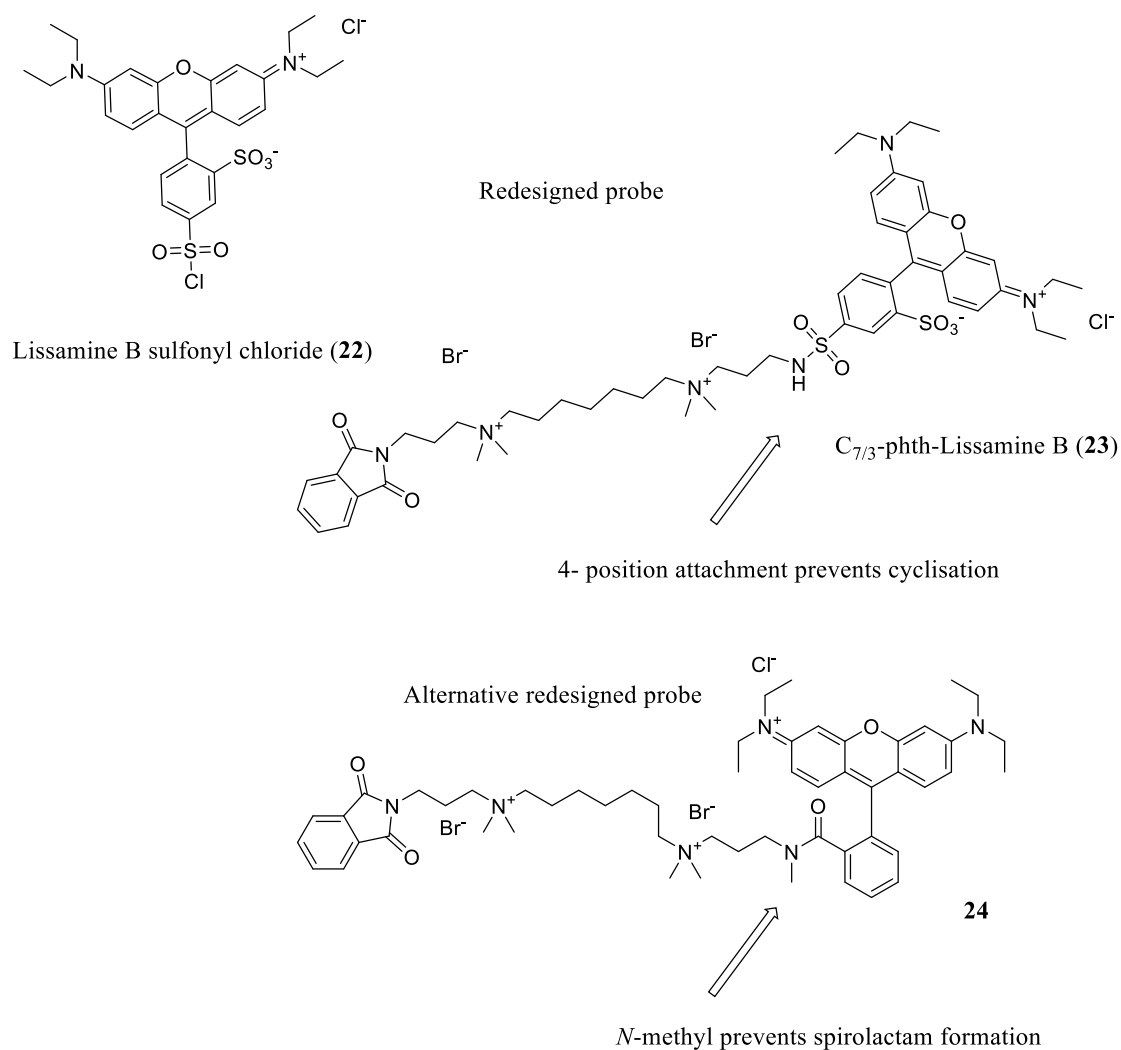
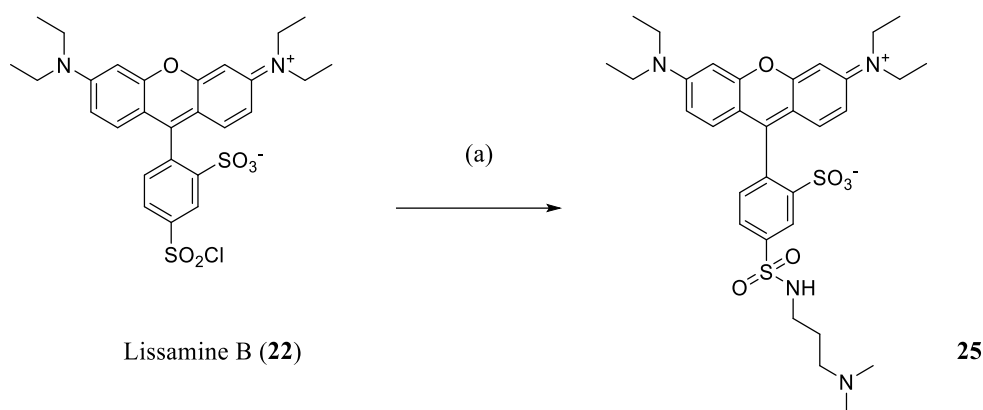


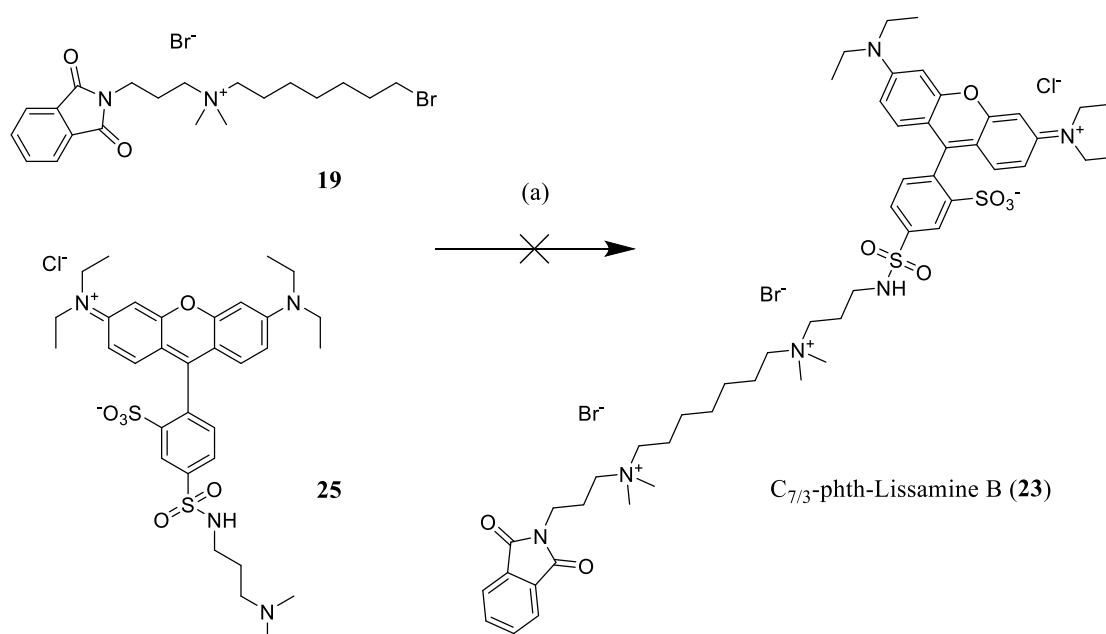
**Figure 10.** Chemical structures of Lissamine B sulfonyl chloride (**22**), our redesigned fluorophore probe, C<sub>7/3</sub>-phth-Lissamine B (**23**) and a potential alternate *N*-methylated design, incorporating Rhodamine B, compound **24**.

The *N*<sup>1</sup>,*N*<sup>1</sup>-dimethylpropane-1,3-diamine linker was attached to the fluorophore, Lissamine B sulfonyl chloride (**22**), by combining the two materials in anhydrous ACN with base and stirring at room temperature for 1 hour (Scheme 4). The reaction was monitored by TLC and, upon completion, the product **25** was isolated by liquid-liquid extraction and aqueous washings. This gave compound **25** in high yields and to a purity sufficient for the subsequent synthetic steps.



**Scheme 4.** Reagents and conditions: (a)  $N^1,N^1$ -dimethylpropane-1,3-diamine, DIPEA, anhydrous ACN, room temperature, 1 h, 89%.

To avoid the significant hydrolysis of the bromide starting material, compound **19**, which we had been observed previously in the synthesis of  $C_{7/3}$ -phth-Rhodamine B (**13**), we used anhydrous ACN as the solvent for the first attempt at the synthesis of  $C_{7/3}$ -phth-Lissamine B (**23**) and once again incrementally increased the temperature over the course of the experiment, with regular monitoring by LC-MS. However, in this case no product formed, even after several days and heating as high as 160 °C in a sealed tube (Scheme 5).



**Scheme 5.** Reagents and conditions: (a) AR grade or anhydrous ACN/ AR grade or anhydrous DMF/ AR grade DMSO, DIPEA, 25  $\rightarrow$  160 °C, 72 h, no reaction.

We repeated the experiment in several different polar aprotic solvent systems including AR grade ACN, AR grade and anhydrous DMF and AR grade DMSO, but no product was detected by LC-MS in any of our experiments (Scheme 5). Since we were unable to produce any detectable product by the aforementioned method, we sought out an alternative synthetic pathway to achieve our title compound, C<sub>7/3</sub>-phth-Lissamine B (**23**). When synthesising the radiolabelled derivative of dimethyl-W84 (**2**), Tränkle *et al.* synthesised a tertiary amine intermediate first, such that the tritium labelled methyl groups could be installed in the final step.<sup>14</sup> In light of this we tried synthesizing the target compound, C<sub>7/3</sub>-phth-Lissamine B (**23**), via a different route which avoided the direct *N*-quaternisation of compound **25** with compound **19**, instead first substituting the bromine of compound **19** with *N*-methylamine first, and then reacting this intermediate, compound **26**, with the bromide derivative of compound **25**, (compound **27**), and finally *N*-quaternising the tertiary amine intermediate **28** with methyl iodide to form our target compound, C<sub>7/3</sub>-phth-Lissamine B (**23**) (Figure 11).

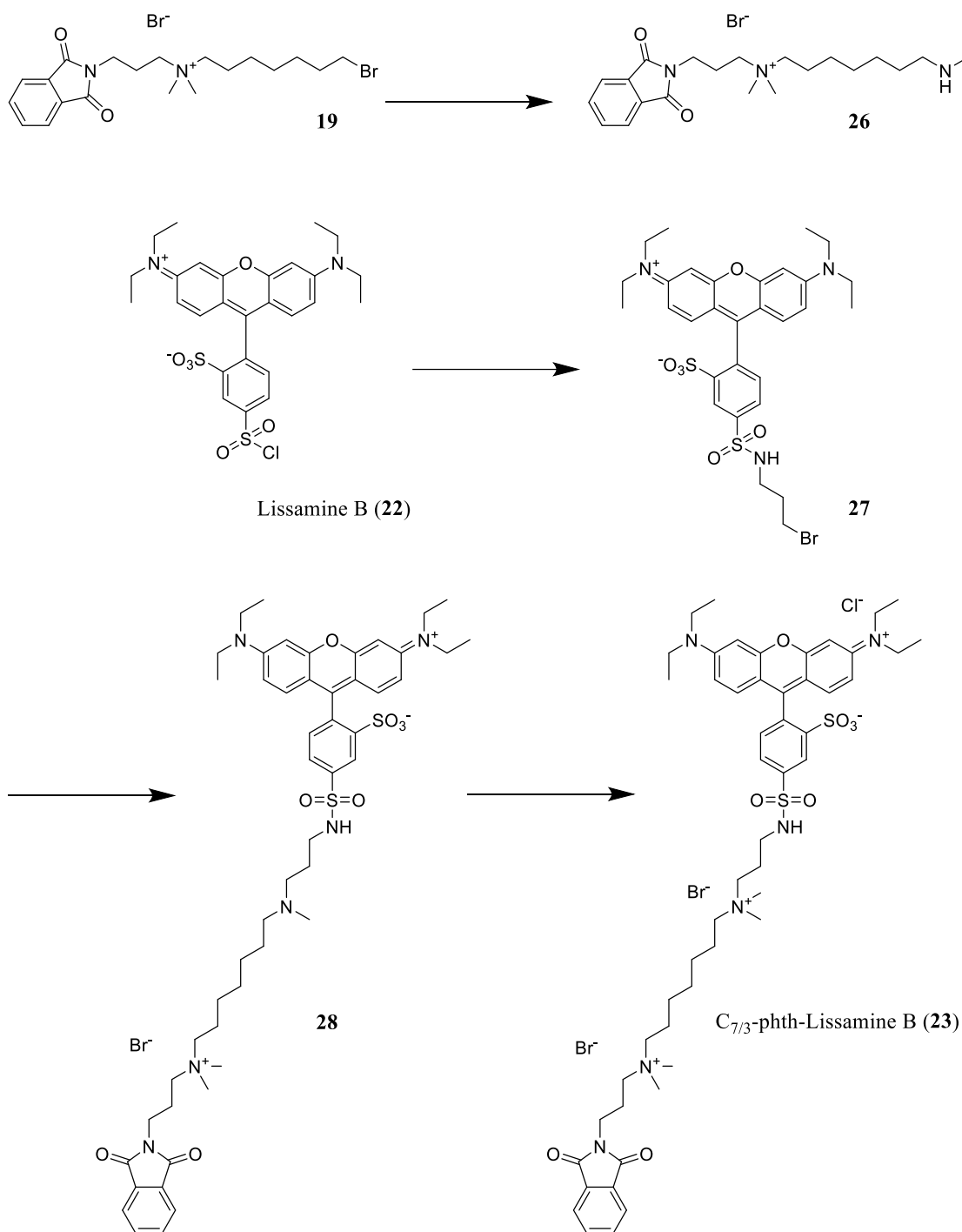
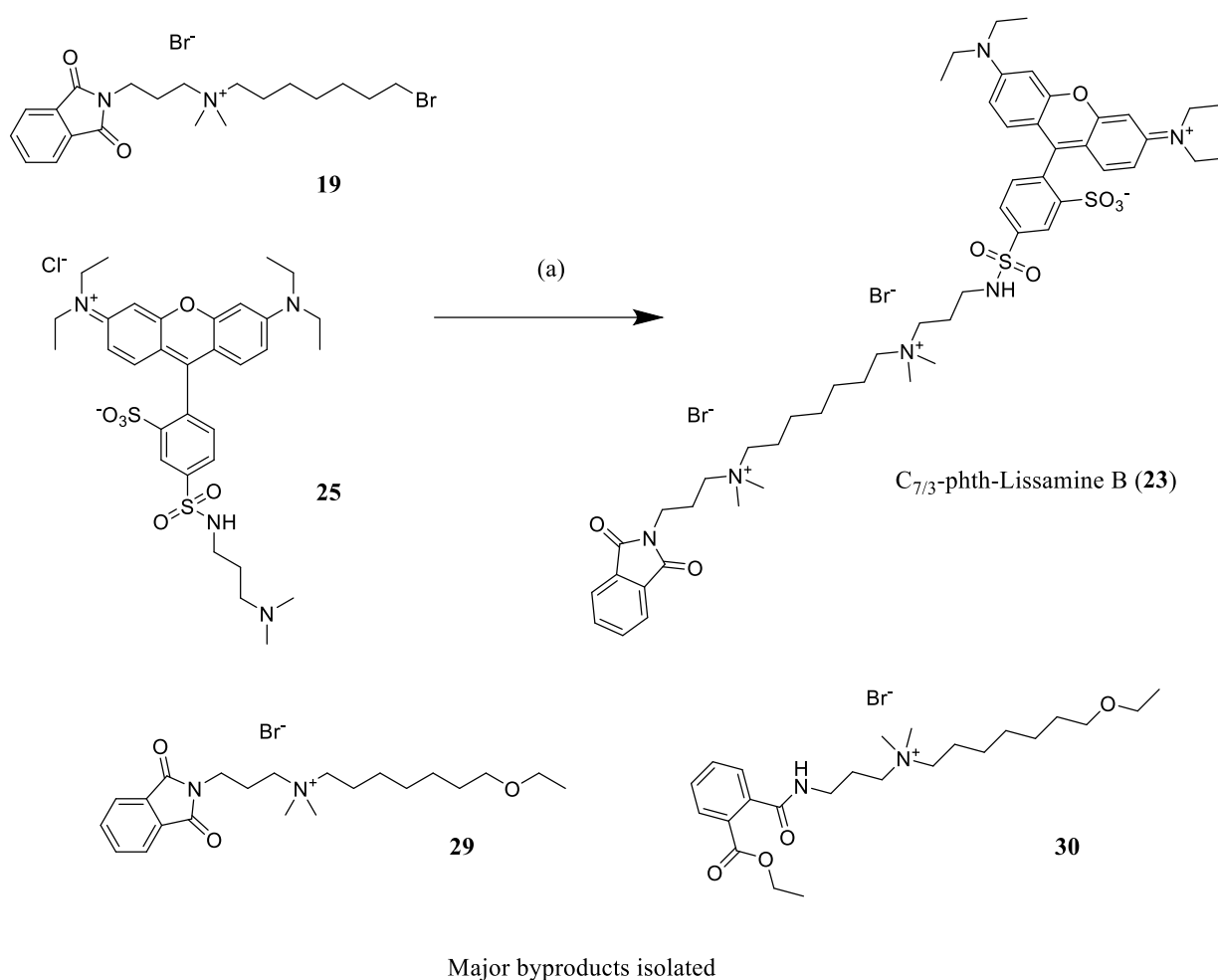


**Figure 11.** Proposed alternate route to the synthesis of C<sub>7/3</sub>-phth-Lissamine B (23).

However, experiments reacting compound **19** with *N*-methylamine with base in ACN or DMF again yielded no detectable product by LC-MS and only byproducts were isolated. Finally, having had no success with aprotic solvents we decided to attempt the reaction again, this time with the polar protic solvent EtOH (Scheme 6), which we had initially avoided

because of the potential for nucleophilic attack of the solvent towards our starting material, compound **19**. As expected, the dominant materials recovered were the mono- and diethoxylated byproducts, **29** and **30**, however a small amount of the target compound, C<sub>7/3</sub>-phth-Lissamine B (**23**), was also produced, along with many other minor byproducts as indicated by LC-MS and HPLC analysis (Scheme 6).



**Scheme 6.** Reagents and conditions: (a) DIPEA, EtOH, 160 °C, 72 h, 4 – 7 %.

This experiment was repeated twice more to ensure its reproducibility and the crude mixtures were separated by up to five iterative purifications on preparative HPLC, to afford the title compound C<sub>7/3</sub>-phth-Lisaamine B (**23**) in yields ranging from 4 - 7%. Although



typically a purity of greater than 95 % is acceptable for a test compound, here we have set the acceptable purity to greater than 99 %. We believed that such extensive purification was necessary to remove other minor, presumably structurally related, fluorescent byproducts, as their presence would decrease the signal-to-noise ratio of the final ligand in assay. The low yields in our experiments are most likely due to the high formation of byproduct as a result of the choice of solvent and temperature, which were both unfortunately necessary for obtaining the desired compound. However, it has also been shown that solvents such as ethylene carbonate, can also be used in the synthesis of di-cationic compounds related to C<sub>7/3</sub>-phth.<sup>44</sup> This approach may also be applicable to the synthesis of C<sub>7/3</sub>-phth-Lissamine B (**23**) to improve yields and to minimize byproduct formation associated with the use of a protic/ nucleophilic solvent such as EtOH. Future work will involve exploring ethylene carbonate and other solvent systems in the reaction of compounds **19** and **25**, in an attempt to improve yields and limit byproduct formation, for purpose of improving efficiency and ease of separation of the target compound, C<sub>7/3</sub>-phth-Lissamine B (**23**).

**Pharmacology.** C<sub>7/3</sub>-phth-Lissamine B (**23**) was first evaluated at the eGFP-tagged M<sub>2</sub> mAChR by competition and dissociation kinetics binding assays, to determine whether it retained the allosteric affinity and cooperativity of the parent ligand, C<sub>7/3</sub>-phth (**6**) (Figure 12).

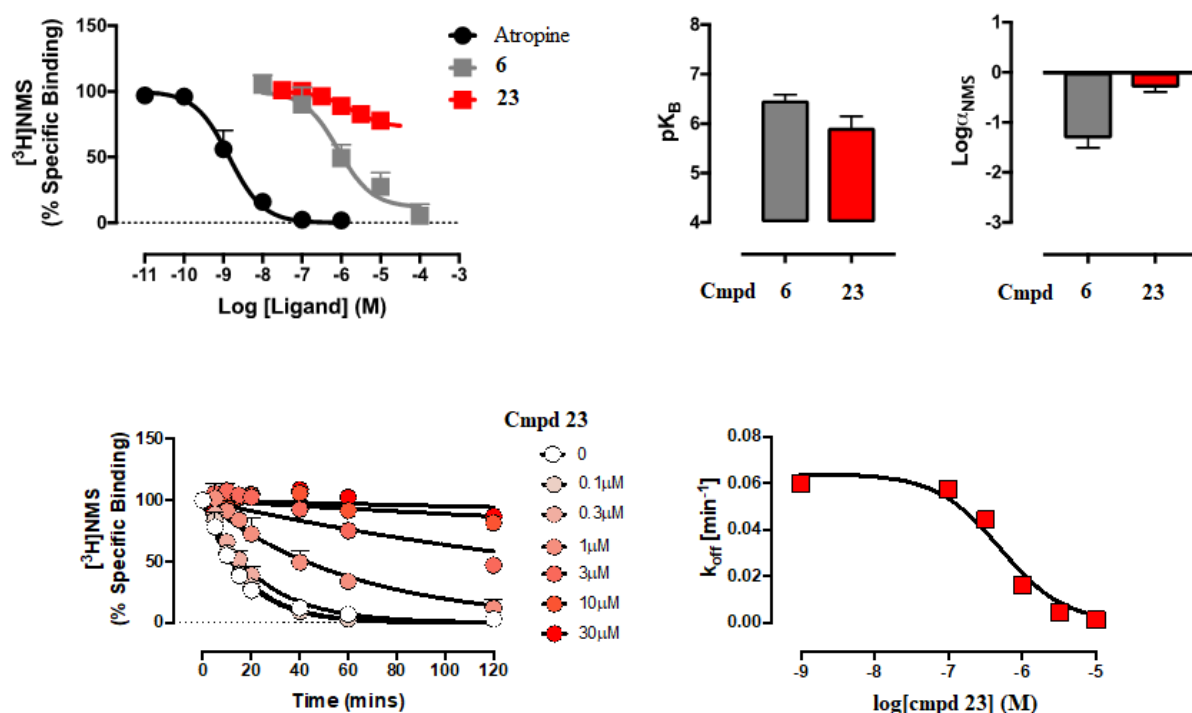


**Figure 12.** Radioligand binding experiments on Flp-In-CHO cells over expressing the eGFP-M<sub>2</sub> mAChR, assessing the competition binding and dissociation kinetics of [<sup>3</sup>H]NMS in the presence of increasing concentrations of C<sub>7/3</sub>-phth-Lissamine B (**23**) and C<sub>7/3</sub>-phth (**6**). (Top left) shows the inhibition of [<sup>3</sup>H]NMS binding by C<sub>7/3</sub>-phth-Lissamine B (**23**), C<sub>7/3</sub>-phth (**6**) and atropine as a control. (Top right) shows the comparison of allosteric affinity (pK<sub>B</sub>) and cooperativity with [<sup>3</sup>H]NMS (log α<sub>NMS</sub>) as determined from the competition binding experiments. (Bottom left) shows the dissociation of [<sup>3</sup>H]NMS over time (mins) in the presence of increasing concentrations of C<sub>7/3</sub>-phth-Lissamine B (**23**). (Bottom right) shows the change in the dissociation rate constant (k<sub>off</sub>) of [<sup>3</sup>H]NMS in the presence of increasing concentrations of C<sub>7/3</sub>-phth-Lissamine B (**23**). All data was analysed using the GraphPad 7 software. Data represent the mean ± S.E. of three independent experiments performed in duplicate.

The competition binding assays revealed that C<sub>7/3</sub>-phth-Lissamine B (**23**) partially displaces [<sup>3</sup>H]NMS from the eGFP-M<sub>2</sub> mAChR indicative of an allosteric modulator (Figure 12, top left), however did so with reduced cooperativity (log α) compared with the parent ligand (C<sub>7/3</sub>-phth) (Figure 9, top right). The affinity of C<sub>7/3</sub>-phth-Lissamine B (**23**) (pK<sub>B</sub> = 5.92 ± 0.23) was apparently reduced compared to C<sub>7/3</sub>-phth (**6**) (pK<sub>B</sub> = 6.47 ± 0.11) but not so much as to make the probe an unviable tool (Figure 9, top right). However, dissociation kinetic binding assays confirmed that C<sub>7/3</sub>-phth-Lissamine B (**23**) retains some negative cooperativity with [<sup>3</sup>H]NMS, strongly suggesting that it interacts allosterically with the eGFP-M<sub>2</sub> mAChR and

with micromolar affinity, comparable to the parent ligand, C<sub>7/3</sub>-phth (**6**) (Figure 12, top left). To independently verify the allosteric affinity and binding mode of C<sub>7/3</sub>-phth-Lissamine B (**23**) (indicated by the competition and kinetic binding assays) interaction radioligand binding experiments were performed with both C<sub>7/3</sub>-phth (**6**) and atropine, on Flp-In-CHO cells over expressing the eGFP-tagged M<sub>2</sub> mAChR (Figure 13).

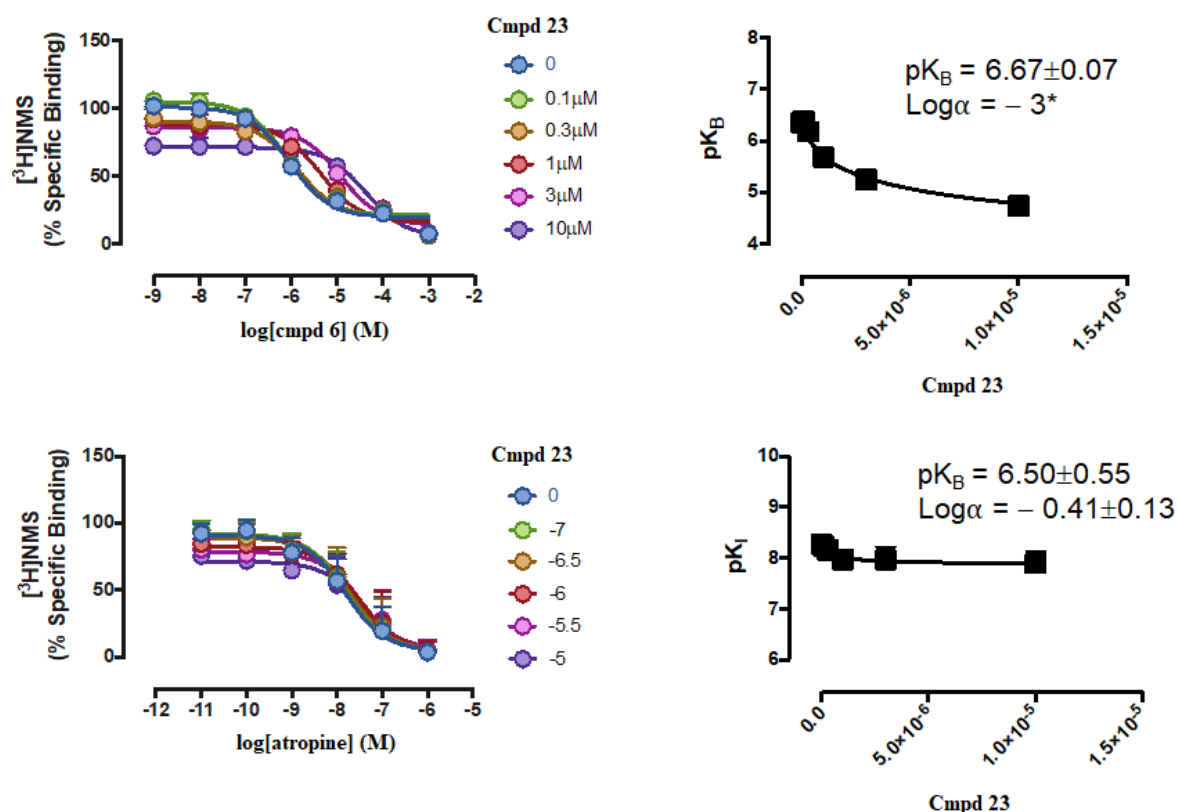


**Figure 13.** Interaction radioligand binding experiments on Flp-In-CHO cells over expressing the eGFP-tagged M<sub>2</sub> mAChR, interacting [<sup>3</sup>H]NMS, C<sub>7/3</sub>-phth-Lissamine B (**23**) and either C<sub>7/3</sub>-phth (**6**) or atropine. (Top left) shows the competition binding curves of [<sup>3</sup>H]NMS, and C<sub>7/3</sub>-phth (**6**) in the presence of increasing concentrations of C<sub>7/3</sub>-phth-Lissamine B (**23**). (Top right) shows a plot of how the allosteric affinity (pK<sub>B</sub>) of C<sub>7/3</sub>-phth (**6**) changes in response to increasing concentrations of C<sub>7/3</sub>-phth-Lissamine B (**23**). (Bottom left) shows the competition binding curves of [<sup>3</sup>H]NMS, and atropine in the presence of increasing concentrations of C<sub>7/3</sub>-phth-Lissamine B (**23**). (Bottom right) shows a plot of how the affinity (pK<sub>i</sub>) of atropine changes in response to increasing concentrations of C<sub>7/3</sub>-phth-Lissamine B (**23**). All data was analysed using the GraphPad 7 software. Data represent the mean ± S. E. of three independent experiments performed in duplicate.

The data shows that C<sub>7/3</sub>-phth-Lissamine B (**23**) was able to displace C<sub>7/3</sub>-phth (**6**) in a concentration dependent manner (Figure 13, top left, top right), indicating that the two ligands likely compete for a common (allosteric) site. Additionally, no evidence for direct competition with the orthosteric ligand atropine was found (Figure 13, bottom left, bottom right). As for [<sup>3</sup>H]NMS the cooperativity of C<sub>7/3</sub>-phth-Lissamine B (**23**) with atropine was found to be low (Figure 13, bottom right). Although this suggests that C<sub>7/3</sub>-phth-Lissamine B (**23**) has lost some of its allosteric modulator characteristics, this property of cooperativity is less important for the intended use of C<sub>7/3</sub>-phth-Lissamine B (**23**) as an allosteric probe than its affinity for the allosteric site (Figure 13). In fact, an allosteric probe which exhibits neutral cooperativity may even be beneficial as it decreases the likelihood of probe dependence-like interactions with other ligands. Experiments competing C<sub>7/3</sub>-phth-Lissamine B (**23**) with [<sup>3</sup>H]NMS indicated that C<sub>7/3</sub>-phth-Lissamine B (**23**) had lower affinity compared with C<sub>7/3</sub>-phth (**6**) (Figure 12). However experiments interacting C<sub>7/3</sub>-phth (**6**) and C<sub>7/3</sub>-phth-Lissamine B (**23**) reveal a more precise measurement, showing that the affinity of both ligands are similar (Figure 13). This most likely arose due to the low cooperativity of C<sub>7/3</sub>-phth-Lissamine B (**23**) and [<sup>3</sup>H]NMS, resulting in high error in the initial measurements of affinity (Figure 12). To evaluate any probe dependency phenomena which may bias our measurements of allosteric affinity, we then evaluated C<sub>7/3</sub>-phth-Lissamine B (**23**) in similar interaction assays as before, this time employing the orthosteric agonist iperoxo (IXO) and PG 1000 (Figure 14). The structure of PG 1000 has not been disclosed, however it behaves as an M<sub>2</sub> mAChR selective antagonist in assays.

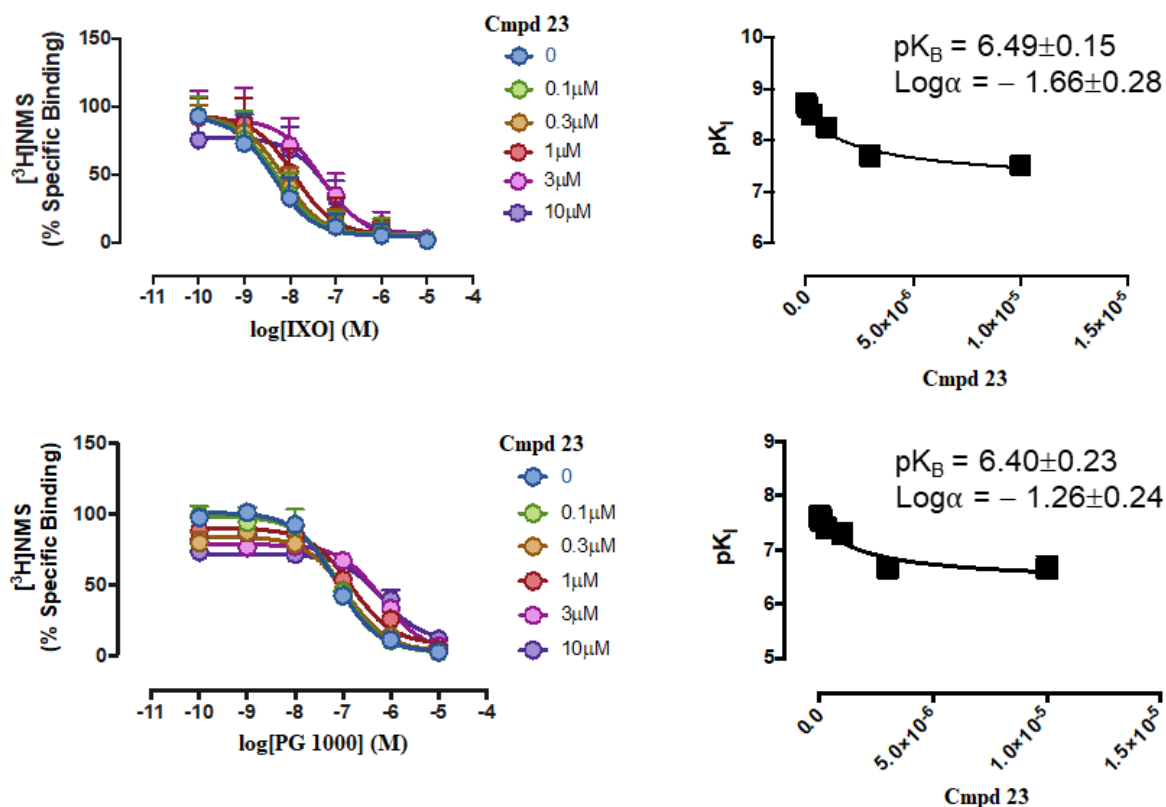


**Figure 14.** Interaction radioligand binding experiments on Flp-In-CHO cells over expressing the eGFP-tagged M<sub>2</sub> mAChR, interacting [<sup>3</sup>H]NMS, C<sub>7/3</sub>-phth-Lissamine B (**23**) and either iperexo (IXO) or PG 1000. (Top left) shows the competition binding curves of [<sup>3</sup>H]NMS, and iperexo (IXO) in the presence of increasing concentrations of C<sub>7/3</sub>-phth-Lissamine B (**23**). (Top right) shows a plot of how the allosteric affinity (pK<sub>i</sub>) of iperexo (IXO) changes in response to increasing concentrations of C<sub>7/3</sub>-phth-Lissamine B (**23**). (Bottom left) shows the competition binding curves of [<sup>3</sup>H]NMS, and PG 1000 in the presence of increasing concentrations of C<sub>7/3</sub>-phth-Lissamine B (**23**). (Bottom right) shows a plot of how the affinity (pK<sub>i</sub>) of PG 1000 changes in response to increasing concentrations of C<sub>7/3</sub>-phth-Lissamine B (**23**). All data was analysed using the GraphPad 7 software. Data represent the mean ± S. E. of three independent experiments performed in duplicate.

C<sub>7/3</sub>-phth-Lissamine B (**23**) was found to partially inhibit the binding of the orthosteric agonists, iperexo and PG 1000, in a concentration dependent manner (Figure 14, top left, top right, bottom left, bottom right), further suggesting that C<sub>7/3</sub>-phth-Lissamine B (**23**) behaves as a weak NAM, which induces an inactive conformation in the eGFP-tagged M<sub>2</sub> mAChR. As with the competitive and dissociation kinetics assays (Figure 12), and the interaction radioligand binding experiments performed with antagonists (Figure 13), the interaction radioligand binding experiments with agonists (Figure 14) indicated that C<sub>7/3</sub>-phth-Lissamine

B (**23**) had an affinity for the eGFP-M<sub>2</sub> mAChR of approximately 1  $\mu$ M. With these experiments we were able to rule out probe dependence as a bias in our affinity measurements for C<sub>7/3</sub>-phth-Lissamine B (**23**) and confirm that it appears to maintain good allosteric affinity for the eGFP-tagged M<sub>2</sub> mAChR, relative to the parent ligand, C<sub>7/3</sub>-phth (**6**) (Figure 12). Having established the allosteric binding mode of C<sub>7/3</sub>-phth-Lissamine B (**23**) it was then subjected to assay by confocal microscopy to evaluate its effectiveness as an allosteric probe (Figure 15).

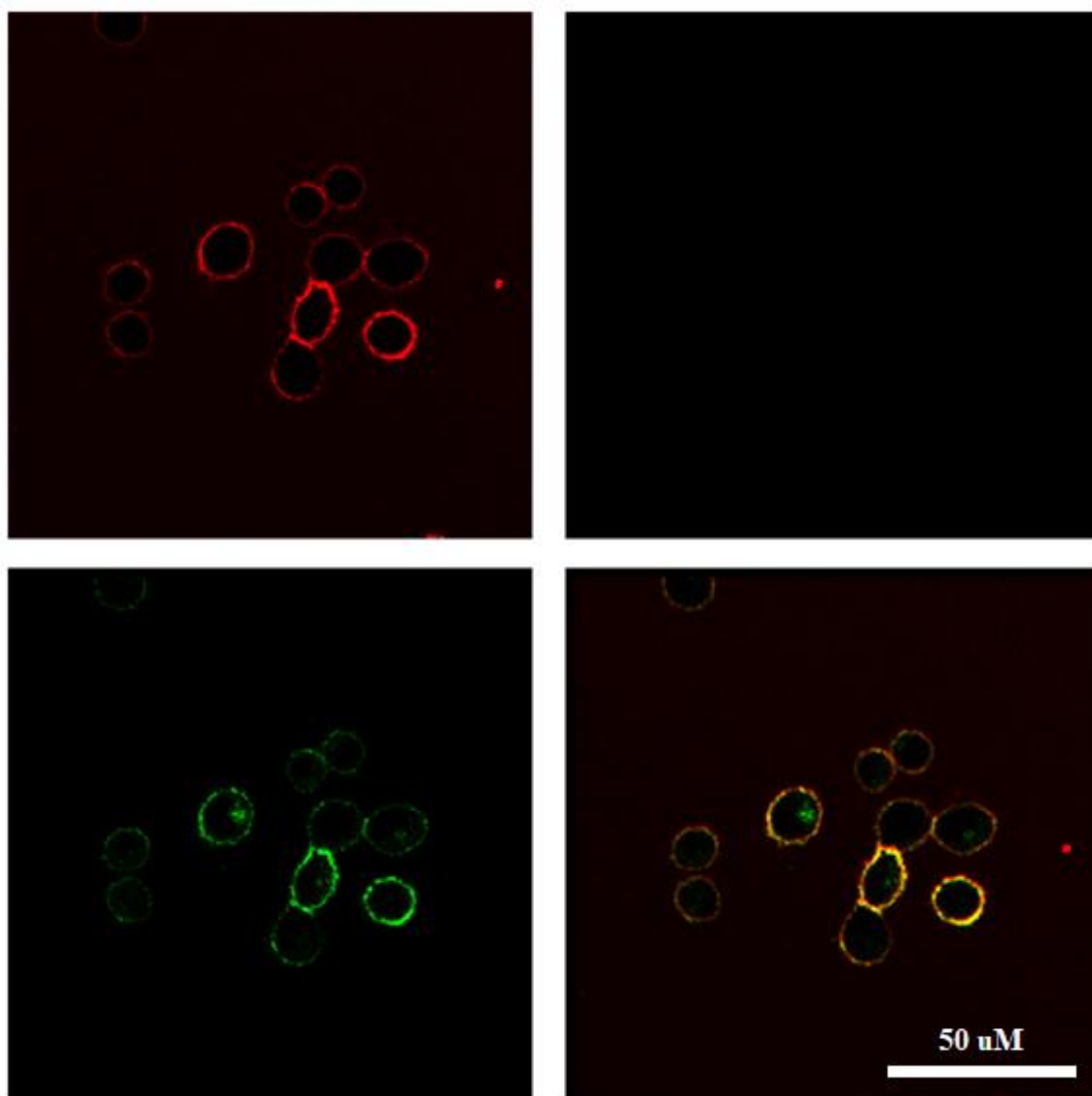


**Figure 15.** Image taken from a representative confocal microscopy experiment. (Top left) shows the red channel which shows the fluorescent probe, C<sub>7/3</sub>-phth-Lissamine B (**23**). (Top right) shows the blank channel. (Bottom left) shows the green channel in which the eGFP-tagged M<sub>2</sub> mAChR can be seen. (Bottom right) shows the overlay of the red and green channels. Expression of eGFP—M<sub>2</sub> mAChRs was found to be ~ 90 000 receptors per cell by saturation radioligand binding. Concentration of C<sub>7/3</sub>-phth-Lissamine B (**23**) used was 1 μM. All experiments were performed at room temperature and images were taken live, before during and after addition of C<sub>7/3</sub>-phth-Lissamine B (**23**). The images above were taken immediately after addition of C<sub>7/3</sub>-phth-Lissamine B (**23**).

Encouragingly, in the red channel  $C_{7/3}$ -phth-Lissamine B (**23**) can be seen localizing to the cell membranes of the eGFP-M<sub>2</sub> mAChR expressing CHO cells (Figure 15, top left). The surrounding solution presents with a faint general fluorescence, possibly due to minor, non-binding, fluorescent impurities in the sample of  $C_{7/3}$ -phth-Lissamine B (**23**), but could also be simply due to free, unbound  $C_{7/3}$ -phth-Lissamine B (**23**) in solution. Despite this a good signal-to-noise ratio was obtained and so a wash-out was not performed as it was unnecessary. The green channel shows the eGFP-tagged receptors, generally distributed around the cell membranes as expected, however some receptors can be seen internalized inside the cells due to receptor trafficking (Figure 15, bottom left). The overlay of both channels shows that, as expected,  $C_{7/3}$ -phth-Lissamine B (**23**) appears to co-localise with the eGFP-M<sub>2</sub> mAChRs around the cell membranes, resulting in the yellow colour seen in the confocal microscopy image (Figure 15, bottom right). Furthermore, this co-localisation is not seen in the internalized receptors, suggesting that very little if any  $C_{7/3}$ -phth-Lissamine B (**23**) is internalized with receptors over the timescale of the assay. Finally, we wished to examine the binding kinetics of  $C_{7/3}$ -phth-Lissamine B (**23**) at the eGFP-tagged M<sub>2</sub> mAChRs by confocal microscopy and confirm that the values obtained were consistent with the binding and kinetic measurements made using radioligand binding techniques performed previously (Figure 16).



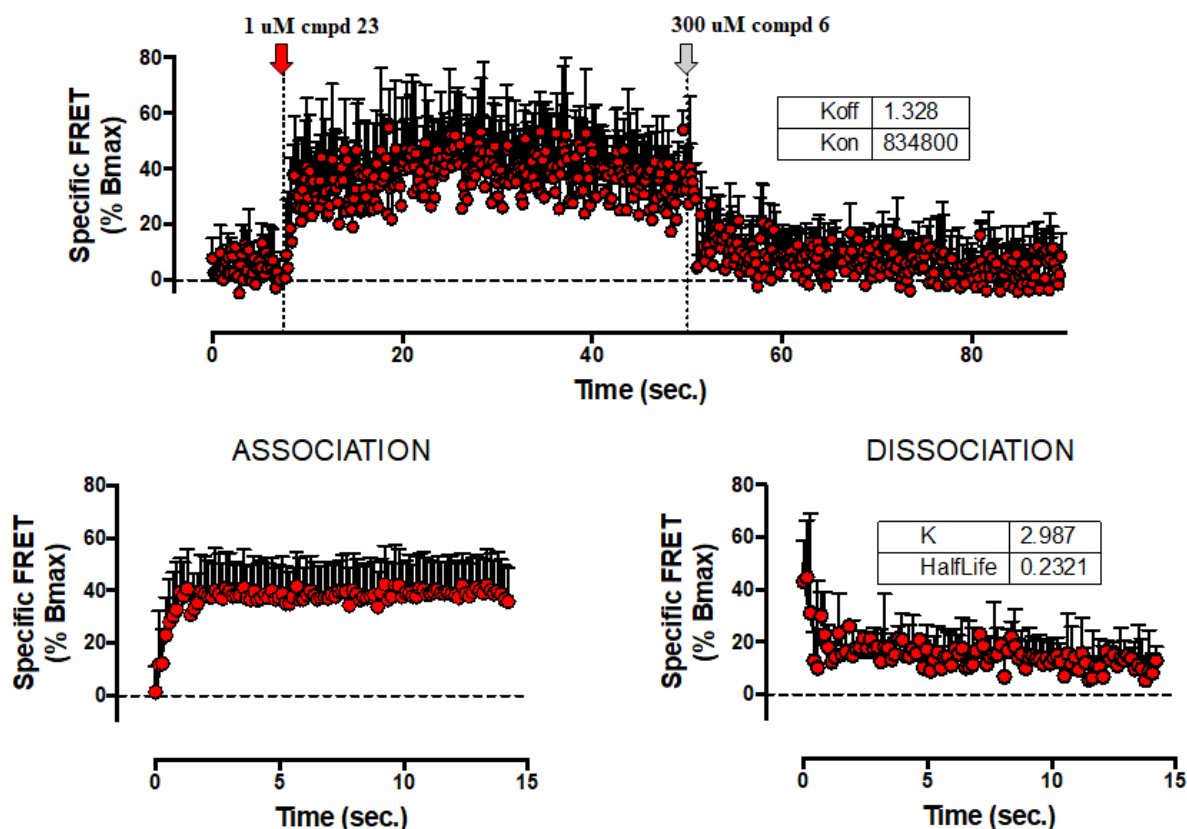


**Figure 16.** Representative experiment of real-time confocal microscopy data analyzing the change in FRET signal at a signal point on the membrane of a Flp-In-CHO cell expressing the eGFP-tagged M<sub>2</sub> mAChR in the presence of C<sub>7/3</sub>-phth-Lissamine B (**23**). (Top) shows the full duration of a kinetic experiment in which 1 μM of C<sub>7/3</sub>-phth-Lissamine B (**23**) is added initially, until association has to come to equilibrium, before adding a saturating concentration (300 μM) of unlabeled C<sub>7/3</sub>-phth (**6**) to induce dissociation. (Bottom left) shows the association phase of C<sub>7/3</sub>-phth-Lissamine B (**23**) binding in isolation for clarity. (Bottom right) shows the dissociation phase of C<sub>7/3</sub>-phth-Lissamine B (**23**) in isolation for clarity.

Real-time confocal microscopy experiments analyzing the change in FRET signal at a point on the cell membrane show that C<sub>7/3</sub>-phth-Lissamine B (**23**) displays fast on and fast off rate kinetics, suggesting that (as expected for an allosteric interaction) the energy of binding and unbinding is relatively low (Figure 16, top). These kinetic FRET experiments also demonstrate that C<sub>7/3</sub>-phth-Lissamine B (**23**) is completely displaced by the parent ligand within the error margins of the assay, C<sub>7/3</sub>-phth (**6**) (Figure 16, top, bottom right), again (as for the radioligand interaction binding data) suggesting that both ligands compete for a common binding site. The affinity for C<sub>7/3</sub>-phth-Lissamine B (**23**) as calculated from the  $k_{on}$  and  $k_{off}$

values from the FRET assays (Figure 16, bottom left) comes out as  $pK_B \sim 5.8$ , which is comparable to the estimated affinity values from the radioligand binding assays of  $pK_B \sim 6.4$  (Figure 12, Figure 13, Figure 14). This good agreement between the affinity values measured from equilibrium and non-equilibrium experiments implies that the nature of ligand binding for C<sub>7/3</sub>-phth-Lissamine B (**23**) is specific. If non-specific binding were occurring the dissociation rate would be artificially decreased in the non-equilibrium assays (and potentially the dissociation curve biphasic) due to some ligand dissociating from the receptor and some from the membrane in tandem. Hence, the calculated affinity from the non-equilibrium experiments would not agree with the equilibrium radioligand binding affinity. However, we found good agreement between the two assays, hence no evidence for non-specific binding. In combination with the radioligand binding data previously discussed these FRET results give a good indication of that C<sub>7/3</sub>-phth-Lissamine B (**23**) behaves as intended as a mAChR allosteric probe and, in conjunction with the eGFP-tagged M<sub>2</sub> mAChR CHO cell line, will be useful a useful tool for the direct measurement of allosteric binding affinity and kinetics of mAChR allosteric ligands.

## ■ CONCLUSIONS

In this chapter we have designed, synthesized and evaluated a novel fluorophore-tagged allosteric probe for the mAChRs. Our initial design ultimately failed to produce the desired fluorescence, and highlighted the importance of including structural features into the ligand which prevent isomerization of the Rhodamine B (**12**) tag to its non-fluorescent spirolactam form. Our re-designed probe overcame this issue, however as with the original design the yields in the synthesis were low and the isolation of the target compound, C<sub>7/3</sub>-phth-Lissamine B (**23**), was difficult, requiring many repeated purifications by preparative HPLC. *N*-quaternisation to form the final product proved to be challenging in polar protic solvents, however, the usage of

EtOH in the final *N*-Quaternisation reaction allowed for the production of some of the desired product, C<sub>7/3</sub>-phth-Lissamine B (**23**), in a repeatable manner. Unfortunately, the yields of C<sub>7/3</sub>-phth-Lissamine B (**23**) were very low, due to the dominant formation of the mono- and diethoxylated starting material, due to the nucleophilic nature of EtOH. We suggest that other, non-nucleophilic, high dielectric constant solvents, such as ethylene carbonate, may be useful for overcoming this issue in future work. The final probe, C<sub>7/3</sub>-phth-Lissamine B (**23**), displayed all of the expected pharmacological traits of the parent ligand (C<sub>7/3</sub>-phth), being a weak NAM at the eGFP-M<sub>2</sub> mAChR with an affinity of approximately 1  $\mu$ M, and not significantly different from that measured for C<sub>7/3</sub>-phth (**6**). Confocal microscopy imaging data shows that C<sub>7/3</sub>-phth-Lissamine B (**23**) and the eGFP-M<sub>2</sub> mAChRs co-localise on the cell membranes. Time-course assays monitoring change in FRET signal in the presence of C<sub>7/3</sub>-phth-Lissamine B (**23**) indicated that C<sub>7/3</sub>-phth-Lissamine B (**23**) displays fast on and off rate kinetics, and the values for affinity obtained from the FRET kinetics assays and the radioligand binding assays are in good agreement. Although here we have only evaluated C<sub>7/3</sub>-phth-Lissamine B (**23**) by FRET assay at the eGFP-M<sub>2</sub> mAChR it is likely that (as with the parent ligand), C<sub>7/3</sub>-phth-Lissamine B (**23**) also displays reasonable affinity at all M<sub>1</sub>-M<sub>5</sub> mAChR subtypes, making it a viable tool for probing the allosteric sites of all of those receptors. Our strategy of incorporating the fluorophore directly into the pharmacophore of C<sub>7/3</sub>-phth (**6**) was fortunately successful and further highlights what has been shown by previous SAR studies of related structures that show there is significant flexibility for substituting the phthalimido ring motif in these compounds with larger aromatic motifs, without the significant loss of allosteric affinity. Future work will involve optimization of the synthesis of C<sub>7/3</sub>-phth-Lissamine B (**23**) to improve overall yields, and to increase the synthetic accessibility of this compound. We intend to develop other eGFP-tagged mAChR subtypes (M<sub>1</sub>, M<sub>3</sub>-M<sub>5</sub> mAChR) and to characterize the pharmacological properties of C<sub>7/3</sub>-phth-Lissamine B (**23**) at these remaining

mAChR subtypes, to evaluate C<sub>7/3</sub>-phth-Lissamine B (**23**) as a general purpose mAChR allosteric probe. Furthermore, we would be interested to know whether C<sub>7/3</sub>-phth-Lissamine B (**23**) could potentially be used in alternate assay formats such as FP, which can be performed using the native untagged receptors, as this would further increase the pharmacological applicability of C<sub>7/3</sub>-phth-Lissamine B (**23**) as a low-cost, throughput scalable, subtype general mAChR allosteric probe.

## ■ EXPERIMENTAL SECTION

**Chemistry.** All materials were reagent grade and purchased commercially from Sigma-Aldrich or Matrix Scientific. Anhydrous solvents were obtained from an MBraun MB SPS-800 Solvent Purification System. Analytical thin layer chromatography (TLC) was performed on Silica Gel 60 F254 pre-coated plates (0.25 mm, Merck ART 5554) and visualised using ultraviolet light, iodine, potassium permanganate or ninhydrin as necessary. Silica gel 40–63 micron (Davisil) was used for silica gel flash chromatography. <sup>1</sup>H NMR spectra were recorded on a Bruker Avance 400 MHz Ultrashield Plus spectrometer at 400.13 MHz. Chemical shifts ( $\delta$ ) for all <sup>1</sup>H NMR spectra are reported in parts per million (ppm) using the central peak of the deuterated solvent chemical shift as the reference: MeOD (3.31), CDCl<sub>3</sub> (7.26) and *d*<sub>6</sub>-DMSO (2.50).<sup>45</sup> Each resonance was assigned according to the following convention: chemical shift ( $\delta$ ) (multiplicity, coupling constant(s) in Hz, number of protons). Coupling constants (*J*) are reported to the nearest 0.1 Hz. In reporting the spectral data, the following abbreviations have been used: s, singlet; d, doublet; t, triplet; q, quartet; p, pentet; m, multiplet; br, broad; app, apparent; as well as combinations of these where appropriate. <sup>13</sup>C NMR spectra were recorded at 100.62 MHz using a Bruker Avance 400 MHz Ultrashield Plus spectrometer. Chemical shifts ( $\delta$ ) for all <sup>13</sup>C NMR spectra are reported in parts per million (ppm), using the center peak of the deuterated solvent chemical shift as the reference: MeOD (49.00), CDCl<sub>3</sub> (77.16) and *d*<sub>6</sub>-

DMSO (39.52).<sup>45</sup> Compounds for which less than 20 mg were obtained were analysed for 3 hr to ensure good a signal-to-noise ratio was obtained. HSQC, HMBC and COSY spectra were obtained using the standard Bruker pulse sequence to assist with structural assignment of the compounds. LC-MS was performed on an Agilent 1200 Series coupled to the 6120 quadrupole mass spectrometer. Elution was also monitored at 254 nm. HRMS analyses were recorded in the specified ion mode using an Agilent 6224 TOF LC-MS coupled to an Agilent 1290 Infinity (Agilent, Palo Alto, CA). Analytical reverse-phase HPLC was performed on a Waters HPLC system using a Phenomenex® Luna C8 (2) 100Å column (150 × 4.6 mm, 5 µm) and a binary solvent system; solvent A: 0.1% TFA/H<sub>2</sub>O; solvent B: 0.1% TFA/CH<sub>3</sub>CN. Isocratic elution was carried out using the following protocol (time, % solvent A, % solvent B): 0 min, 100, 0; 10 min, 20, 80; 11 min, 20, 80; 12 min, 100, 0; 20 min, 100, 0; at a flow rate of 1.0 mL/min monitored at 214 and/ or 254 nm using a Waters 996 Photodiode Array detector. Preparative HPLC was performed using an Agilent 1260 infinity coupled with a binary preparative pump and Agilent 1260 FC-PS fraction collector, using Agilent OpenLAB CDS software (Rev C.01.04) and an Altima 5 µM C8 22 mm × 250 mm column. The following buffers were used: buffer A, H<sub>2</sub>O; buffer B, MeCN, with sample being run at a gradient of 5% buffer B to 100% buffer B over 20 min at a flow rate of 20 mL/min. Characterisation requirements for final compounds were set as: <sup>1</sup>H NMR, <sup>13</sup>C NMR, LC-MS, HPLC (254 nm and 214 nm) purity >95%.

***N*<sup>1</sup>-(3-(3'-(Diethylamino)-6'-(diethylammonio)-3-oxospiro[isoindoline-1,9'-xanthen]-2-yl)propyl)-*N*<sup>7</sup>-(3-(1,3-dioxoisindolin-2-yl)propyl)-*N*<sup>1</sup>,*N*<sup>1</sup>,*N*<sup>7</sup>,*N*<sup>7</sup>-tetramethylheptane-1,7-diaminium dibromide (13).** Compound **19** (87 mg, 0.18 mmol) and compound **20** (94 mg, 0.18 mmol) and DIPEA (2 drops) were combined in AR grade ACN (2 mL) and stirred in a sealed tube. The temperature was gradually increased over 24 h from room temperature to 160

°C and held at that temperature for an additional 48 hrs. The solution was then allowed to cool and the solvent removed *in vacuo*. The crude material was then purified by FCC with DCM:MeOH (9:1) as the eluent to give the product as a light pink, viscous oil; 6.9 mg, 5%. <sup>1</sup>H NMR (CDCl<sub>3</sub>) δ 7.92 – 7.88 (m, 1H), 7.86 – 7.79 (m, 2H), 7.75 – 7.70 (m, 2H), 7.54 – 7.42 (m, 2H), 7.17 – 7.06 (m, 1H), 6.42 – 6.35 (m, 4H), 6.29 (dd, *J* = 9.0, 2.6 Hz, 2H), 4.14 (t, *J* = 5.0 Hz, 2H), 3.89 – 3.75 (m, 4H), 3.70 – 3.51 (m, 6H), 3.40 – 3.23 (m, 12H), 3.04 (s, 6H), 2.32 – 2.22 (m, 2H), 1.94 – 1.61 (m, 10H), 1.53 – 1.32 (m, 4H), 1.16 (t, *J* = 7.0 Hz, 12H); <sup>13</sup>C NMR (CDCl<sub>3</sub>) δ 168.7, 168.4, 153.7, 152.9, 148.0, 145.0, 139.1, 134.5, 132.0, 128.8, 128.7, 124.2, 123.8, 123.1, 113.7, 108.4, 97.9, 65.3, 65.0, 64.7, 63.2, 62.8, 62.5, 51.7, 51.5, 50.1, 44.6, 37.0, 35.1, 27.1, 24.8, 22.8, 22.4, 22.3, 22.1, 12.8; *m/z* MS (TOF ES<sup>+</sup>) C<sub>53</sub>H<sub>73</sub>N<sub>6</sub>O<sub>4</sub><sup>3+</sup> [M]<sup>2+</sup> calcd, 285.9; found, 285.8; LC-MS: *t*<sub>R</sub> = 3.09 min.

**2-(3-(Dimethylamino)propyl)isoindoline-1,3-dione (18).** Phthalic anhydride (888 mg, 6.00 mmol) and *N*<sup>1</sup>,*N*<sup>1</sup>-dimethylpropane-1,3-diamine (153 mg, 1.50 mmol) were combined in AcOH (15 mL) and heated to reflux for 24 h, monitoring periodically by TLC. The solvent was removed *in vacuo* and the crude material was purified by FCC on silica with DCM:MeOH (1:1) as the eluent, giving the product as a crop of fine white needles; 301 mg, 86%. <sup>1</sup>H NMR (*d*<sub>6</sub>-DMSO) δ 7.93 – 7.81 (m, 4H), 3.64 (t, *J* = 6.5 Hz, 2H), 3.19 – 3.06 (m, 2H), 2.74 (s, 6H), 2.03 – 1.91 (m, 2H); <sup>13</sup>C NMR (*d*<sub>6</sub>-DMSO) δ 168.2, 134.6, 131.9, 123.2, 54.5, 42.4, 34.8, 23.6; *m/z* MS (TOF ES<sup>+</sup>) C<sub>13</sub>H<sub>16</sub>N<sub>2</sub>O<sub>2</sub> [M+H]<sup>+</sup> calcd, 233.1; found, 233.2. LC-MS: *t*<sub>R</sub> = 4.34 min.

**7-Bromo-*N*-(3-(1,3-dioxoisoindolin-2-yl)propyl)-*N,N*-dimethylheptan-1-aminium bromide (19).** Compound **18** (730 mg, 3.15 mmol), 1,7-dibromoheptane (1.63 g, 6.32 mmol) and DIPEA (406 mg, 3.15 mmol) were combined in ACN (20 mL) and heated to reflux for 6 hrs. The solution was allowed to cool and the solvent removed *in vacuo*. The crude material was then recrystallized from EtOAc, adding minimal PE upon cooling to induce crystallization, giving a crop of white needles which were vacuum filtered, washed with a small volume of PE

and dried under vacuum; 1.263 g, 82%.  $^1\text{H}$  NMR ( $d_6$ -DMSO)  $\delta$  7.93 – 7.82 (m, 4H), 3.66 (t,  $J$  = 6.3 Hz, 2H), 3.53 (t,  $J$  = 6.7 Hz, 2H), 3.46 – 3.40 (m, 2H), 3.27 – 3.18 (m, 2H), 2.97 (s, 6H), 2.04 (p,  $J$  = 6.7 Hz, 2H), 1.79 (p,  $J$  = 6.7 Hz, 2H), 1.65 – 1.55 (m, 2H), 1.43 – 1.17 (m, 6H);  $^{13}\text{C}$  NMR ( $d_6$ -DMSO)  $\delta$  168.2, 134.6, 131.9, 123.3, 63.2, 60.9, 53.8, 35.3, 34.8, 32.2, 27.7, 27.4, 25.7, 21.7, 18.3;  $m/z$  MS (TOF ES $^+$ )  $\text{C}_{20}\text{H}_{30}\text{BrN}_2\text{O}_2^+$   $[\text{M}]^+$  calcd, 409.2; found, 408.8. LC-MS:  $t_{\text{R}}$  = 5.05 min.

***N*-(6-(Diethylamino)-9-(2-((3-(dimethylamino)propyl)carbamoyl)phenyl)-3H-xanthen-3-ylidene)-*N*-ethylethanaminium chloride (20).** Rhodamine B (*N*-(9-(2-carboxyphenyl)-6-(diethylamino)-3H-xanthen-3-ylidene)-*N*-ethylethanaminium chloride) (1.44 g, 3.00 mmol),  $N^1,N^1$ -dimethylpropane-1,3-diamine (500 mg, 3.00 mmol) and HCTU (1.24 g, 3.00 mmol) were combined in DCM:DMF (1:1, 30 mL) and stirred at room temperature. DIPEA (1.16 g, 9.00 mmol) in DCM:DMF (1:1, 4.5 mL) was added to the stirring solution, dropwise over 30 mins. After the addition, the solution was stirred overnight. The DCM was then removed under vacuum and  $\text{dH}_2\text{O}$  (150 mL) was added and the product extracted with EtOAc (3 x 35 mL), which was washed with sat.  $\text{NaHCO}_3$  solution (3 x 10 mL), dried over  $\text{MgSO}_4$  and the solvent removed under vacuum. The crude material was then purified by FCC with DCM:MeOH (19:1) as the eluent, giving the title compound as a red foam; 711 mg, 42%.  $^1\text{H}$  NMR ( $\text{CDCl}_3$ )  $\delta$  7.91 – 7.87 (m, 1H), 7.50 – 7.37 (m, 2H), 7.12 – 7.02 (m, 1H), 6.47 – 6.39 (m, 2H), 6.37 (d,  $J$  = 2.6 Hz, 2H), 6.25 (dd,  $J$  = 8.9, 2.6 Hz, 2H), 3.32 (q,  $J$  = 7.0 Hz, 8H), 3.17 – 3.07 (m, 2H), 2.09 (t,  $J$  = 7.5 Hz, 2H), 2.02 (s, 6H), 1.15 (t,  $J$  = 7.0 Hz, 12H);  $^{13}\text{C}$  NMR ( $\text{CDCl}_3$ )  $\delta$  168.1, 153.6, 153.5, 148.8, 132.3, 131.7, 129.1, 128.1, 123.9, 122.8, 108.2, 106.0, 97.9, 57.5, 46.9, 45.2, 38.7, 26.2, 12.7;  $m/z$  MS (TOF ES $^+$ )  $\text{C}_{33}\text{H}_{42}\text{N}_4\text{O}_2$   $[\text{M}+\text{H}]^+$  calcd, 528.3; found, 528.0. LC-MS:  $t_{\text{R}}$  = 3.22 min.

**2-(6-(Diethylamino)-3-(diethyliminio)-3H-xanthen-9-yl)-5-(*N*-(3-((7-((3-(1,3-dioxoisindolin-2-yl)propyl)dimethylammonio)heptyl)dimethylammonio)propyl)**

**sulfamoyl)benzenesulfonate ditrifluoroacetate (23).** Compound **19** (44 mg, 0.11 mmol), compound **25** (70 mg, 0.11 mmol) and DIPEA (1 drop) were combined in EtOH (2.5 mL) and heated to 160 °C in a sealed tube for 72 hrs. The solvent was removed *in vacuo* and the crude material purified by iterative runs of preparative HPLC by the protocol listed in the general methods, giving the title compound as a crop of fine red prisms; 8.7 mg, 7%. <sup>1</sup>H NMR (MeOD)  $\delta$  8.62 (d,  $J$  = 1.9 Hz, 1H), 8.11 (dd,  $J$  = 8.0, 1.9 Hz, 1H), 7.92 – 7.78 (m, 4H), 7.56 (d,  $J$  = 7.9 Hz, 1H), 7.10 (d,  $J$  = 9.4 Hz, 2H), 7.02 – 6.92 (m, 4H), 3.76 (t,  $J$  = 6.6 Hz, 2H), 3.67 (q,  $J$  = 7.1 Hz, 8H), 3.53 – 3.33 (m, 8H), 3.16 – 3.309 (m, 8H), 3.06 (s, 6H), 2.16 (p,  $J$  = 6.5 Hz, 2H), 2.11 – 2.02 (m, 2H), 1.93 – 1.69 (s, 4H), 1.57 – 1.35 (m, 6H), 1.30 (t,  $J$  = 7.0 Hz, 12H); <sup>13</sup>C NMR (MeOD)  $\delta$  169.8, 159.4, 157.6, 157.2, 147.4, 143.2, 135.7, 135.6, 133.4, 132.9, 129.2, 127.8, 124.3, 115.2, 115.0, 97.1, 65.4, 65.1, 62.9, 62.3, 51.8, 51.3, 46.8, 41.2, 40.9, 38.2, 35.8, 26.8, 24.4, 23.3, 23.2, 23.1, 12.8;  $m/z$  MS (TOF ES<sup>+</sup>) C<sub>52</sub>H<sub>72</sub>N<sub>6</sub>O<sub>8</sub>S<sub>2</sub><sup>2+</sup> [M]<sup>2+</sup> calcd, 486.2; found, 486.0. LC-MS:  $t_R$  = 3.25 min; HPLC:  $t_R$  = 4.17 min, purity (254) = 98.1%, purity (214) = 97.4%.

**2-(6-(Diethylamino)-3-(diethyliminio)-3H-xanthen-9-yl)-5-(N-(3-(dimethylamino)propyl)sulfamoyl)benzenesulfonate (25).** Lissamine B sulfonyl chloride (5-(chlorosulfonyl)-2-(6-(diethylamino)-3-(diethyliminio)-3H-xanthen-9-yl)benzenesulfonate) (115 mg, 0.199 mmol) and *N*<sup>1</sup>,*N*<sup>1</sup>-dimethylpropane-1,3-diamine (82 mg, 0.80 mmol) were combined in anhydrous THF and the solution stirred at room temperature for 1 hr. The solvent was removed *in vacuo* and the crude dissolved in dH<sub>2</sub>O (30 mL) and extracted into DCM (3 x 15 mL). The combined organic extracts were washed with sat. NaHCO<sub>3</sub> (30 mL), dried over MgSO<sub>4</sub> and the solvent removed under vacuum to give the product as fine red prisms; 69 mg, 54%. <sup>1</sup>H NMR (CDCl<sub>3</sub>)  $\delta$  8.79 (d,  $J$  = 1.9 Hz, 1H), 8.00 (dd,  $J$  = 7.9, 1.9 Hz, 1H), 7.31 (d,  $J$  = 9.5 Hz, 2H), 7.20 (d,  $J$  = 7.8 Hz, 1H), 6.79 (dd,  $J$  = 9.5, 2.5 Hz, 2H), 6.67 (d,  $J$  = 2.5 Hz, 2H), 5.30 (s, 1H), 3.63 – 3.47 (m, 8H), 3.24 (t,  $J$  = 5.9 Hz, 2H), 2.52 (t,  $J$  = 5.9 Hz,



2H), 2.32 (s, 6H), 1.75 (p,  $J = 6.0$  Hz, 2H), 1.30 (t,  $J = 7.1$  Hz, 12H);  $^{13}\text{C}$  NMR ( $\text{CDCl}_3$ )  $\delta$  157.9, 155.7, 149.0, 148.1, 146.3, 140.5, 133.8, 131.1, 127.9, 124.5, 123.5, 117.1, 114.6, 95.8, 57.9, 46.0, 45.6, 42.4, 25.0, 12.7, 8.2;  $m/z$  MS (TOF  $\text{ES}^+$ )  $\text{C}_{32}\text{H}_{42}\text{N}_4\text{O}_6\text{S}_2$   $[\text{M}+\text{H}]^+$  calcd, 643.3; found, 642.7; LC-MS:  $t_R = 4.89$  min.

#### Isolated byproducts from the synthesis of compound 6.

***N*-(3-(1,3-Dioxoisindolin-2-yl)propyl)-7-ethoxy-*N,N*-dimethylheptan-1-aminium bromide (29).**  $^1\text{H}$  NMR (MeOD)  $\delta$  7.60 – 7.51 (m, 2H), 7.14 – 7.05 (m, 2H), 3.68 (q,  $J = 7.2$  Hz, 6H), 3.35 (s, 6H), 3.30 – 3.17 (m, 6H), 2.12 – 2.01 (app m, 2H), 1.91 – 1.80 (app m, 2H), 1.78 – 1.66 (app m, 2H), 1.60 – 1.38 (m, 10H), 1.28 (t,  $J = 4.5$  Hz, 3H);  $m/z$  MS (TOF  $\text{ES}^+$ )  $\text{C}_{22}\text{H}_{35}\text{N}_2\text{O}_3^+$   $[\text{M}]^+$  calcd, 375.3; found, 375.0; LC-MS:  $t_R = 3.82$  min.

**7-Ethoxy-*N*-(3-(2-(ethoxycarbonyl)benzamido)propyl)-*N,N*-dimethylheptan-1-aminium bromide (30).**  $^1\text{H}$  NMR (MeOD)  $\delta$  7.60 – 7.51 (m, 2H), 7.14 – 7.05 (m, 2H), 3.68 (q,  $J = 7.2$  Hz, 6H), 3.35 (s, 6H), 3.30 – 3.17 (m, 6H), 2.12 – 2.01 (app m, 2H), 1.91 – 1.80 (app m, 2H), 1.78 – 1.66 (app m, 2H), 1.60 – 1.38 (m, 10H), 1.28 (t,  $J = 4.5$  Hz, 3H);  $m/z$  MS (TOF  $\text{ES}^+$ )  $\text{C}_{24}\text{H}_{41}\text{N}_2\text{O}_4^+$   $[\text{M}]^+$  calcd, 421.3; found, 421.0. LC-MS:  $t_R = 3.71$  min.

#### ■ REFERENCES

- (1) Langmead, C. J.; Watson, J.; Reavill, C. Muscarinic acetylcholine receptors as CNS drug targets. *Pharmacol. Ther.* **2008**, *117*, 232-43.
- (2) Foster, D. J.; Choi, D. L.; Conn, P. J.; Rook, J. M. Activation of M1 and M4 muscarinic receptors as potential treatments for Alzheimer's disease and schizophrenia. *Neuropsychiatr. Dis. Treat.* **2014**, *10*, 183-91.
- (3) Bymaster, F. P.; Felder, C.; Ahmed, S.; McKinzie, D. Muscarinic Receptors as a Target for Drugs Treating Schizophrenia. *Curr. Drug Targets CNSNeurol. Disord.* **2002**, *1*, 163-81.
- (4) Raedler, T. J.; Bymaster, F. P.; Tandon, R.; Copolov, D.; Dean, B. Towards a muscarinic hypothesis of schizophrenia. *Mol. Psychiatry* **2006**, *12*, 232-46.
- (5) Christopoulos, A. Allosteric binding sites on cell-surface receptors: novel targets for drug discovery. *Nat. Rev. Drug Discov.* **2002**, *1*, 198-210.
- (6) Conn, P. J.; Christopoulos, A.; Lindsley, C. W. Allosteric modulators of GPCRs: a novel approach for the treatment of CNS disorders. *Nat. Rev. Drug Discov.* **2009**, *8*, 41-54.

- (7) Flanagan, C. A. Chapter 10 - GPCR-radioligand binding assays. In *Methods in Cell Biology*, K. Shukla, A., Ed. Academic Press: **2016**; Vol. 132, pp 191-215.
- (8) Kenakin, T. P. Chapter 3 - Drug-Receptor Theory. In *A Pharmacology Primer (Fourth Edition)*, Kenakin, T. P., Ed. Academic Press: San Diego, **2014**; pp 45-62.
- (9) Kenakin, T. P. Chapter 4 - Pharmacological Assay Formats: Binding. In *A Pharmacology Primer (Fourth Edition)*, Kenakin, T. P., Ed. Academic Press: San Diego, **2014**; pp 63-83.
- (10) Christopoulos, A.; Kenakin, T. G Protein-Coupled Receptor Allostereism and Complexing. *Pharmacol. Rev.* **2002**, *54*, 323-74.
- (11) Christopoulos, A. Quantification of Allosteric Interactions at G Protein Coupled Receptors Using Radioligand Binding Assays. *Curr. Protoc. Pharmacol.* **2000**, *11*, 1.22.1-40.
- (12) Kenakin, T. P. Chapter 7 - Allosteric Modulation. In *A Pharmacology Primer (Fourth Edition)*, Kenakin, T. P., Ed. Academic Press: San Diego, **2014**; pp 155-180.
- (13) Schober, D. A.; Croy, C. H.; Xiao, H.; Christopoulos, A.; Felder, C. C. Development of a Radioligand, [3H]-LY2119620, to Probe the Human M2 and M4 Muscarinic Receptor Allosteric Binding Sites. *Mol. Pharmacol.* **2014**, 116-23.
- (14) Tränkle, C.; Weyand, O.; Voigtlander, U.; Mynett, A.; Lazareno, S.; Birdsall, N. J.; Mohr, K. Interactions of orthosteric and allosteric ligands with [3H]dimethyl-W84 at the common allosteric site of muscarinic M2 receptors. *Mol. Pharmacol.* **2003**, *64*, 180-90.
- (15) Croy, C. H.; Schober, D. A.; Xiao, H.; Quets, A.; Christopoulos, A.; Felder, C. C. Characterization of the Novel Positive Allosteric Modulator, LY2119620, at the Muscarinic M2 and M4 Receptors. *Mol. Pharmacol.* **2014**, *86*, 106-15.
- (16) Tränkle, C.; Mies-Klomfass, E.; Cid, M. H.; Holzgrabe, U.; Mohr, K. Identification of a [3H]Ligand for the Common Allosteric Site of Muscarinic Acetylcholine M2 Receptors. *Mol. Pharmacol.* **1998**, *54*, 139-45.
- (17) Smith, D. L.; Davoren, J. E.; Edgerton, J. R.; Lazzaro, J. T.; Lee, C. W.; Neal, S.; Zhang, L.; Grimwood, S., Characterization of a Novel M1 Muscarinic Acetylcholine Receptor Positive Allosteric Modulator Radioligand, [3H]PT-1284. *Mol. Pharmacol.* **2016**, *90* (3), 177-87.
- (18) Kuder, K.; Kiec-Kononowicz, K. Fluorescent GPCR ligands as new tools in pharmacology. *Curr. Med. Chem.* **2008**, *15*, 2132-43.
- (19) Chen, L.; Jin, L.; Zhou, N. An update of novel screening methods for GPCR in drug discovery. *Expert Opin. Drug Discov.* **2012**, *7*, 791-806.
- (20) Jones, L. H.; Randall, A.; Napier, C.; Trevethick, M.; Sreckovic, S.; Watson, J. Design and synthesis of a fluorescent muscarinic antagonist. *Bioorg. Med. Chem. Lett.* **2008**, *18*, 825-7.
- (21) Hern, J. A.; Baig, A. H.; Mashanov, G. I.; Birdsall, B.; Corrie, J. E.; Lazareno, S.; Molloy, J. E.; Birdsall, N. J. Formation and dissociation of M1 muscarinic receptor dimers seen by total internal reflection fluorescence imaging of single molecules. *Proc. Natl. Acad. Sci. U. S. A.* **2010**, *107*, 2693-8.
- (22) Daval, S. B.; Valant, C.; Bonnet, D.; Kellenberger, E.; Hibert, M.; Galzi, J.-L.; Ilien, B. Fluorescent Derivatives of AC-42 To Probe Bitopic Orthosteric/Allosteric Binding Mechanisms on Muscarinic M1 Receptors. *J. Med. Chem.* **2012**, *55*, 2125-43.
- (23) Stoddart, L. A.; White, C. W.; Nguyen, K.; Hill, S. J.; Pfleger, K. D. Fluorescence- and bioluminescence-based approaches to study GPCR ligand binding. *Br. J. Pharmacol.* **2016**, *173*, 3028-37.
- (24) Bajar, B. T.; Wang, E. S.; Zhang, S.; Lin, M. Z.; Chu, J., A Guide to Fluorescent Protein FRET Pairs. *Sensors (Basel)* **2016**, *16* (9), 1488.
- (25) Haga, K.; Kruse, A. C.; Asada, H.; Yurugi-Kobayashi, T.; Shiroishi, M.; Zhang, C.; Weis, W. I.; Okada, T.; Kobilka, B. K.; Haga, T.; Kobayashi, T., Structure of the human M2 muscarinic acetylcholine receptor bound to an antagonist. *Nature* **2012**, *482*, 547.

- (26) Christopoulos, A.; Sorman, J. L.; Mitchelson, F.; El-Fakahany, E. E. Characterization of the subtype selectivity of the allosteric modulator heptane-1,7-bis-(dimethyl-3'-phthalimidopropyl) ammonium bromide (C7/3-phth) at cloned muscarinic acetylcholine receptors. *Biochem. Pharmacol.* **1999**, *57*, 171-9.
- (27) Muth, M.; Bender, W.; Scharfenstein, O.; Holzgrabe, U.; Balatkova, E.; Tränkle, C.; Mohr, K. Systematic Development of High Affinity Bis(ammonio)alkane-type Allosteric Enhancers of Muscarinic Ligand Binding. *J. Med. Chem.* **2003**, *46*, 1031-40.
- (28) Bock, A.; Bermudez, M.; Krebs, F.; Matera, C.; Chirinda, B.; Sydow, D.; Dallanoce, C.; Holzgrabe, U.; De Amici, M.; Lohse, M. J.; Wolber, G.; Mohr, K. Ligand Binding Ensembles Determine Graded Agonist Efficacies at a G Protein-coupled Receptor. *J. Biol. Chem.* **2016**, *291*, 16375-89.
- (29) Bock, A.; Chirinda, B.; Krebs, F.; Messerer, R.; Bätz, J.; Muth, M.; Dallanoce, C.; Klighenthal, D.; Tränkle, C.; Hoffmann, C.; De Amici, M.; Holzgrabe, U.; Kostenis, E.; Mohr, K. Dynamic ligand binding dictates partial agonism at a g protein-coupled receptor. *Nat. Chem. Biol.* **2014**, *10*, 18-20.
- (30) Disingrini, T.; Muth, M.; Dallanoce, C.; Barocelli, E.; Bertoni, S.; Kellershohn, K.; Mohr, K.; De Amici, M.; Holzgrabe, U. Design, Synthesis, and Action of Oxotremorine-Related Hybrid-Type Allosteric Modulators of Muscarinic Acetylcholine Receptors. *J. Med. Chem.* **2006**, *49*, 366-72.
- (31) Holzgrabe, U.; Mohr, K. Allosteric modulators of ligand binding to muscarinic acetylcholine receptors. *Drug Discov. Today* **1998**, *3*, 214-22.
- (32) Jäger, D.; Schmalenbach, C.; Prilla, S.; Schrobang, J.; Kebig, A.; Sennwitz, M.; Heller, E.; Tränkle, C.; Holzgrabe, U.; Hölte, H.-D.; Mohr, K. Allosteric Small Molecules Unveil a Role of an Extracellular E2/Transmembrane Helix 7 Junction for G Protein-coupled Receptor Activation. *J. Biol. Chem.* **2007**, *282*, 34968-76.
- (33) Mudd, G.; Pi, I. P.; Fethers, N.; Dodd, P. G.; Barbeau, O. R.; Auer, M. A general synthetic route to isomerically pure functionalized rhodamine dyes. *Methods Appl. Fluoresc.* **2015**, *3*, 045002.
- (34) Beija, M.; Afonso, C. A. M.; Martinho, J. M. G. Synthesis and applications of Rhodamine derivatives as fluorescent probes. *Chem. Soc. Rev.* **2009**, *38*, 2410-33.
- (35) Baker, J. G.; Middleton, R.; Adams, L.; May, L. T.; Briddon, S. J.; Kellam, B.; Hill, S. J. Influence of fluorophore and linker composition on the pharmacology of fluorescent adenosine A1 receptor ligands. *Br. J. Pharmacol.* **2010**, *159*, 772-86.
- (36) Matera, C.; Flammini, L.; Quadri, M.; Vivo, V.; Ballabeni, V.; Holzgrabe, U.; Mohr, K.; De Amici, M.; Barocelli, E.; Bertoni, S.; Dallanoce, C. Bis(ammonio)alkane-type agonists of muscarinic acetylcholine receptors: synthesis, in vitro functional characterization, and in vivo evaluation of their analgesic activity. *Eur. J. Med. Chem.* **2014**, *75*, 222-32.
- (37) Petrov, R. R.; Ferrini, M. E.; Jaffar, Z.; Thompson, C. M.; Roberts, K.; Diaz, P. Design and evaluation of a novel fluorescent CB2 ligand as probe for receptor visualization in immune cells. *Bioorg. Med. Chem. Lett.* **2011**, *21*, 5859-62.
- (38) Diaz, P.; Phatak, S. S.; Xu, J.; Astruc-Diaz, F.; Cavasotto, C. N.; Naguib, M. 6-Methoxy-N-alkyl Isatin Acylhydrazones as a Novel Series of Potent Selective Cannabinoid Receptor 2 Inverse Agonists: Design, Synthesis, and Binding Mode Prediction. *J. Med. Chem.* **2009**, *52*, 433-44.
- (39) Yates, A. S.; Doughty, S. W.; Kendall, D. A.; Kellam, B. Chemical modification of the naphthoyl 3-position of JWH-015: In search of a fluorescent probe to the cannabinoid CB2 receptor. *Bioorg. Med. Chem. Lett.* **2005**, *15*, 3758-62.
- (40) Matera, C.; Flammini, L.; Quadri, M.; Vivo, V.; Ballabeni, V.; Holzgrabe, U.; Mohr, K.; De Amici, M.; Barocelli, E.; Bertoni, S.; Dallanoce, C. Bis(ammonio)alkane-type agonists of

muscarinic acetylcholine receptors: synthesis, in vitro functional characterization, and in vivo evaluation of their analgesic activity. *Eur. J. Med. Chem.* **2014**, *75*, 222-32.

(41) Nassif-Makki, T.; Trankle, C.; Zlotos, D.; Bejeuhr, G.; Cambareri, A.; Pfletschinger, C.; Kostenis, E.; Mohr, K.; Holzgrabe, U. Bisquaternary ligands of the common allosteric site of M2 acetylcholine receptors: search for the minimum essential distances between the pharmacophoric elements. *J. Med. Chem.* **1999**, *42*, 849-58.

(42) Yue, X.-l.; Li, C.-r.; Yang, Z.-y. A novel colorimetric and fluorescent probe for trivalent cations based on rhodamine B derivative. *J. Photochem. Photobiol.* **2018**, *351*, 1-7.

(43) An, K.-L.; Shin, S.-R.; Jun, K.; Lee, J.-Y.; Hwang, J.-Y.; Son, Y. Synthesis of Rhodamine-based Chemosensor and Determination of Spectral Properties AU - Lee, Sang-Oh. *Mol. Cryst. Liq. Cryst.* **2014**, *604*, 193-201.

(44) Dror, R. O.; Green, H. F.; Valant, C.; Borhani, D. W.; Valcourt, J. R.; Pan, A. C.; Arlow, D. H.; Canals, M.; Lane, J. R.; Rahmani, R.; Baell, J. B.; Sexton, P. M.; Christopoulos, A.; Shaw, D. E. Structural basis for modulation of a G-protein-coupled receptor by allosteric drugs. *Nature* **2013**, *503*, 295-9.

(45) Gottlieb, H. E.; Kotlyar, V.; Nudelman, A. NMR Chemical Shifts of Common Laboratory Solvents as Trace Impurities. *J. Org. Chem.* **1997**, *62*, 7512-5.

# Chapter Six

## Conclusions and Future Directions

### Chapter 2

We attempted in this chapter to employ the bitopic hybrid ligand concept for the design of an  $M_1$  mAChR selective agonist, identifying that these ligands strangely possessed  $M_2/M_4$  mAChR selectivity at non-optimal linker lengths. Subsequent synthesis and evaluation of truncated derivatives of the hybrid ligands revealed that the  $M_2/M_4$  mAChR selectivity was not due to a bitopic interaction, being most pronounced in the *N*-decyl derivative of iperoxo (IXO-C10), which bears no allosteric pharmacophore with which to make a bitopic interaction.

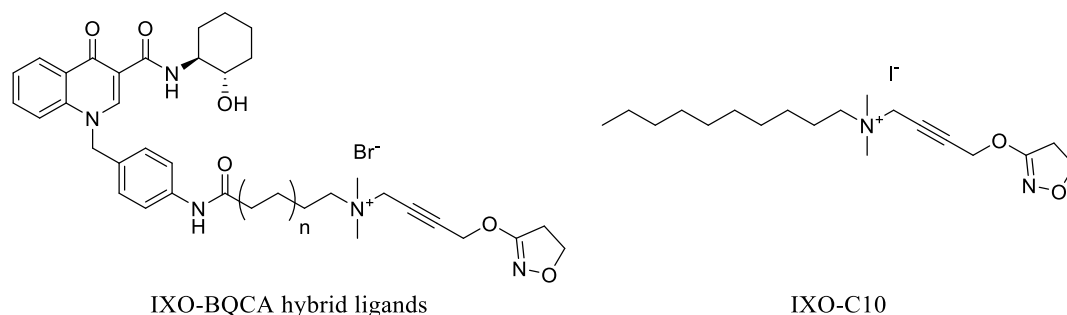


**Figure 1.** General chemical structure of our IXO-BQCA hybrid ligands and the most selective ligand found in chapter 2, IXO-C10.

Our hybrid ligands, though clearly not bitopic, possess similar selectivity to other mAChR hybrid ligands which have been reported to act bitopically at the mAChRs.<sup>1-3</sup> Since completing this study, further work has been published which suggests that some of these compounds gain their  $M_2/M_4$  mAChR selectivity via conformational restriction of the allosteric domain (leading to  $G_i$  bias) which explains why many of our truncated hybrid ligands possess  $M_2/M_4$  mAChR selectivity.<sup>4</sup> To our knowledge, no group has yet reported a mAChR hybrid ligand agonist which possesses selectivity for another subtype (or subset of subtypes) besides the  $M_2/M_4$  mAChR, and it seems reasonable to propose that all of these hybrid ligands act via this mechanism of conformational restriction and not via a bitopic mechanism. Furthermore, if

these hybrid ligands can only gain selectivity via conformational restriction of the allosteric domain then designing selective mAChR agonists for any other subtypes besides the M<sub>2</sub>/M<sub>4</sub> mAChRs may be an impossibility. Despite this, we found a significant difference in efficacy for IXO-C10 between the M<sub>2</sub> and M<sub>4</sub> mAChRs, suggesting that there may be another mechanism/s at play which could allow for differentiation between the M<sub>2</sub> and M<sub>4</sub> mAChR subtypes besides bitopic interactions and conformational restriction of the allosteric domain. However, we suggest that the approach of conjoining known orthosteric and allosteric ligands may not be suitable for designing selective agonists for the mAChRs.

### Chapter 3

In chapter 3 we explored the SAR of our iperoxo-based hybrid ligands which we had identified in chapter 2. Substitution of the allosteric pharmacophore yielded compounds with a surprising range of pharmacology, from non-selective and relatively high efficacy, to highly selective (differentiating between the M<sub>2</sub> and M<sub>4</sub> mAChRs and having no activity at the M<sub>1</sub>/M<sub>3</sub>/M<sub>5</sub> mAChRs) and with relatively lower efficacy overall.

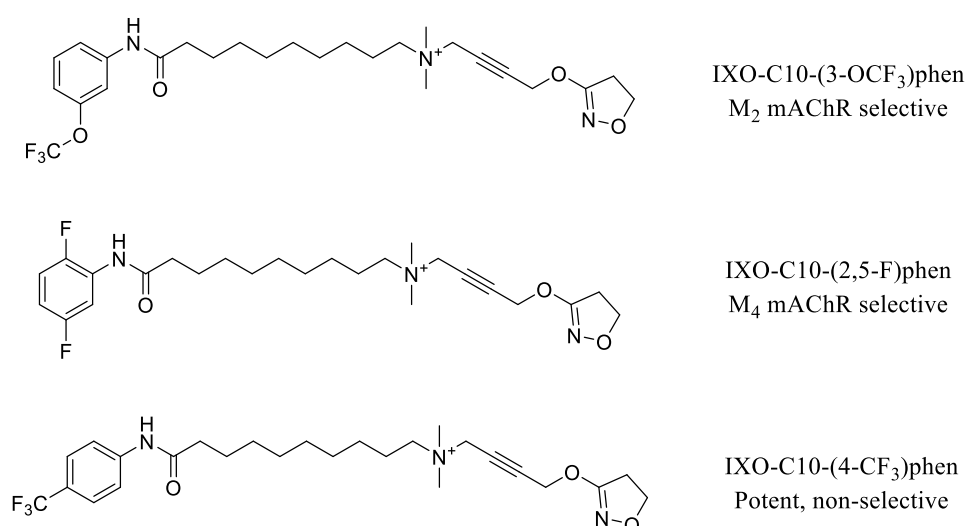


**Figure 2.** Chemical structures of hybrid ligands identified in chapter 3 with M<sub>2</sub> mAChR selectivity, M<sub>4</sub> mAChR selectivity and no mAChR selectivity.

The hybrid ligands identified which possess significantly different efficacy between the M<sub>2</sub> and M<sub>4</sub> mAChRs, as for IXO-C10 in chapter 2, again suggest that some of these hybrid ligands may act via a mechanism other than conformational restriction of the allosteric domain, which has been suggested to only result in G<sub>i</sub> bias.<sup>4</sup> We identified an inverse correlation between the efficacy of the hybrid ligands and their selectivity, which suggested that we would be unable to optimise these ligands for both efficacy and M<sub>4</sub> mAChR selectivity further. Also of note was the hybrid ligands which possessed high efficacy and were non-selective, a phenomena which we could not account for by the mechanism of conformational restriction of the allosteric domain, by which they were presumed to act, due to their apparent lack of G<sub>i</sub> bias.<sup>4</sup> From these results we were again lead to the hypothesis that there may be an alternate mechanism/s at play in the action of these hybrid ligands at the mAChRs, and this possibility was explored in detail in the following chapter. To our knowledge, this is the first hybrid ligand study to attempt to build hybrid ligands ‘from the ground up’, as opposed to the more standard approach which is commonly adopted, in which known ligands are combined. Our results show that this approach is indeed viable, leading to several novel hybrid ligands with selectivity for the M<sub>2</sub> over the M<sub>4</sub> mAChRs (or vice versa), or other interesting pharmacology, and propose that this approach be adopted by others to increase the diversity of mAChR hybrid ligand structures, such as to better reveal the potential scope of mAChR hybrid ligands in the future.

## **Chapter 4**

In chapters 2 and 3, which explored the SAR surrounding iperoxo-based hybrid ligands, we noted several observations which we could not account for from a molecular mechanistic perspective. Initially, based on their chemical structure and pharmacology, we expected that our hybrid ligands simply disrupted the allosteric vestibule (as has been observed in related hybrid ligands), resulting in G<sub>i</sub> bias, and that their pharmacology would be essentially identical, regardless of the substituted allosteric pharmacophore. However, (as noted in chapter 3) the



significant variation in pharmacology with allosteric substitution, the identification of hybrid ligands which differentiated between the  $G_i$  coupled  $M_2$  and  $M_4$  mAChRs, and the identification of a significant inverse correlation between efficacy and selectivity of our entire set of hybrid ligands, lead us to hypothesise that there may be an alternative mechanism/s involved in their action at the mAChRs. We subjected our hybrid ligands to molecular pharmacological and *in silico* analysis, and our results suggested that these ligands can adopt two possible conformations, one which non-selectively maintains efficacy, relative to iperoxo, and another which disrupts the allosteric vestibule, resulting in efficacy attenuation. This model gives an explanation for our aforementioned anomalous results. Firstly, it allows for the structure of the allosteric pharmacophore of our hybrid ligands to determine its binding orientation by interacting with alternate regions of the receptor (outside of the allosteric vestibule), explaining the significant differences in pharmacology between closely structurally related hybrid ligands. Secondly, the model allows for each hybrid ligand to bind in differing ratios of the two orientations at different subtypes, allowing for differences in efficacy at the  $G_i$  coupled  $M_2$  and  $M_4$  mAChRs. Finally, this model explains the correlation between efficacy and selectivity as resulting from differing proportions of hybrid ligands bound in each state of this two-state system, as determined by their allosteric substituent. Future work will involve analysis of these hybrid ligands for their  $G_i$  bias, via [ $^{35}\text{S}$ ]GTP $\gamma$ S assay, to assess the extent to which  $G_i$  bias and binding conformation influence their selectivity. Additionally, we wish to identify the region outside of the ‘typical’ allosteric of the  $M_2$  and  $M_4$  mAChRs to which the non-selective hybrid ligands bind, as our results indicate that the proportion of bound hybrid ligand which binds to this site may allow for selectivity between these two subtypes. Modelling work has suggested that this alternate binding site resides between transmembrane helices 1, 2 and 7 (TM1, TM2 and TM7) and this could be explored in more detail using mutagenesis of the  $M_2$  and  $M_4$  mAChRs. Ultimately, we believe that understanding the structural differences

of this region (TM1, TM2 and TM7) will aid in the rational design of hybrid ligand agonists which differentiate between the M<sub>2</sub> and M<sub>4</sub> mAChR subtypes, and this in turn may aid in the rational design of drugs which selectively target either of these two receptors for their therapeutic benefits.

## Chapter 5

In chapter 5 we turned our attention to the rational design of a fluorophore-tagged mAChR allosteric probe. Here we have designed, synthesised and evaluated a mAChR allosteric probe which has the potential to be used as a, low-cost general purpose allosteric probe at all M<sub>1</sub>-M<sub>5</sub> mAChR subtypes.

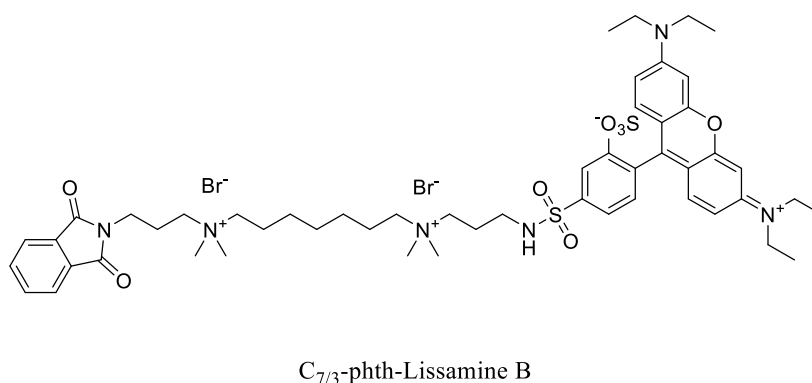


**Figure 3.** Chemical structure of the final fluorophore-tagged mAChR allosteric probe.

This probe bears none of the common issues of waste and safety associated with radiolabelled probes and has advantages not possible with radiolabelled probes, including applications in confocal microscopy imaging studies looking at receptor trafficking and localisation in real-time. Our design strategy involved incorporating the fluorophore directly into the ligand pharmacophore, a strategy which is typically risky, as the fluorophore is unlikely to make a good receptor-ligand interaction by mere chance. However we suggest that this strategy may be well suited to the design of mAChR allosteric probes, given the flexible ‘open’ nature of allosteric vestibules in these receptors.<sup>5</sup> Although here the probe was only evaluated

at the eGFP-tagged M<sub>2</sub> mAChR in FRET based assays, the parent ligand shows comparable affinity across all mAChR subtypes (i.e. it is selective at the level of cooperativity), and it is likely that this probe will work as an allosteric probe at all M<sub>1</sub>-M<sub>5</sub> mAChRs. Future work will involve the characterisation of the probe at the remaining eGFP-tagged M<sub>1</sub>, M<sub>3</sub>-M<sub>5</sub> mAChRs to assess its usefulness at these subtypes. Furthermore, here the probe has only been assessed in FRET based assays, which require an eGFP-tagged receptor. However we suspect that the probe may also work in fluorescence polarisation (FP) based assays, which do not require an eGFP-tagged receptor. This would increase the general applicability of this tool, and could be investigated in future work.<sup>6</sup> Finally, despite its pharmacological success, the synthesis of the probe was unfortunately very low yielding, and so future chemistry work will involve the improvement and optimisation of the synthesis to fix this issue.

## Conclusion

The identification of subtype selective ligands for the mAChRs has been a significant challenge in medicinal chemistry since the realisation that differentiated mAChR subtype existed. The overall goal of this thesis was to increase our understanding of selectivity in mAChR ligands, and (in chapter 5) to facilitate the development of future selective ligands which may have potential therapeutic benefit. Future work will involve the further development of these compounds and ideas such as to allow for their employment in the rational design and discovery of novel therapeutic agents which selectively target a single mAChR subtype.

## ■ REFERENCES

- (1) Disingrini, T.; Muth, M.; Dallanoce, C.; Barocelli, E.; Bertoni, S.; Kellershohn, K.; Mohr, K.; De Amici, M.; Holzgrabe, U. Design, Synthesis, and Action of Oxotremorine-Related Hybrid-Type Allosteric Modulators of Muscarinic Acetylcholine Receptors. *J. Med. Chem.* **2006**, *49*, 366-72.
- (2) Bock, A.; Bermudez, M.; Krebs, F.; Matera, C.; Chirinda, B.; Sydow, D.; Dallanoce, C.; Holzgrabe, U.; De Amici, M.; Lohse, M. J.; Wolber, G.; Mohr, K. Ligand Binding Ensembles

Determine Graded Agonist Efficacies at a G Protein-coupled Receptor. *J. Biol. Chem.* **2016**, *291*, 16375-89.

(3) Bock, A.; Chirinda, B.; Krebs, F.; Messerer, R.; Bätz, J.; Muth, M.; Dallanocce, C.; Kligenthal, D.; Tränkle, C.; Hoffmann, C.; De Amici, M.; Holzgrabe, U.; Kostenis, E.; Mohr, K. Dynamic ligand binding dictates partial agonism at a g protein-coupled receptor. *Nat. Chem. Biol.* **2014**, *10*, 18-20.

(4) Bermudez, M.; Bock, A.; Krebs, F.; Holzgrabe, U.; Mohr, K.; Lohse, M. J.; Wolber, G. Ligand-Specific Restriction of Extracellular Conformational Dynamics Constrains Signaling of the M2 Muscarinic Receptor. *ACS Chem. Biol.* **2017**, *12*, 1743-48.

(5) Avlani, V. A.; Gregory, K. J.; Morton, C. J.; Parker, M. W.; Sexton, P. M.; Christopoulos, A. Critical Role for the Second Extracellular Loop in the Binding of Both Orthosteric and Allosteric G Protein-coupled Receptor Ligands. *J. Biol. Chem.* **2007**, *282*, 25677-86.

(6) Rossi, A. M.; Taylor, C. W. Analysis of protein-ligand interactions by fluorescence polarization. *Nat. Protoc.* **2011**, *6*, 365-87.

# Appendix

# **Supplementary Information**

## **Chapter Two**

### **Subtype Selectivity and Efficacy of Iperoxo-BQCA Muscarinic Acetylcholine Receptor Hybrid Ligands**

#### **Contents**

*Methods and schemes for the synthesis and characterization of intermediate compounds*

*Methods for pharmacological analysis of target compounds*

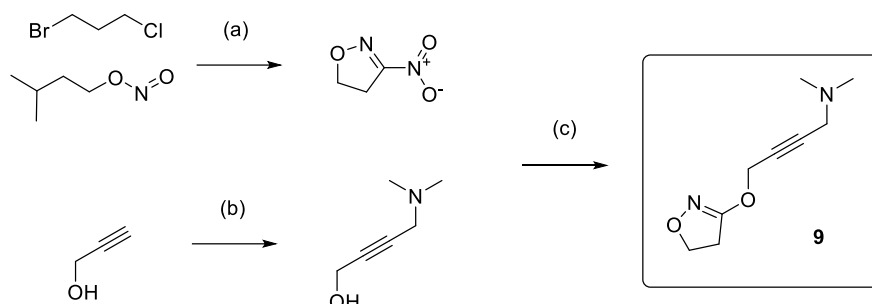
**Supplementary Figure 1 – Peak ERK 1/2 phosphorylation time course assays for target compounds**

**Supplementary Figure 2 – Allosteric interaction data for BQCA-derivative 3 and iperoxo 1**

## ■ EXPERIMENTAL SECTION

**Chemistry.** Synthesis of 1-(4-nitrobenzyl)-4-oxo-1,4-dihydroquinoline-3-carboxylic acid (**5**),<sup>40</sup> *N*-desmethyliperoxo (**9**) and subsequently iperoxo (**1**)<sup>39</sup> was carried out according to literature procedures.

### Synthesis of iperoxo-base **9**.<sup>a</sup>



<sup>a</sup>Reagents and conditions: (a) NaNO<sub>2</sub>, DMSO, RT, 70%; (b) dimethylamine HCl, HCHO (aqueous 40% w/w), CuSO<sub>4</sub>·5H<sub>2</sub>O, KOH<sub>aq</sub> (2 M), H<sub>2</sub>O, 85 °C, 29%; (c) NaH (60% in mineral oil), anhydrous THF, reflux, 48%.

**3-Nitro-4,5-dihydroisoxazole (13).** A solution of NaNO<sub>2</sub> (3.51 g, 50.8 mmol) and isopentyl nitrite (5.12 mL, 38.1 mmol) in DMSO (45 mL) was stirred at room temperature, under N<sub>2</sub>. 1-Bromo-3-chloropropane (2.53 mL, 25.4 mmol) was added dropwise over 30 min and the solution stirred for 24 h. The mixture was poured into ice water (75 mL) and extracted with dichloromethane (3 × 40 mL), dried over anhydrous MgSO<sub>4</sub> and the solvent removed under vacuum. The bulk of excess DMSO was removed by vacuum distillation at 65 °C (5 mmHg), the remainder being removed by dissolving the crude material in ethyl acetate (10 mL) and washing with brine, drying over anhydrous MgSO<sub>4</sub>, and removing the organics under vacuum. The target compound was obtained as a viscous yellow oil; 3.04 g, 70 %. <sup>1</sup>H NMR (CDCl<sub>3</sub>) δ 4.84 (t, *J* = 10.9 Hz, 2H), 3.45 (t, *J* = 10.9 Hz, 2H). <sup>13</sup>C NMR (CDCl<sub>3</sub>) δ 75.5, 40.8, 30.7. *m/z* MS (TOF ES<sup>+</sup>) C<sub>3</sub>H<sub>4</sub>N<sub>2</sub>O<sub>3</sub> [M+H]<sup>+</sup> calcd 117.0; found, 117.0. LC-MS *t*<sub>R</sub>: 3.33 min.

**4-(Dimethylamino)but-2-yn-ol (14).** Dimethylammonium HCl (10.9 g, 134 mmol) was dissolved in minimal distilled water and the pH adjusted to 10 with aqueous KOH (2 M).

CuSO<sub>4</sub>·5H<sub>2</sub>O (860 mg, 3.44 mmol), 40% aqueous formaldehyde (18.5 mL, 182 mmol) and propargyl alcohol (6.5 mL, 107 mmol) were dissolved in minimal distilled water and added, and the pH again adjusted this time to 8. The solution was then heated, with stirring, under N<sub>2</sub>, to 85 °C for 3 h. The crude reaction mixture was reduced under vacuum and then extracted using a continuous liquid-liquid extractor over 18.5 h, utilising 90% DCM/ 10% *i*-PrOH as the solvent system. The crude extract was purified by vacuum filtering through a silica ‘plug’ with chloroform as the mobile phase. Concentration of the organics *in vacuo* afforded the target compound as a yellow-orange oil; 3.45 g, 29%. <sup>1</sup>H NMR (CDCl<sub>3</sub>) δ 4.27 (t, *J* = 1.9 Hz, 2H), 3.25 (t, *J* = 1.9 Hz, 2H), 2.28 (s, 6H). <sup>13</sup>C NMR (CDCl<sub>3</sub>) δ 84.1, 80.1, 50.7, 48.0, 44.1. *m/z* MS (TOF ES<sup>+</sup>) C<sub>6</sub>H<sub>11</sub>NO [M+H]<sup>+</sup> calcd, 114.1; found, 114.4. LC-MS *t*<sub>R</sub>: 1.38 min.

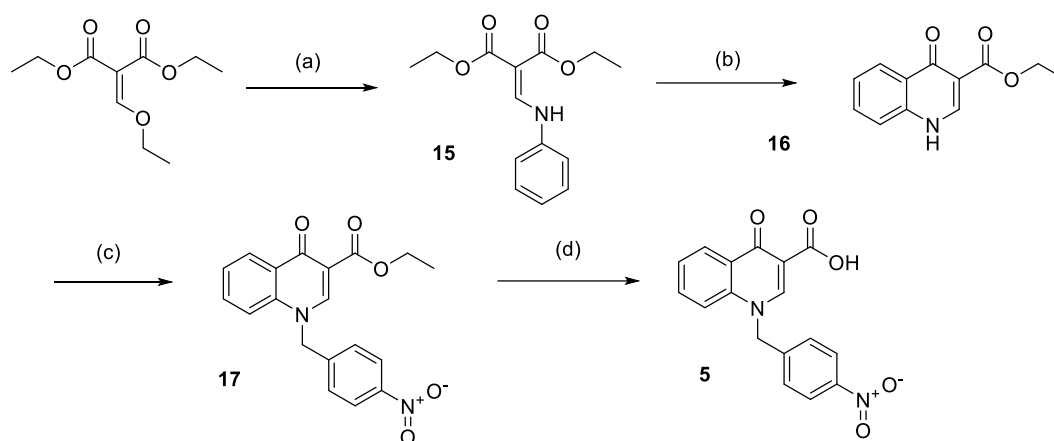
**4-((4,5-Dihydroisoxazol-3-yl)oxy)-*N,N*-dimethylbut-2-yn-1-amine (9).** 4-(Dimethylamino)but-2-ynol (**14**) (2.97 g, 25.6 mmol) was stirred in dry THF (50 mL), under N<sub>2</sub>. 60% NaH in mineral oil (1.54 g, 38.5 mmol) was carefully added in portions, and stirring continued at room temperature for 45 min – 1 h. 3-Nitro-4,5-dihydroisoxazole (**13**) (3.00 g, 26.5 mmol) in dry THF (5 mL) was added dropwise over 15 min. The solution was then refluxed for 24 h and monitored by LC-MS. After cooling the solution was poured into distilled water (50 mL) and extracted gently with chloroform (5 × 50 mL), dried over anhydrous MgSO<sub>4</sub>, and the solvent removed under vacuum to yield a crude brown oil. This oil was then chromatographed on silica (stationary phase: silica, gradient mobile phase: 100% chloroform – 90% chloroform/ 10% methanol) to give the target compounds as a clear yellow oil; 2.24g, 48%. <sup>1</sup>H NMR (*d*<sub>6</sub>-DMSO) δ 4.80 (t, *J* = 1.9 Hz, 2H), 4.30 (t, *J* = 9.6 Hz, 2H), 3.28 (t, *J* = 1.8 Hz, 2H), 3.00 (t, *J* = 9.6 Hz, 2H), 2.17 (s, 6H). <sup>13</sup>C NMR (CDCl<sub>3</sub>) δ 167.0, 83.4, 78.6, 69.8, 58.1, 48.0, 44.2, 33.1. *m/z* MS (TOF ES<sup>+</sup>) C<sub>9</sub>H<sub>14</sub>N<sub>2</sub>O<sub>2</sub> [M+H]<sup>+</sup> calcd, 183.1; found, 183.3. LC-MS *t*<sub>R</sub>: 1.49 min.



**4-((4,5-Dihydroisoxazol-3-yl)oxy)-*N,N,N*-trimethylbut-2-yn-1-aminium iodide (1).**

Compound **9** (200 mg, 1.20 mmol) was dissolved in ACN (10 mL). A large excess of iodomethane was added and the solution stirred overnight at room temperature. The solvent was removed under vacuum and the crude material recrystallized from boiling MeOH. White solid; 350.1 mg, 90%.  $^1\text{H}$  NMR ( $d_6$ -DMSO)  $\delta$  4.94 (t,  $J$  = 1.7 Hz, 2H), 4.46 (t,  $J$  = 1.7, 2H), 4.32 (t,  $J$  = 9.6 Hz, 1H), 3.14 (s, 9H), 3.02 (t,  $J$  = 9.6 Hz, 2H).  $^{13}\text{C}$  NMR ( $d_6$ -DMSO)  $\delta$  166.7, 86.0, 76.3, 69.6, 57.2, 55.1, 52.0, 32.2.  $m/z$  MS (TOF ES+)  $\text{C}_{10}\text{H}_{17}\text{N}_2\text{O}_2^+ [\text{M}]^+$  calcd, 197.1; found 197.1. LC-MS  $t_R$ : 1.03 min.

**Synthesis of BQCA-derivative **5**.<sup>a</sup>**



<sup>a</sup>Reagents and conditions: (a) aniline (neat), 110 °C, 83%; (b) Eaton's reagent (P<sub>4</sub>O<sub>10</sub>/methansulfonic acid 1:10 w/w), 95 °C, 71%; (c) *p*-nitrobenzyl bromide, K<sub>2</sub>CO<sub>3</sub>, KI, DMF, RT, 82%; (d) LiOH.H<sub>2</sub>O, 1:1 THF:H<sub>2</sub>O, RT, 85%.

**Diethyl 2-((phenylamino)methylene)malonate (15).** Aniline (1.60 g, 17.2 mmol) and diethyl ethoxymethylenemalonate (3.71 g, 17.1 mmol) were combined neat and heated to 110 °C on an oil bath, with stirring, under N<sub>2</sub>, and the reaction was monitored by TLC. After 8 h the reaction was cooled on ice at which point it solidified. The solid was removed by vacuum filtration and washed with cold petroleum ether. The organics were then concentrated under vacuum and the resulting precipitate filtered. The crude product was then recrystallised from petroleum ether giving a yellow crystalline solid; 3.76 g, 83%.  $^1\text{H}$  NMR (CDCl<sub>3</sub>)  $\delta$  11.01 (d,  $J$  =

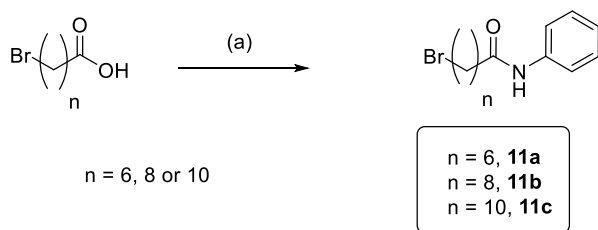
13.5 Hz, 1H), 8.53 (d,  $J = 13.7$  Hz, 1H), 7.41 – 7.33 (m, 2H), 7.19 – 7.11 (m, 3H), 4.31 (q,  $J = 7.1$  Hz, 2H), 4.25 (q,  $J = 7.1$  Hz, 2H), 1.38 (t,  $J = 7.1$  Hz, 3H), 1.33 (t,  $J = 7.1$  Hz, 3H).  $m/z$  MS (TOF ES<sup>+</sup>) C<sub>14</sub>H<sub>17</sub>NO<sub>4</sub> [M+H]<sup>+</sup> calcd, 264.1; found, 264.2. LC-MS  $t_R$ : 3.83.

**Ethyl 4-oxo-1,4-dihydroquinoline-3-carboxylate (16).** Diethyl 2-((phenylamino)methylene)malonate (**15**) (3.73 g, 14.2 mmol) was dissolved in Eaton's reagent (15 mL, P<sub>4</sub>O<sub>10</sub>/ methanesulfonic acid 1:10 w/w) and heated to 95 °C, with stirring, under N<sub>2</sub>. After 5 h the solution was cooled to room temperature and poured into sufficient saturated NaHCO<sub>3</sub> solution to neutralise the residual methanesulfonic acid, and stirred for 15 min. The precipitate was then vacuum filtered, washed with distilled water and petroleum ether and dried under vacuum overnight, giving a fine orange crystalline solid; 2.17 g, 71%. <sup>1</sup>H NMR (*d*<sub>6</sub>-DMSO)  $\delta$  13.45 (br s, 1H) 8.54 (s, 1H), 8.15 (dd,  $J = 8.1, 1.1$  Hz, 1H), 7.70 (ddd,  $J = 8.4, 7.0, 1.5$  Hz, 1H), 7.61 (dd,  $J = 8.2, 0.5$  Hz, 1H), 7.41 (ddd,  $J = 8.1, 7.0, 1.1$  Hz, 1H), 4.21 (q,  $J = 7.1$  Hz, 2H), 1.28 (t,  $J = 7.1$  Hz, 3H).  $m/z$  MS (TOF ES<sup>+</sup>) C<sub>12</sub>H<sub>11</sub>NO<sub>3</sub> [M+H]<sup>+</sup> calcd, 218.1; found, 218.1. LC-MS  $t_R$ : 4.84 min.

**Ethyl 1-(4-nitrobenzyl)-4-oxo-1,4-dihydroquinoline-3-carboxylate (17).** Ethyl 4-oxo-1,4-dihydroquinoline-3-carboxylate (**16**) (445 mg, 2.05 mmol), K<sub>2</sub>CO<sub>3</sub> (349 mg, 2.53 mmol), KI (39 mg, 0.24 mmol) and 4-nitrobenzyl bromide (545 mg, 2.52 mmol) were dissolved in DMF (6 mL) and stirred, under N<sub>2</sub>, at room temperature for 24 h. The reaction mixture was poured onto ice/ distilled water (20 mL) and the yellow precipitate was collected by vacuum filtration, and washed with ethyl acetate to remove any excess 4-nitrobenzyl bromide, giving the product as a light yellow crystalline solid; 591 mg, 82%. <sup>1</sup>H NMR (CDCl<sub>3</sub>)  $\delta$  8.62 (s, 1H), 8.57 (dd,  $J = 8.0, 1.4$  Hz, 1H), 8.27 – 8.19 (m, 2H), 7.56 (ddd,  $J = 8.6, 7.1, 1.7$  Hz, 1H), 7.44 (ddd,  $J = 8.0, 7.2, 0.9$  Hz, 1H), 7.34 (d,  $J = 8.9$  Hz, 2H), 7.15 (d,  $J = 8.4$  Hz, 1H), 5.50 (s, 2H), 4.43 (q,  $J = 7.1$  Hz, 2H), 1.43 (t,  $J = 7.1$  Hz, 3H).  $m/z$  MS (TOF ES<sup>+</sup>) C<sub>19</sub>H<sub>16</sub>N<sub>2</sub>O<sub>5</sub> [M+H]<sup>+</sup> calcd, 353.1; found, 353.2. LC-MS  $t_R$ : 7.71 min.

**1-(4-Nitrobenzyl)-4-oxo-1,4-dihydroquinoline-3-carboxylic acid (5).** Ethyl 1-(4-nitrobenzyl)-4-oxo-1,4-dihydroquinoline-3-carboxylate (**17**) (3.19 g, 9.06 mmol), was dissolved in THF (20 mL) and the solution degassed by bubbling N<sub>2</sub> through it for 30 min. LiOH.H<sub>2</sub>O (1.69 g, 42.2 mmol) in distilled water (20 mL) was added and the solution stirred at room temperature, under N<sub>2</sub>, for 48 h. After this time, the reaction was stopped and the THF was removed under vacuum. The aqueous solution then carefully acidified to pH 3 and the bright yellow precipitate was filtered and washed with minimal cold distilled water. The crude material was then ground under hot acetone and vacuum filtered leaving the product as a yellow crystalline solid; 2.79 g, 85%. <sup>1</sup>H NMR (*d*<sub>6</sub>-DMSO)  $\delta$  15.11 (s, 1H), 9.36 (s, 1H), 8.41 (dd, *J* = 8.1, 1.4 Hz), 8.19 (d, *J* = 8.8 Hz, 2H), 7.89 – 7.82 (m, 1H), 7.75 (d, *J* = 8.6 Hz, 1H), 7.63 (t, *J* = 7.5 Hz, 1H), 7.53 (d, *J* = 8.7 Hz, 2H), 6.05 (s, 2H). <sup>13</sup>C NMR (*d*<sub>6</sub>-DMSO)  $\delta$  177.5, 166.5, 151.1, 147.4, 144.8, 139.5, 132.9, 128.3, 128.0, 127.0, 124.8, 124.5, 118.4, 117.7, 55.2. *m/z* MS (TOF ES<sup>+</sup>) C<sub>17</sub>H<sub>12</sub>N<sub>2</sub>O<sub>5</sub> [M+H]<sup>+</sup> calcd, 325.1; found, 325.1. LC-MS *t*<sub>R</sub>: 5.81 min.

#### Synthesis of truncated hybrid ligand intermediates 11a-c.<sup>a</sup>



<sup>a</sup>Reagents and conditions: aniline, HCTU, DIPEA, 1:1 DMF:DCM, RT, 75-88%.

**General procedure for the synthesis of 11a-c.** Aniline (10.0 mmol, 1.0 eq.), HCTU (11.0 mmol, 1.1 eq.) and the appropriate terminal-bromoalkanoic acid (10.0 mmol, 1.0 eq.) were dissolved in DMF (150 mL) and stirred under N<sub>2</sub> at room temperature. DIPEA (2.33 g, 18.0 mmol, 1.8 eq.) in DCM (150 mL) was added dropwise over 30 min, and stirring continued for 6 h. The DCM was removed under vacuum and the reaction mixture was then diluted with

distilled water (200 mL). The precipitate was filtered and then suspended in a 1:1 solution of saturated  $\text{NaHCO}_3$  (aq) and distilled water (300 mL) and stirred vigorously for 30 min, before being vacuum filtered again. The resulting solid was then re-dissolved in DCM (100 mL) and washed with sat.  $\text{NaHCO}_3$  solution (50 mL),  $\text{dH}_2\text{O}$  (50 mL) and brine (50 mL) before being dried over anhydrous  $\text{MgSO}_4$  and the solvent removed *in vacuo* to afford the target compound.

**7-Bromo-N-phenylheptanamide (11a)** Off-white solid; 808 mg, 88%.  $^1\text{H}$  NMR ( $\text{CDCl}_3$ )  $\delta$  8.84 (s, 1H), 7.54-7.49 (m, 2H), 7.33-7.28 (m, 2H), 7.09 (t,  $J = 7.2$  Hz, 1H), 3.40 (t,  $J = 6.8$  Hz, 2H), 2.36 (t,  $J = 7.6$  Hz, 2H), 1.86 (p,  $J = 6.8$  Hz, 2H), 1.74 (p,  $J = 7.6$  Hz, 2H), 1.52-1.35 (m, 4H).  $^{13}\text{C}$  NMR ( $\text{CDCl}_3$ )  $\delta$  171.38, 138.10, 129.09, 124.30, 119.93, 37.62, 34.00, 32.62, 28.42, 27.96, 25.45.  $m/z$  MS (TOF  $\text{ES}^+$ )  $\text{C}_{13}\text{H}_{18}\text{BrNO}$   $[\text{M}+\text{H}]^+$  calcd, 284.1; found, 284.1. LC-MS  $t_R$ : 3.36 min.

**9-Bromo-N-phenylnonamide (11b)** Off-white solid; 1.23 g, 75%.  $^1\text{H}$  NMR ( $\text{CDCl}_3$ )  $\delta$  8.94 (s, 1H), 7.54-7.49 (m, 2H), 7.32-7.26 (m, 2H), 7.08 (t,  $J = 7.2$  Hz, 1H), 3.39 (t,  $J = 6.8$  Hz, 2H), 2.34 (t,  $J = 7.6$  Hz, 2H), 1.83 (p,  $J = 6.8$  Hz, 2H), 1.70 (p,  $J = 7.6$  Hz, 2H), 1.46-1.26 (m, 8H).  $^{13}\text{C}$  NMR ( $\text{CDCl}_3$ )  $\delta$  171.75, 138.16, 129.03, 124.22, 119.96, 37.77, 34.13, 32.84, 29.26, 29.22, 28.66, 28.17, 25.67.  $m/z$  MS (TOF  $\text{ES}^+$ )  $\text{C}_{15}\text{H}_{22}\text{BrNO}$   $[\text{M}+\text{H}]^+$  calcd, 312.1; found, 312.1. LC-MS  $t_R$ : 3.58 min.

**11-Bromo-N-phenylundecanamide (11c)** Off-white solid; 5.65 g, 77%.  $^1\text{H}$  NMR ( $\text{CDCl}_3$ )  $\delta$  9.07 (s, 1H), 7.56-7.48 (m, 2H), 7.32-7.26 (m, 2H), 7.08 (t,  $J = 7.2$  Hz, 1H), 3.39 (t,  $J = 6.8$  Hz, 2H), 2.35 (t,  $J = 7.6$  Hz, 2H), 1.83 (p,  $J = 6.8$  Hz, 2H), 1.71 (p,  $J = 7.6$  Hz, 2H), 1.45-1.23 (m, 10H).  $^{13}\text{C}$  NMR ( $\text{CDCl}_3$ )  $\delta$  171.77, 138.13, 129.04, 124.25, 119.97, 37.85, 34.19, 32.90, 29.45, 29.43, 29.41, 29.33, 28.81, 28.24, 25.74.  $m/z$  MS (TOF  $\text{ES}^+$ )  $\text{C}_{17}\text{H}_{26}\text{BrNO}$   $[\text{M}+\text{H}]^+$  calcd, 340.1; found, 340.1. LC-MS  $t_R$ : 3.71 min.

## Pharmacology.

*Time-course assays.* Cells were plated in 180  $\mu\text{L}$  media per well. Stock solutions of iperoxo **1** and the test ligands were made up in DMSO ( $10^{-2}$  M). Dilutions of all ligands were made up in FBS-free media at ten times ( $10\times$ ) the required concentration and added to stock plates. Cells were incubated at 37 °C with 20  $\mu\text{L}$  of iperoxo ( $10^{-6}$  M) or test ligand solution ( $10^{-5}$  M) at the time points: 30, 20, 15, 12, 10, 8, 5, 3 and 1 min, before terminating the assay. 10% (v/v) FBS and vehicle were added at 6 min as positive and negative controls.

*Data analysis.* All data analysis was managed using Prism 6 software (GraphPad Software, San Diego, CA). Experiments measuring radioligand equilibrium whole cell binding interactions between compounds **1** and **3** were fitted to the allosteric ternary complex model (1):

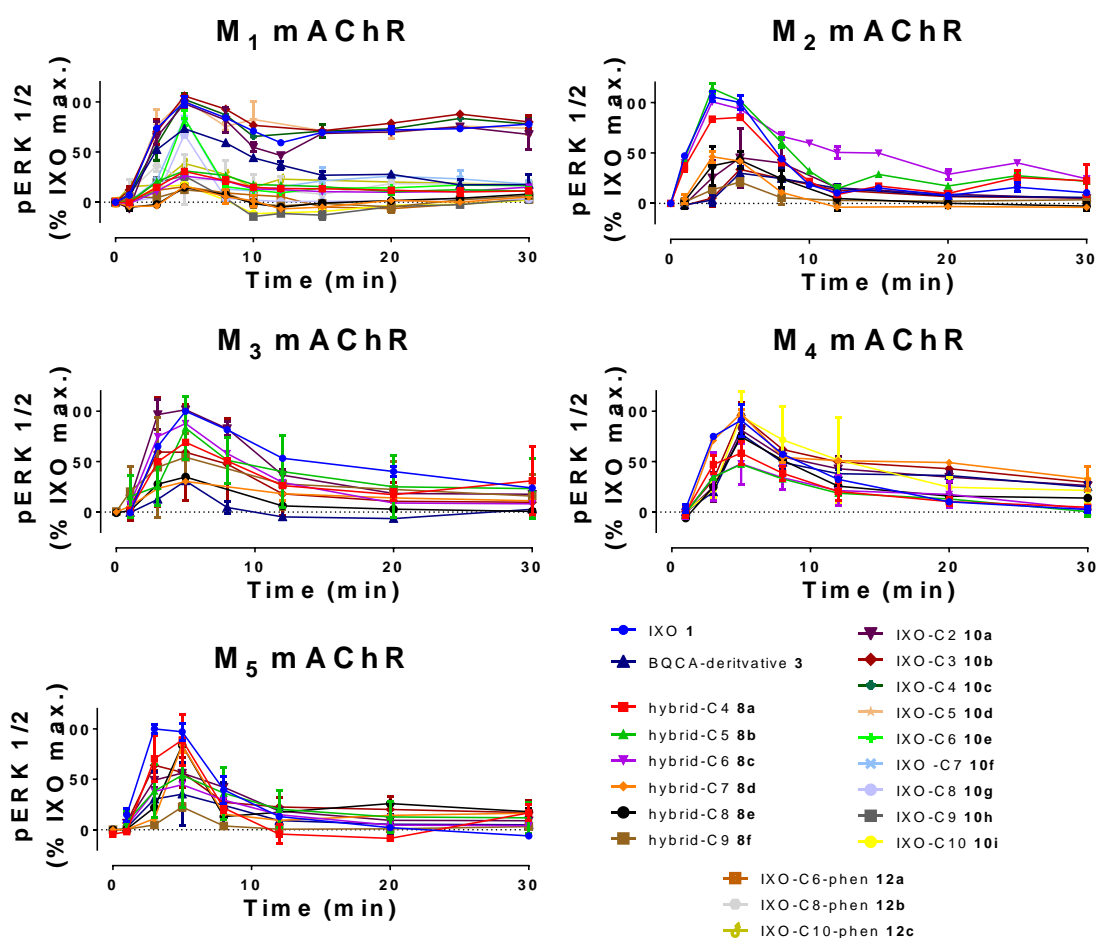
$$Y = \frac{[A]}{[A] + \left( \frac{K_A K_B}{(\alpha' [B] + K_B)} \right) \left( 1 + \frac{[I]}{K_I} + \frac{[B]}{K_B} + \frac{\alpha [I][B]}{K_I K_B} \right)} \quad (1)$$

where Y is the percentage (vehicle control) specific binding, [A], [B] and [I] are the concentrations of [ $^3\text{H}$ ]NMS, **3**, and **1** respectively,  $K_A$  and  $K_B$  are the equilibrium dissociation constants of [ $^3\text{H}$ ]NMS and the allosteric ligand, respectively,  $K_i$  is the equilibrium dissociation constant of **1**, and  $\alpha$  and  $\alpha'$  are the cooperativities between the allosteric ligand and [ $^3\text{H}$ ]NMS or **1**, respectively. Values of  $\alpha$  (or  $\alpha'$ )  $> 1$  denote positive cooperativity; values  $< 1$  denote negative cooperativity, and values  $= 1$  denote neutral cooperativity. Functional experiments measuring the interactions between **1** and **3** were fitted to the operational model of allosterism (2) to derive functional estimates of modulator affinity, cooperativity, and efficacy.

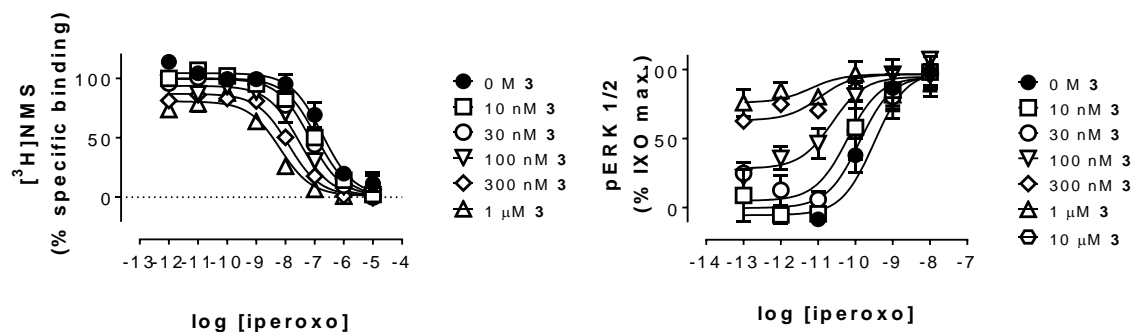
$$E = \frac{E_{\max}(\tau_A[A](K_B + \alpha\beta[B]) + \tau_B[B]K_A)^n}{([A]K_B + K_A K_B + [B]K_A + \alpha[A][B])^n + (\tau_A[A](K_B + \alpha\beta[B]) + \tau_B[B]K_A)^n} \quad (2)$$

where  $E_{\max}$  is the maximum attainable system response for the pathway under investigation; [A] and [B] are the concentrations of orthosteric and allosteric ligands, respectively;  $K_A$  and  $K_B$  are the equilibrium dissociation constants of the orthosteric and allosteric ligands,

respectively;  $\tau_A$  and  $\tau_B$  are the operational measures of orthosteric and allosteric ligand efficacy (which incorporate both signal efficiency and receptor density), respectively;  $n$  is a transducer slope factor linking occupancy to response;  $\alpha$  is the binding cooperativity parameter between the orthosteric and allosteric ligand;  $\beta$  denotes the magnitude of the allosteric effect of the modulator on the efficacy of the orthosteric agonist. The equilibrium dissociation constant of BQCA-derivative was fixed to that determined from the competition binding experiments.



**Supplementary figure 1. Time-course assays measuring the change in pERK 1/2 response in the presence of compounds 1,3 8a-f, 10a-i and 12a-c at the M<sub>1</sub>-M<sub>5</sub> mAChRs.** Experiments were performed on Flp-In-CHO cells stably expressing the M<sub>1,2,4-5</sub> mAChRs or CHO-K1 expressing the M<sub>3</sub> mAChR. Functional response to each ligand was compared to the maximum induced ERK 1/2 phosphorylation in the presence of iperoxo 1 at 1  $\mu$ M. Each data point represents the mean  $\pm$  S. E. of 2 independent experiments, performed in duplicate.



**Supplementary figure 2. Functional interaction assays measuring the change in iperoxo binding (Left) and function (Right) in the presence of 3 at the M<sub>1</sub> mAChR.** Experiments were performed on Flp-In-CHO cells stably expressing the M<sub>1</sub> mAChR. (Left) Whole-cell [ $^3\text{H}$ ]NMS inhibition binding curves were measured for iperoxo with increasing concentrations of 3. Functional response of iperoxo with increasing concentrations of 3 was estimated by measuring the induced ERK 1/2 phosphorylation as a percentage of the maximum inducible phosphorylation by the full agonist (iperoxo), at the time of peak phosphorylation, as determined previously by time-course assays (Supplementary Information). The curve of the graphs were generated by fitting an allosteric ternary complex model to the data, and constraining the models parameters based on experimental measurements of the properties of 3. Each data point represents the mean  $\pm$  S. E. of 3 independent experiments, performed in duplicate.

# **Supplementary Information**

## **Chapter Three**

### **Structure-Activity Relationship Study of Iperoxo-Based Muscarinic Acetylcholine Receptor Hybrid Ligands**

#### **Contents**

**Methods for the synthesis and characterization of intermediate compounds**

**Methods for pharmacological analysis of target compounds**

**Supplementary Figure 1** – Peak ERK 1/2 phosphorylation time course assays for McN-A-343-based hybrid ligands (14a-c) at the M<sub>1</sub>-M<sub>4</sub> mAChRs

**Supplementary Figure 2** – Peak ERK 1/2 phosphorylation time course assays for piperazinyl-linker hybrid ligands (17a-c) at the M<sub>3</sub>/ M<sub>4</sub> mAChRs

**Supplementary Figure 3** – Peak ERK 1/2 phosphorylation time course assays for NH and OH substituted linker hybrid ligands (18a-c, 19a-d) at the M<sub>3</sub>/ M<sub>4</sub> mAChRs

**Supplementary Figure 4** – Peak ERK 1/2 phosphorylation time course assays for phenyl ring substituted hybrid ligands (20a-r) at the M<sub>3</sub>/ M<sub>4</sub> mAChRs

**Supplementary Figure 5** – Peak ERK 1/2 phosphorylation time course assays for the most interesting phenyl ring substituted hybrid ligands (19a,l,m,o,r) at the M<sub>1</sub>/ M<sub>2</sub>/ M<sub>5</sub> mAChRs



## ■ EXPERIMENTAL SECTION

### Chemistry.

**General procedure for the synthesis of n-bromoalkanamides 21a-h.** Amine (10.0 mmol, 1.0 eq.), HCTU (11.0 mmol, 1.1 eq.) and the appropriate terminal-bromoalkanoic acid (10.0 mmol, 1.0 eq.) were dissolved in DMF (15 mL) and stirred under N<sub>2</sub> at room temperature. *N,N*-Diisopropylethylamine (DIPEA) (30.0 mmol, 3.0 eq.) in DCM (15 mL) was added dropwise over 30 min, and stirring continued for 16 h. The DCM was removed under vacuum and the reaction mixture was then diluted with distilled water (20 mL). The precipitate was filtered and then suspended in a 1:1 solution of sat. NaHCO<sub>3</sub> (aq) and distilled water (30 mL) and stirred vigorously for 30 min, before being vacuum filtered again. The resulting solid was then re-dissolved in DCM (10 mL) and washed with sat. NaHCO<sub>3</sub> solution (5 mL), dH<sub>2</sub>O (5 mL) and brine (5 mL) before being dried over anhydrous MgSO<sub>4</sub> and the solvent removed *in vacuo* to afford the target compound.

**11-Bromo-*N*-methylundecanamide (21a).** Off-white solid; 103 mg, 67%. <sup>1</sup>H NMR (CDCl<sub>3</sub>)  $\delta$  5.46 (br s, 1H), 3.40 (t, *J* = 6.9 Hz, 2H), 2.80 (d, *J* = 4.8 Hz, 3H), 2.15 (t, *J* = 8.0 Hz, 2H), 1.88-1.79 (m, 2H), 1.71-1.55 (m, 2H), 1.46-1.21 (m, 12H). <sup>13</sup>C NMR (CDCl<sub>3</sub>)  $\delta$  173.9, 36.9, 34.2, 33.0, 29.5, 29.4, 29.3, 29.2, 28.9, 28.3, 26.4, 25.9. *m/z* MS (TOF ES<sup>+</sup>) C<sub>12</sub>H<sub>24</sub>BrNO [M+H]<sup>+</sup> calcd; 278.1; found, 278.2. LC-MS *t*<sub>R</sub>: 3.81 min.

**11-Bromo-*N*-(3-fluorophenyl)undecanamide (21b).** Off-white solid; 250 mg, 81%. <sup>1</sup>H NMR (CDCl<sub>3</sub>)  $\delta$  7.97 (s, 1H), 7.50 (dt, *J* = 11.0, 2.2 Hz, 1H), 7.25-7.14 (m, 2H), 6.76 (tdd, *J* = 8.2, 2.5, 1.5 Hz, 1H), 3.38 (t, *J* = 6.9 Hz, 2H), 2.34 (t, *J* = 7.6 Hz, 2H), 1.82 (p, *J* = 8.7 Hz, 2H), 1.69 (p, *J* = 7.4 Hz, 2H), 1.46-1.20 (m, 12H). <sup>13</sup>C NMR (CDCl<sub>3</sub>)  $\delta$  172.0, 163.0 (d, *J*<sub>CF</sub> = 244.4 Hz), 139.9 (d, *J*<sub>CF</sub> = 10.8 Hz), 130.0 (d, *J*<sub>CF</sub> = 9.4 Hz), 115.1, 110.7 (d, *J*<sub>CF</sub> = 21.2 Hz), 107.4 (d, *J*<sub>CF</sub> = 26.2 Hz), 38.8, 34.2, 32.9, 29.5, 29.4, 29.3, 29.2, 28.8, 28.2, 25.6. *m/z* MS (TOF ES<sup>+</sup>) C<sub>17</sub>H<sub>25</sub>BrFNO [M+H]<sup>+</sup> calcd; 358.1; found, 357.9. LC-MS *t*<sub>R</sub>: 4.78 min.

**11-Bromo-*N*-(4-fluorophenyl)undecanamide (21c).** Off-white solid; 181 mg, 76%.  $^1\text{H}$  NMR ( $\text{CDCl}_3$ )  $\delta$  7.60 (br s, 1H), 7.51-7.44 (m, 2H), 7.01-6.91 (m, 2H), 3.39 (t,  $J = 6.9$  Hz, 2H), 2.33 (t,  $J = 7.5$  Hz, 2H), 1.88-1.78 (m, 2H), 1.75-1.64 (m, 2H), 1.44-1.22 (m, 12H).  $^{13}\text{C}$  NMR ( $\text{CDCl}_3$ )  $\delta$  171.8, 160.5, 134.2 (d,  $J_{\text{CF}} = 2.8$  Hz), 121.8 (d,  $J_{\text{CF}} = 7.8$  Hz), 115.6 (d,  $J_{\text{CF}} = 22.4$  Hz), 37.6, 34.2, 32.9, 29.5, 29.4, 29.3, 29.2, 28.8, 28.2, 25.7.  $m/z$  MS (TOF  $\text{ES}^+$ )  $\text{C}_{17}\text{H}_{25}\text{BrFNO}$   $[\text{M}+\text{H}]^+$  calcd; 358.1; found, 357.9. LC-MS  $t_{\text{R}}$ : 4.77 min.

**11-Bromo-*N*-(2-methoxyphenyl)undecanamide (21d).** Off-white solid; 84.7 mg, 77%.  $^1\text{H}$  NMR ( $\text{CDCl}_3$ )  $\delta$  8.38 (dd,  $J = 8.0, 1.7$  Hz, 1H), 7.75 (br s, 1H), 7.03 (td,  $J = 7.8, 1.7$  Hz, 1H), 6.95 (td,  $J = 7.7, 1.5$  Hz, 1H), 6.87 (dd,  $J = 8.0, 1.5$  Hz, 1H), 3.88 (s, 3H), 3.40 (t,  $J = 6.8$  Hz, 2H), 2.38 (t,  $J = 7.6$  Hz, 2H), 1.84 (dp,  $J = 8.6, 6.9$  Hz, 2H), 1.73 (p,  $J = 7.5$  Hz, 2H), 1.47-1.22 (m, 12H).  $^{13}\text{C}$  NMR ( $\text{CDCl}_3$ )  $\delta$  171.4, 156.7, 127.9, 123.6, 121.3, 119.9, 110.0, 55.8, 38.2, 34.2, 33.0, 29.5, 29.4, 29.3, 29.2, 28.9, 28.3, 25.7.  $m/z$  MS (TOF  $\text{ES}^+$ )  $\text{C}_{18}\text{H}_{28}\text{BrNO}_2$   $[\text{M}+\text{H}]^+$  calcd; 370.1; found, 369.9. LC-MS  $t_{\text{R}}$ : 4.01 min.

**11-Bromo-*N*-(3-methoxyphenyl)undecanamide (21e).** Off-white solid; 148 mg, 71%.  $^1\text{H}$  NMR ( $\text{CDCl}_3$ )  $\delta$  7.26 (,  $J = 1.5$  Hz, 1H), 7.22 (br s, 1H), 7.12 (t,  $J = 7.5$  Hz, 1H), 6.88 (dt,  $J = 7.5, 1.5$  Hz, 1H), 6.58 (dt,  $J = 7.3, 1.5$  Hz, 1H), 3.78 (s, 3H), 3.40 (t,  $J = 6.8$  Hz, 2H), 2.32 (t,  $J = 7.6$  Hz, 2H), 1.89-1.80 (m, 2H), 1.72 (q,  $J = 7.4$  Hz, 2H), 1.47-1.24 (m, 12H).  $^{13}\text{C}$  NMR ( $\text{CDCl}_3$ )  $\delta$  171.4, 160.3, 139.4, 129.7, 111.9, 110.2, 105.5, 55.4, 38.8, 34.2, 32.9, 29.5, 29.4, 29.3, 29.2, 28.9, 28.3, 25.7.  $m/z$  MS (TOF  $\text{ES}^+$ )  $\text{C}_{18}\text{H}_{28}\text{BrNO}_2$   $[\text{M}+\text{H}]^+$  calcd; 370.1; found, 369.9. LC-MS  $t_{\text{R}}$ : 3.90 min.

**11-Bromo-*N*-(4-methoxyphenyl)undecanamide (21f).** Off-white solid; 123 mg, 86%.  $^1\text{H}$  NMR ( $\text{CDCl}_3$ )  $\delta$  7.43-7.37 (m, 2H), 7.09 (br s, 1H), 6.88-6.82 (m, 2H), 3.78 (s, 3H), 3.40 (t,  $J = 6.8$  Hz, 2H), 2.32 (t,  $J = 7.6$  Hz, 2H), 1.89-1.80 (m, 2H), 1.72 (q,  $J = 7.4$  Hz, 2H), 1.47-1.24 (m, 12H).  $^{13}\text{C}$  NMR ( $\text{CDCl}_3$ )  $\delta$  171.3, 156.5, 131.2, 121.8, 114.3, 55.6, 37.8, 34.2, 33.0,

29.5, 29.4, 29.3, 29.2, 28.9, 28.3, 25.8. *m/z* MS (TOF ES<sup>+</sup>) C<sub>18</sub>H<sub>28</sub>BrNO<sub>2</sub> [M+H]<sup>+</sup> calcd; 370.1; found, 369.9. LC-MS *t*<sub>R</sub>: 3.83 min.

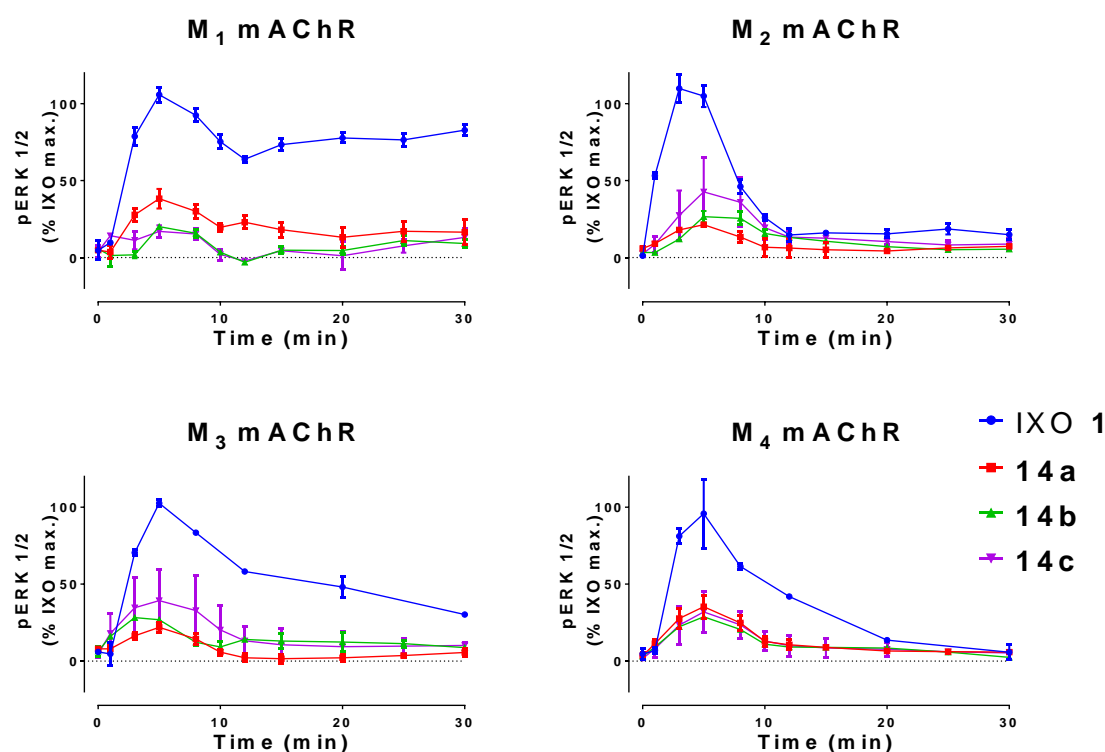
**11-Bromo-*N*-(3-(trifluoromethyl)phenyl)undecanamide (21g).** Off-white solid; 148 mg, 77%. <sup>1</sup>H NMR (CDCl<sub>3</sub>) δ 7.83 (s, 1H), 7.73 (d, *J* = 8.0 Hz, 1H), 7.63 (s, 1H), 7.41 (t, *J* = 7.9 Hz, 1H), 7.35-7.31 (m, 1H), 3.40 (t, *J* = 6.9 Hz, 2H), 2.38 (t, *J* = 7.6 Hz, 2H), 1.84 (p, *J* = 8.7 Hz, 2H), 1.71 (p, *J* = 7.5 Hz, 2H), 1.48-1.23 (m, 12H). <sup>13</sup>C NMR (CDCl<sub>3</sub>) δ 172.0, 138.7, 131.4 (q, *J*<sub>CF</sub> = 32.3 Hz), 129.6, 122.7, 124.0 (q, *J*<sub>CF</sub> = 272.4 Hz), 120.8, 116.6, 37.8, 34.2, 32.9, 29.5, 29.4, 29.3, 29.2, 28.8, 28.3, 25.6. *m/z* MS (TOF ES<sup>+</sup>) C<sub>18</sub>H<sub>25</sub>BrF<sub>3</sub>NO [M+H]<sup>+</sup> calcd; 408.1; found, 407.9. LC-MS *t*<sub>R</sub>: 4.91 min.

**11-Bromo-*N*-(4-(trifluoromethyl)phenyl)undecanamide (21h).** Off-white solid; 202 mg, 58%. <sup>1</sup>H NMR (CDCl<sub>3</sub>) δ 7.96 (s, 1H), 7.71-7.63 (m, 2H), 7.57-7.49 (m, 2H), 3.39 (t, *J* = 6.9 Hz, 2H), 2.38 (t, *J* = 7.6 Hz, 2H), 1.83 (p, *J* = 8.7 Hz, 2H), 1.70 (p, *J* = 7.5 Hz, 2H), 1.47-1.20 (m, 12H). <sup>13</sup>C NMR (CDCl<sub>3</sub>) δ 172.3, 141.4, 128.2 (app d, *J*<sub>CF</sub> = 18.0 Hz), 126.2 (q, *J*<sub>CF</sub> = 3.8 Hz), 124.2 (q, *J*<sub>CF</sub> = 272.0 Hz), 119.5, 124.0, 37.8, 34.2, 32.9, 29.5, 29.4, 29.3, 29.2, 28.8, 28.2, 25.6. *m/z* MS (TOF ES<sup>+</sup>) C<sub>18</sub>H<sub>25</sub>BrF<sub>3</sub>NO [M+H]<sup>+</sup> calcd; 408.1; found, 407.8. LC-MS *t*<sub>R</sub>: 4.91 min.

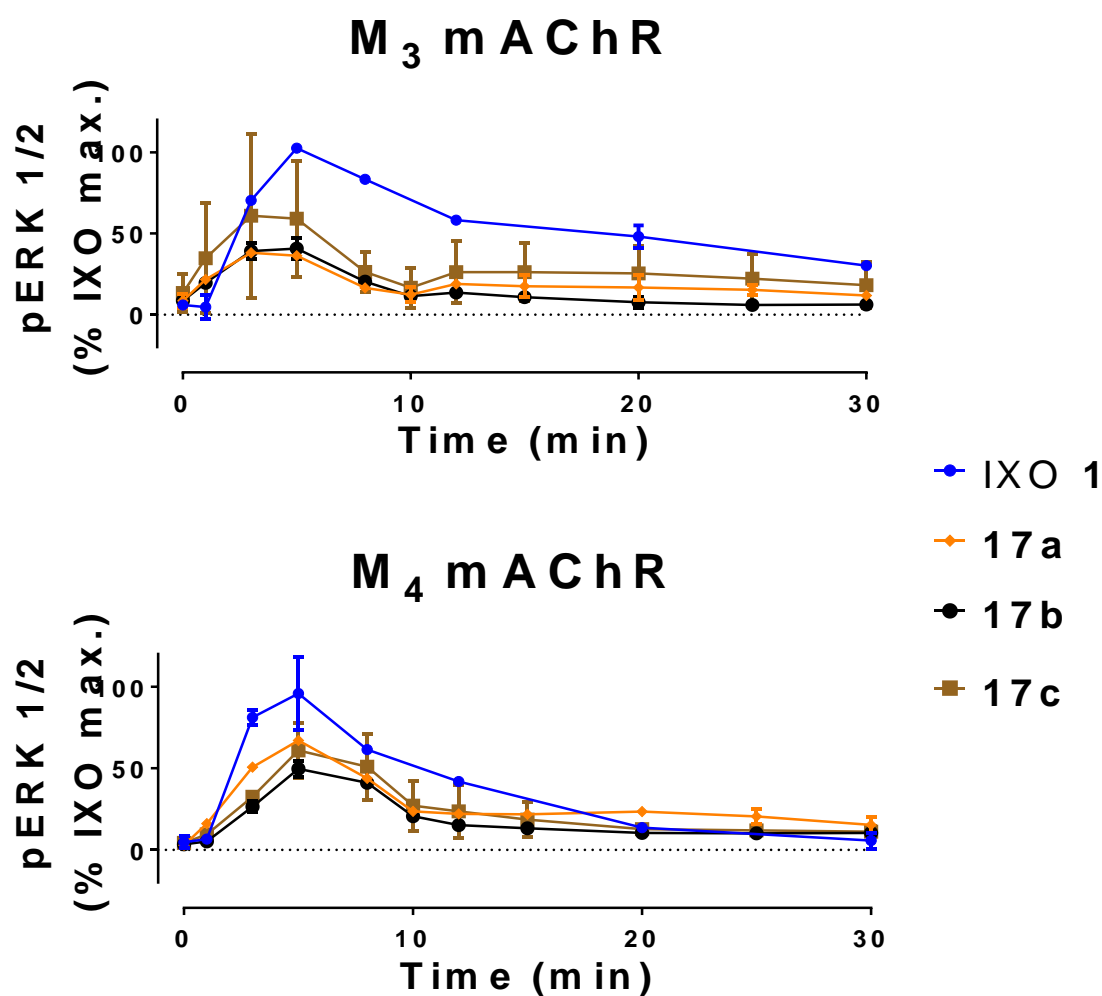
### Pharmacology.

*Time-course assays.* Cells were plated in 180 μL media per well. Stock solutions of iperoxo **1** and the test ligands were made up in DMSO (10<sup>-2</sup> M). Dilutions of all ligands were made up in FBS-free media at ten times (10×) the required concentration and added to stock plates. Cells were incubated at 37 °C with 20 μL of iperoxo (10<sup>-6</sup> M) or test ligand solution (10<sup>-5</sup> M) at the time points: 30, 20, 15, 12, 10, 8, 5, 3 and 1 min, before terminating the assay. 10% (v/v) FBS and vehicle were added at 6 min as positive and negative controls.

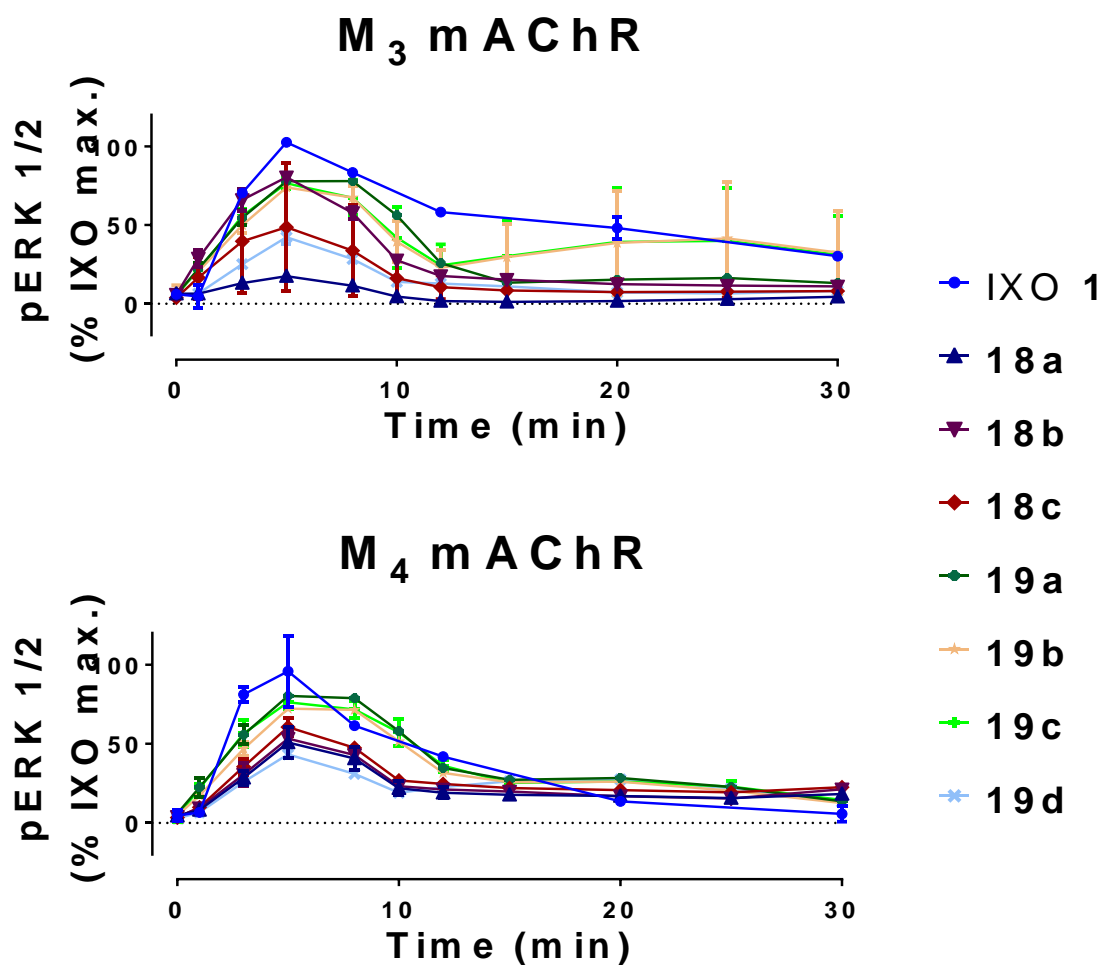
*Data analysis.* All data analysis was managed using Prism 6 software (GraphPad Software, San Diego, CA).



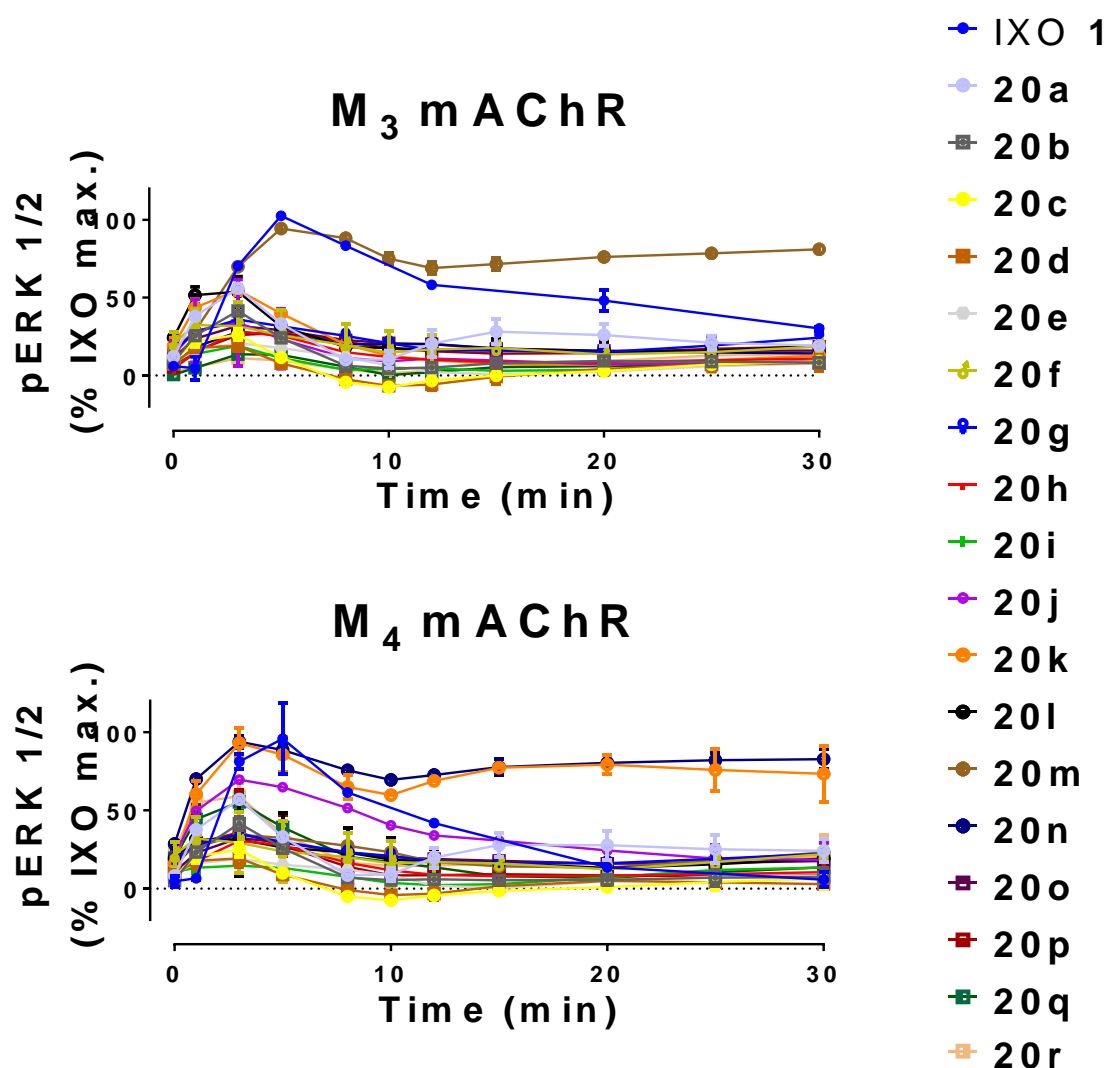
**Supplementary Figure 1. Time-course assays measuring the change in pERK 1/2 response for McN-A-343-based hybrid ligands (14a-c) at the M<sub>1</sub>-M<sub>4</sub> mAChRs.** Experiments were performed on Flp-In-CHO cells stably expressing the M<sub>1</sub>/M<sub>2</sub> or M<sub>4</sub> mAChRs or CHO-K1 expressing the M<sub>3</sub> mAChR. Functional response to each ligand was compared to the maximum induced ERK 1/2 phosphorylation in the presence of iperoxo 1 at 1  $\mu$ M. Each data point represents the mean  $\pm$  S. E. of 2 independent experiments, performed in duplicate.



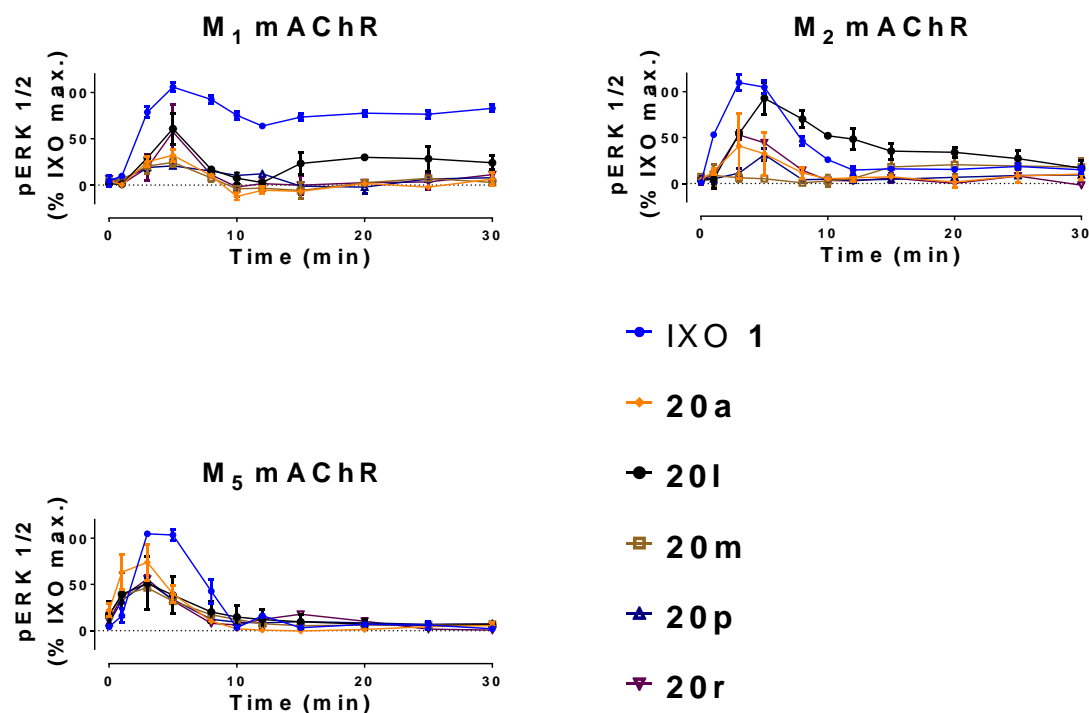
**Supplementary figure 2. Time-course assays measuring the change in pERK 1/2 response for piperazinyl-linker hybrid ligands (17a-c) at the M<sub>3</sub>/ M<sub>4</sub> mAChRs.** Experiments were performed on CHO-K1 cells stably expressing the M<sub>3</sub> mAChR or Flp-In-CHO cells expressing the M<sub>4</sub> mAChR. Functional response to each ligand was compared to the maximum induced ERK 1/2 phosphorylation in the presence of iperoxo **1** at 1  $\mu$ M. Each data point represents the mean  $\pm$  S. E. of 2 independent experiments, performed in duplicate.



**Supplementary figure 3. Time-course assays measuring the change in pERK 1/2 response for NH and OH substituted linker hybrid ligands (18a-c, 19a-d) at the M<sub>3</sub>/ M<sub>4</sub> mAChRs.** Experiments were performed on CHO-K1 cells stably expressing the M<sub>3</sub> mAChR or Flp-In-CHO cells expressing the M<sub>4</sub> mAChR. Functional response to each ligand was compared to the maximum induced ERK 1/2 phosphorylation in the presence of iperoxo **1** at 1  $\mu$ M. Each data point represents the mean  $\pm$  S. E. of 2 independent experiments, performed in duplicate.



**Supplementary figure 4. Time-course assays measuring the change in pERK 1/2 response for phenyl ring substituted hybrid ligands (20a-r) at the M<sub>3</sub>/ M<sub>4</sub> mAChRs.** Experiments were performed on CHO-K1 cells stably expressing the M<sub>3</sub> mAChR or Flp-In-CHO cells expressing the M<sub>4</sub> mAChR. Functional response to each ligand was compared to the maximum induced ERK 1/2 phosphorylation in the presence of iperoxo **1** at 1  $\mu$ M. Each data point represents the mean  $\pm$  S. E. of 2 independent experiments, performed in duplicate.



**Supplementary figure 5. Time-course assays measuring the change in pERK 1/2 response for the most interesting phenyl ring substituted hybrid ligands (20a,l,m,p,r) at the M<sub>1</sub>/M<sub>2</sub>/M<sub>5</sub> mAChRs** Experiments were performed on Flp-In-CHO cells stably expressing the M<sub>1</sub>/M<sub>2</sub>/ or M<sub>5</sub> mAChRs. Functional response to each ligand was compared to the maximum induced ERK 1/2 phosphorylation in the presence of iperoxo **1** at 1  $\mu$ M. Each data point represents the mean  $\pm$  S. E. of 2 independent experiments, performed in duplicate.



# **Supplementary Information**

## **Chapter Four**

### **Investigation into the Molecular Mechanism of Efficacy and Selectivity of Iperoxo-Based Muscarinic Acetylcholine Receptor Hybrid Ligands**

#### **Contents**

*Methods for pharmacological analysis of target compounds*

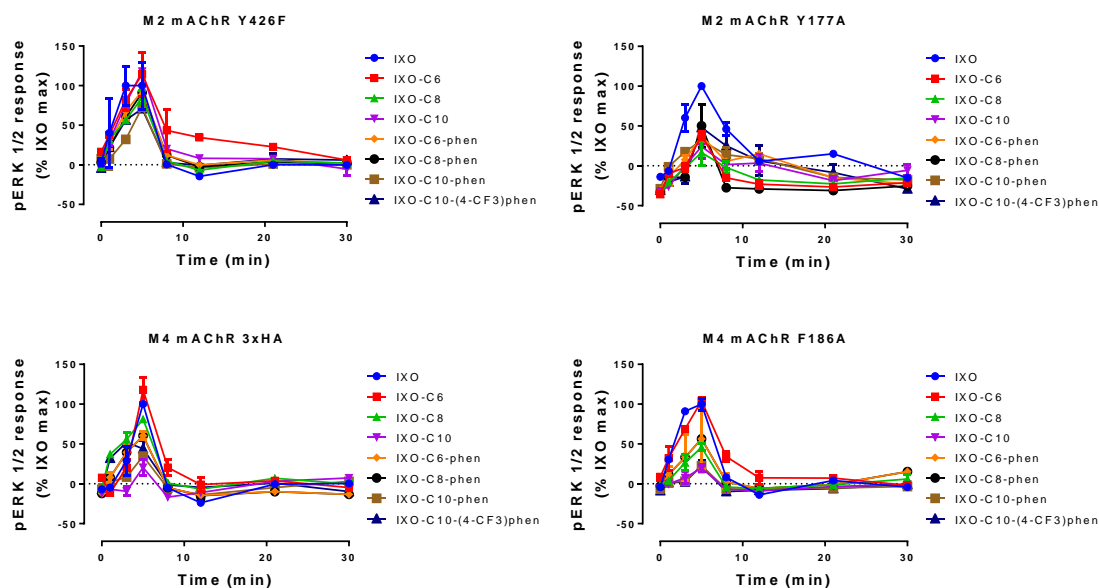
**Supplemental figure 1 – Peak ERK 1/2 phosphorylation time course assays for target compounds at mutant M<sub>2</sub> and M<sub>4</sub> mAChRs**

## ■ EXPERIMENTAL

### Pharmacology.

*Time-course assays.* Cells were plated in 180  $\mu$ L media per well. Stock solutions of iperoxo (IXO) and the test ligands were made up in DMSO ( $10^{-2}$  M). Dilutions of all ligands were made up in FBS-free media at ten times ( $10\times$ ) the required concentration and added to stock plates. Cells were incubated at 37  $^{\circ}$ C with 20  $\mu$ L of iperoxo ( $10^{-6}$  M) or test ligand solution ( $10^{-5}$  M) at the time points: 30, 20, 15, 12, 10, 8, 5, 3 and 1 min, before terminating the assay. 10% (v/v) FBS and vehicle were added at 6 min as positive and negative controls.

*Data analysis.* All data analysis was managed using Prism 7 software (GraphPad Software, San Diego, CA).



**Supplementary figure 1. Time-course assays measuring the change in pERK 1/2 response in the presence of compounds IXO, IXO-C6, IXO-C8, IXO-C10, IXO-C6-phen, IXO-C8-phen, IXO-C10-phen and IXO-C10-(4-CF<sub>3</sub>)phen at the M<sub>2</sub> Y426F, M<sub>2</sub> Y177A, M<sub>4</sub> 3xHA and M<sub>4</sub> F186A mutant mACHRs.** Experiments were performed on Flp-In-CHO cells stably expressing the M<sub>2</sub> Y426F, M<sub>2</sub> Y177A, M<sub>4</sub> 3xHA and M<sub>4</sub> F186A mutant mACHRs. Functional response to each ligand was compared to the maximum induced ERK 1/2 phosphorylation in the presence of iperoxo (IXO) at 1  $\mu$ M. Each data point represents the mean  $\pm$  S. E. of 2 independent experiments, performed in duplicate.